Identification of Sea Breezes, their Climatic Trends and Causation, with Application to the Adelaide Coast

ZAHRA PAZANDEH MASOULEH

BENG (CIVIL & STRUCTURAL), MSCENG (Coastal)

A THESIS SUBMITTED FOR THE DEGREE OF
DOCTOR OF PHILOSOPHY

SCHOOL OF CIVIL, ENVIRONMENTAL AND MINING ENGINEERING
July 2015

Table of contents

List of Figures

List of Tables

Abstract

Nearshore processes along the sandy beaches of Adelaide are driven by the prevailing wind and waves. While the narrow entrance of Gulf St. Vincent and the shallow waters attenuate the ocean swell waves, the locally generated southerly to south-westerly waves are behind the net northward littoral drift transport. An important factor in the generation of local waves are the sea breezes, which for Gulf St Vincent result from a combination of a southerly ocean breeze and westerly gulf breezes, and a key question in this time when the climate is said to be changing is whether there is evidence that these sea breezes are changing.

This study, therefore, investigates the existence of long-term changes to the gulf breeze; hereafter referred to as the sea breeze, over the period of August 1955 to June 2008.

In the study of the local climate a set of criteria were developed to define and identify the sea breeze days on which the locally generated coastal winds are generally dominant in the afternoon. Considering the limitation of meteorological observations, the criteria employed the three-hourly near surface data, the 12-hourly upper air levels recorded data, and the surface temperatures of Gulf St. Vincent, provided by Advanced High Resolution Radiometer (AVHRR).

Applying the methods, the period of study is divided into sea breeze and non-sea breeze days, where the characteristic afternoon wind in both categories is analysed. Although the annual percentage of observed sea breeze cases does not show any significant change over the period of the study, the results have demonstrated the presence of an increasing trend in the intensity of afternoon winds, more evidently for the selected sea breeze days.

Through regression analysis of the results, the rise of the southerly component of the wind has been found to have a strong correlation with the surface temperature of the

land, whereas the growth of the westerly component was not correlated with any local climate drivers.

Following this important result, the study then went on to determine what might be driving this change. As the importance of urbanization on the climate of wind has been extensively studied by previous researchers, the growth of the Adelaide metropolitan area was conjectured to affect the wind climate at the planetary boundary layer.

A next-generation mesoscale numerical model, Weather Research and Forecasting (WRF), was employed to simulate the climate of the area with and without the metropolitan area of Adelaide, where the city was replaced by the native vegetation of the land. From the simulations it appears that the westerly components of the winds are strongly affected by changes to the nature of the land, due to a combination of changes to the surface roughness length and modification of the surface heat budget components.

The main findings of the statistical and numerical study of the wind climate of Adelaide are:

1. The wind climate in and around Gulf St. Vincent has shown a statistically significant change over the last 50 years.
2. While there has been no significant change in the number of sea breeze days, the current wind climate has significantly higher wind speeds more evidently on sea breeze days. This is likely to have an important effect on the coast, particularly if the trend continues.
3. Through the component-wise analysis of wind, the change in the intensity of south-north component of wind intensity was found to be correlated to the increasing trend of land surface temperature. This is likely to explain one of the key drivers of the change in wind climate.

4. A numerical modelling exercise demonstrated the importance of the growth of the metropolitan area of Adelaide with the change in surface roughness and the change to the surface energy budget being two key elements of the change.

In the end, there is still a need for future study to examine the possible effects of prolonged changes of wind characteristics on the dynamics of the shoreline, particularly in regard to the littoral sediment transport system.

Statement of Originality

I, Zahra Pazandeh Masouleh certify that this work contains no material which has been accepted for the award of any other degree or diploma in my name, in any university or other tertiary institution and, to the best of my knowledge and belief, contains no material previously published or written by another person, except where due reference has been made in the text. In addition, I certify that no part of this work will, in the future, be used in a submission in my name, for any other degree or diploma in any university or other tertiary institution without the prior approval of the University of Adelaide and where applicable, any partner institution responsible for the joint-award of this degree.

I give consent to this copy of my thesis, when deposited in the University Library, being made available for loan and photocopying, subject to the provisions of the Copyright Act 1968.

I also give permission for the digital version of my thesis to be made available on the web, via the University's digital research repository, the Library Search and also through web search engines, unless permission has been granted by the University to restrict access for a period of time.

Signature:

Date:

Acknowledgement

I would like to express my deep and sincere gratitude to my supervisors: Professor David Walker and Professor John Crowther, for their valuable guidance, consistent encouragement, understanding, patience, and most importantly, their friendship throughout the research work.

I am extremely grateful to my main supervisor Prof. David Walker, for his guidance and all the useful discussions and brainstorming sessions, especially during the difficult conceptual development stage. His deep insights helped me at various stages of my research. I also remain indebted for his understanding and support during my maternity leave. My sincere gratitude is reserved for Prof. John Crowther for his invaluable insights and suggestions. I really appreciate his willingness to meet me at short notice every time and going through several drafts of my thesis. I remain amazed that despite his busy schedule, he was able to go through the final draft of my thesis and meet me in less than a week with comments and suggestions on almost every page. He is an inspiration. I also acknowledge the contribution of Dr. Murray Townsend to my thesis and his support as a member of my PhD supervision panel is highly appreciated. I thank Mr. Darren Ray, senior meteorologist at South Australian Regional Climate Services Centre of Bureau of Meteorology for his supports and helps with meteorological data.

Sincere thanks are extended to the former computing officer, Dr. Stephen Carr and the school administrative staff, for their help.

I wish to thank my fellow postgraduates in the School of Civil, Environmental and Mining Engineering for their assistance and friendship. Special thanks to my very good friends Li Li, Jaya and Nimasha, who have made this journey so much more enjoyable. I owe a lot to my parents, who encouraged and helped me at every stage of my personal and academic life, and longed to see this achievement come true. Lastly, I would like to dedicate this thesis to my precious daughter, Aida and my loving, supportive, encouraging, and patient husband Arash Asadi whose faithful support through this Ph.D. is so appreciated.

List of Abbreviation

AAO	Antarctic Oscillation
ACST	Australian Central Standard Time
AFWA	Air Force Weather Agency
AHD	Australian Height Datum
AOI	Antarctic Oscillation Indices
ARW	Advanced Research WRF
AVHRR	Advanced Very High Resolution Radiometer
CBD	Central Business District
CGA	Synchrotac Cup Anemometer
CSIRO	Commonwealth Scientific and Industrial Research Organisation
CTL	Control Run
DST	Daylight Saving Time
ENSO	El Niño Southern Oscillation
ETA	Eta Model
FAA	Federal Aviation Administration
FSL	Forecast System Laboratory
GCM	General Circulation Models
GDAS	Global Data Assimilation System
GTS	Global Telecommunications System
IOA	Index Of Agreement
IOD	Indian Ocean Dipole
LH	Latent Heat
LW	Long Wave radiation
MB	Mean Biass Error
MM5	PSU/NCAR mesoscale model
MO	Monin–Obukhov similarity theory
NCAR	National Center for Atmospheric Research
NCEP	National Center for Environmental Prediction
NCEP FNL	global reanalysis datasets (final data analysis) from the US National Centers for Environmental Prediction
NESL	parallel language developed at Carnegie Mellon
NMM	Non-hydrostatic Mesoscale Model
NOAA	National Oceanic and Atmospheric Administration
NRMSE	Normalized root mean square error
NTV	Native Vegetation (model)
NVIS	National Vegetation Information System

PBL	Planetary Boundary Layer
pchip	Piecewise Cubic Hermite Interpolating Polynomial
PTA	Dines Pressure Tube Anemometer
Qv	mixing ratio for water vapour
RAAF	Royal Australian Air Force
RCM	Regional Climate Models
RMSD	Root Mean Square Difference
RMSE	Root Mean Square Error
RSM	Reynolds Stress equation Model
SH	Sensible Heat
SLP	Sea-Level Pressure
SOI	Southern Oscillation Index
SW	Short Wave radiation
UCI	Urban Cool Island
UHI	Urban Heat Island
USGS	U.S. Geological Survey
WMP	Warmer Months Prediction
WPS	WRF pre-processing system
WRF	Weather Research and Forecasting
WSM3	WRF Single Moment 3 classes

1. Introduction

1.1. Background and motivation for the research

The dynamics of over 30 kilometres of coastline at Adelaide (Figure 1.1), South Australia, are very vulnerable to changes in the wind and wave climates. The issue is made more urgent as unwise coastal developments have altered the dynamics of the coast to such extent that, nowadays, the natural coastal processes do not sustain the beaches. Each year the placement of over 160,000 cubic metres of sand at strategic locations on the beaches is required to protect the coastal infrastructure and maintain the coastal sand dune buffers(Tucker *et al.*, 2005).

The wave-induced littoral drift is the most important sand movement mechanism in the nearshore zone, with the combination of wind-generated currents, mainly produced by south-westerly winds, and northerly tidal currents moving the sands in a net northward direction.

As a locally generated wind, the sea breezes not only affect the wave climate but also contribute to the wind-blown formation of sand dunes. These breezes are created as a result of temperature differences between the land and sea surface and therefore are very sensitive to the temperature of the land surface.

A study by Plummer *et al.* (1995) suggests that, since 1950 the average annual maximum and minimum temperatures of South Australia have increased by 0.1 - 0.2 °C and 0.2 - 0.3 °C per decade, respectively. Moreover, the results of simulation of the Australian continent with pre-European vegetation by Mcalpine *et al.* (2007), confirm the important role of land surface cover on near surface wind speed as it modifies the roughness length of the surface as well as the surface evaporation and latent and sensible

heat flux. The results show an overall increase of 0.2 m s^{-1} in the 10 m height wind speed of South Australia.

It is also relevant that for the cities located in the vicinity of the coast, the interaction of urban heat island and sea-land breeze circulation has been observed to affect the sea-land circulation pattern. It can change the sea breeze wind speed and the timing of its arrival (Yoshikado, 1992).

The combination of the abovementioned factors and the globally increased mean sea level is likely to change the wave climate of the sandy shoreline of Adelaide (Tucker *et al.*, 2005). The combination of concerns regarding the local coastal climate, increasing land temperatures, rising sea level pressure and the effects of urbanization and land cover change inspired the current research to study the sea breeze characteristics of the Adelaide coastline since 1955 using the record of local meteorological observations.

1.2. Research scope and Objective

The metropolitan city of Adelaide, with a population of 1.23 million, is the fifth-largest city of Australia. It is located between Gulf St Vincent to the west and the low-lying Mount Lofty Ranges to the east, with over 30 km of shoreline that is oriented approximately north-northwest/south-southeast. The sandy beaches of Adelaide are impacted by sea waves generated mainly by the west-southwest winds (Tucker *et al.*, 2005). The climate of Adelaide has been described as Mediterranean with hot, dry summers and mild wet winters. Figure 1.1 shows Adelaide and the surrounding areas of interest.

The Gulf is relatively shallow with the deepest part being up to 40 metres. It is joined to the Southern Ocean through the deep and narrow Backstairs Passage and Investigator Strait. The presence of Kangaroo Island restricts and attenuates the entrance of large ocean swell that leaves the sandy beaches responsive to changes of locally generated waves.

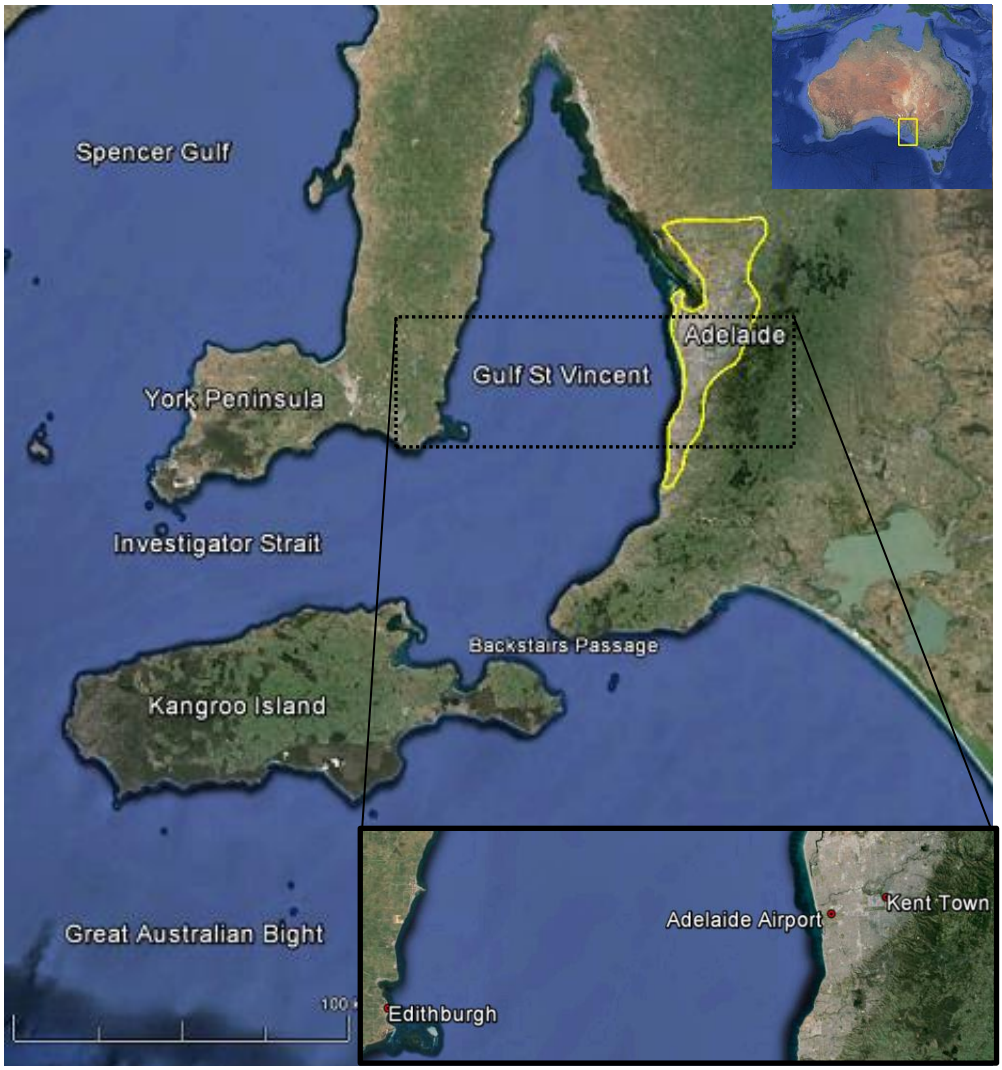

Figure 1.1. The location of metropolitan Adelaide (Google Earth)

The significant wave heights of the Gulf rarely exceed 2 metres while for 50% of the time the significant wave height is 0.5 metres or less. These waves, which strike the coastline at an oblique angle, are generated by predominantly south westerly winds (South Australian Coast Protection Board, 1993) and induce a littoral sediment transport in that direction. These winds, as demonstrated by Physick and Byron-Scott (1977), are a combination of westerly sea breezes from Gulf St Vincent (gulf breeze) and southerly breezes from the Southern Ocean, known as the ocean breeze.

Although the arrival time of these two breezes is different, by late in the afternoon they integrate and generate a south-westerly wind. These breezes have been observed to arrive as early as 07:00 ACST (Australian Central Standard Time) and cease as late as 21:00. As far as the previous observational study of sea breeze of Adelaide goes, the wind on the eastern side of the Gulf turns to an onshore direction in the early morning, which is associated with the arrival of the gulf breeze and reaches its maximum velocity before noon, followed by a decrease in speed until mid-afternoon when the maximum ocean breeze hits the land. The arrival of the gulf breeze is associated with a drop in temperature and a rise in humidity. Due to the shallow depth of the Gulf, and relatively warmer water, the breeze generated over the Gulf carries moist air, while the ocean breeze arrival is denoted by the arrival of a late cool and drier air mass.

The importance of locally generated waves on the sand transport of the Adelaide coast has been stressed in a number of reports commissioned by the Department of Environment, Water and Natural Resource of the Government of South Australia (Cooper and Pilkey, 2012). As one of the main driving forces behind the locally generated waves, a long-term change to the sea breeze characteristic is considered to have a significant role on the Adelaide coastal process and beach morphology. This fact prompted the current study of the available meteorological records in order to identify any possible changes to the sea breeze system. As part of the project, the considerable urban growth of the city and land cover alteration of the surrounding areas after settlement was also investigated as it was believed to amplify the local changes to the climate of the region.

The central question is whether there is any local change to the climate of sea breeze over the Adelaide metropolitan areas due to urbanization and anthropogenic land cover change and, if so, how serious it is.

To achieve the answer, this study develops a selection algorithm to detect sea breeze occurrences for the period 1955-2008 (where the data are available). The Adelaide

Airport station, with the longest surface level and upper air level records, has been chosen as the key station as it is close to the shoreline, and a fully developed sea breeze with inland penetration arrives at the station in the afternoon. These sea breezes normally reach the land a few hours after the time that the maximum temperature gradient over the land and sea occurs. The rotation of wind from an offshore to onshore direction is the main indication of the arrival of sea breezes. An observational study performed by Physick and Byron-Scott (1977), illustrated the sea breeze features, including the effects that occur on the other side of the Gulf. For the locally generated winds over the Gulf, the onshore component of the wind has been observed to accelerate to its maximum intensity sometime in the afternoon. The general behaviour of wind on sea breeze days was compared for two coastal stations at both sides of the Gulf. In line with the overall objective of the study, the time of start, cessation and the maximum wind occurrence is discussed.

To examine the contribution of urbanization in the meso-scale climate of the sea breeze, numerical modelling was utilized to simulate the weather of the region. The model's performance was validated using observed meteorological records. Different land cover scenarios were simulated and the results compared to estimate the possible modification to the meso-scale weather of the region due to human activities.

1.3. Overview of Thesis

This research is designed to provide an understanding of the sea breeze climate of Adelaide and the progressive change in it as a result of the continuous growth of the urban area. It includes the following chapters:

Chapter 2. Literature review: The main focus of this chapter is an extensive review of previous work on global climate change, urban heat island and their impacts on the coastal cities weather. It includes an extensive explanation of the parameters and processes involved in the alteration of near surface climate as result of land cover

change. Examples of observation and numerical studies of climate of numbers of cities (including Australia) are presented.

Chapter 3: The climate of the study area: This chapter looks at the climate of the area, and specifically the wind climate. The major climatic drivers of South Australia are also defined in this chapter.

Chapter 4. Detection and Validation of Sea Breezes: In this chapter meteorological data from Adelaide Airport station are investigated to select sea breeze events for the duration of 1955 to 2008 while observational record from Edinburgh meteorological station on the other side of the Gulf St Vincent are used to evaluate the selection algorithm. The changes in the wind characteristics on selected days are demonstrated and, where possible, the timing of sea breeze onset and cessation is determined. Since some of the climate oscillations of oceans have been observed to have an impact on the weather of coastal cities, the change of sea breeze properties such as intensity was tested against some relevant indices such as the SOI (Southern Oscillation Index).

Chapter 5. Modelling the urban weather: The numerical model, Weather Research and Forecasting (WRF) is explained, configured and utilized to reproduce the weather of the Adelaide region. After the evaluation of the model's performance, the effect of urbanization on local weather of the city is explained using the result of two simulations. The contribution of land cover change on the structure of wind, more specifically during warmer months with more frequent sea breeze cases, is analyzed in this chapter. Moreover the changes to the wind regime of observed sea breeze days (from the selection algorithm) of simulation period are discussed at the end.

Chapter 6. Summary and Conclusions: The importance of sea breeze study for Adelaide coastline is set out and the impact of urbanization on sea breeze change is quantified, using the results from the previous chapters and finally the areas for further studies are recommended.

2. Literature Review

2.1. Introduction to Adelaide Coastal Climate

The Adelaide plains are located in South Australia, between Gulf St Vincent and the Mount Lofty ranges. The climate of the plains is described as Mediterranean, with warm and dry summers and wet and cool winters. The coastline consists of fine to medium grade sands that, before the European settlement in 1836, was formed as sand dunes with an average width of 200 to 300 metres and a height of up to 15 metres. With the development of the Adelaide metropolitan area, and predominantly after the 1920's, the dunes were mined and levelled and vegetation removed for residential purposes. The unstable condition of sand dunes resulted in major damage of near-shore properties in the 1940's and 50's storms (Tucker *et al.*, 2005).

Most of Adelaide's current metropolitan shoreline is exposed to slow littoral drift and a net northerly movement of sand, driven by wave action. These low to medium energy waves are generated by south westerly winds that blow over Gulf St Vincent and in summer months are dominantly controlled by the arrival of sea breezes. These sea breezes are composed of westerly winds from Gulf St Vincent, called the gulf breeze and southerly sea breezes from over the Southern Ocean (Physick and Byron-Scott, 1977).

A study of Australian coastal zones by Voice *et al.* (2006), stresses the vulnerability of sandy beaches to the change of wave climate and rise in mean sea level. There have been a number of studies on the change of sea level on Australian beaches (Belperio, 1993; Watson, 2005; Church *et al.*, 2006; Australian Bureau of Meteorology, 2010) suggesting an increase rate of 2.2 mm per year for inner Port Adelaide. On the other hand, wave climate is dominantly controlled by the sea breeze system. The following section describes the sea breeze climate and the local and global factors that contribute to the possible changes in its climate.

2.2. Sea breeze Circulation System

The phenomenon of the coastal sea breeze has been noted from the earliest times. Aristotle, for example, planned the city of Alexandria in such a way that the alignment of the main streets was designed to make use of the cooling effect of the sea breeze, while still providing shelter from other less favourable winds (Watson, 2005). Later the term "sea-breeze" was mentioned in a book written in 1697 by Dampier which was first published by Argonaut Press in London (Dampier, 1927), however the theory of sea breezes has been extensively studied only since 1955, with the work by Clarke (1955)on sea breeze observations (Abbs and Physick, 1992).

As a result of different thermal properties of the land and the sea, the land surface temperature increases more rapidly in the morning than the adjacent water temperature, producing a steeper thermal gradient over the land than over the sea in the lower levels of the atmosphere. This drives a cooling breeze known as a sea breeze which blows from the sea toward the land (Simpson, 1994). The sea breeze passing across the sea carries significant humidity and as it penetrates over the land it increases the relative humidity there. Onset of the sea breeze is followed by a drop in the surface temperature of the land (Sumner, 1977; Kala *et al.*, 2010). In the presence of a light gradient wind, the sea breeze forms as a circulating flow with an offshore component, known as a return flow, in the upper levels of the atmosphere. The sea breeze depths can extend to a height of 1000 m (approximately 900 hPa) above mean sea level on the South Australian coast (Stone, 1969; Finkele *et al.*, 1995). Without the effect of gradient wind the horizontal expansion of sea breeze cells over the water is believed to be greater than those over the land as a result of smaller surface friction over water. The inland penetration of the sea breeze in mid latitudes can reach to maximum of 50 km, while in tropical and subtropical zones it has been observed to extend to 150 km (Abbs and Physick, 1992).

Based on the driving processes, sea breezes can be characterized by an intensified wind from the offshore direction in the afternoon. During the night time, due to the greater cooling rate of the land, a reverse wind can blow from the land towards the sea: a land-

breeze. The dynamics of the sea breeze circulation are affected by synoptic conditions and the presence of a moderate opposing gradient wind can modify the climatology of a sea breeze, delaying its inland penetration (Frizzola and Fisher, 1963). Bigot and Planchon (2003), for example, argue that a strong confronting synoptic wind with a speed greater than 6 to 8 m s^{-1} can disrupt sea breeze generation.

Sea breezes have been observed to influence precipitation (Baker *et al.*, 2001), air pollution (Grossi *et al.*, 2000) and coastal processes (Masselink and Pattiaratchi, 1998; Masselink and Pattiaratchi, 2001). In fact, it has been suggested that there can be a significant impact from the sea breeze on locally generated waves as it can change the general sedimentation pattern (Psuty, 2005). As a demonstration of the importance of the sea breeze in some coastal locations, Hendrickson and MacMahan (2009) found that the presence of a sea breeze could increase the height of the waves by up to 25% in Monterey Bay, California.

2.3. Geophysical variable that affect sea breezes

There are a number of environmental parameters that affect the formation and characteristics of sea breezes; these parameters were summarized in work by Crosman and Horel (2010). These parameters are as shown in Figure 2.1.

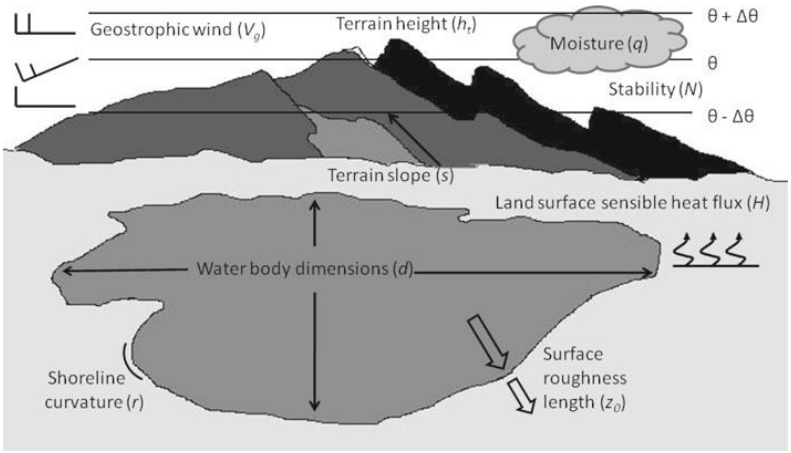

Figure 2.1. Geophysical variable that control sea and lake breezes (Coriolis parameter *f* not shown) adapted from Crosman and Horel (2010).

The key parameters are:

- Ambient geostrophic wind: Geostrophic wind affects the sea breeze development and propagation. While a strong offshore geostrophic wind prevents sea breeze formation, a moderate one slows the penetration of sea breeze (Finkele *et al.*, 1995; Finkele, 1998). In the study by Finkele (1998), for the Coorong region in South Australia, an offshore geostrophic wind of 7.5 m s^{-1} prevented any inland penetration of the sea breeze.

- Atmospheric stability: Based on Monin–Obukhov similarity theory (Monin and Obukhov, 1954), the wind velocity at the height of z is influenced by the stability of the atmosphere at this level. This factor and the roughness length of the surface were included to correct the wind speed profile equation as below (Barthelmie, 1999):

$$U = \frac{u_*}{\kappa}\left[ln\left(\frac{z}{z_0}\right) - \Psi\left(\frac{z}{L}\right)\right] \quad (2.1)$$

where Ψ is the stability correction to wind speed, κ is the von Karman constant, L is Monin–Obukhov length and u_* is the friction velocity.

- Atmospheric moisture: The cloudiness of the sky as a result of atmospheric moisture will obstruct the incoming solar radiation, leading to a relatively cooler surface that reduces the temperature difference between the land and water.

- Water body dimensions: The width and the depth of the water body are the two main factors that determine the temperature of the water surface. It is mentioned by Physick (1976) that for larger bodies of water (lakes in his cases) the pressure gradient of attributed temperature difference is greater and results in comparatively greater propagation rate.

- Terrain morphology (height and slope): The presence of hilly terrain can stop further inland penetration of the sea breeze (Abbs and Physick, 1992). It has also been found that the interaction of mountain and sea breeze circulations modifies, and in some cases intensifies, the near-surface circulations (Mahrer and Pielke, 1977).

- Coriolis parameter: The presence of Coriolis force deflects the direction of wind away from the direction of pressure gradient force. The effect of Coriolis force is opposite in the northern and southern hemispheres. Masselink and Pattiaratchi (2001) have noted that the Coriolis force does not affect the sea breeze at the start , however the afternoon anti-clockwise shift of the wind is slightly associated with the presence of the Coriolis force.

- Surface aerodynamic roughness length (z_o): The friction force, as a product of surface roughness, determines the speed of near surface wind (Equation 2.1); therefore for the areas with greater roughness length, the sea breeze speed is relatively less than that over bare land covers.

- Shoreline curvature: This factor determines the convergence or divergence of the sea breeze, which in some cities has been observed to generate a strong updraft, helping to clear the air pollution, while in some other cities, it produces a smog front (Abbs and Physick, 1992).

- The land surface sensible heat flux: Different properties and energy balances of the surface cause a different heating rate of the surface which leads to a pressure gradient force that operates from sea to land, which establishes the land sea temperature difference. Urbanization and land cover alteration are the main factors that are responsible for the change of land surface heat flux. As the city of Adelaide was built adjacent to a coastline, the development of the metropolis predominantly modifies the surface energy balance.

2.4. Surface energy budget

The importance of surface morphology and the thermal properties of land cover have been noticed in most urban climate research (Sailor, 1995; Kusaka and Kimura, 2000; Gero and Pitman, 2006; Lin *et al.*, 2008; Chen *et al.*, 2011). These parameters impact urban climate in different ways: change in surface energy balance due to alteration of the thermal properties of city buildings, reduction in leaf area index, change in albedo, and a change in long wave radiation emitted from the earth.

The surface radiation budget is written as Equation 2.2 (Oke, 1988) in which Q^* is net radiation, Q_H is turbulent sensible heat flux, Q_E is turbulent latent heat flux and Q_S is net heat storage flux.

$$Q^* + Q_F = Q_H + Q_E + Q_S \qquad (2.2)$$

The Q_F parameter is describing any additional source of energy that is attributed to the nature of urban areas such as the energy perturbation of urban areas. Although urbanization is mainly responsible for a change of Q_F, it should be noted that any change in the nature of the land modifies the surface evaporation and soil moisture and increases the heat storage capacity of the area. These facts lead to the formation of a relatively warmer near-surface atmospheric layer that is referred to as the urban heat island effect. Apart from temperature, the obstacle forms of buildings strongly influence the near

surface atmospheric layer known as roughness sublayer, especially at the city boundaries. It changes both the mean wind field and the turbulent field and the effects of the latter can extend to over several kilometres downstream and tens of metres upwards (Mestayer *et al.*, 2003).

2.5. Urban Boundary Layers

The urban boundary layer (Figure 2.2), as part of the planetary boundary layer, consists of four layers: the urban canopy layer, roughness layer, inertial sub-layer and mixed layer (Oke, 1988; Rotach, 1993; Rotach *et al.*, 2005). It is identified as a layer above the city surface with a height several times larger than the average building height. Its character is affected by the nature of the city (roughness and surface temperature). As Uno and Ueda (1988) observed in his study of the city of Sapporo in Japan, the urban boundary layer can reach a height of 59 m. The city of Sapporo has a population of 1.6 million and an average building height of 25 m and the 30-40% of the city is covered by buildings.

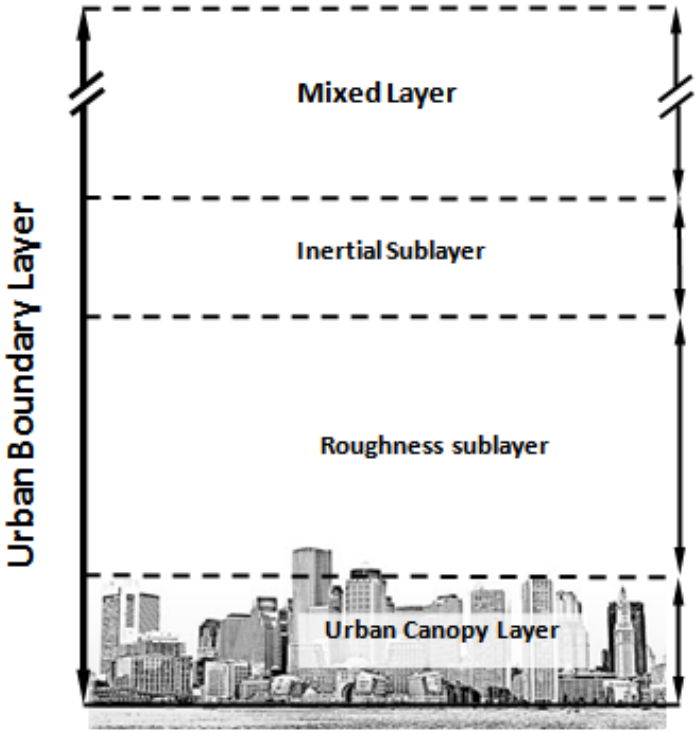

Figure 2.2. The urban layer stratifications (after Oke, 1988)

The urban canopy layer ranges from the ground to average height of buildings and includes the space between buildings and below the roof tops in which the climate is dominated by the surface thermal and aerodynamic nature of urban land cover (albedo, orientation, thermal property, etc.). The release of stored heat from the building surface of the urban canopy layer is slower than the rural environment and it increases the temperature difference between them, and reaches its maximum several hours after sunset (Johnson *et al.*, 1991). Urban surface morphology studies emphasize the importance of the urban canopy layer in the development of urban heat island rather than the anthropogenic heat emission (Uno and Ueda, 1988; Arnfield, 2003; Zhang *et al.*, 2008).

The roughness sub-layer with height of up to 5 times of the height of surface roughness elements (buildings and trees) is affected by the extended urban turbulent flow (Nelson

et al., 2007). In this layer, the turbulent flux of momentum, energy, moisture and pollution are height dependent.

The inertial sub-layer, with a height of 10% of the height of urban boundary layer and located above the roughness layer, is where turbulent vertical fluxes are roughly constant, and the flow field is horizontally homogeneous hence under ideal circumstances (e.g. stationary conditions). The Monin–Obukhov (MO) similarity theory (Monin and Obukhov, 1954) is applied in this layer (Rotach *et al.*, 2005; Nelson *et al.*, 2007; Castillo *et al.*, 2011).

The convective mixed layer, known as the urban outer layer and capped by an inversion layer, is where the convective mixing occurs on a large-scale and its components and stability are driven by buoyancy forces (Castillo *et al.*, 2011).

At the inversion layer, at the top of the urban boundary layer, the vertical potential temperature gradient changes from negative to positive, unlike the layer beneath which makes it more distinguishable from the urban boundary layer and this inversion traps aerosols emitted from the earth's surface. At the top of the inversion layer, the atmospheric potential temperature lapse rate turns positive, and makes the atmosphere above a homogeneous stable layer (Uno and Ueda, 1988).

The structure of urban boundary layer is mainly controlled by urban morphology and radiation fluxes.

2.6. Thermal Properties and the Urban Street Canyon Effect

Changes to the thermal properties of the surface due to land cover modification from vegetation to artificial increases the absorption of short wave radiation during the day and therefore alters the re-emission of the long wave radiation during the night and creates what is referred to as a nocturnal urban heat island. Furthermore, a reduction in the evaporation rate due to faster water canalization and changes in the surface pavement

specifications modify the energy balance between latent and sensible heat and lower transpiration as a result of low vegetation cover. Canyon geometry has a multiple effect on the energy budget of the city by reducing the long wave radiation within city streets and reflecting the short wave radiation between the canyon surfaces. The sheltering nature of the canyon alters the turbulent transfer of heat inside the city canopy layer. Anthropogenic climate modification, due to heat and pollution intensification, releases heat to the atmosphere and changes the city energy balance (Johnson *et al.*, 1991). Through a sensitivity test over the city of Taipei, it has been noticed that an increase of 100 W m^{-2} in the simulation can increase the surface temperature of the surface by nearly 0.31 ^{0}C (Lin *et al.*, 2008).

2.7. Urban Heat Island

As cities develop, the land surface is modified from natural/semi-natural vegetation to buildings and roads. This modification has been observed to change the temperature of the air in the lower surface layer where higher temperatures have been recorded for the cities compared to surrounding rural/non-urbanized areas (Figure 2.3). This is known as an urban heat island. The main causative factors of heat island formation can be summarized as (Oke *et al.*, 1991):

1. Change of the surface substance: due to modification of land cover material the albedo, emissivity and heat capacity of materials alters, leading to greater sensible heat. On the other hand lower vegetative cover and the presence of surface water drainage systems in the urban environment reduce the evaporation from the surface and decrease the latent heat.

2. Increase in anthropogenic heat and pollution: this factor impacts the incoming long-wave radiation receipt and warms up the urban environments.

3. Canyon effect of urban buildings: the presence of sheltering features of urban buildings modifies the heat transmission and short wave and long wave radiation through the streets.

As the heat storage of materials that make up the surface of urban areas are greater than those of natural materials, and due to difference in net long wave radiation emission and thermal admittance between urban and rural environment at night time, urban areas are exposed to slower nocturnal cooling compared to the neighbouring rural area and consequently stay warm for some hours after sunset. This fact is known as a nocturnal urban heat island (Oke, 1981).

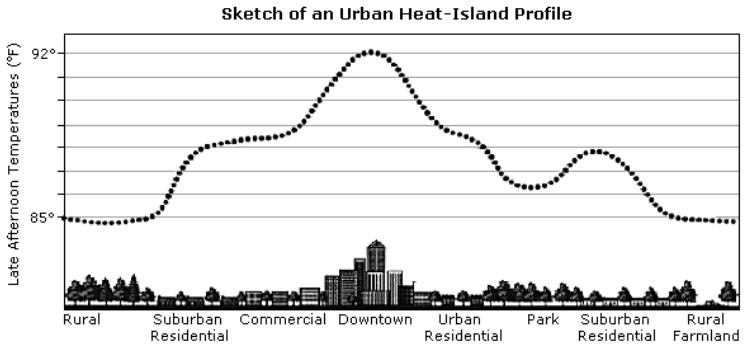

Figure 2.3. The Thermal Differential of City and its adjacent areas (Goodman, 1999)

However, as a result of shading effects of buildings in some cities surrounded by large urban parks the temperature has been observed to be comparatively lower than the neighbouring green areas during the daytime as a result of the shading effects of the buildings and this has been named as an urban cool island (Freitas *et al.*, 2007; Shigeta *et al.*, 2009).

For the city of Adelaide, observations by Erell and Williamson (2007) over four months revealed a temperature difference of up to 9 ^{o}C between a city park ring and the central business district (CBD), which happened mainly before sunrise. However, their observation of 9 day temperature of Adelaide CBD canyon in May 2000 (Erell and

Williamson, 2006) indicated that on a sunny day, the temperature of near surface canyon of the CBD can be cooler than neighbouring suburbs up to 5°C.

2.7.1. Heat Island Types and Circulation

Based on the Voogt and Oke (2003) classification, there are three special types of urban heat island known as surface heat island, canopy layer heat island and boundary layer heat island.

1. Surface Heat Islands, which can be typically depicted by thermal infrared image of cities, refers to the highest temperature of urban surface such as buildings and roads.

2. The canopy layer heat island produced by streets micro-climate processes, in which the air temperature over the canopy layer is higher in urban areas compared to the natural surroundings.

3. The boundary layer heat island, that is based at about roof level and in which the urban boundary layer can extend upwards, and in some cases can reach the height of 1 km.

The presence of a boundary layer heat island increases the depth or thickness of the urban boundary layer and creates an isolated atmospheric island over the city, known as urban plume, that leads to an internal thermal advection and consequently forms a wind circulation over the city (Oke, 1987; Eliasson and Holmer, 1990). Figure 2.4 shows the circulation over an urban area in calm weather conditions, with the crest of the profile approximately over the centre of the city. With a rise in the temperature differential between the city and its rural surrounding, the circulation intensity increases. Generally, the primary factors contributing to the intensity of heat island circulation are the size of the urban area, the temperature gradient between the city and surrounding area, and the basic stratification of the atmosphere (Yoshikado, 1992). The urban heat island

circulation has been observed to start after sunset when the cooling process of the city is slower than that in the natural neighbouring areas (Eliasson and Holmer, 1990; Haeger-Eugensson and Holmer, 1999).

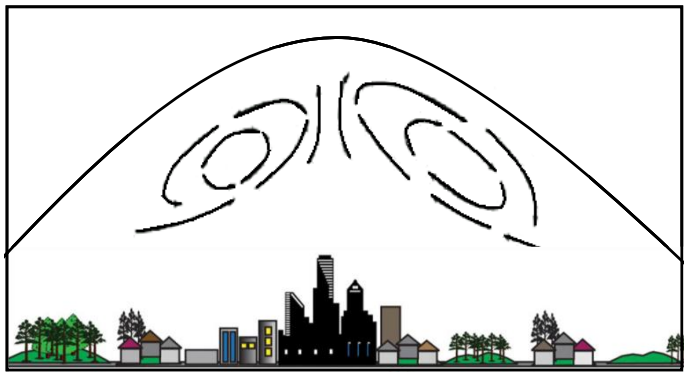

Figure 2.4. A schematic diagram of urban plum and the heat island circulation

Although a light gradient of regional wind increases the vertical component of heat island circulation higher speed winds reduce the vertical component of urban heat island more abruptly than the horizontal component and lead to a decline of the circulation intensity. As the speed of local winds grow the boundary layer dome skews (becomes quite asymmetrical) along with the leeward shifts of the peak point and the height of heat island circulation decreases (Yoshikado, 1992; Freitas *et al.*, 2007).

2.7.2. Urban heat island impact

Urban-modified climate of the city and formation of heat island circulation have a range of effects due to the increase of the air temperature and can cause damage to human health (Rosenzweig *et al.*, 2005; Zhang *et al.*, 2008). For instance urban heat island effects increase the number of heat wave cases and consequently has shown a higher potential for heat related mortality (Patz *et al.*, 2005). The chemical processing of emitted pollutants is also affected due to rise in the temperature (Makar *et al.*, 2006). Moreover, the stagnation of concentrated pollution over cities as a consequence of heat island circulation increases the smoke exposure impact on people (Dong and Dong, 2012).

2.7.3. Characteristics of Urban Heat Island in Different Cities Worldwide

There have been large number of urban heat island intensity studies in both northern hemisphere countries such as the United States, South Korea, Mexico and Greece (Jauregui, 1997; Kim and Baik, 2002; Cynthia *et al.*, 2005; Han, 2008)and southern hemisphere countries such as Australia and Brazil (Morris and Simmonds, 2000; Freitas *et al*., 2007). Based on a city's climate, size, population, distance from the sea and morphology, there can be a vast diversity in urban heat island characteristics as they differ in precipitation, anthropogenic modification intensity, urban ventilation, their thermal inertia and leaf area index. For instance, urban heat island intensity is larger in the dry season nights and this will vary with climate type. In Seoul, it is larger in autumn and winter (Kim and Baik, 2002)while in Mexico City it is larger during summer nights (Jauregui, 1997).

There are a number of studies in which the presence of an urban cooling island have been recognized during the day and this has been related to urban canopy structure known as sky view factor In this case, building shadows decrease the direct solar radiation incident on the area and keep the city centre cooler than lower density suburban areas. An example of such phenomena is illustrated in Figure 2.5 from the study of urban cool island in Okayama city in Japan by (Yoshinori *et al.*, 2009).

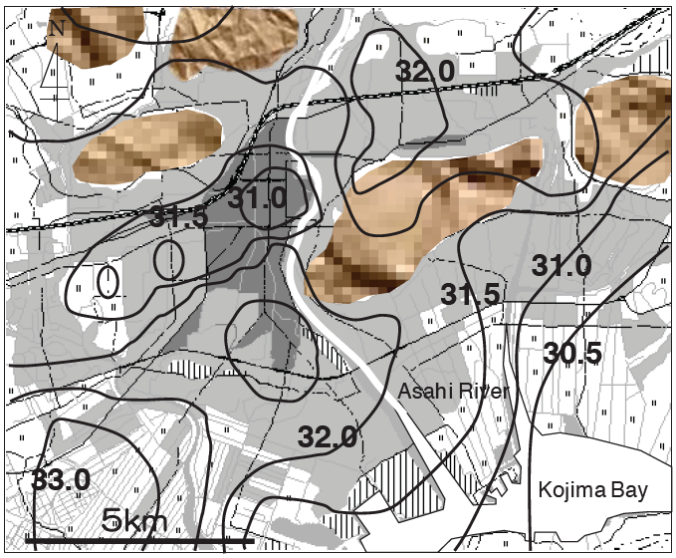

Figure 2.5. Temperature distribution in daytime of 13 of August 2009, Okayama city in Japan - dark grey and brown shading represents commercial areas and mountain respectively (Shigeta *et al.*, 2009)

For Australian cities, in the 1970s different research efforts have been conducted on urban heat island observation that indicate the presence of a strong urban rural temperature difference of 6.8 °C over the city of Melbourne. For the city of Adelaide, with a population of 870,000 people in 1974, the city's air temperature was observed to be 4.4 °C higher than the surrounding rural area (Torok *et al.*, 2001). In the most recent study of Adelaide canyon temperature that has been taken place over the period of 5 months , the urban heat island intensity, measured as the difference between the temperature of the CBD and surrounding suburbs, has been observed to reach to up to 9 °C after sunset, while the daily urban cool island (due to presence of urban canyon effect) can be as high as 5 °C (Erell and Williamson, 2006; Erell and Williamson, 2007).

For the city of Melbourne, it has been observed that for 75% of the days in the period of 1973-1999, the city was hotter than its surroundings (Morris and Simmonds, 2000).

2.7.4. Interaction of Urban Heat Island and Sea breeze

For cities located in the neighbourhood of the coast, the urban heat island circulation, attributed to the presence of the city, interacts with the sea breeze circulation (Yoshikado, 1994; Ohashi and Kida, 2002; Cenedese and Monti, 2003; Freitas *et al.*, 2007). A numerical study by Ohashi and Kida (2002) suggests that the interaction normally happens in the morning and intensifies the sea breeze circulation and with the inland penetration of sea breeze acting similarly to regional wind, shifts the centre of heat island circulation toward the inland suburban areas. However a numerical study by Dandou *et al.* (2009) emphasizes on overall decrease of surface wind intensity as a result of building frictional effects. The significance of the interaction is governed by the combination of the the size of city, its distance from the coast and the intensity of urban heat island (Yoshikado, 1994; Cenedese and Monti, 2003; Freitas *et al.*, 2007).

In small cities located along the shore (i.e. zero distance from the shore), the urban heat island circulation does not develop to the mature stage before the arrival of the sea breeze. As the size of the city grows and is shifted inland, the interaction between the sea breeze and urban heat circulation modify the onset, penetration and intensity of sea breeze. For a larger city a sufficient distance from the sea, the existence of rural-urban circulation over the inland side of the city (opposed to the sea breeze circulation) increases the sea breeze front intensity as it penetrates to the city and modifies the convergence flow pattern over the city (Yoshikado, 1992; Yoshikado, 1994; Cenedese and Monti, 2003; Freitas *et al.*, 2007). On the other hand, the presence of cities prevents further inland penetration of the sea breeze. This, in addition to the change of surface roughness, is a result of sea breeze and heat island circulation (Freitas *et al.*, 2007).

The stagnant region of the suburban area on the inland side of a coastal city and the presence of heat island circulation leads to a delay in the inland penetration of the sea breeze which, as a consequence, has a significant effect on the development of the daytime heat island. An expansion of the urban width increases the height of the thermal internal boundary layer and the vertical and horizontal velocity of circulation. The same

result is expected with an anthropogenic heat enhancement (Sarkar *et al.*, 1998; Cenedese and Monti, 2003).

A laboratory experiment by Cenedese and Monti (2003), reveals the effect of sea breeze on sea breeze circulation to be similar to the impact of a regional onshore flow as it moves the centre of heat island plumes, where the urban heat island intensity controls the magnitude of the shift. Figure 2.6, taken from their work, illustrate the deformation of heat island circulation in the presence of a sea breeze. This fact has also been concluded in a numerical study of the interaction of sea breeze and urban heat island by Yoshikado (1992).

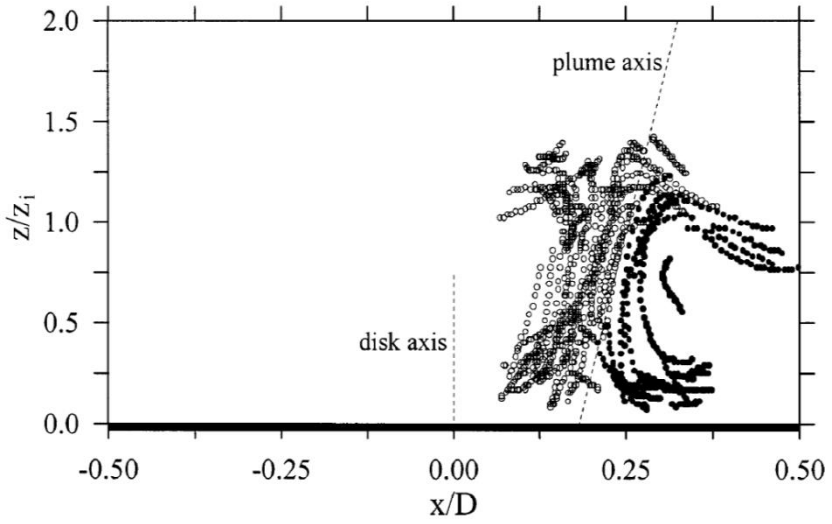

Figure 2.6. An example of the longest trajectories that originated upwind (open circles) and downwind (full circles) of the plume axis in the presence of a sea breeze, taken from a study by Cenedese and Monti (2003), x/D = 0 represents the centre of the urban area.

Although there has been much research on the interaction of urban heat island and sea breeze circulation (Yoshikado, 1992; Yoshikado, 1994; Kambezidis *et al.*, 1995; Sarkar *et al.*, 1998; Kusaka and Kimura, 2000; Marshall *et al.*, 2004; Childs and Raman, 2005; Freitas *et al.*, 2007; Chen *et al.*, 2011), the contribution of long-term modification to the characteristics of the sea breeze has not yet been covered in any study. Therefore, as one of the objectives of the current study, there was a substantial need to develop an

algorithm to identify sea breeze cases for as long a time period as possible for which the appropriate meteorological observations were available.

2.8. Sea Breeze Detection Methods

Identification of sea breeze days has been an objective of many previous studies (Stone, 1969; Borne *et al.*, 1998; Furberg *et al.*, 2002; Bigot and Planchon, 2003; Dunsmuir *et al.*, 2003), wherein most of them the characteristics of a sea breeze day have been studied. It is evident from these studies that the availability of meteorological data, topography and climate of the study area determine the accuracy of the selection method (Azorin-Molina *et al.*, 2011).

In most of the sea breeze day selection methods, the surface wind characteristics have been taken into account since the presence of an intense offshore wind prevents the formation of a sea breeze. Therefore the diurnal reversal of wind direction from offshore to onshore was used as an identifier for a sea breeze day in research carried out by different researchers (Stone, 1969; Steyn and Faulkner, 1986; Pattiaratchi *et al.*, 1997; Borne *et al.*, 1998; Tijm *et al.*, 1999; Masselink and Pattiaratchi, 2001; Furberg *et al.*, 2002; Miller and Keim, 2003; Azorin-Molina and Martin-Vide 2007; Azorin-Molina and Chen, 2009). A rapid change in the intensity of wind was considered in some cases: Masselink and Pattiaratchi (2001) Azorin-Molina and Martin-Vide (2007) and Azorin-Molina *et al*. (2011).

An abrupt drop in the surface temperature of the land along with a sudden increase in the humidity can also be a feature of the onset of a sea breeze. Where records of autographic instruments such as hygrographs and thermographs are available, the formation of a sea breeze is, therefore, observable. This indicator was introduced in studies by Stone (1969), Sumner (1977), Physick and Byron-Scott (1977), Abbs (1986) and Azorin-Molina *et al*. (2011).

In the study by Borne *et al*. (1998), a steady-state condition of the 700 hPa wind was included in the sea breeze day criteria, as the climate at this level was considered to be unaffected by the sea breeze circulation, whereas Dunsmuir *et al.* (2003) included the change of the 900 hPa wind as an indicator for sea breeze occurrence, since the sea breeze return flow has been observed to extend to this level.

A day with a sky conditions known as broken sky (cloud cover of 5 to seven oktas) or overcast (8 oktas) is assumed to reduce the possibility of sea breeze occurrence as it slows down the heating process of the land. This factor, and the presence of a temperature gradient over the land and sea, was employed in studies by Furberg *et al*. (2002), Borne *et al*.(1998), Miller and Keim (2003) and Steyn (2003).

In practice, researchers will use a combination of several of these identifiers. For example, Borne *et al.* (1998) used a set of six filters to determine a sea breeze day considering the change in the characteristics of the upper air level and surface level wind. They attempted to evaluate the accuracy of the method, by comparing the days they identified as sea breeze days with those of an independent researcher. Although the activities associated with the start of a sea breeze were neglected in their method, the comparison showed an agreement of greater than 75%. In fact, the difference between the number of sea breeze cases, are mainly attributed to the selection algorithm (Azorin-Molina *et al.*, 2011) and cannot be referred to strictly as the accuracy of the method. Furberg *et al.* (2002), following the work of Steyn and Faulkner (1986), selected sea breeze days as those with a higher temperature over the land as the main factor, together with a dominant offshore wind during the night and early morning and an onshore wind during the daytime. Azorin-Molina *et al.* (2011) introduced two selection algorithms, where each was based on different aspects of sea breeze climatology. Their manual technique considered the shift in the wind direction as well as changes in temperature and relative humidity for a sea breeze occurrence, while their computer-based method examined different features of sea breeze processes in a day. Their methods were evaluated using the results of independent, previous researchers. The manual approach

was compared with the output of a method developed by a researcher from the regional climate group from the University of Goteborg (Sweden), while the computer-based approach was examined against a selection technique developed by Prtenjak and Grisogono (2007).

One of the conclusions reached by Azorin-Molina *et al.* (2011) is that the selection of sea breeze days is strongly related to the criteria employed and yet, for a study where long-term patterns and behaviour are being sought, this is an issue. In terms of verifying a sea breeze detection method, it is not clear that simply comparing one method to another provides much benefit. There is a need, therefore, for a sea breeze detection method that can be verified based on meteorological arguments. This formed one of the aims of the current study.

Simultaneously to the observational method on urban-modified climate of sea breeze, numerical simulations were provided to reproduce the sea breeze climate for different scenarios of adjacent land cover. These models help to investigate different possibilities and also project potential future climate changes. As part of the study, the contributions of urban land cover to the wind characteristic of sea breeze days were simulated and possible consequences were discussed.

2.9. Numerical Simulation of climate

With an increasing awareness of greenhouse impact on change to the climate of different regions, there has been a considerable interest by the scientific community in simulating complex physical systems using numerical models. The history of development of these models was described by Lynch (2008). These models, which are primarily developed as the General Circulation Models (GCM), use mathematical equations to simulate the interactions of the atmosphere, oceans, land surface, and ice on a global scale. The GCMs, also use Atmospheric Circulation Models as a core to provide the circulation of the atmosphere. To be able to simulate the regional climate, a downscaling approach was

used and the general analysis of global models were supplied as initial and boundary conditions for the Regional Climate Models (RCM), which employ the detailed topography and physical parameterization to simulate climate at the mesoscale level, in higher resolution.

The atmospheric models are principally governed by the physical conservations of mass, momentum and energy (Kiehl and Ramanathan, 2006). Different models use different approaches to solve the physical equations and therefore they require different types of data for validation Schneider and Dickinson (1974).

The general form of conservation law in Cartesian coordinates can be written as Equation 2.3.

$$\frac{d\Phi}{dt} + \nabla.(F + \Omega V) - H = 0 \quad (2.3)$$

in which, ∇ is divergence (shown in Equation 2.4 for velocity), Ω is any quantity (such as mass, energy and momentum), therefore ΩV is the transport flux, F is flux of Ω in the absence of fluid transport and H is a source or sink of Ω.

$$\nabla.v = \frac{\partial u}{\partial x} + \frac{\partial v}{\partial y} + \frac{\partial w}{\partial z} \quad (2.4)$$

Deriving the equation for heat of a single phase material, the amount of heat per unit volume is $\rho c_p T$, where c_p is the specific heat (energy per unit mass per degree Kelvin) at constant pressure and T is the temperature. Considering the heat flux in the absence of transport as $F = -k\nabla\mathrm{T}$, where k is the thermal conductivity and the heat transport flux is $\rho c_p T\, V$, the simple equation of conservation of the heat is

$$\frac{d\rho c_p T}{dt} + \nabla.\left(\rho c_p T V\right) = \nabla.k\nabla\mathrm{T} + \mathrm{H} \quad (2.5)$$

in which H is the combination of all sources of heat (ρQ). For a constant $c_p$and k, and using Equation (2.3), this equation can be rewritten as

$$\frac{dT}{dt} + V.\nabla \mathrm{T} = \kappa \nabla^2 \mathrm{T} + \mathrm{H}/\rho c_p \qquad (2.6)$$

where $\kappa = k/\rho c_p$, is the thermal diffusivity.

Equation 2.5 is called the thermodynamic equation and, as mentioned, is in Cartesian coordinates. Expressing the equation of motion in pressure coordinates, where the coordinate of constant geopotential altitude is replaced by the isobaric surface, the scalar equation, considering the Coriolis force as $f = 2\Omega sin\phi$, will be

$$\left(\frac{d}{dt}\right)_p = \frac{\partial}{\partial t} + \frac{v}{a\cos\phi}\left(\frac{\partial}{\partial \lambda}\right)_p + \frac{v}{a}\left(\frac{\partial}{\partial \phi}\right) + \omega\frac{\partial}{\partial p} \qquad (2.7)$$

in which p is pressure, ω is vertical velocity in term of rate of change of pressure (i.e. $\frac{dp}{dt}$.) and λ,ϕ represent longitude and latitude, respectively.

Considering the flux form of the thermodynamic equation for atmosphere, the predictive equation for temperature can be written as Equation 2.8 (Kiehl and Ramanathan, 2006) in which Q_{rad} is net radiative heating, V is horizontal vector velocity, Q_{con} is net condensational heating, D_H is diffusive and boundary layer heating.

$$c_p \frac{\partial T}{\partial t} = -c_p V.\nabla T + c_p \omega\left(\frac{\kappa T}{p} - \frac{\partial T}{\partial p}\right) + \tilde{Q}_{rad} + \tilde{Q}_{con} \qquad (2.8)$$

Similarly conservation of mass leads to the continuity of atmospheric circulation as in Equation 2.9 (Kiehl and Ramanathan, 2006)

$$\frac{\partial \omega}{\partial p} = -\nabla.V \qquad (2.\ 9)$$

The conservation of momentum, is obtained from Newton's second law of motion and in the form of atmospheric circulation is written in Equation 2.10.

$$\frac{\partial v}{\partial t} = -\mathrm{v}.\nabla \mathrm{v} - \omega \frac{\partial V}{\partial p} + fk \times \mathrm{v} - \nabla\Phi + D_M \tag{2.10}$$

where k, is the unit vector in the vertical direction, Φ is the geopotential (Equation 2.11) and $\mathrm{D_M} = \left(\mathrm{D_\lambda}, \mathrm{D_\phi}\right)$ is the turbulent transfer of momentum.

$$\frac{\partial \Phi}{\partial p} = -\frac{RT}{p} \tag{2.11}$$

where, R is the gas constant. Equations 2.8, 2.9 and 2.10, along with equation of state 2.12, and continuity equation for moist air 2.13, are the atmospheric primitive equations (Trenberth, 1992).

$$p = \frac{RT}{v} \tag{2.12}$$

$$\frac{\partial q}{\partial t} = -\mathrm{v}.\nabla \mathrm{q} - \omega \frac{\partial q}{\partial p} + E - C - D_q \tag{2.13}$$

Development of climate modelling is facilitated by observational data, either from field or global satellites, or a combination of both, and the models are constantly evaluated against observational records. These models not only have been used to understand the atmospheric climatic system and forecast future possible climate, but have been performed to reproduce the mechanism of climate in past and more importantly to examine different case scenarios.

2.9.1. Regional Climate Models (RCMs)

Regional Climate Models, as described by Pielke and Roger (2013), are mainly affected by surface terrain and topography such as valleys, sea and urban areas and their mesoscale features are forced by geographically- induced circulations.

Similar to GCMs, a mesoscale model numerically solves equations of conservation of mass, energy and momentum, in limited area domains and therefore uses outputs from global climate simulations or analysis to derive their boundary condition information: a process called nesting.

RCMs benefit from downscaling, either dynamical or statistical techniques to provide the ability of nesting for even higher resolution (Feser *et al.*, 2011). The dynamical approaches, known as spectral nudging, utilize low-pass filtering methods to compute the reference climate at higher resolution, while the statistical downscaling applies statistical relationships to compute the inner nesting variable from nesting parents. In order to prevent any deviation arising between the global and the regional models as a result of downscaling, the widely used technique of spectral nudging is applied and was first suggested for use in regional atmosphere modelling by Von Storch *et al.* (2000).

There are two interactive modes of one-way or two-way nesting approaches, of which the latter benefits from feedback of higher resolution information interactively while in the former, the information for the higher resolution is derived from coarser resolution regions (Giorgi and Mearns, 1991).

Figure 2.7 shows a schematic of a nesting in a regional climate model within a global climate model (Rasch, 2012).

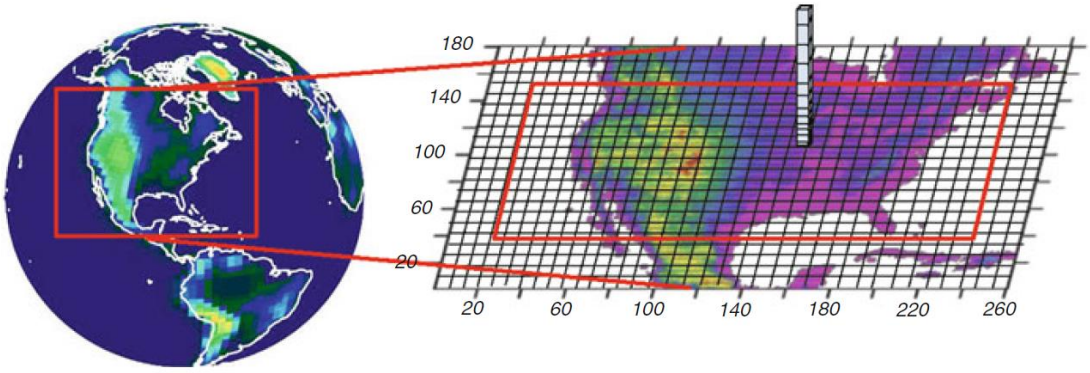

Figure 2.7. an example of Nesting in a regional climate model with the horizontal grid shown in black line, boundary of buffer zone in red line and vertical column indicating the atmospheric layers by the model, from Rasch (2012).

Like GCMs, the regional models are also evaluated primarily using observational data; however intercomparison of models can significantly improve systematic errors and uncertainties.

The history of mesoscale climate modelling and some case studies has been extensively explained by Pielke and Roger (2013).

2.9.2. Application of RCMs

Mesoscale models have helped scientists to understand regional climate processes and have been used in previous studies to test different hypotheses. The contribution of different regional forcings on climate variability was examined using RCMs (Rasch, 2012). Furthermore the Earth's physical geographical features at the mesoscale were simulated by RCMs.

2.9.2.1. Simulation of Sea-land breeze

The circulation of sea and land breezes over flat terrain has been the most studied mesoscale phenomena in both observational and theoretical method (Pielke and Roger, 2013). It has firstly been modelled using a two-dimensional nonlinear numerical model by Estoque (1962) and followed by many since (Moroz, 1967; Physick, 1976; Mahrer

and Pielke, 1977). With an improvement in computing capability, three dimensional simulation of these phenomena was performed following Mcpherson (1970) in work on the effect of coastline irregularity on the sea breeze circulation. The important role of sea breeze in pollution distribution was also studied using three dimensional models (Pielke and Roger, 2013).

2.9.2.2. Simulation of Land cover change and urban Climate

Like sea breeze circulation, the effects of urban circulation on local weather were simulated after the influence of urbanization on climate and consequently on human health were discovered. With an increasing number of pollution-related deaths, meteorological models have been used to simulate the transport and dispersion of pollutants as well as the effect of urban developments on the wind, temperature and moisture.

The effect of heat islands on synoptic scale weather was modelled in a series of recent studies (Mihalakakou *et al.*, 2004; Gero and Pitman, 2006; Freitas *et al.*, 2007; Lo *et al.*, 2007; Han and Jin Baik, 2008; Simpson *et al.*, 2008; Zhang *et al.*, 2008; Cheng and Chan, 2012).

Moreover the role of changes in land surface on climate change of different regions around the world was simulated using numerical models. For Australia, 200 years of change to the surface land use were simulated by Narisma and Pitman (2003), employing a mesoscale model (MM5), suggesting that change of native vegetation cover of the land to non-irrigated and non-harvested grass land reduces the surface evaporation and leads to rainfall reduction as well as increase in mean and maximum temperature. In a different study by Gero and Pitman (2006), the effect of land cover properties on storms in the Sydney basin were modelled and it was found that velocities within storms developing near the southern boundary of the basin, are greater with current agricultural land cover, compare to the native pre-European vegetation.

2.9.3. Weather Research and Forecasting Model (WRF)

The National Center for Atmospheric Research (NCAR) is one of the pioneers in climate modelling, starting in the early 1960s and continuing with state of the art, comprehensive climate models. In the 1990's the collaboration of NCAR, National Center for Environmental Prediction (NCEP) from the National Oceanic and Atmospheric Administration (NOAA), Forecast System Laboratory (FSL), the Air Force Weather Agency (AFWA), the Naval Research Laboratory, the University of Oklahoma and the Federal Aviation Administration (FAA) developed a next-generation mesoscale model, known as Weather Research and Forecasting (WRF) model, to serve both purposes of research and operational forecasting. The equations employed in the model are relatively simple, yet sophisticated enough to include cloud microphysics and land-surface dynamics, to simulate complex atmospheric processes.

The pre-processing system of WRF (WPS), converts the outputs of Global Data Assimilation System (GDAS) to an understandable format to be used as initial and boundary condition for WRF model.

The WRF system is designed with two separate dynamical cores, the Non-hydrostatic Mesoscale Model (NMM) and the Advanced Research WRF (ARW), and offers numerous options to describe physical processes in the atmosphere and for energy and momentum exchanges with the land and sea surfaces. With the broad spectrum application across scales ranging from metres to thousands of kilometres, the modular single-source code of WRF is efficient in massively parallel computing environments (Janjic *et al.*, 2010).

2.9.3.1. The major feature of ARW and the governing equations

The ARW core solves fully compressible Euler non-hydrostatic equations in a terrain following vertical coordinate system to simulate the three dimensional real-data atmospheric system with one-way, two-way or moving nest options. The numerous physics options of the model offer different categories of:

- Microphysics: this option provides atmospheric heat and moisture tendencies such as water vapour, cloud and precipitation processes.

- Cumulus parameterization: the effects of shallow clouds and sub-grid-scale convection are performed here.

- Planetary boundary layer (PBL) is responsible for unresolved turbulent heat fluxes due to eddy transport within the planetary boundary layer and throughout the atmosphere.

- Surface layer: this scheme is responsible for friction velocity and exchange coefficient that enable the calculation of surface hat and moisture fluxes by the land surface models and surface stress in planetary boundary layer scheme.

- Land surface model: provides heat and moisture flux over land points and sea-ice points, using atmosphere information from the radiation scheme, radiative forcing from radiation scheme and precipitation forcing from microphysics and cumulus scheme.

- Atmospheric radiation: atmospheric heating due to the absorption, emission, reflection and scattering of shortwave and long wave radiation from the Sun and the ground and within the atmosphere are provided with these schemes.

Four types of lateral boundary condition are possible within the model known as: symmetric, open, specified and periodic. The bottom boundary condition sets the normal velocity to zero while the top boundary enforces the Cartesian vertical velocity to be zero.

The interaction between the model's physical parameterizations is shown in Figure 2.8. PBL represent planetary boundary layer scheme, SW and LW are shortwave and long wave radiation, SH and LH are sensible and latent heat, and Qv is mixing ratio for water vapour.

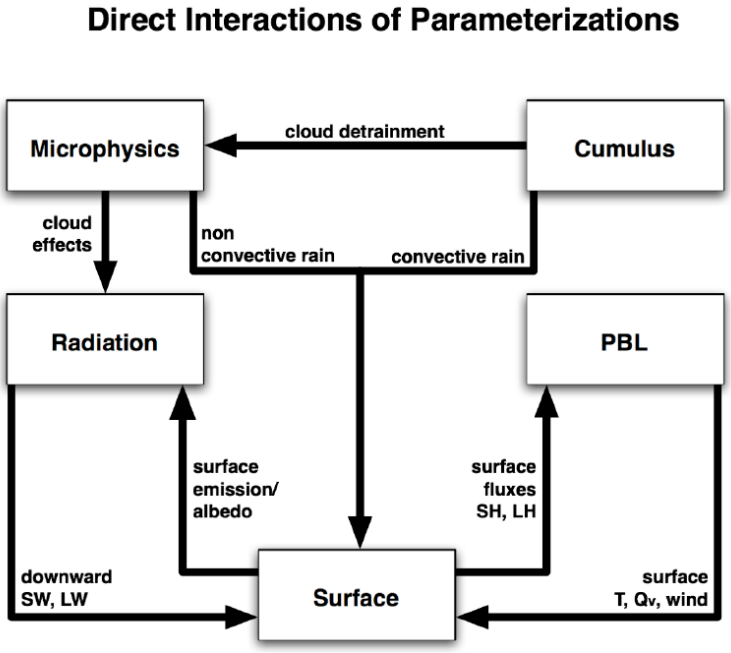

Figure 2.8. The interactions between the five major physical parameterizations used in the WRF-ARW (Dudhia, 2010)

Similar to Equation 2.7, the total derivation operator in any coordinate system can be written as

$$\left(\frac{d}{dt}\right)_p = \frac{\partial}{\partial t} + \vec{v}.\nabla_\pi + \dot{\pi}\frac{\partial}{\partial \pi} \tag{2.16}$$

where π represents the choice of coordinate system, $\dot{\pi} = \frac{D\pi}{Dt}$ and $\vec{v} = (v, v)$ is the two-dimensional Cartesian wind vector.

The ARW equations use the terrain-following hydrostatic-pressure vertical coordinate denoted by η and defined as

$$\eta = \frac{p_h - p_{ht}}{p_{hs} - p_{ht}} = \frac{p_h - p_{ht}}{\mu} \tag{2.14}$$

in which p_h is the hydrostatic component of pressure (at top is p_{ht} and surface is p_{hs}); and η decreases monotonically from 1 at the surface to 0 at the upper boundary layer of model domain.

The flux form variables in the model are:

$$\vec{V} = \mu_d \vec{v} = (\mu_d u, \mu_d v, \mu_d w) = (U,V,W) \tag{2.15}$$

$$\Theta = \mu_d \theta \tag{2.16}$$

$$\Omega = \mu_d \dot{\eta} \tag{2.17}$$

where μ_d represents the mass of dry air in the column.

Derived from first principles, the continuity equation and the Navier Stokes equations, the moist Euler equations for x,y,z momentums in the model are written as (Skamarock *et al.*, 2007).:

$$\text{x-momentum: } \frac{\partial U}{\partial t} + \frac{\partial (Uu)}{\partial x} + \frac{\partial (Vu)}{\partial y} + \frac{\partial (\Omega u)}{\partial \eta} + \mu_d \alpha \frac{\partial P}{\partial x} + \frac{\alpha}{\alpha_d}\frac{\partial P}{\partial \eta}\frac{\partial \varphi}{\partial x} = F_U \tag{2.18}$$

$$\text{y-momentum: } \frac{\partial V}{\partial t} + \frac{\partial (Uv)}{\partial x} + \frac{\partial (Vv)}{\partial y} + \frac{\partial (\Omega u)}{\partial \eta} + \mu_d \alpha \frac{\partial P}{\partial y} + \frac{\alpha}{\alpha_d}\frac{\partial P}{\partial \eta}\frac{\partial \varphi}{\partial y} = F_V \tag{2.19}$$

$$\text{z-momentum: } \frac{\partial W}{\partial t} + \frac{\partial (Uw)}{\partial x} + \frac{\partial (Vw)}{\partial y} + \frac{\partial (\Omega w)}{\partial \eta} + g(\mu_d - \frac{\alpha}{\alpha_d}\frac{\partial P}{\partial \eta}) = F_W \tag{2.20}$$

Also the conservation of heat, mass and water are as shown in Equations 2.21 to 2.23:

Conservation of heat: $\frac{\partial \Theta}{\partial t} + \frac{\partial (\mathrm{U}\theta)}{\partial \mathrm{x}} + \frac{\partial (\mathrm{V}\theta)}{\partial \mathrm{y}} + \frac{\partial (\Omega \mathrm{w})}{\partial \eta} = F_{\Theta}$ (2.21)

Conservation of mass: $\frac{\partial \mu_d}{\partial t} + \frac{\partial \mathrm{U}}{\partial \mathrm{x}} + \frac{\partial \mathrm{V}}{\partial \mathrm{y}} + \frac{\partial \Omega}{\partial \eta} = 0$ (2.22)

Conservation of water: $\frac{\partial \mathrm{Q_m}}{\partial t} + \frac{\partial (\mathrm{U q_m})}{\partial \mathrm{x}} + \frac{\partial (\mathrm{V q_m})}{\partial \mathrm{y}} + \frac{\partial (\Omega \mathrm{q_m})}{\partial \eta} = F_{\mathrm{Q_m}}$ (2.23)

$Q_{\mathrm{m}} = \mu_d \mathrm{q_m}$ with $\mathrm{q_m}$ mixing ratio for water vapour, cloud, rain, ice . a_d is the inverse density of the dry air and a is the inverse density of the full parcel $(1/\rho)$.

The equation for material derivative of the definition of geopotential is written as

$$\frac{\partial \varphi}{\partial t} + \mu_d^{-1}\left(\frac{\partial (\mathrm{U}\varphi)}{\partial \mathrm{x}} + \frac{\partial (\mathrm{V}\varphi)}{\partial \mathrm{y}} + \frac{\partial (\Omega \varphi)}{\partial \eta} - \mathrm{gW}\right) = 0 \quad (2.24)$$

The hydrostatic equation used in the model is:

$$\frac{\partial \varphi}{\partial \eta} = \mu_d a_d \quad (2.25)$$

and the equation of state is:

$$\mathrm{p} = \mathrm{p_0}\left(\frac{R_d \theta_m}{p_0 a_d}\right)^{\gamma} \quad (2.26)$$

where $\gamma = c_{\mathrm{p}}/c_{\mathrm{v}}$=1.4 and $\mathrm{p_0}$=1000 hPa with $\theta_m = \theta\left[1 + (\mathrm{R_v}/\mathrm{R_d})\mathrm{q_v}\right]$ and where $\varphi = \mathrm{gz}$ is the geopotential, Θ is the potential temperature, p is pressure, F is forcing terms for U, V,W, θ (horizontal component of velocity in x, y direction, vertical component of velocity and potential temperature respectively).

The Advection in WRF is simulated using the following equation:

$$\frac{\partial \varphi}{\partial t} = -\frac{\partial (\mathrm{U}\varphi)}{\partial \mathrm{x}} = -\mathrm{U}\frac{\partial \varphi}{\partial \mathrm{x}} \tag{2.27}$$

To include the map projection in the equations, a map scale ratio of earth is defined as $m = \frac{(\Delta \mathrm{x}, \Delta \mathrm{y})}{\text{distance on the earth}}$ which redefines the momentum variable as $\mathrm{U}=\mu_d \mathrm{u}/m$, $\mathrm{V}=\mu_d \mathrm{v}/m$, $\mathrm{W}=\mu_d \mathrm{w}/m$, $\Omega=\mu_d \dot{\eta}/m$.

The right hand side of Equations 2.18, 2.19 and 2.20 contains the Coriolis and curvature terms, which can be written as:

$$F_{U_{cor}} = +\left(f + \mathrm{u}\frac{\partial m}{\partial y} - \mathrm{v}\frac{\partial m}{\partial x}\right)\mathrm{V} - \mathrm{eW}\cos\alpha_r - \frac{\mathrm{uW}}{r_e} \tag{2.28}$$

$$F_{\mathrm{V}_{cor}} = -\left(f + \mathrm{u}\frac{\partial m}{\partial y} - \mathrm{v}\frac{\partial m}{\partial x}\right)\mathrm{U} - \mathrm{eW}\sin\alpha_r - \frac{\mathrm{vW}}{r_e} \tag{2.29}$$

$$F_{W_{cor}} = +e(\mathrm{U}\cos\alpha_r - \mathrm{V}\sin\alpha_r) + \left(\frac{\mathrm{uU}+\mathrm{vV}}{r_e}\right) \tag{2.30}$$

where α_r is local rotation angle between y-axis and the meridians, Ψ is the latitude, $f = 2\Omega_\mathrm{e}\sin\Psi$, $= 2\Omega_\mathrm{e}\cos\Psi$, $\Omega_\mathrm{e}$is the angular rotation rate of the earth and r_e is the radius of the earth.

The meso-scale meteorological model, WRF, has been used in a variety of coastal situations to investigate this interaction between the ocean and adjacent coast. Studies have looked at the ability of the model to reproduce temperature behaviour (Giannaros *et al.*, 2013) and to predict the comfort levels in the city (Giannaros and Melas, 2012). The effect of coastal circulation on pollutant transport has also been a focus of many studies (Challa *et al.*, 2009; Yerramilli *et al.*, 2010; Hernández-Ceballos *et al.*, 2013). Others, not necessarily associated with coastal sites, have looked at modelling the effect of increasing temperatures due to the urban heat island effect and the implications for urban

infrastructure (Lin *et al.*, 2008; Miao *et al.*, 2009; Salamanca *et al.*, 2010; Cheng *et al.*, 2012; Tomlinson *et al.*, 2013).

Performance of WRF models in precipitation forecast of Indian monsoon was compared against other atmospheric models (MM5, RSM, ETA) in a paper by Das *et al.* (2008) . It was shown that the WRF and MM5 models have performed better where the quantity of rainfall was favoured, however the distribution of rainfall was predicted relatively more accurately with RSM and ETA models.

In Australia, the WRF model has been employed for different purposes, from reproducing a storm event in Sydney basin (Gero, 2006) to simulation of drought situations (Meng *et al.*, 2011) and fire weather- the weather condition that increase the risk of large-scale bush fire- (Clarke *et al.*, 2013) in south-east Australia. In addition, the performance of the model's different schemes have been evaluated for different regions of the continent (Evans and Matthew, 2010; Evans *et al.*, 2012; Andrys *et al.*, 2013; Evans and Mccabe, 2013).

The sensitivity of the model's performance to physics parameterization on simulation of rainfall events in South-East Australia has been tested, using 36 multi-physics ensemble (Evans *et al.*, 2012). The physics options of planetary boundary layer, cumulus, micro-physics and radiation schemes were all tested. They concluded that in modelling the precipitation, the cumulus physics scheme plays a decisive role, while mean sea level pressure and wind are more sensitive to both cumulus and planetary boundary layers scheme.

In a different study, WRF-ARW was implemented over the Houston area by Chen *et al.* (2011) to simulate the interaction between an urban heat island and sea breeze circulation. They applied the WRF models, coupled to an Urban Canopy Model (UCM), to simulate the UHI of the Houston metropolitan area. The models evaluation has shown an acceptable performance in capturing the nocturnal heat island intensity and diurnal

wind rotation, however the rate of rural daily temperature range were comparatively underestimated whereas the wind velocity at low level (below 1 km) was overestimated by 2-3 m s^{-1} .

The overall performance of the models for different regions in the world is closely associated with the choice of the model's physical schemes and the studied atmospheric variable and is advised to be evaluated against observations (Chen *et al.*, 2011).

2.10. Summary

The present chapter has reviewed the previous studies of urban heat island and sea breezes in different cities and explained the state of the art numerical modelling that has been used to study development of these phenomena in past, present and future. Apart from relatively old studies of Adelaide sea breezes, less is known about the characteristic of this phenomenon and its climate over the time. On the other hand, the development of the city of Adelaide has been recently observed to affect the near surface temperature. As the metropolitan of Adelaide expansion has been accelerated since 1950, there is a potentiality for the sea breeze system to be affected by these changes. Therefore, the current study aims to investigate the changes to the sea breeze regime associated with human settlement along the coast of the city of Adelaide.

3. Climate of the Study Area

3.1. Description of the Adelaide Metropolitan Area

The city of Adelaide, located in the southern part of the Adelaide plains surrounded by Gulf St Vincent to the west and the Mount Lofty ranges to the east (of which the highest point is 726 metres above mean sea level) has a Mediterranean climate with warm to hot, dry summers and cool to mild winters. Humidity is usually low and oppressive conditions rarely last for longer than one or two days. With the current population of 1.23 million (Australian Bureau of Statistics, 2011), the city is the fifth largest city of Australia. Since 1955 the metropolitan area has shown an extensive increase of over 700,000 in population with relatively minor growth in the central business district. The Adelaide metropolitan coastline is approximately 30 km long from Kingston Park to Outer Harbor and oriented approximately from north-northwest to south-southeast.

3.2. The main feature of climate in Adelaide

The location of the sub-tropical high pressure ridge is mainly responsible for the aridity of most of the continent and determines the climate of Australia. The counter-clockwise wind circulation around anticyclones in the southern hemisphere generates a general westerly flow on the southern part of the sub-tropical ridge which is normally centred between 30° and 35° S in winter and moves to between 35° and 40° S in summer. In southern Australia, the occasional slow-moving anticyclones generate prolonged periods of excessive hot weather known as heat-waves, which normally occur in much of the inland areas; however the coastal regions can also be affected by this extremely hot weather for a few days. A lack of major topographic obstructions in Australia allows the occasional band of moisture and cloud to extend from the northwest to the south of the continent which brings rainfall to southern Australia. In the period from 1977 to 2000, the average daily maximum temperature and rainfall for Adelaide varied from 15.2 °C

and 79.9 mm in July to 29.3 ºC and 12.7 mm in February (Australian Bureau of Statistics, 2012).

3.2.1. Wind climate

The seasonal wind-rose for 9 am and 3 pm for Adelaide airport station from 1995-2004 are shown in figure 3.1.

Although the morning wind of autumn and winter months blows from the north and north-east direction, there is not any dominant direction for the 9 am winds of warmer seasons, however as shown in Figure 3.1, around 40 percent of afternoon wind in autumn and spring and more than half of the afternoon winds in summer has been observed to arrive from a south-westerly direction. The sea breeze flow in these months contributes most of the south-westerly component.

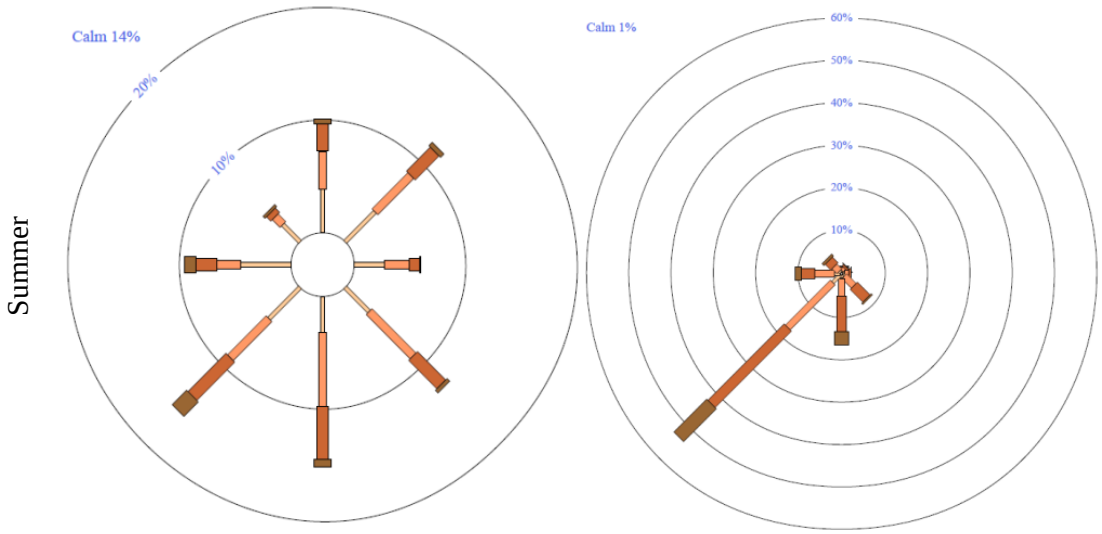

Figure 3.1.a. Seasonal wind rose in Adelaide for summer, 9 am on left and 3 pm on right (Australian Burea of Meteorology, 2014a)

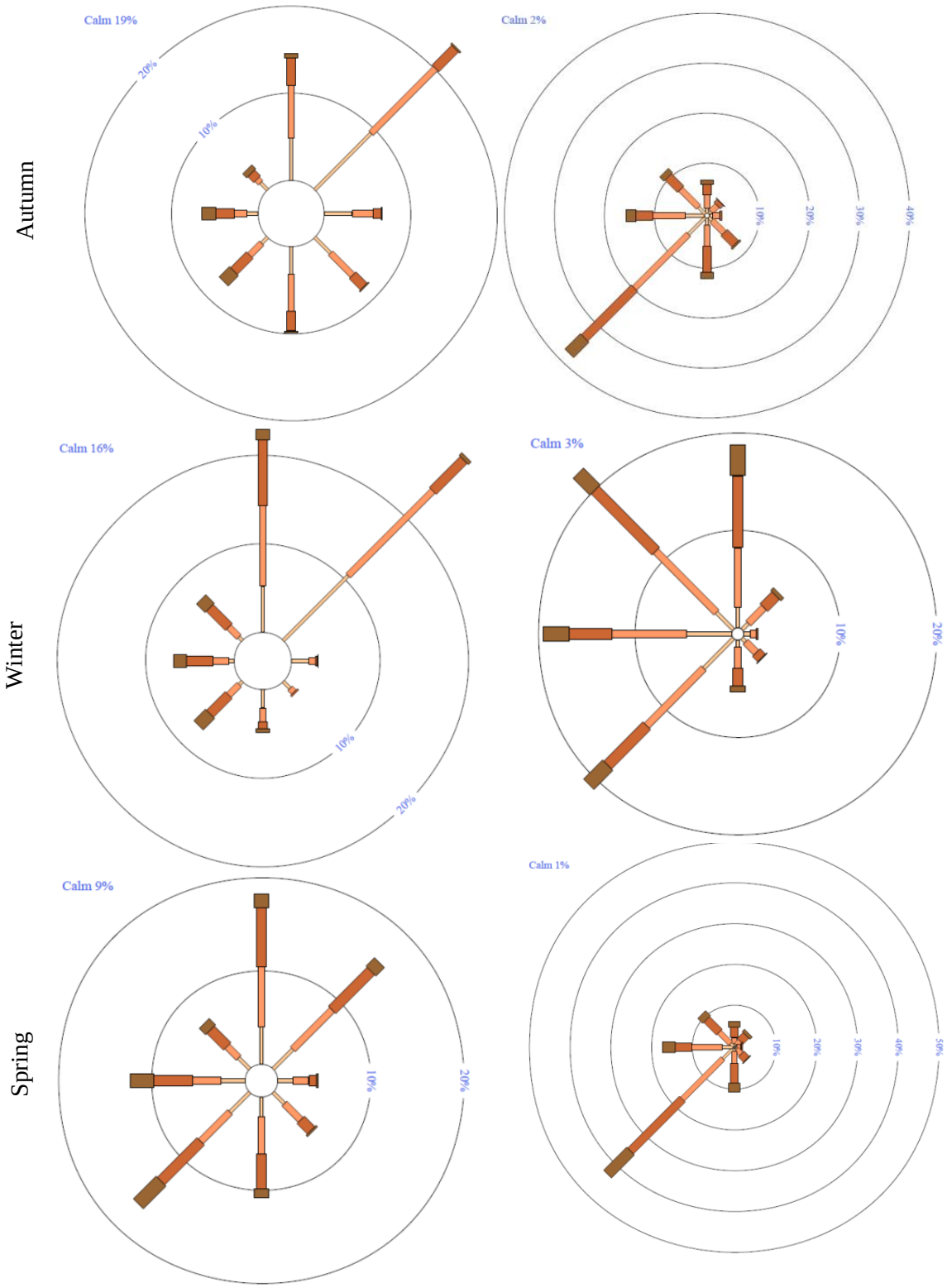

Figure 3.1.b. Seasonal wind rose in Adelaide, 9 am on left and 3 pm on right (Australian Burea of Meteorology, 2014a)

During the warmer months, another common wind, known as a gully wind is experienced mainly at night from the adjacent foothills of the Mount Lofty ranges, occasionally extending to several kilometres westward. Gully winds are basically the north-easterly winds that have been funnelled by the gullies of the western side of the Mouth Lofty ranges (Sha *et al.*, 1996).

3.3. South Australian Major Climate Drivers

Although the climate of South Australia differs from one year to the next, there are a few atmospheric phenomena that mainly control the general climate of the region. The main climate drivers for South Australia are listed and discussed in the following sections (Australian Bureau of Meteorology, 2010) .

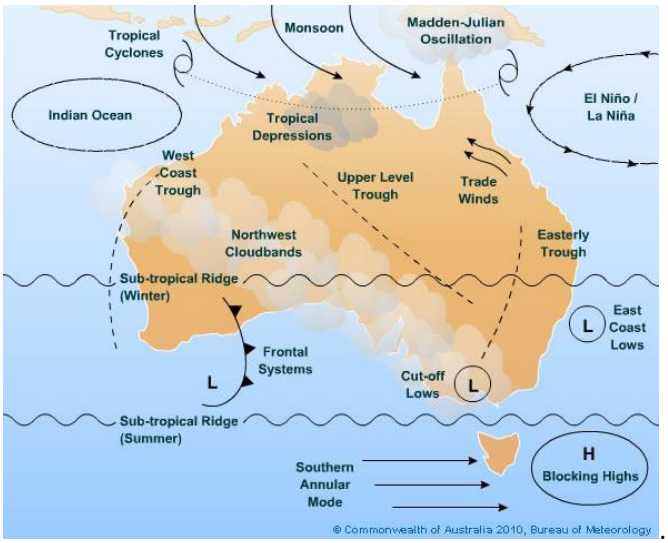

Figure 3.2. Climatic drivers of Australia (Australian Bureau of Meteorology, 2010)

3.3.1. The El Niño Southern Oscillation

The well-known El Niño Southern Oscillation (ENSO) has been measured using the pressure difference between Tahiti and Darwin, and is normally related to the change of surface temperature of the equatorial Pacific Ocean. This oscillation cycles between two

extremes of El Niño and La Niña. For Australia the El Niño phase is associated with droughts, while La Niña years bring more rainfall and floods (Australian Bureau of Meteorology, 2010). Although there have been more studies on the effects of the Southern Oscillation events on rainfall in Australia, as it generally affects the pressure system over the continent, hypothetically, there is a possibility that the South Australian temperature is influenced by this phenomenon. It has also been reported that presence of either of the phases lowers the sea surface heights of Australian southern coasts as a result of the existence of anomalous longitudinal subsurface flow (Holbrook *et al.*, 2009).

3.3.2. The Indian Ocean Dipole

This climatic system, similar to the Southern Oscillation, is defined using the temperature anomalies of the western equatorial Indian Ocean and the eastern part. When it is in phase with ENSO it enhances the impact of El Niño and La Niña events over Australia and while out of phase ENSO and IOD lessen their impacts.

A positive IOD (Indian Ocean Dipole) was observed to reduce the rainfall amount over Southern Australia whereas a negative value increases it.

3.3.3. Southern Annular Mode

Known as Antarctic Oscillation (AAO) the Southern Annular Mode is characterized by north – south movement of the westerly wind belt across the south of the Australian continent that influences the strength and position of cold fronts and mid-latitude storm systems. A positive value of the AAO Index represents strong westerly winds towards Antarctica and normally weakens the higher pressures and westerly winds over southern Australia, whereas a negative value shows the presence of westerly wind bands that expand towards the equator and bring stronger low pressure systems over southern Australia with an increase in storms and rains.

The Southern Annular Mode indices have been recorded since 1979 and are available through the Climate Prediction Center of the National Oceanic and Atmospheric Administration (Climatic Prediction Center, 2005).

3.3.4. Sub-Tropical Ridge

The sub-tropical ridge is a band of high pressure which is a major driver of southern Australia's climate and mainly brings cold fronts in winter and produces fine and dry weather in summer. Although the location of the ridge varies from the central part of Australia during winter to the southern part of the continent in summer, the daily latitudinal movement of the ridge is very small; however as argued by Drosdowsky (2005) some studies suggest a shift of 3 degrees south to the summer's centre of the ridge in the long-term, which has brought more droughts to Tasmania.

A study by Williams and Stone (2009) reveals the significant effect of the monthly anomaly of the latitude of the ridge (L as it has been referred to) on seasonal rainfall of Australia. They also suggest the presence of a significant relation between L and the Antarctic Oscillation Index and Southern Annular Mode.

In addition to these systems already mentioned, there are also a few synoptic features that greatly impact the climate of South Australia, mainly the rainfall pattern and amounts, and are listed in the following sections.

3.3.5. Cloud bands

Cloud bands are described as the presence of a predominant layer of clouds that stretch from the north-west to the south-east of Australia. They are generally classified into two types: oceanic and continental. The difference between the two types is in the northern extension of the cloud cluster which in the case of the oceanic cloud bands stretch to the oceans. The effect of cloud bands on the Australian rainfall has been previously studied

by Wright (1997), in which he highlighted the 20 percent contribution of this system to cool seasons rainfall over the agricultural part of South Australia.

3.3.6. Frontal Systems

A frontal system is generally a transition of a cold front from west to east across the Southern Ocean and in intense cases is associated with heavy rainfall. Frontal systems can happen at any time of the year but have been mainly observed during the cold months, namely May to August.

3.3.7. Cut-Off Lows

Similar to a frontal system, a cut-off low which is associated with the presence of a low pressure system over southern Australia, affects cold seasons by bringing more rainfall to the region.

3.3.8. Blocking Highs

This system happens when the travelling high-pressure cells move to the south (about -45° latitude) and slow down to a speed of less than 20 degrees of longitude in a week. In colder months, when the sea surface temperature is higher than the land, the system is generally observed to locate over the Australian continent, while in summer, it is generally found over the sea. Blocking highs have been documented to be responsible for some of South Australian hot and dry conditions.

The climate drivers of South Australia and their impacts are summarized by climate tools for Australian farmers as in Table 3.1.

Table 3.1: Climatic drivers of South Australia

Climate driver	Time of Impact	Duration	Potential impact
Frontal System	all year round with great impact during winter	between a few days to a week	more rainfall
Cut-Off Lows	all year round (most common in autumn and winter)	between a few days to a week	sustained, and often heavy, rainfall and strong and gusty winds and high seas
Northwest Cloud Bands	March to October, with the highest frequency between April and September	between a few days to a week	bring widespread, and often heavy, rainfall
Blocking Highs	all year round	from several days to several weeks	hot and dry conditions if the high is in the Tasman Sea
			increased chance of cut-off lows if the high is south of the Bight
	winter and spring		fog and frost if the high is centered near South Australia
The Sub-Tropical Ridge	all year round	ongoing	colder southwesterly winds and showery condition in winter
			lowers the temperature and more rainfall in summer
Southern Annular Mode	all year round	10 days to two weeks	Negative Phase- increase rainfall
			positive phase- less rain and higher temperature in winter
			positive phase - more rain and lower temperature in summer and spring
Indian Ocean Dipole	May to November, with the greatest impact between June and October	up to several months	positive phase-less rain
			Negative Phase- more rain
El Niño Southern Oscillation (ENSO)	all year round	seasons to year	El Niño- Warmer surface temperature and less rainfall
			La Nina -cool surface temperature and more rainfall

3.4. Previous study of sea breezes in the region

Previous studies of sea breezes in the region suggest the presence of an opposite sea and land breeze for the two sides of a semi enclosed body of water such as St Vincent's Gulf. In the study of sea breeze presented by Physick and Byron-Scott (1977) for the period of 1972 to 1974 the sea breezes have been categorized into five different groups, based on the daily synoptic situation. A summary of the wind characteristic on sea breeze days is illustrated in Table 3.2, adopted directly from their work. In their classification, there has not been any evidence of sea breeze formation on the days with a strong gradient wind from the south to northeast direction (clockwise), however the days with light variable synoptic winds in Adelaide have been observed to experience sea breezes with the maximum intensity of 4.5 m s^{-1} sometime between 14:00 and 16:00

local standard time. The change of wind to an onshore direction was documented to occur between 08:00 and 11:00 in Adelaide and cease sometime between 17:00 and 20:00. The characteristics of wind during sea breeze days on a site on the opposite side of the gulf have also been included. As the study was undertaken more than 30 years ago, the observations may not be relevant to the current weather pattern and the ongoing effects of urbanization.

Table 3.2: A summary of sea breeze day characteristic adopted from Physick and Byron-Scott (1977)

Gradient wind	south to south-east		south-east to east		east to north-east		north-east to north-		Light variable	
Shoreline	Adelaide	York Peninsula	Adelaide	York Peninsula	Adelaide	York Peninsula	Adelaide	York Peninsula	Adelaide	York Peninsula
Pre-dawn strength (m s-1)	4.0	south to south-east winds at 6.0-7.0 ms-1 throughout the day and night	2.0-2.5	5.0	4.0	<6.0	5.0	3.5	2.0	3.0
and direction	south-east		east to north-east	south-east	north-east	north to north-east	north	north-east	north-east	north-west
Time of changeover from land to sea (CST)	1100		0900-1000	-	1000-1300	0700-0800	variable	-	0800	0600-0800
Direction to which wind changes	south to south-west		south-west		north-west then south-west	north-east then south-east	north-west	east to north-east	west then south-west	north-east
Maximum velocity (m s-l)	7.0		4.0-5.0	7.0	4.5	4.5	7.0	4.5	4.5	4.0-5.0
and time (CST)	1400		1400	1700-1800	1400	1600-1700	1500	1400-1600	1400-1600	1100-1200 and 1600-1700
Time of changeover from sea to land (CST)	1700		1900	-	1900	-	1600-1700	2100	2000	2000
Direction to which wind changes	south-east		south-east to east	-	south to south-east	-	north to north-east	north to north-west	south-east	variable
Strength (m s-l) and	2.0		1.0-1.5	6.0	3.5-4.0	1.0-1.5	3.0	3.0	2.0	1.0
direction at midnight	south-east		north-east	south to south-east	norh-east	north to north-east	north to north-east	north to north-west	east to north-east	variable

About 20 years later, a numerical study by Finkele (1998) examined sea breezes inland and offshore propagation speeds under the presence of an offshore gradient wind. The model was evaluated against observational measurements at South Australia's Coorong coast from another study by Finkele *et al.* (1995). Finkele (1998) found that geostrophic winds, with a strong offshore component of more than 7.5 m/s, prevented inland propagation of sea breezes.

4. Adelaide Sea breeze

4.1. Adelaide Mesoscale Meteorology

As previously mentioned, Adelaide has a temperate Mediterranean climate with hot, dry summers and mild winters. The presence of a subtropical high pressure belt has been observed over the region in December, with a displacement to the south in following months. The report on climate change for South Australia by the Commonwealth Scientific and Industrial Research Organisation, known as CSIRO, (Mcinnes *et al.*, 2002) reveals an average increase of 0.17°C per decade in South Australia's maximum temperature since 1950, a rate of increase that is comparatively faster than the Australian continent as a whole. It has also been predicted that the annual average temperature of the Adelaide area will increase by 0.3° to 1.3° by 2030 and 0.6° to 3.8° by 2070 (Suppiah *et al.*, 2006).

Previous studies of the Adelaide metropolitan heat characteristics were mainly focused on the architectural effects of street canyons and energy consumption on the climate of the central business district (CBD), suggesting the presence of a night-time Urban Heat Island (UHI) and daytime Urban Cool Island (UCI). It has also been observed that, by the arrival of a sea breeze in the afternoon of summer months, the temperature of the CBD area decreased significantly, however the UHI intensity increases as heated air above the western suburbs reaches the city, leaving the city warmer than the suburbs and surrounding parklands (Erell and Williamson, 2007; Guan *et al.*, 2013). It should be noted that the UHI in the work by Erell and Williamson (2007) has been considered as a temperature difference between the CBD and the surrounding suburbs.

The climate of the Adelaide sea breeze is largely influenced by the presence of Mt Lofty to the east. An analysis of the wind spectra by Lyons (1975), confirmed that locally generated winds, (sea breezes for coastal sites, and gully winds for foothills) in summer

are the major source of kinetic energy of wind flows, while the synoptic winds are significantly dominant during the winter. The Adelaide shoreline has been observed to experience an interaction of two sea breeze systems, one generated over Gulf St Vincent, bringing warm moist air, while the other arrives later in the day generated over the Southern Ocean and is mainly referred to as a continental sea breeze. The arrival of the latter is characterised by a cooler and drier air mass. With continuous surface observation of the weather, the arrival of the two breezes can be observed through changes in temperature and relative humidity (Physick and Byron-Scott, 1977).

4.2. Detection and Validation of Sea Breezes

As mentioned earlier, sea breeze detection has been an objective of a number of studies, where the defining criteria vary, based on the availability of the observed meteorological records. The longest meteorological data for a coastal location near Adelaide were collected at the Adelaide Airport station. The data, as shown in Table 4.1, include 3-hourly surface readings of the temperature, wind speed and direction and 6-hourly upper air wind speed and direction.

For the current study where the long-term change to the wind characteristics of sea breezes is the aim, there have been a number of obstacles in terms of data availability. As has been explained in the literature review, a sea breeze day can be detected either thorough its commencement features such as an abrupt change in the surface climatic observation (i.e. decrease in temperature, increase in humidity or sudden increase in onshore wind velocity (Physick and Byron-Scott, 1977; Sumner, 1977)) or it can be recognized using a continuous characteristic of the day such as a gradual shift of wind to an onshore direction (Borne *et al.*, 1998). In order to select a day as a sea breeze day, and considering the frequency of observation (3-hourly), the selection criteria were formed to first select the days with the potential of sea breeze occurrence and then detect the surface wind characteristics of a fully developed sea breeze. Therefore the Adelaide Airport station, as a coastal site with the longest surface and upper air level records, was

selected. Later in the chapter, the characteristics of selected sea breeze days on the other side of the gulf are also analysed using the Edithburgh station on Yorke Peninsula.

4.2.1. Adelaide Airport

With the establishment of Adelaide Airport at West Beach in 1954/55, a meteorological station was established at the airport, which has recorded meteorological data from 1955, providing both surface data and observations from the upper air levels. The station height is 2 m above Australian Height Datum (AHD) with the barometer located at the height of 8.2 metres.

The frequency of surface data records has been increased from 8 times per day in 1955 to 48 time a day since January 1985. The meteorological data that have been recorded are listed in Table 4.1.

Table 4.1: Adelaide airport station. Data supplied by Australian Burea of Meteorology (2014a)

Observation	Commence Month	Frequency(average daily)	Single day missed	Full month missing
Air Temperature	February 1955	8.0	15	0
Dew Point	February 1955	8.0	15	0
Mean Sea Level Pressure	February 1955	8.0	15	0
Soil Temperature	February 1955	2.0	26	0
Total Cloud Amount	February 1955	8.0	15	0
Wind Speed	February 1955	8.0	15	0
Wind Direction	February 1955	8.0	15	0
Upper Air Data				
Upper Air Temperature	June 1954	2.0	256	0
Upper Air Wind Speed	January 1955	4.0	55	15
Upper Air Wind Direction	January 1955	4.0	55	15

There has been some replacement of observation equipment for the station, the details of which are attached as Appendix A along with the location of the instruments. The observations of wind speed and direction at surface level were started in 1955 using a Dines pressure tube anemometer (PTA) which was later replaced by a Synchrotac cup anemometer (CGA) in 1988. As mentioned in a study by Miller *et al.* (2013), previous work on a comparison of different anemometer types indicates that the mean wind speed observation with two instruments shows comparatively close results. However the experiments undertaken by Smith (1981) and Logue (1986) suggest a slight overestimation of the mean wind recorded by cup generator anemographs compared to pressure tube anemographs. It has been documented that for the mean wind speeds greater than Beaufort 5, regardless of the time of the day, the mean ratio of observation by cup-generators are less than 1.25% higher than the records of pressure-tube anemographs, whereas for the class of 3 and 4 on the Beaufort scale, the daytime wind has been observed to be up to 5% overestimated for the stations where a cup generator was used (Logue, 1986).

In contrast, wind gusts recorded by cup-generators have been observed to be approximately underestimated by 5 percent in most cases. These correction rates have been illustrated in a graph, shown in Figure 4. 1 (Logue, 1986).

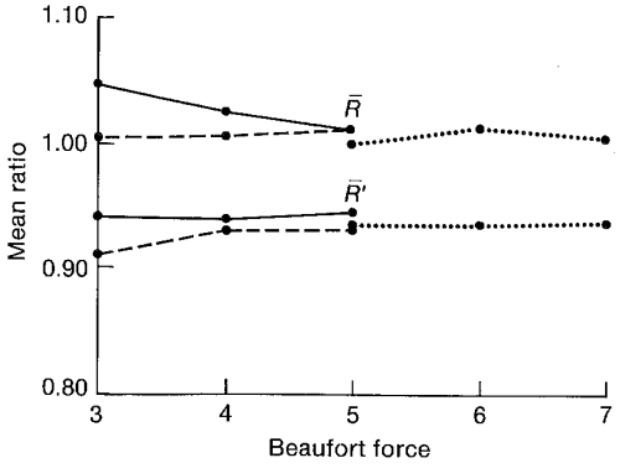

Figure 4.1. Mean ratios CGA/PTA for mean wind speed ($\bar{R}$) and gust wind ($\bar{R}$) of day (solid line) and night (pecked line) and all observation (dotted line), from (Logue, 1986)

Following Logue (1986), the wind speeds were corrected for the purpose of this study to bring them all to a common standard. The adjustments were applied to daytime wind of Beaufort force 3 and 4, applying the 1.05 and 1.025 increase of mean wind speed records of the Dines pressure-tube anemometer.

4.2.2. Edithburgh

As the sea breeze has been observed to occur on the other side of the Gulf, the station of Edithburgh, located at the southern end of Yorke Peninsula, was selected to investigate the characteristics of wind on the identified sea breeze days.

The station is located at the distance of 1 km from the shoreline, 6 m above mean sea level. The observations started in 1984, but continuous hourly records of the near surface wind and temperature only started from 1993. Figure 4.2 illustrates the location of the selected stations.

Figure 4.2. Location of Adelaide airport and Edithburgh stations.

4.2.3. The Sea Breeze Identification algorithm

To identify sea breeze days for Adelaide a set of criteria (or filters) has been developed to detect sea breeze formation and its subsequent penetration inland. Since analysis of long-term variations in sea breeze characteristics was the main objective of the study, it was necessary to obtain consistent meteorological observations for a long period with the highest possible temporal resolution. The Australian Bureau of Meteorology supplied meteorological data from 1955 for Adelaide Airport, which were used in this study, including three-hourly observations of wind speed and direction (10 m above ground level) and air temperature (1.2m above ground level) and six-hourly observations of the weather at upper air levels (using radiosondes). In the study by Crooks and Brooks (1987), the sea breeze was observed to arrive at the coast with an angle of between 190 and 310 degrees (inclusive); as the readings of wind direction are at the interval of 10 degrees, in order to include these values, the sea breeze sector is referred as an angle between 180 to 320 (exclusive) in the current study.

The records from the Advanced Very High Resolution Radiometer (AVHRR) from NOAA, discussed in (Townshend, 1994), were supplied to provide the surface temperature of Gulf St Vincent. The data collection started in 1981 but for the period 24 August 1981 to 13 December 2008, there were only 2081 records available (approximately 21%). In order to produce an estimated value for sea surface temperature, the data were interpolated using Matlab's (Matlab, 2010) piecewise cubic interpolation of spline and pchip (Piecewise Cubic Hermite Interpolating Polynomial). The results were averaged for each day of the year over the period from 1981 to 2008 and were considered as sea surface temperatures for each day of the year from 1956 (Figure 4.4). The correlation between available data and estimated values is 0.98 with a standard error of 0.65 ^{o}C. The sensitivity of the algorithm to the sea surface temperature is provided later in this chapter.

Previous studies, as explained in the literature review, tried to use distinguishable characteristics of a sea breeze day in order to identify them from synoptic scale flows,

therefore they have mostly utilized available near surface or upper level air records of meteorological stations. The selection criteria in this study were customized to be applied to the longest available record of data and to be able to detect sea breeze related modifications to the weather and reject large scale changes. Consequently, the following filters were introduced and implemented to select a sea breeze day:

1. Presence of a positive temperature difference between land and sea surface

2. Early afternoon wind speed at 700 hPa with an offshore component of no greater than 7.5 m s^{-1}.

3. One of the following conditions in surface wind observations:

    - Presence of a calm condition or an offshore wind in the early morning with a rotation to the sea breeze sector in the afternoon followed by a calm or offshore wind in evening and late night.

    - In days where morning or evening winds are predominantly a light breeze from the sea breeze sector, the afternoon wind intensity should exceed 1.5 m s^{-1}.

4. Moreover, for a day to be considered as a sea breeze day, the afternoon wind direction was required to be from the sea breeze sector for 2 subsequent readings (at least 3 hours flow).

Although the vertical temperature gradient over the land initiates the formation of sea breeze circulation, the presence of a temperature difference between the sea and land surfaces is the fundamental driver of sea breeze development; therefore, greater temperature over the land has been included as the first condition for a day to be selected as a sea breeze day. The temperature of Adelaide Airport station was used as the land surface temperature. The more inland station of Kent Town (approximately 8.5 kilometres further inland) has shown an average temperature difference of 0.64 degree

higher than the airport, (since the start of its operation in 1977). The second criterion excludes the days with strong opposing gradient winds (Finkele, 1998), and only considers the days for which there is a greater potential for a sea breeze to form.

The last filter considers the fact that the main specification of a sea breeze is the rotation of wind to the onshore direction accompanied by an increase in wind speed. Filters 1, 3 and 4 have been applied to the surface wind observations.

4.2.4. Method Assumptions

Wind speeds of less than 2 m s^{-1} were taken as a light breeze (Beaufort scale); therefore weaker afternoon winds were ignored in the selection process. The increase in velocity of more than 1.5 m s^{-1}, as explained by Azorin-Molina and Martin-Vide (2007), were previously applied in different sea breeze studies.

Due to the low frequency of observations (3-hourly surface and 12-hourly upper air level records), the selection method is likely to underestimate the sea breeze days frequency as some potential sea breezes with shorter duration are not detected. However the selected cases provide a set of days with fully developed sea breeze conditions that continue for at least 3 hours.

4.3. The Results

The selection algorithm was applied to the data set using Visual Basic codes developed by the author. Since there were periods of missing data in the observational records that were used in the detection method, the sea breeze cases for each time period are presented as the percentage of sea breeze occurrence.

For the period of study, August 1955 to June 2008, which included 95% data coverage for surface and upper air level observation, 26.6% of the days (4893 days) were identified as sea breeze days.

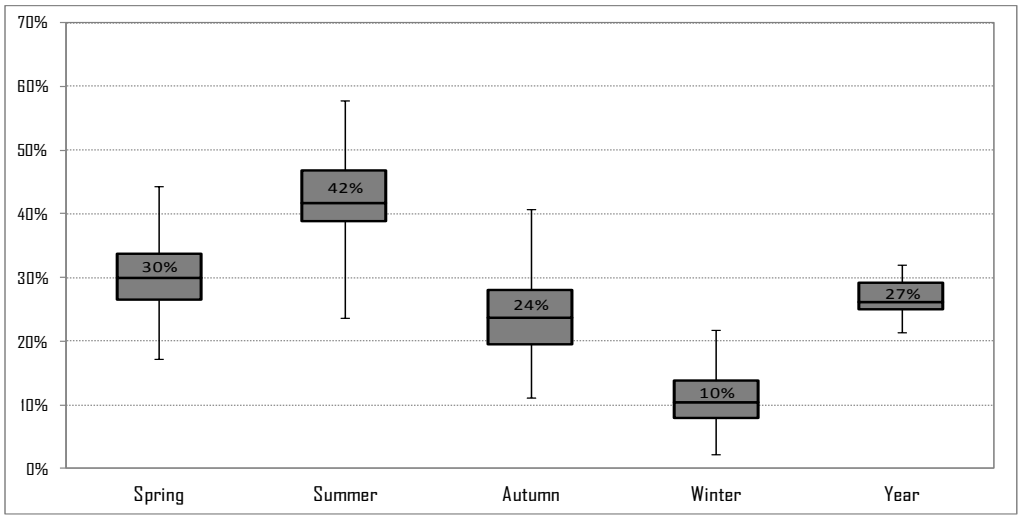

Figure 4. 3. The frequency of sea breeze event for each season, the box shows the lower and the upper quartile.

The percentages of possible sea breeze cases (hereafter sea breeze cases) in each season are plotted in Figure 4.3. Seasons are defined as: March to May as autumn, June to August as winter, September to November as spring and December to February as summer.

As expected, summer months have the most sea breezes with an average of 42% and a maximum of 58% of the days, while on average only 10% of winter days were observed to have sea breezes. This frequency of sea breeze occurrence in Adelaide coastline is less than that on the coastline of Perth in Western Australia, studied by Masselink and Pattiaratchi (2001). For the period of their study (1949-1997), on average, more that 197 days of the year (54%) and about 62% of days in summer were identified as sea breeze days. The lower potentiality of sea breeze events in Adelaide is attributed to the location of the coastline and the more restricted selection algorithm. Being located along the shore of the Indian Ocean, the sea breeze system of the coastline of Perth is known to be one of the strongest and most active systems in the world (Pattiaratchi *et al.*, 1997). On the other hand, the selection of sea breeze days in the study by Masselink and

Pattiaratchi (2001) was solely based on the behaviour of surface winds at 9 am (local time) and 3 pm and therefore may overestimate the number of sea breeze days.

4.4. Sensitivity analysis

4.4.1. Sea surface temperature

As there has been an assumption made for the temperature of the sea surface, a sensitivity test was carried out to examine the change in the number of selected sea breeze days, applying the actual value of temperature for days when actual sea surface data were available.

For the days where the actual record of sea surface temperature was available, the criteria were applied again and the number of sea breeze days' number was computed.

Figure 4.4 shows the assumed sea surface temperature (solid line) compared with the actual measurement with the radiometer. The land surface temperature is also included as black dots.

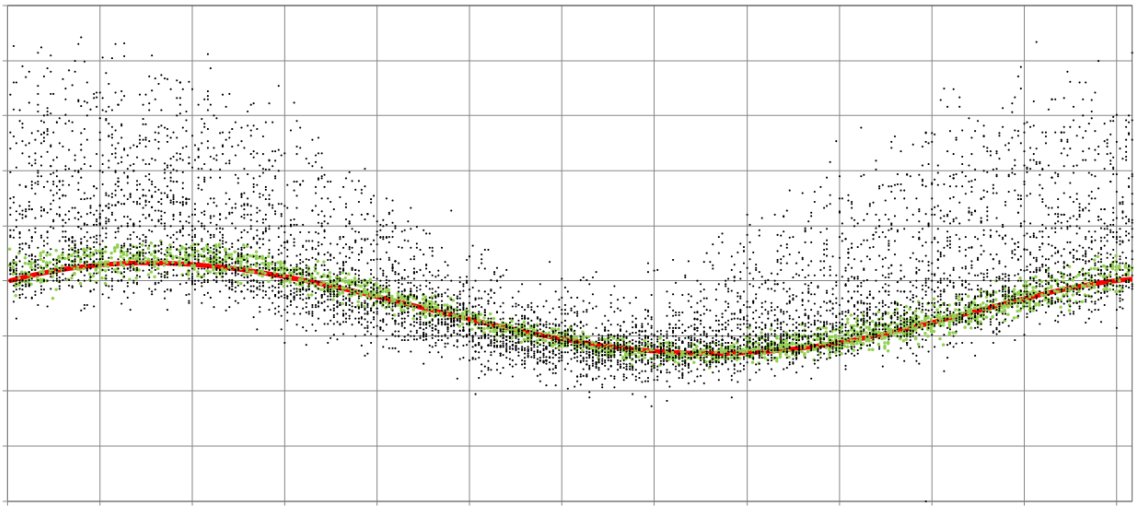

Figure 4.4. Available (green dots) and averaged (red line) sea surface temperature against the observed land surface temperature for each day of the year

In the colder months (150to 270 days) with lower dispersion, there is a good agreement between the measured and replaced sea surface temperatures compared to warmer months. However for the warmer months as the observed land surface temperatures are notably higher than sea surface temperatures, the averaging of the temperature of sea surface does not imply any significant error.

It should be noted that since the start of sea surface temperature measurement with AVHRR (a very high resolution radiometer) in August 1981, the records are only available for 21% of the days. Using the explained method for sea breeze detection on the 2033 days with actual sea surface temperature data only 633 days were selected as sea breeze days (31.1%). On the other hand, applying the averaged sea surface temperature (used in selection algorithm) for the same days, resulted in 643 cases (32.6 %) of sea breeze days, increasing the numbers by only 1.5 %. As there were no sea surface temperatures available prior to 1981, and the total error of using the average value only caused an error of 6.6%, the averaged values of sea surface temperature for each day of the year were used for the entire time period of study.

4.4.2. Sensitivity to land surface temperature

As mentioned in the literature review, previous studies on sea breeze identification used a temperature difference between land and sea as one of the characteristics of a sea breeze day. While in some studies, any positive difference between averaged daily air temperature over land surface and sea surface temperature were accepted (Furberg *et al.*, 2002), others use a minimum threshold between the land maximum temperature and sea surface temperature (Borne *et al.*, 1998). Watts (1955) found that a temperature difference of as little as 2 degrees was enough for sea breeze formation.

In this study, the temperature at 1.2 m height of Adelaide Airport station was used as the near surface air temperature, however due to its location the airport station is comparatively cooler than other inland stations.

From 1977, the station at Kent Town was operated at a distance of 8.5 km inland from Airport station. To test the sensitivity of the temperature criteria, in the selection algorithm, the first criterion was replaced by presence of a greater than 2 ^{o}C temperature difference between land and sea surface, in which the near surface (1.2m) air temperatures of Kent Town were considered as land temperature. Reapplying the new criteria resulted in a change of less than 3.2 percent in the number of sea breeze days.

4.4.3. Sensitivity to surface level wind speed criteria

In the selection algorithm a wind speed of equal to or less than 1.5 m s^{-1} was chosen as a light wind, based on Beaufort scale, however the wind speed observations were recorded with irregular intervals (0, 0.5, 0.6, 1, 1.1, 1.4, 1.5, 2.1, 2.2, 2.5, 2.6 ,… m s^{-1}). In order to analyse the sensitivity of the selection criteria to the value chosen to represent a light wind, an error of ± 0.5 m s^{-1} was applied to the observed data.

It was found that a positive error of 0.5 m s^{-1} in wind speed will decrease the number of sea breeze days from 4893 to 4876 days (0.3%), while a -0.5 m s^{-1} change results in an increase of 37 days to the number of sea breeze days (0.7%). Based on this it was assumed that the sea breeze day algorithm was not sensitive to the specification of the value for a light wind.

4.5. Characteristic of the wind at opposing shoreline of St Vincent Gulf

The selected sea breeze days based on the Adelaide data were examined using the wind data from the meteorological station at Edithburgh, located on the western side of St Vincent Gulf. As the collection of observation of this site started from 1993, the corresponding period was examined for both sites.

The hodographs of the wind for averaged sea breeze and non-sea breeze days are shown in Figure 4.5 where each point on the hodograph refers to the end of the vector of

averaged wind at that time. The hodographs were plotted over the map outline of the area to make comparison and evaluation easier.

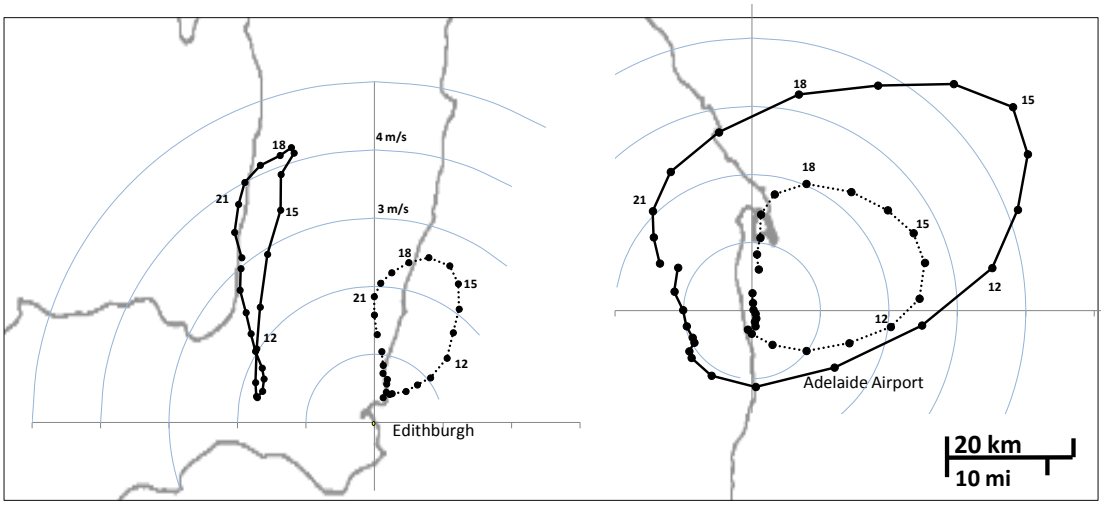

Figure 4.5. Wind hodograph of sea breeze (full line) and non-sea breeze days (dotted line) for both sides of the gulf (1993-2008). The circles show the wind speed at the interval of 1 m/s.

The averaging was done for each component of wind over the period of 16 years for sea breeze and non-sea breeze days separately. There is an evident difference between the behaviour of the sea breeze and non-sea breeze days at Edithburgh. It is worth noting that the chosen sea breeze days for all locations have been based on application of the detection filters to the Adelaide Airport observations.

The directions of afternoon wind on the afternoon of non-sea breeze days are similar for Adelaide and Edithburgh, whereas the sea breeze day winds show a different characteristic at the Edithburgh station. Figure 4.6 shows the U and V components of averaged west-to-east and south-to-north components, respectively, at Edithburgh and Adelaide for sea breeze and non-sea breeze days, as selected for Adelaide. For sea breeze days, the night-time U-component (between 21:00 and 09:00 the next day) is from the east (i.e. negative) for both locations but stronger at Edithburgh due to its more exposed location. During the early part of the sea breeze day the U-component changes sign from offshore to onshore and increases in strength at Adelaide Airport, whereas at

Edithburgh, the U-component becomes more negative and more onshore as expected for a sea breeze at Edithburgh, being on the opposite side of Gulf St. Vincent (Figure 4.6a). Later in the sea breeze day, the U-component weakens in magnitude at both locations, becoming offshore at Adelaide but not at Edithburgh. This difference may be explained by the relative strength of sea breezes and land breezes on the larger land mass (Xian and Pielke, 1991) east of Adelaide compared with the narrow peninsula to the north and west of Edithburgh. The V-components have a similar pattern at both locations but are stronger at Edithburgh due to its greater exposure to southerlies (Figure 4.6c). The V-component on sea breeze days becomes negative at Adelaide but not at Edithburgh, probably again connected with the greater local land mass and the offshore land breeze at Adelaide. The fact that the observed sea breeze direction is not perpendicular to the shoreline is due to the location of the Gulf in the vicinity of the ocean, and the presence of the continental sea breeze from the south, which shifts the resultant wind southerly as has been previously noted by Physick and Byron-Scott (1977).

For non-sea breeze days the U-components at both Edithburgh and Adelaide are similarly positive and peak during the afternoon, albeit more strongly at Adelaide because it is less sheltered from westerlies than Edithburgh (Figure 4.6b). The V-components for non-sea breeze days have a similar pattern at both locations but are stronger at Edithburgh due to its greater exposure to southerlies (Figure 4.6d).

Thus the hodographs and wind components at Adelaide and Edithburgh show quite similar behaviour on non-sea breeze days but are significantly different on sea breeze days due to Edithburgh's location on the opposite side of Gulf St. Vincent. The differences are consistent with the circulation patterns expected on a sea breeze day at Adelaide. Other differences may be explained by the differences in exposure and local land mass.

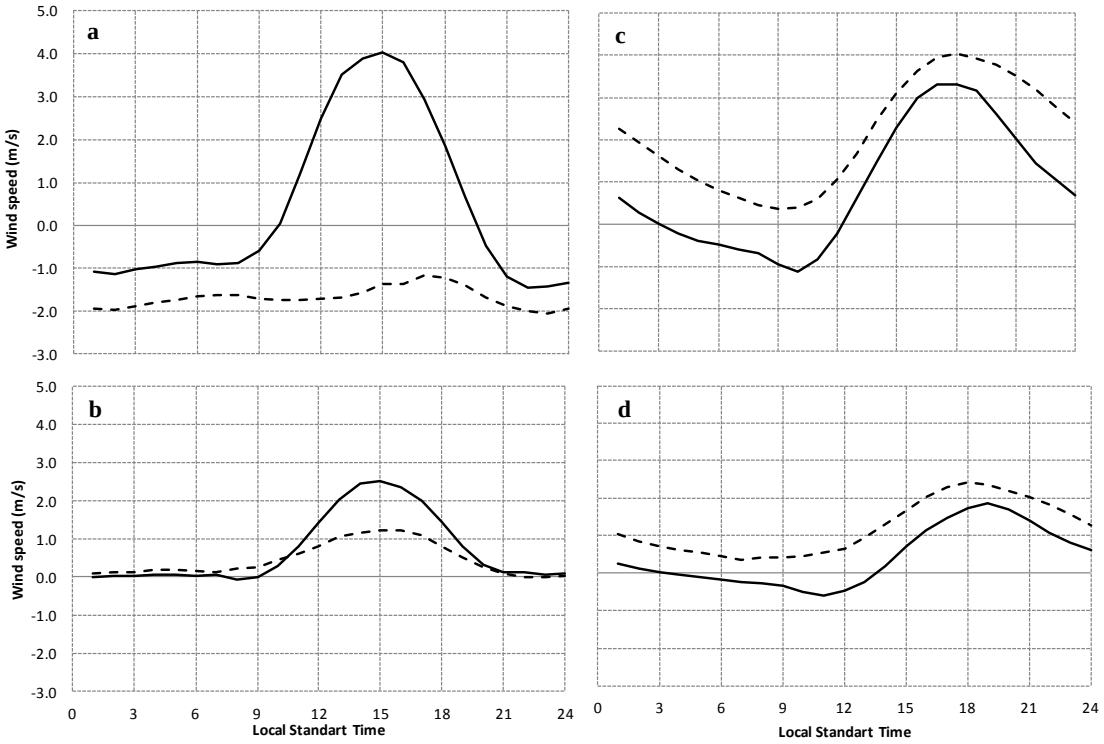

Figure 4.6. Average sea breeze days' U-component (a) and V-component (c) of Adelaide Airport (solid line) and Edithburgh (dashed line). Same for non-sea breeze days (b) and (d) respectively.

4.6. Long-term trend

4.6.1. Some considerations on statistical analysis of data

There have been a few changes in weather observation practice, which make it difficult to come to a conclusion about the long-term changes in the surface wind observations.

Apart from changes to the instrumentation that have been applied to observation data, the commencement of daylight saving and change in the frequency of observation can have a large impact on the time series analysis of observations. The change in daylight saving was important because while data collection continued at 3 hourly intervals they were shifted from the pattern of 00:00, 03:00, 06:00, etc. during the non-daylight saving days to 23:00, 02:00, 05:00 etc. during the daylight saving days. Therefore, to avoid any systematic error in the long-term analysis of wind data due to implementation of

Daylight Saving Time (DST) since 1972, and the change of observational frequency in 1985, the data were analysed for three separate time periods of 1955-1972, 1972-1985 and 1985-2007.

For the period of 1972 to 1985 the DST in South Australia started from early October each year and ended at early March of the next year. Therefore, through seasonal averaging of data i.e. summer (Dec-Feb), autumn (Mar-May), winter (June-Aug) and spring (Sep-Nov), this change to the local time would affect spring and summer observations. In order to avoid any possible error in averaging, the period of 1972-1985 has not been included in the spring and summer analysis, whereas since autumn months are not affected by the time advancement of DST the long-term analysis of data is applicable. As a consequence the following analyses are discussed on a seasonal basis, excluding winter months due to the lower number of sea breeze cases.

As discussed earlier, the afternoon winds of sea breeze days are a combination of a locally generated gulf breeze (from the west), and southerly ocean breezes, while the Coriolis induced rotation of wind may slightly shift the afternoon wind anticlockwise. To individually assess the alteration of each of the breezes, south-north (V) and west-east (U) components of wind were examined separately.

4.6.2. Summer

The three months of December to February are regarded as summer months. As already mentioned, the introduction of daylight saving from 31/10/1971 to 27/02/1972 meant that the 3 hourly records of winds were shifted one hour and this makes the comparison inappropriate, therefore the period of 1972-1984 was omitted from observations and the remaining data were analysed for trend detection.

To avoid any misinterpretation of data as a result of the reduction in the number of records, a plot of the U component of averaged sea breeze days, 15:00 wind for two

cases of (a) entire observations and (b) with exclusion of 1972-1984 are shown in Figure 4.7.

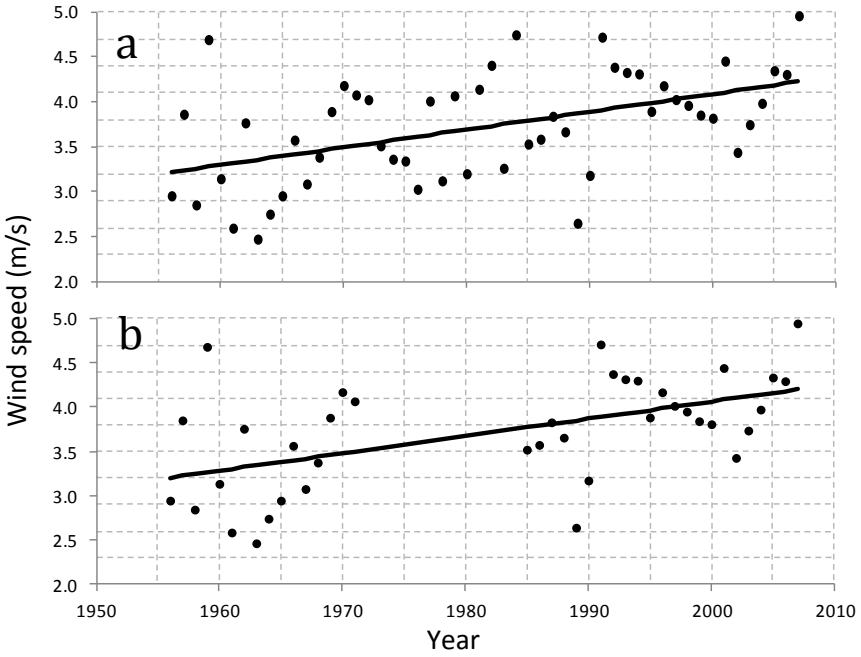

Figure 4.7. U component of 15:00 hour for entire period (a) and excluding 1972-1984 (b).

The change of data collection time from 15:00 to 14:00 on 13 years observational record does not make any significant impact on the growth rate of the 15:00 wind intensity on sea breeze days, as the linear regression slopes of (a) and (b) are 0.0198 and 0.0195 per year, respectively.

There is a similar pattern of behaviour for other observational records, as shown in Figure 4.8.

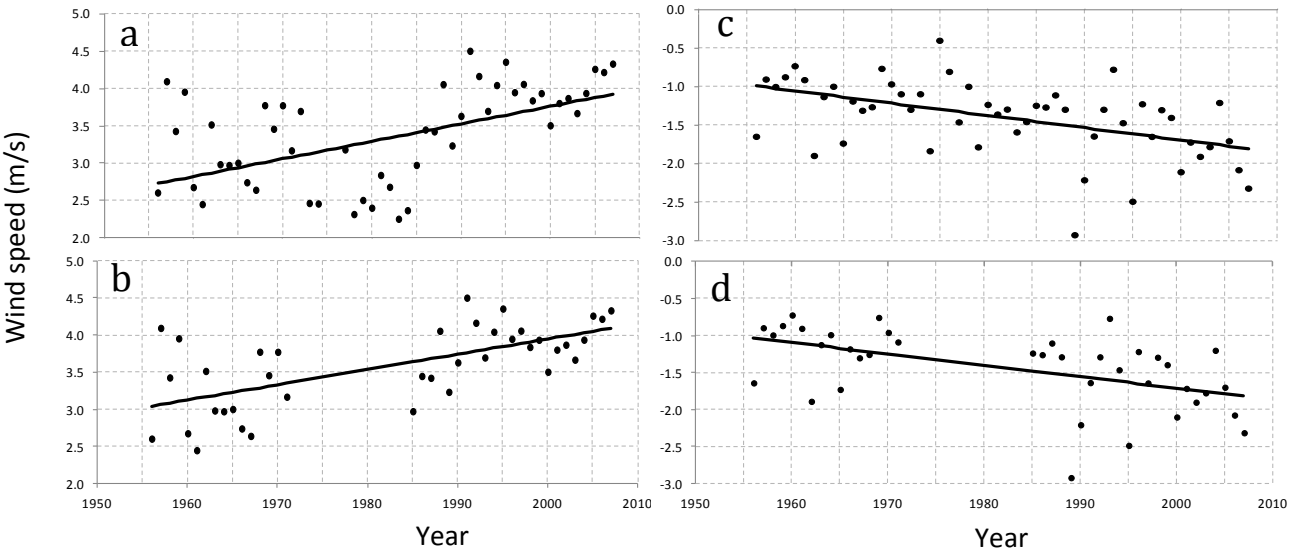

Figure 4.8. U component of 12:00 hour for entire period (a) and excluding 1972-1984 (b) and similarly for 21:00 data (c,d).

As mentioned in the literature review, the arrival of the locally generated sea breeze, the gulf breeze, has been observed to be as early as 10:00 (Physick and Byron-Scott, 1977) and as the next readings of the data were at 12:00, the wind components at 15:00, 18:00 and 21:00 were examined, and the results presented in Table 4.2.

The linear regression analyses were applied to the values and some selected statistical measurements used to determine the significance of the trend lines.

- Regression coefficient: defines the rate of change of dependent variable (wind speed in this case).

- Standard error: defines the standard deviation of sampling distribution and is calculated as the square root of the variance of the regression coefficient.

- R^2 (R square): known as the coefficient of determination, is the percent of the total variation in the dependent variable (wind speed) that is explained by the independent variables (time).

- t statistic: determines how significant the difference between the regression coefficient and zero line is at 95 percent significance level, whereas the p-value defines the actual level of significance of the regression coefficient. The (two tail) p-value of 0.01 (from Table 4.3) implies 1-(2×0.01)= 98% confidence that the coefficient of V component wind speed of 18:00 is about 0.0018.

- The normalized root mean square error (NRMSE): a non-dimensional form of root mean square error (RMSE) and is calculated by dividing RMSE by the average observed values.

- Durbin-Watson Statistic: this statistical test detects the presence of first order autocorrelation between time series values. A value of 2 of this test means that there is not any autocorrelation in the sample. The 1% significant point of lower and upper critical value for the data size of 52 are 1.324 and 1.403, therefor the value of less than 1.324 or more than 2.767 (4-1.324) reject the null hypothesis of non-autocorrelated errors in favour of the hypothesis of positive first-order autocorrelation. If the test statistic value lies between the two limits (1.324 and 1.403 or 2.597 and 2.767), the test is inconclusive.

Table 4.2 Results of regression analysis of U-wind component in summer –excluding the 1972-1984 records, the significant regression values are bolded.

U	Time	Regression Coefficients	standard error	R^2	f stat	t stat	p-value	NRMSE of residuals	Durbin-Watson stat
SB	12:00	0.020	0.42	0.42	26.44	5.14	0.00	0.12	0.90
	15:00	**0.019**	**0.53**	**0.29**	**15.02**	**3.88**	**0.00**	**0.14**	**2.07**
	18:00	0.005	0.68	0.02	0.62	0.79	0.44	0.91	1.39
	21:00	**-0.015**	**0.45**	**0.27**	**13.46**	**-3.67**	**0.00**	**-0.31**	**1.89**
NON_SB	12:00	0.001	0.91	0.00	0.01	0.10	0.92	0.41	2.06
	15:00	0.002	1.06	0.00	0.04	0.19	0.85	0.50	2.25
	18:00	-0.006	1.08	0.00	0.37	-0.61	0.55	1.04	2.00
	21:00	-0.007	0.76	0.03	1.04	-1.02	0.31	1.25	1.97

The value of the two tail F distribution (f stat) at 95% level is 5.3.

Analysis of the regression results indicates that the slope parameter is significantly different from zero at the 5% level for afternoon wind of sea breeze days at 12:00, 15:00 and 21:00, suggesting an increase in the wind intensity over time. however the Durbin-Watson value of 0.9 reject the null hypothesis and it means that there is an autocorrelation between the data. By comparison, the non-sea breeze days afternoon winds do not show any significant changes to the wind strength.

Having over 35 data points, the large values of the t-statistic (critical value of two tail T test for sample size of more than 30 at 95% significance level is 2.04), along with significantly low p-values (< 0.05) and considerably lower normalized root mean square errors of residuals indicate the presence of a significant increasing trend at the 5% level in the strength of the mentioned afternoon wind of sea breeze days. Moreover, the value of the standard error of regression of the mentioned afternoon wind component is comparatively lower than other times. The changes in the 15:00 and 21:00 hour wind intensities for the same 52 year period were analysed and found to be 1.01 ± 0.53 m s^{-1} and -0.8 ± 0.44 m s^{-1}, respectively. The negative sign of the regression coefficient demonstrates the easterly direction of 21:00 hour winds.

The north- south component analysis is given in Table 4.3.

Table 4.3 regression analysis of V-wind component in summer –excluding the 1972-1984 records

V	Time	Regression Coefficients	standard error	R^2	f stat	t stat	p-value	NRMSE of residuals	Durbin-Watson stat
SB	12:00	0.004	0.65	0.01	0.53	0.72	0.47	0.38	2.21
	15:00	0.005	0.69	0.02	0.69	0.83	0.41	0.17	1.76
	18:00	**0.014**	**0.53**	**0.18**	**8.15**	**2.86**	**0.01**	**0.13**	**1.52**
	21:00	**0.018**	**0.45**	**0.33**	**18.41**	**4.29**	**0.00**	**0.23**	**1.40**
NON_SB	12:00	-0.003	0.67	0.01	0.19	-0.44	0.66	0.24	1.54
	15:00	-0.001	0.77	0.00	0.01	-0.11	0.91	0.18	1.92
	18:00	0.005	0.61	0.00	0.75	0.86	0.39	0.13	2.09
	21:00	**0.013**	**0.50**	**0.17**	**7.42**	**2.72**	**0.01**	**0.14**	**1.72**

In the case of the V component of afternoon winds on sea breeze days, it is clear that the 18:00 and 21:00 hour southerly winds are progressively growing with an average of 0.74 ± 0.53 m s^{-1} and 0.94 ± 0.45 m s^{-1} increases over the period of 52 years. However, as shown in Table 4.3, the south to north component of the 21:00 hour wind on non-sea breeze days is suggesting an increase, similar to the 18:00 hours sea breeze days, of 0.67 ± 0.50 m s^{-1} from 1956 to 2007. It suggests that generally the afternoon south-easterly wind at 21:00 is increasing, which might be associated with more continental scale changes to the wind regime. The Durbin-Watson test of data reject the presence of any autocorrelation for 18:00 of sea breeze abd 21:00 of non-sea breeze days; however the results for 21:00 hours sea breeze days is inconclusive. It is worth noting that the regression coefficient with a t value of greater than 1.96 and the corresponding p-value of 0.025 and below are significant at a 95 percent level. Figure 4.9 illustrates the southerly component of averaged summer wind at 18:00 and 21:00 of sea breeze days and 21:00 of non-sea breeze days, excluding the period of 1972-1984.

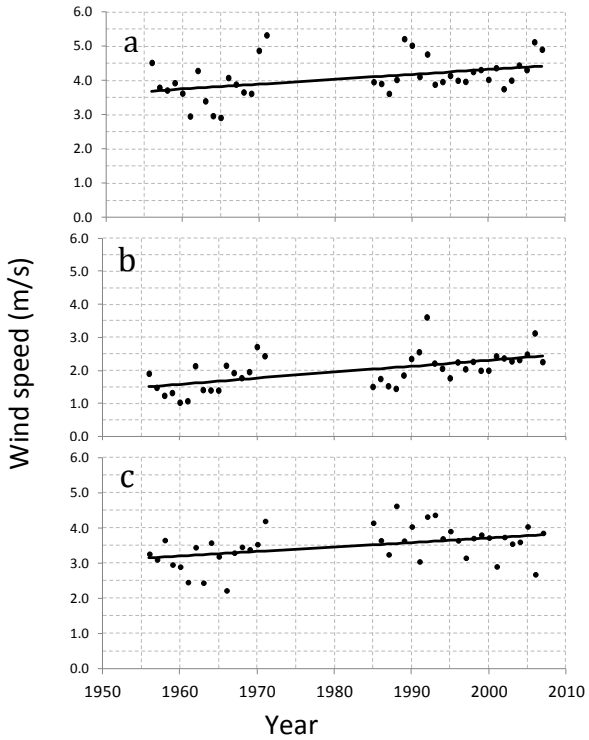

Figure 4.9. V component of 18:00 (a) and 21:00 (b) winds of sea breeze days and 21:00 (c) wind of non-sea breeze days.

4.6.3. Autumn

The autumn months of March, April and May were not affected by daylight saving time advancement, since for the period 1972-1985 the DST normally ended within the first week of March, therefore the analysis includes the entire data set.

Similar tables to those shown previously are provided for autumn for the duration of 1956 to 2007.

Table 4.4 Result of regression analysis of U-wind component in autumn

U	Time	Regression Coefficients	standard error	R^2	f stat	t stat	p-value	NRMSE of residuals	Durbin-Watson stat
SB	12:00	0.010	0.53	0.08	4.64	2.15	0.04	0.18	1.63
	15:00	**0.019**	**0.49**	**0.27**	**18.42**	**4.29**	**0.00**	**0.15**	**1.90**
	18:00	0.001	0.53	0.00	0.01	-0.08	0.94	0.91	1.78
	21:00	**-0.020**	**0.37**	**0.41**	**35.07**	**-5.92**	**0.00**	**-0.40**	**1.90**
NON_SB	12:00	0.004	0.73	0.01	0.42	0.65	0.52	0.52	2.17
	15:00	0.009	0.87	0.03	1.37	1.17	0.25	0.46	1.90
	18:00	-0.011	0.67	0.03	3.23	-1.80	0.08	1.10	1.98
	21:00	**-0.019**	**0.49**	**0.26**	**17.16**	**-4.14**	**0.00**	**1.12**	**2.28**

The westerly component of averaged summer wind at 18:00 and 21:00 of sea breeze days and 21:00 of non-sea breeze days are plotted in Figure 4.10.

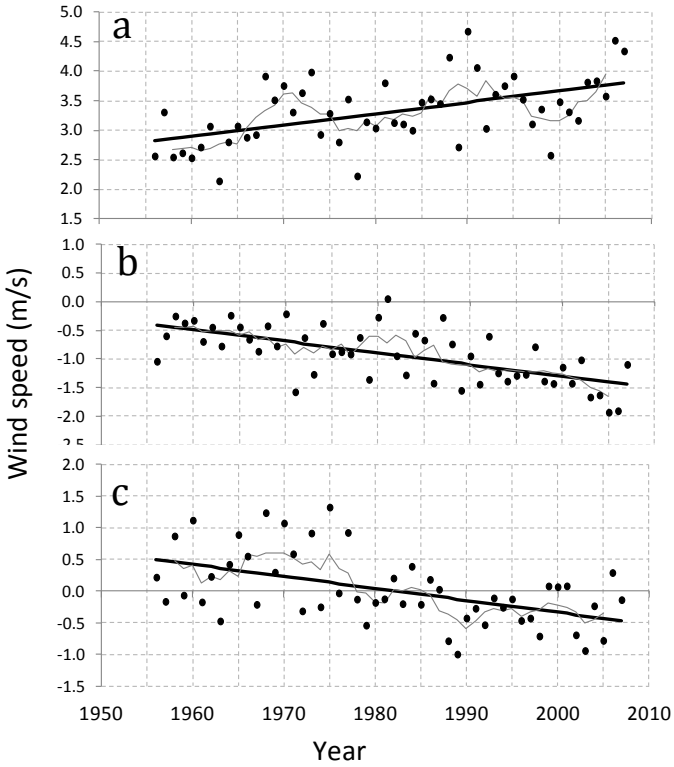

Figure 4.10. U component of 15:00 (a) and 21:00 (b) wind of sea breeze and 21:00 (c) wind of non-sea breeze days. The grey line shows the five years moving average.

Similar to the summer months, the westerly wind component is showing a rising trend, particularly at 15:00 with an average increase of 1.0 ± 0.47 m s^{-1} within the 52 years of the study, a growth of between 16% and 45% in the velocity of averaged wind. In the same period the easterly wind at 21:00 was found to have a comparable growth of 1.0 ± 0.37 m s^{-1} (between 75% to 152% increase in averaged wind speed) for identified sea breeze days. In the case of non-sea breeze days, the averaged wind vector at 21:00 has shown a change of direction from offshore to onshore within the period of study.

From Table 4.5, the sea breeze V component from 15:00 to 21:00 is showing an increasing trend, with rises in velocity of 1.07 ± 0.78 m s^{-1}, 1.43 ± 0.57 m s^{-1} and 1.04 ± 0.48 m s^{-1}, respectively. Considering an averaged velocity of 2.57 m s^{-1}, 2.42 m s^{-1} and 0.96 m s^{-1} in southerly wind component at these times of the day, the percentage of increase is relatively higher for 21:00 winds (between 60% and 156%). Nevertheless, the

southerly components of wind of 15:00, 18:00 and 21:00 in non-sea breeze cases have also increased 0.84 ± 0.72 m s^{-1}, 0.69 ± 0.48 m s^{-1} and 0.66 ± 0.36 m s^{-1}, respectively. With an average of 1.41 m s^{-1}, 1.85 m s^{-1} and 1.03 m s^{-1} for the period of 1956 to 2007, the percentage of increase in the wind velocity is relatively lower than on sea breeze days. There should be noted that for all of the mentioned time, there is no autocorrelation between the time series values.

Table 4.5 Result of regression analysis of V-wind component in autumn

V	Time	Regression Coefficients	standard error	R^2	f stat	t stat	p-value	NRMSE of residuals	Durbin-Watson stat
SB	12:00	0.009	0.79	0.03	1.38	1.17	0.25	1.27	2.30
	15:00	**0.021**	**0.78**	**0.14**	**8.05**	**2.84**	**0.01**	**0.3**	**2.40**
	18:00	**0.028**	**0.60**	**0.33**	**25.02**	**5.00**	**0.00**	**0.25**	**1.94**
	21:00	**0.020**	**0.48**	**0.29**	**20.58**	**4.54**	**0.00**	**0.48**	**2.26**
NON_SB	12:00	0.007	0.69	0.02	1.22	1.10	0.27	1.33	1.80
	15:00	**0.016**	**0.74**	**0.10**	**5.52**	**2.35**	**0.02**	**0.52**	**1.73**
	18:00	**0.013**	**0.50**	**0.10**	**8.36**	**2.89**	**0.01**	**0.27**	**2.09**
	21:00	**0.013**	**0.37**	**0.22**	**13.78**	**3.71**	**0.00**	**0.36**	**2.07**

In Figure 4.11 the southerly component winds at 15:00, 18:00 and 21:00 for both cases are plotted.

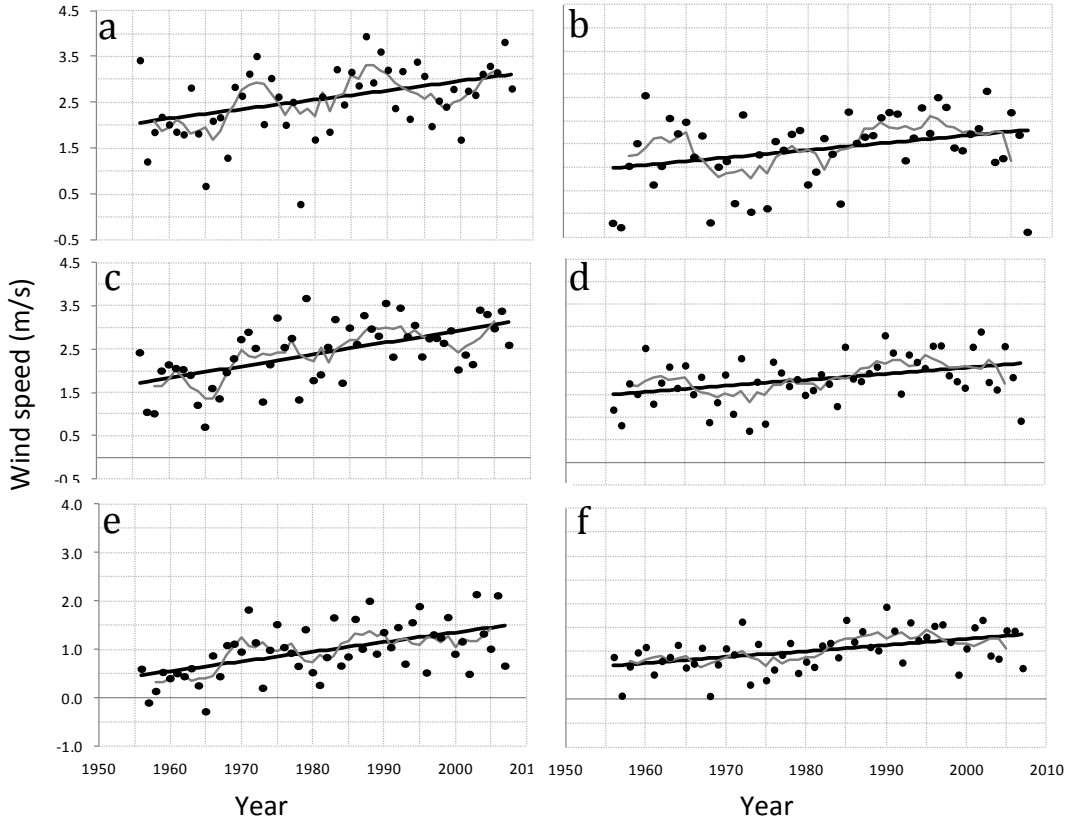

Figure 4.11. V component of sea breeze (left) and non-sea breeze (right) at 15:00 (a,b), 18:00 (c,d) and 21:00 (e,f).

4.6.4. Spring

For the three months of September to November, the same considerations as the summer months have been applied, noting that due to unavailability of the data in 1992, this year was omitted from the analysis.

Table 4.6 Result of regression analysis of U-wind component in spring –excluding the 1972-1984 and 1992 records

U	Time	Regression Coefficients	standard error	R^2	f stat	t stat	p-value	NRMSE of residuals	Durbin-Watson stat
SB	12:00	0.010	0.47	0.12	5.13	2.27	0.03	0.13	1.56
	15:00	**0.014**	**0.39**	**0.29**	**14.45**	**3.80**	**0.00**	**0.11**	**1.76**
	18:00	**0.013**	**0.48**	**0.17**	**7.62**	**2.76**	**0.01**	**0.89**	**1.45**
	21:00	**-0.021**	**0.40**	**0.46**	**30.11**	**-5.49**	**0.00**	**0.33**	**1.47**
NON_SB	12:00	0.010	0.88	0.04	1.54	1.24	0.22	0.34	2.33
	15:00	0.006	0.99	0.01	0.44	0.66	0.51	0.36	2.07
	18:00	0.005	1.03	0.01	0.28	0.53	0.60	0.66	2.20
	21:00	0.004	0.88	0.01	0.24	-0.49	0.63	0.93	2.39

The coefficient of determination (R^2), in Tables 4.2, 4.4 and 4.6, suggest that the increase is more significant for the seasons of summer and autumn; however as highlighted in the Table 4.6, the perpendicular wind component to the shore (U) is showing an increase in velocity at all afternoon times on selected sea breeze days, most noticeably at late afternoon, while there are not any significant changes to the remaining days afternoon wind behaviour. The growth of wind intensity for 15:00 and 21:00 are 0.72 ± 0.39 m s^{-1} and 1.08 ± 0.4 m s^{-1} respectively, whereas the easterly component of wind of selected sea breeze days is showing a distinctive rise of 1.24 ± 0.62 m s^{-1} for the period of 53 years on the intensity of 18:00 hour wind (between 21% to 135% of averaged wind intensity). The averaged afternoon U component of wind on sea breeze days are plotted in Figure 4.12. For 12:00 the p-value of 0.03 implies that the regression coefficient is not significant at preferred level of 95 percent, but is significant at 1-(2×0.03) =94% level. The Durbin-Watson statistic test reject presence of any autocorrelation for all of the afternoon time data.

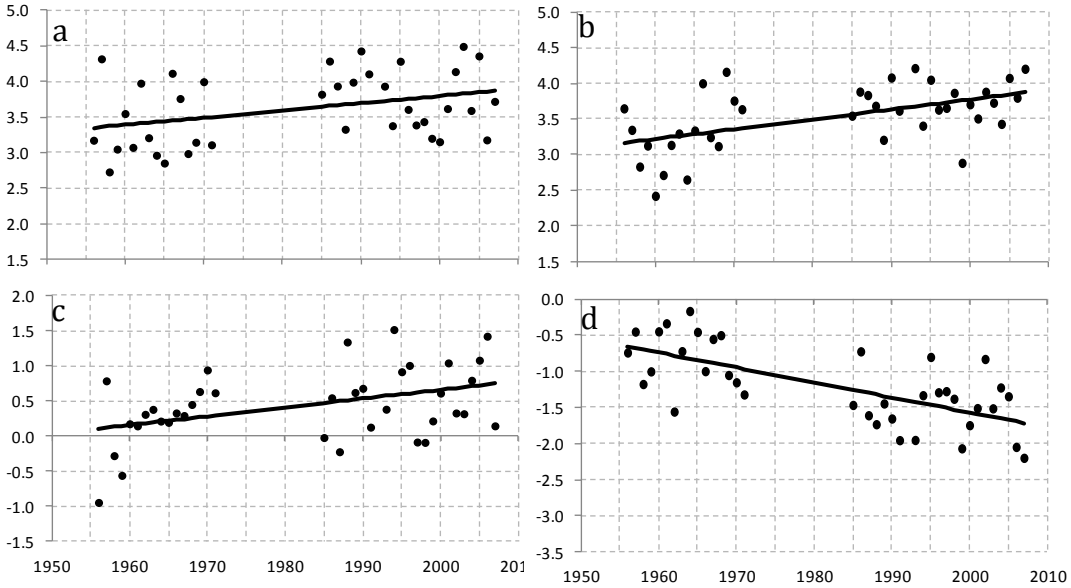

Figure 4.12. The U component of sea breeze day 12:00 (a), 15:00 (b), 18:00 (c) and 21:00 (d) wind.

In the case of V-wind component, similarly there is not any significant change in the wind velocity of non-sea breeze days. However observation of the southerly component at 18:00 and 21:00 wind on sea breeze days is suggesting an increase of 1.24 ± 0.62 m s^{-1} and 0.76 ± 0.45 m s^{-1} in velocity. The 1.83 and 1.53 value for autocorrelation test means that there is no autocorrelation between in the time series.

Table 4.7 Result of regression analysis of V-wind component in spring –excluding the 1972-1984 and 1992 records

V	Time	Regression Coefficients	standard error	R^2	f stat	t stat	p-value	NRMSE of residuals	Durbin-Watson stat
SB	12:00	0.003	0.80	0.00	0.15	0.39	0.70	1.19	2.15
	15:00	0.015	0.81	0.10	4.04	2.01	0.05	0.32	2.03
	18:00	**0.024**	**0.62**	**0.32**	**16.60**	**4.07**	**0.00**	**0.25**	**1.81**
	21:00	**0.015**	**0.45**	**0.25**	**11.96**	**3.46**	**0.00**	**0.48**	**1.53**
NON_SB	12:00	-0.017	0.99	0.08	3.13	-1.77	0.09	1.21	2.12
	15:00	-0.014	0.94	0.06	2.44	-1.56	0.13	0.61	2.10
	18:00	-0.004	0.83	0.06	0.20	-0.45	0.66	0.37	2.05
	21:00	-0.002	0.63	0.00	0.16	-0.39	0.70	0.41	2.03

Despite the presence of a growth in the intensity of 15:00 southerly wind on sea breeze days, shown in Figure 4.13(a), considering the value of t test and p-value, it is not significant at the 95% confidence level.

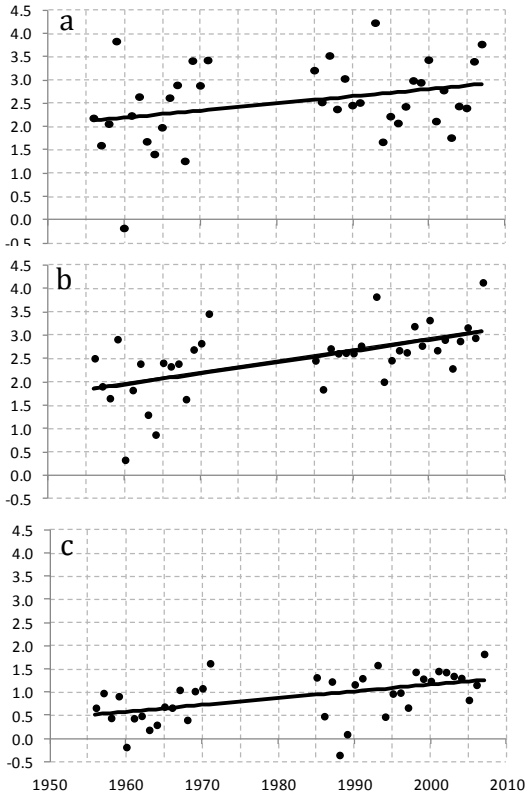

Figure 4.13. The V component of sea breeze day 15:00 (a), 18:00 (b) and 21:00 (c) wind.

4.7. Daily cycle of wind

Hodographs of the average of selected sea breeze winds for the duration of the study (1955-2007) were plotted for the non-sea breeze days (Figure 4.14).

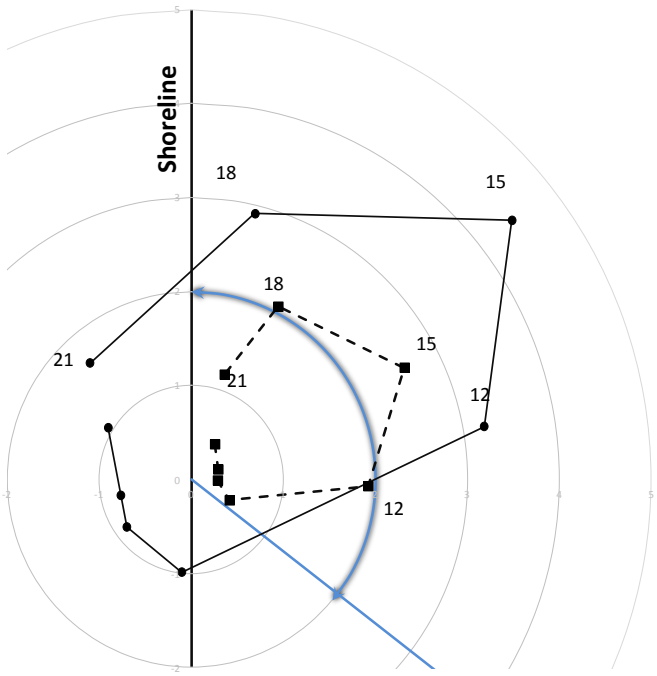

Figure 4.14. Sea breeze (solid line) and non-sea breeze days (dashed line) hodograph (1955-2007) for Adelaide airport. The sea breeze sector (180°-320°) is illustrated as a blue curve. The circles show the wind speed at the interval of 1 m/s.

Evidently, on sea breeze days, the shoreline is facing a complete rotation from onshore to offshore with the maximum wind intensity happening around 15:00 local standard time.

For the period 1985-2007, where the half hourly surface observation is available, the time of sea breeze onset and cessation have been analysed. Therefore the time that an onshore wind intensity increases or an offshore wind shifts to the sea breeze sector (from 180 to 320 degrees), has been considered as the start of the sea breeze, and the rotation of wind to offshore direction or a decline of its strength has been assumed as its end.

As one of the characteristic parameters of a sea breeze day, the frequency of average time of start, end and maximum sea breeze intensity are plotted in Figure 4.15.

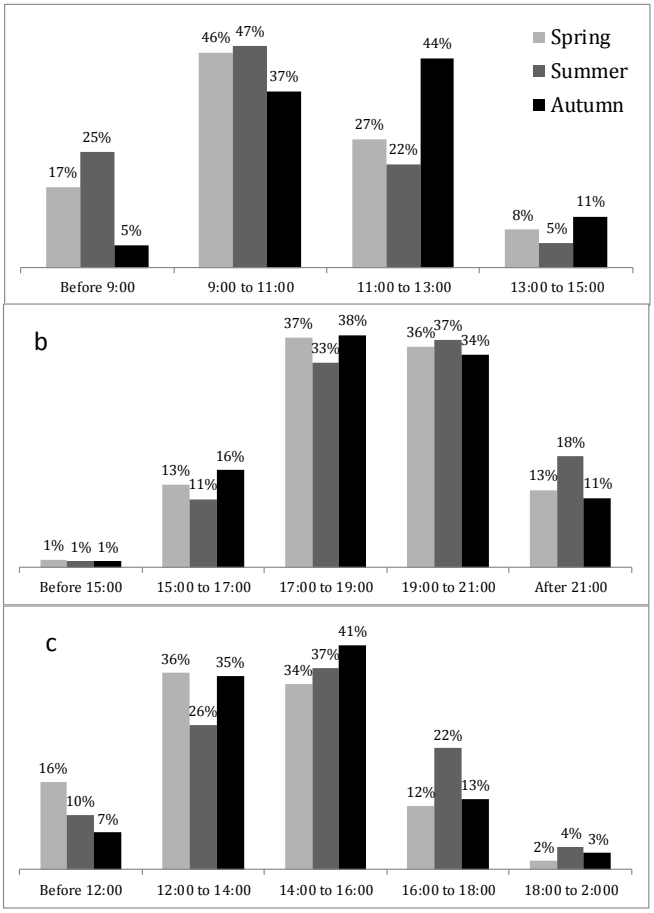

Figure 4.15. The frequency of time of sea breeze start (a) cessation (b) and maximum (c) (1985-2007) in each season.

As the number of sea breeze cases in winter months (June, July and August) is relatively low (less than 10 % of the winter days), these months were excluded from the figures.

Apparently sea breezes start comparatively later in autumn than summer and spring, which is related to approximately 1 hour's delay in the time of sunrise. It is also observed that the summer sea breezes cease relatively later than in the other two seasons, attributed to the 14 hours duration of daytime compared to autumn and spring with 11.3 and 12.9 hours.

Where most sea breezes of spring and autumn reach their maximum intensity sometime between 12:00 to 16:00 hours, there have been 22% of cases in summer, where the

maximum sea breeze reaches the Adelaide Airport after 16:00. The most observed time of sea breeze start, end and maximum for each month is plotted in Figure 4.16.

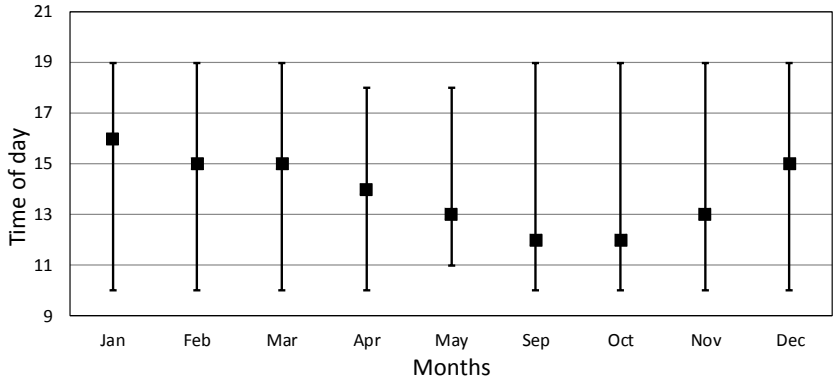

Figure 4.16. Monthly averages of sea breeze start-end and maximum (1985-2007).

For each month (excluding winter) the maximum sea breeze intensity is averaged over the period of 1985-2007. The result suggests a maximum wind velocity of 7.1 m s^{-1} in January to 4.9 m s^{-1} in May, while the direction on which the wind blows is constantly from south west (varies from 225 degrees in January to 256 in September).The maximum wind velocity and associated direction is shown in Figure 4.17.

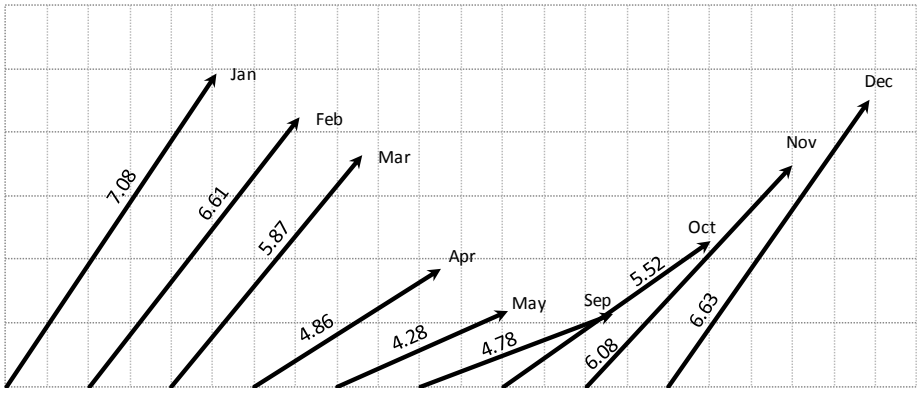

Figure 4.17. Average of maximum sea breeze direction and speed (1985-2007). The numbers on the arrows are the wind speed in m s^{-1}.

It is evident in Figure 4.17 that the maximum wind intensity on sea breeze days has a considerably stronger southerly component during the warmer months of December to February, whereas in September the maximum wind approximately blows from the direction perpendicular to the shore line.

4.8. Analysis and discussion

The annual percentage of sea breeze occurrences for the period 1956 to 2007 is plotted in Figure 4.18. Analysis shows that there is not any significant change to the frequency of sea breeze events for the period of the study, however the number of selected sea breeze days does vary with time.

On the other hand, the intensity of the afternoon wind has shown a distinctive trend for the same time period. Section 4.5 has addressed these changes extensively and Table 4.1 demonstrates the summary of the time where the changes were observed.

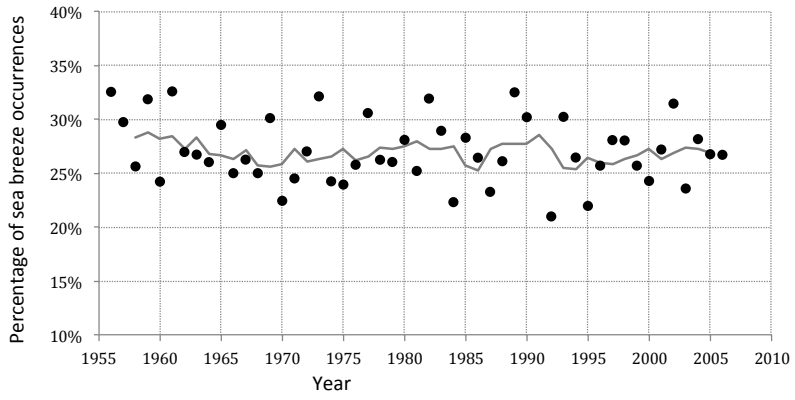

Figure 4.18. Percentage of annual sea breeze events for the period of 1956-2007, the line shows the 5-year moving average.

It is concluded from the results of the statistical analysis of the 3-hourly wind intensity, that irrespective of the season, the 15:00 hour westerly onshore winds in the set of identified sea breeze days are progressively increasing over time, whereas for non-sea breeze days there has not been any significant change to the intensity of the observed

wind. Similarly, the 21:00 hour easterly wind on sea breeze days has shown a comparative increase of velocity, the only exception is in autumn where non-sea breeze days have followed a similar growth pattern to non-sea breeze days. Moreover, the easterly wind at 12:00 in summer and 18:00 in spring are suggesting an increasing trend in the intensity.

Table 4.8 The time of observed significant increase of the component of afternoon and evening winds

	Spring		Summer		Autumn	
	sea breeze days	Non sea breeze days	sea breeze days	Non sea breeze days	sea breeze days	Non sea breeze days
U	15:00, 18:00, 21:00	-	15:00, 21:00	-	15:00, 21:00	21:00
V	18:00, 21:00	-	18:00, 21:00	21:00	15:00, 18:00, 21:00	15:00, 18:00, 21:00

For the south-north wind direction, there is a greater tendency of intensification in the late afternoon southerly wind speed. This is the time that has been documented for the arrival of the Southern Ocean breeze in the Adelaide region, normally with some delays from the near shore observations. In most cases, either the increase only was observed for sea breeze days or the growth rate for sea breeze cases has been predominantly greater than for non-sea breeze days.

As the maximum intensity of gulf breezes previously observed to arrive on land by mid-afternoon, followed by late arrival of ocean breeze (Physick and Byron-Scott, 1977), the growth of the 15:00 hour westerly wind and the 18:00 hour southerly wind indicate the presence of a progressive modification to the driving forces behind the sea breeze.

The correlations between the average intensity of the wind component for each subsequent reading are summarized in Table 4.9. The high correlation factors shown for the V readings (0.86 to 0.96) demonstrate that the southerly winds (V) are generally caused by synoptic scale flows that are steady over the whole afternoon. This is similar for the non-sea breeze days' westerly winds (U) where the correlations vary between 0.84 and 0.87. On the other hand, because the sea breeze days westerly components are considered to be result of locally generated winds, they vary independently and have much lower correlation coefficients (0.32 to 0.44).

Table 4.9 The correlation between each afternoon wind component and the next reading.

	U			V		
	12:00 and 15:00	15:00 and 18:00	18:00 and 21:00	12:00 and 15:00	15:00 and 18:00	18:00 and 21:00
Sea breeze days	0.44	0.40	0.32	0.87	0.88	0.86
Non-sea breeze days	0.84	0.87	0.85	0.96	0.96	0.96

Examples of the correlation are plotted in Figure 4.19.

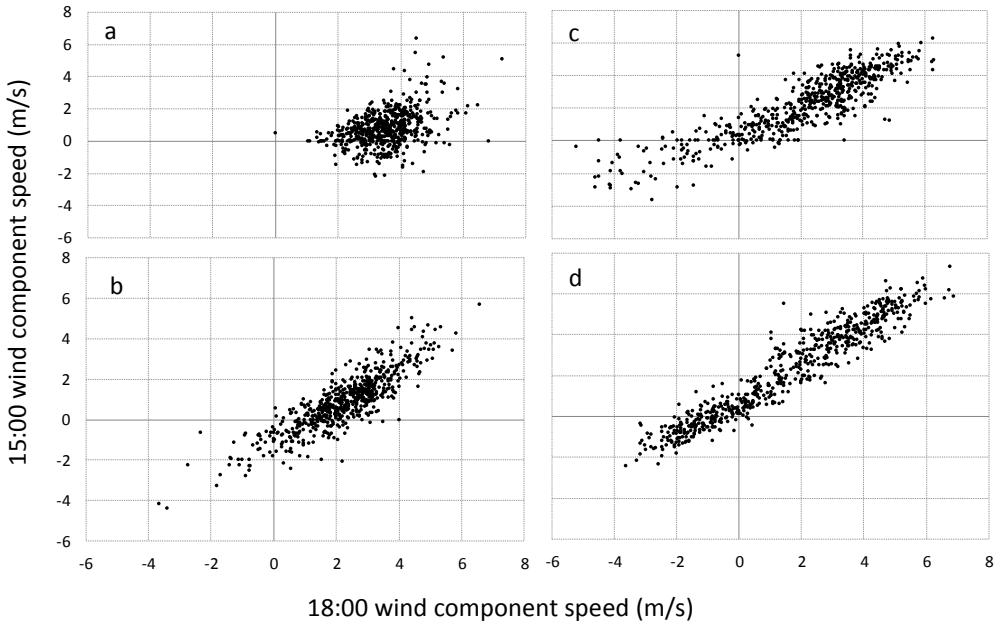

Figure 4.19. The 18:00 (X axes) against 15:00 (Y axes) wind component for Sea breeze days U(a) , V (c) component (m s^{-1}) and similarly for non-sea breeze days (b, d)

4.8.1. Effect of Change to the Land surface temperature

As the temperature difference between the land and sea is the essential causative factor of a sea breeze circulation, it implies that the increase to the intensity of the afternoon wind on sea breeze days might be related to a possible increase in the temperature of land surface or decrease of sea surface temperature which the latter is not supported by the global sea surface warming .To test this hypothesis the data from Adelaide Airport station were used. The anomalies of the 1.2 metre height maximum and minimum

temperature of the station are plotted in Figure 4.20. The anomalies are the departure of temperature from long-term average of 1956 to 2007.

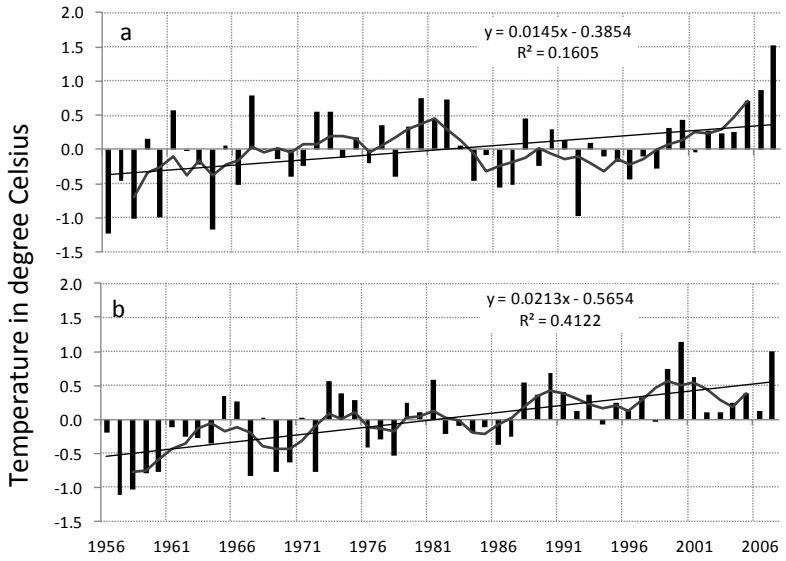

Figure 4.20. Anomaly of 1.2 m maximum (a) and minimum (b) temperatures in Adelaide Airport.

Evidently there are upward trends in both maximum and minimum temperatures. However, as is indicated on the graph, the rate of increase in minimum temperature is considerably higher than that of the daily maximum. One of the main factors that contribute to different daily heating rate is the change of the land surface cover to substances with greater heat storing capacities.

To examine the role of increasing temperature in afternoon wind intensity, the monthly averaged maximum temperatures of sea breeze and non-sea breeze days were compared against the afternoon wind component of south-north and west-east and the results are summarised in Table 4.10. Regardless of the day's categorization as sea breeze or non-sea breeze , the afternoon southerly winds intensity, associated with continental sea breeze, are significantly correlated (0.63 to 0.81) with the maximum daily temperature, so that the increase of wind velocity in these cases can be partially explained by a rise in maximum daily temperature.

Table 4.10 Correlation coefficient between monthly averaged U and V components of wind and maximum temperature for sea breeze and non-sea breeze days.

		15:00	18:00	21:00
U (west-east)	Sea breeze days	0.08	-0.12	-0.48
	Non-sea breeze days	-0.22	-0.22	-0.30
V (south-North)	Sea breeze days	0.63	0.73	0.66
	Non-sea breeze days	0.75	0.80	0.81

Given that the V component of afternoon wind is mainly associated with the arrival of the ocean breeze, while the U component is mainly attributed to the locally generated gulf breeze, distinctly higher correlation demonstrates the role of land surface temperature on ocean breeze intensity. It should be emphasised that the near surface temperature of Adelaide airport station has been used in this analysis and as this station is located in the vicinity of the shoreline and constantly exposed to the cooling effect of onshore winds; its temperature should not be considered as surface temperature of Adelaide metropolitan areas.

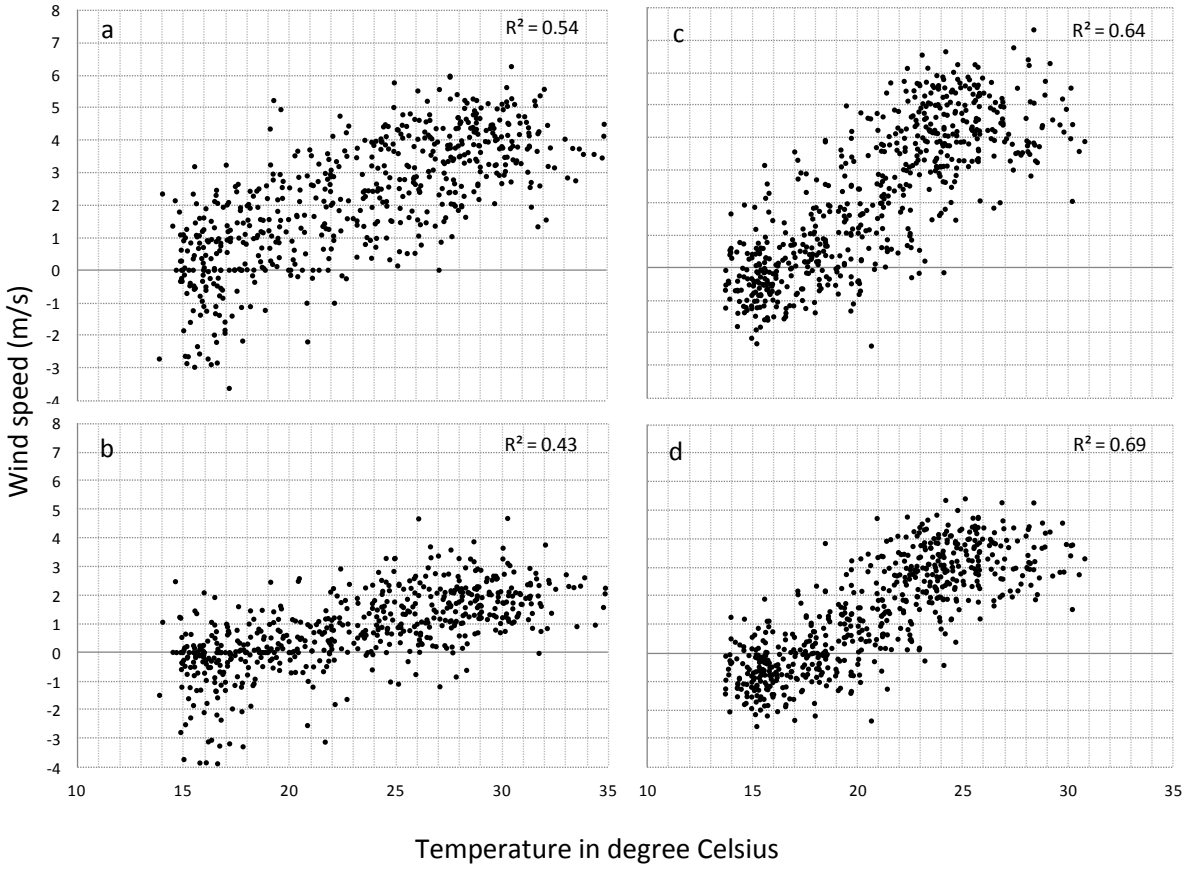

Figure 4.21. Plot of maximum temperature against monthly averaged V components of wind on sea breeze days, at 18:00 (a) and 21:00(b) and non-sea breeze days (c, d respectively) .

As the maximum daily temperature has a strong correlation with the afternoon V component of the wind for both cases of sea breeze and non-sea breeze, the increase in the surface temperature is likely to be the major causative factor of growth of southerly wind components.

Since the warmer months are shown to have higher percentage of sea breeze events, the de-trended values of maximum temperature were compared against the percentage of sea breeze occurrence to identify any correlation. Figure 4.22 shows the percentage of observed sea breeze days against the mean maximum monthly temperature at Adelaide airport. It suggests an increase of 10 percent in the likelihood of sea breeze occurrence in a month if the mean maximum temperature of the month increases by 5 degrees.

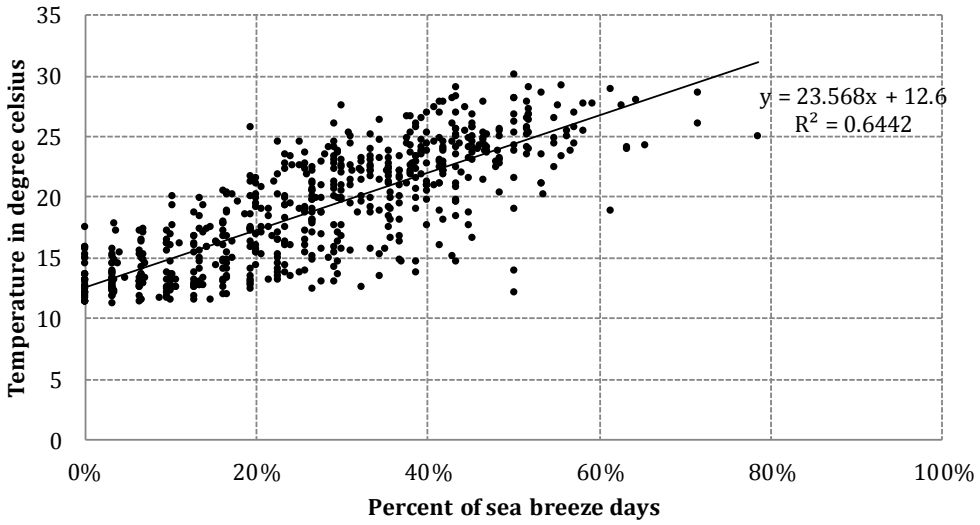

Figure 4.22. Plot of monthly averaged maximum temperature and the percentage of selected sea breeze days.

4.8.2. Effect of Other Climate Drivers

In Chapter 3, the climate drivers for the region of South Australia were discussed of which a few have been characterised, using an index value. As these phenomena generally have an oscillatory pattern, they do not correlate with any continuous events such as temperature trend or, in this case, the intensity of the afternoon winds but it might amplify or lessen them to some extent. Therefore the fluctuations of each component of afternoon wind around the trend line, the de-trended values (Figure 4.23), were compared against the oscillation indices. The phenomena with indices are El Niño - Southern Oscillation, Indian Ocean Dipole and Southern Annular Mode.

The Southern Oscillation Index (SOI) as the monthly averaged pressure difference between Tahiti and Darwin has been recorded since 1876 and the values are provided by Australian Burea of Meteorology (2014b).

The Indian Ocean Dipole (IOD) is measured as the temperature anomaly of the western equatorial Indian Ocean and the eastern part and has been recorded since 1958. The data were provided by the National Oceanic and Atmospheric Administration (NOAA) and

are available from the Japan Agency for Marine-earth Science and Technology database (Jamst, 2014).

The Southern Annular Mode or Antarctic Oscillation Indices (AOI) have been documented since 1979 and are available through the Climate Prediction Centre of the National Oceanic and Atmospheric Administration (Climatic Prediction Center, 2005). It has been calculated from sea-level pressure (SLP) anomalies south of 20S.

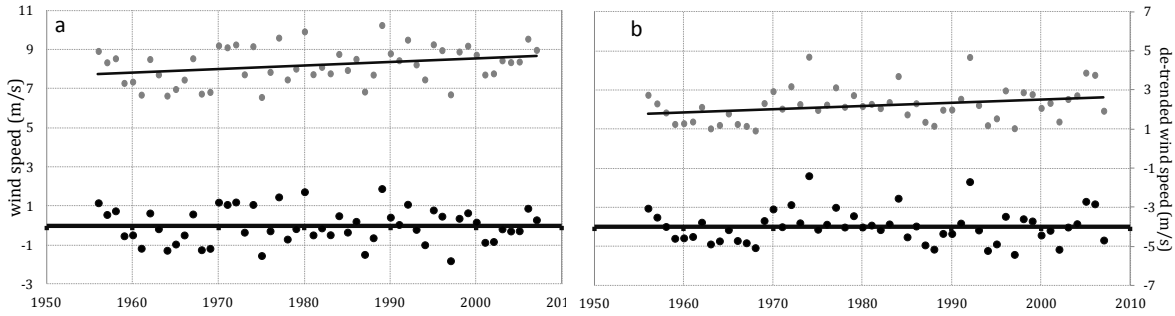

Figure 4.23. Averaged southerly wind component of January 18:00 (a) and 21:00 (b) with actual value (gray dots) and de-trended value (black dots).

Despite the potential for some interactions, correlation analysis of each of the indices with the de-trended monthly averaged wind intensity of each component has shown no significant relation between any of these climate drivers and the intensity of afternoon winds. Although applying 3 years and 5 years filtering increases the correlation for some cases, the high correlations are sporadic and irregular. It does not provide any distinctive conclusion to support the hypothesis of the presence of any significant correlation between one of the indices and the afternoon wind components. The results of the analysis are attached in Appendix B.

4.8.3. Effect of local climate drivers and urban heat island

The comparison of the afternoon wind component with the land surface temperature and driving forces of the South Australian climate have verified the climatic forces behind an increasing trend of afternoon northerly wind component of both sea breeze and non-sea

breeze days and afternoon easterly component of non-sea breeze days, however there has not been any relation between afternoon U-component of sea breeze days with these elements. As the westerly sea breezes of the coastal city of Adelaide have been generated over the Gulf St Vincent, it is more likely to be driven by local climatic forces.

With a growth of more than 150 percent in the population of Adelaide metropolitan area from 1954 to 2011(Australian Bureau of Statistics, 2012), shown in Figure 4.24, the dwelling density of the city has increased significantly. This change will not only increase the energy consumption but is also accompanied with a conversion of natural land surfaces to buildings and roads. Therefore the city's local environment is going through an increasing anthropogenic modification that leads to formation of an urban heat island.

The ongoing development of urban areas with heat-holding structures generates heat storage processes during the daytime, and increases the sensible heat flux. As a result, the air above the urban canopy, in absence of any considerable anthropogenic heat, have been observed to increase to a similar temperature as nearby rural areas in daytime and significantly higher temperatures at night. However, continuous growth in the population of the city and an increasing demand for energy amplifies the daytime temperatures by increasing the anthropogenic heat emission. This fact, along with the increase of residential density, contributes to a modification of the surface energy balance and can result in greater surface temperatures of the region.

Figure 4.24 shows the distribution of population density in metropolitan area and the residential development during 1910-2011, denoting the CBD residential density to be lower than nearby suburbs.

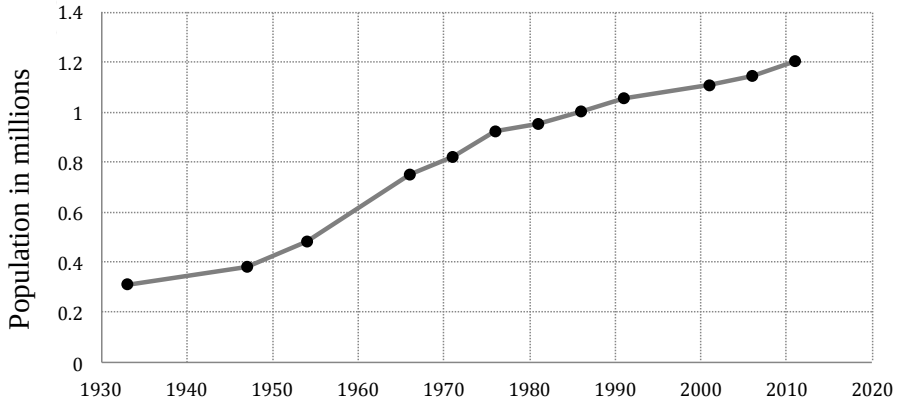

Figure 4.24. Adelaide Metropolitan population (Australian Bureau of Statistics, 2012).

The majority of the growth and expansion of Adelaide metropolitan has occurred between 1960 and 1986, with a conversion of north-east and southern surroundings.

As explained in the literature review (Section 2.7.4), the concurrence of urban heat island circulation and sea breeze circulation, in coastal cities, has been known as an interaction of two circulations, which might enhance or diminish one another. Therefore, in the case of the developing city of Adelaide, there is a possibility of afternoon wind increase being linked to the continuous change of the urban surface. Apart from the increase in the anthropogenic heat in urban areas, the expansion of the city results in change to the thermal property of material and the surface roughness.

It has been discussed in Section 2.4 that the change to the heat balance of the surface in urban areas, forms a relatively warmer land surface and in the case of coastal cities this results in stronger sea breeze activities. At the same time, a rise in the height of the buildings will lead to an increase in the roughness length of the surface. As the near surface wind speed is determined by surface friction force, an increase to the roughness length decreases the propagation speed of sea/land breezes.

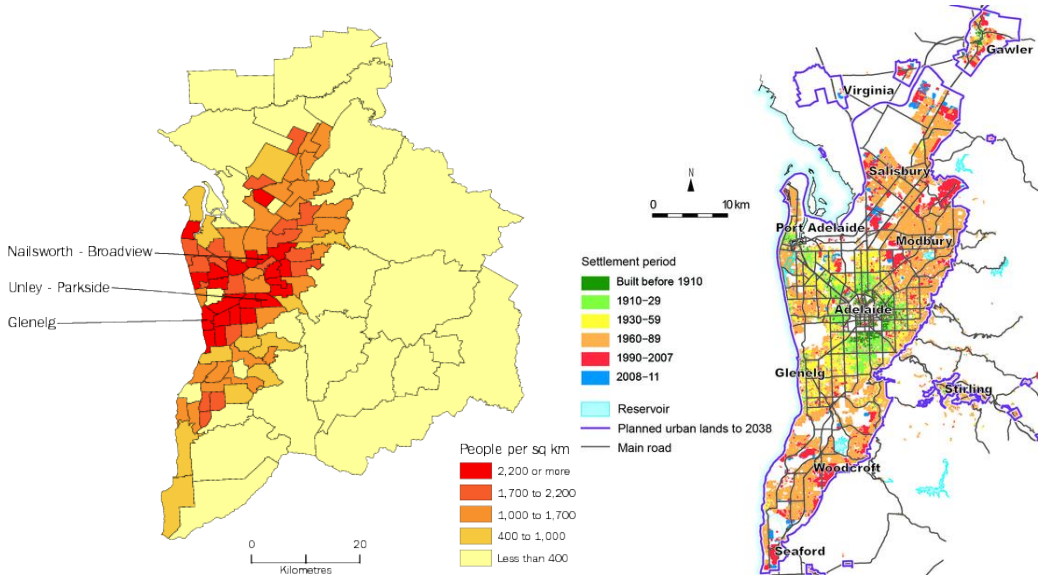

Figure 4.25. Adelaide City expansion since 1910 (State of Environment, 2011) on right and population density in 2012 (Abs, 2013) on left.

To test the possible contribution of land development and urbanization on the characteristic of afternoon wind regime, the weather of the region was reproduced using a sophisticated numerical model: Weather Research and Forecasting (WRF). The simulations were conducted for two different land covers: one with the urban in its current condition, and the other with urban being replaced by its previous native vegetation. In the next chapter, the possible changes to the near surface wind conditions are discussed and the changes to the sea breeze intensity examined.

5. Numerical Modelling of the urban climate

In the previous chapter, the long-term changes to the southerly and westerly components of the afternoon wind were discussed and it was concluded that the increase of land surface temperature has significantly contributed to the long-term growth of the southerly component of afternoon winds, which are largely associated with the arrival of the continental ocean breeze. However, comparison of the westerly components of wind with the various driving forces of South Australian climate did not show any correlation.

As mentioned in the previous chapter, the study of the South Australian sea breeze by Physick and Byron-Scott (1977) suggested that the afternoon westerly component of the sea breeze is associated with a locally generated sea breeze, referred to as the gulf breeze, and this implies the possibility of the effect of urban-modified weather (anthropogenic climate modification) on the wind characteristics of the Adelaide metropolitan area.

Previous studies have suggested the presence of an urban heat island over the city of Adelaide (Coppin, 1979; Oke, 1982; Elnahas and Williamson, 1997; Erell and Williamson, 2007) where Erell and Williamson (2007) have found a temperature difference of 6.7 °C at sunrise between the CBD and the parklands ring around the city. This suggests the presence of a nocturnal urban heat island over the area. It has also been concluded that during the day, ignoring the considerable anthropogenic heat, the city centre would be cooler than the surrounding area, owing to the effects of street canyons.

In this chapter the contribution of Adelaide metropolitan areas establishment and growth to the local climate of the Adelaide plain is assessed by simulating the weather of the region. For this purpose, the Weather Research and Forecasting model (WRF) was chosen from several numerical modelling options, due to its proven capability to simulate the weather of coastal cities (Lin *et al.*, 2008; Evans and Matthew, 2010; Chen

et al., 2011; Mohan and Bhati, 2011; Carvalho *et al.*, 2012a; Evans *et al.*, 2012; Hernández-Ceballos *et al.*, 2013).

The simulations were conducted for two case scenarios: the first a control run (CTL), which replicates the weather of the area with its present condition as an urban, built-up area, and the second a run with the metropolitan area being turned back to its native vegetation (NTV) as reported in Bradshaw (2012). It should be noted that the conversion of the land does not include cropland and pastures.

5.1. WRF model principles

The Weather Research and Forecasting (WRF) model was developed by collaboration between the US National Center for Atmospheric Research (NCAR), the US National Centers for Environmental Prediction (NCEP), the US National Oceanic and Atmospheric Administration (NOAA), US Forecast System Laboratory (FSL), the US Air Force Weather Agency (AFWA), the US Naval Research Laboratory, the University of Oklahoma and the US Federal Aviation Administration (FAA) and provides multi-nested domains to facilitate broad use across scale ranges from metres to thousands of kilometres and offers multiple dynamic cores and physical schemes. The model contains sets of preliminary processing programs known as WPS (WRF Pre-processing System), for producing initial and lateral boundary conditions, which converts existing gridded data from an external source (including meteorological data, topography and land use index) to a WRF legible format. Later the data will be processed with forward integration by the Advanced Research WRF (ARW) solver. The major features of ARW and the governing equations were discussed in the literature review in Section 2.9.3.1.

5.2. Models initial and boundary conditions

The WRF model's pre-processing system, WPS, produces the initial and lateral boundary conditions for WRF, supplied by the operational global reanalysis datasets

(final data analysis) from the US National Centers for Environmental Prediction (NCEP FNL). The data are produced by the Global Data Assimilation System (GDAS), using observational data, collected by Global Telecommunications System (GTS)and other sources. These data include the surface pressure, sea level pressure, geopotential height, air temperature, sea surface temperature, soil temperatures moistures and liquids, ice cover, mixing ration for rain, cloud and ice, relative humidity, u- and v- winds, vertical motion, vorticity and ozone concentration on a 1.0 × 1.0 degree grid and were provided every six hours, since August 1999, for 36 sigma levels from the surface to 50 mb by the US National Centers for Environmental Prediction (2000). In the vertical, level data are available for total of 26 mandatory levels from 1000 mb to 10 mb, in the surface boundary layer, and at some sigma layers, the tropopause, and a few others.

The terrestrial input data in the Model are adapted from NESL's Mesoscale and Microscale Meteorology Database which provided land use and topography data with a resolution of 10 minutes, 2 minutes and 30 seconds.

In order to be able to simulate the area in a high resolution of 3 km by 3 km, the option of two-way nesting was used. This option allows the model to simulate all domains simultaneously and interpolate the finer grid boundary condition from coarse grid forecasts and replace the data from one domain to another at any time step.

With the limitation of downscaling ratio of maximum 5, the 1 degree by 1 degree (approximately 111.12 km) input files needed to go through telescoping nesting to a parent domain (D1) of 27 km by 27 km, modelling the central and eastern Australia, to a second domain (D2) of 9 km by 9 km, covering South Australia, and to the finest domain (D3) of 3 km by 3 km. which is centred at latitude 35.39^{o} south and longitude of 137.85^{o} and spanning the Adelaide plain, Gulf St Vincent, Yorke Peninsula and Kangaroo Island. The location and dimension of the three domains are shown in Figure 5.1.

Figure 5.1. Layout of model domains, D1, D2 and D3, with enlarged Domain 3 shown on the right (Google Earth, 2013).

5.3. Simulation set-up

The outputs from WPS were fed to the WRF modelling system for reproduction of the weather over southern Australia, with the finer domain located over the metropolitan area of Adelaide.

The WRF model allows different physical parameter combinations to simulate different climate zones. Out of all possible combinations, the WRF/Noah LSM/Urban-Canopy Coupled Models were adopted in order to represent the nature of man-made surfaces of the urban canopy, including shadowing from buildings and surface reflection.

The NOAH land surface model was added to the PSU/NCAR mesoscale model of MM5 and, as described by Chen and Dudhia (2001), is able to reproduce the seasonal variation of soil moisture and represent the dynamics of land forcing at fine scales. The model is a 4-layer soil temperature and one layer canopy model in which the root zone, evapotranspiration, soil drainage and runoff have been considered. Coupled with the urban canopy model, this model improves the urban simulation and considers the surface

emissivity and surface albedo to provide the sensible and latent heat flux to the boundary-layer scheme.

In this study, the Noah LSM is coupled with a single layer urban canopy model (Figure 5.2). This model, introduced by Kusaka *et al.* (2001) considers the urban geometry, shadowing effects of buildings, the logarithmic profile of the wind, and energy and momentum exchange between the urban surface and atmosphere to provide the surface temperature in, and heat fluxes from roof, wall and roads. The three different categories of density of urban area, and the added option of an anthropogenic diurnal heating cycle allows more accurate simulation of the urban heat island effects.

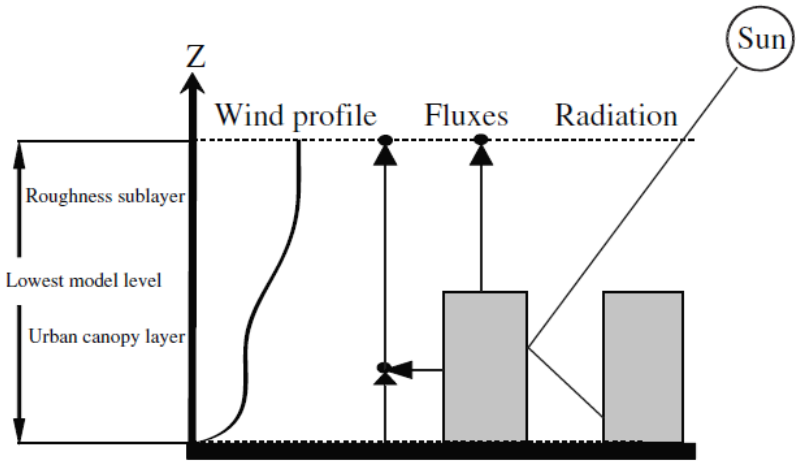

Figure 5.2. Schematic of single-layer urban canopy model (from Chen *et al*., 2011)

Other physical options that were selected for the current study include:

- Microphysics scheme of WRF Single Moment 3 classes (WSM3): Three hydrometeor categories of vapour, cloud water/ice and rain/snow make the scheme computationally efficient and result in a realistic distribution of clouds and an increase in the accuracy of the vertical heating profile of the freezing/melting processes (Hong *et al.*, 2004). As the simulated area of southern Australia generally does not experience days with temperatures below freezing,

the WSM3 is sufficiently capable of simulating thunderstorms and heavy rainfalls, two more observed types of weather in the region.

- Radiation Schemes: the absorption, reflection, emission and scattering process in the atmosphere and at the surfaces are provided by radiation schemes; hence these are the main forces that regulate the surface energy budget. Clouds, water vapour distribution, and the concentration of carbon dioxide, ozone and trace gases control the radiation within the atmosphere. The temperature at the surface and the height of the planetary boundary layer are governed by accurate calculation of both shortwave and longwave radiation. WRF radiation schemes treat the atmosphere in individual columns with a thickness of much less than the horizontal grid length(Skamarock *et al.*, 2007).

- The NCAR Community Atmosphere Model (CAM) for shortwave and longwave radiation scheme: with 19 discrete intervals for shortwave and 2 for the longwave spectrum, this scheme has the ability to handle the optical properties of several aerosol types and absorption by trace gases. The scattering and absorption of cloud water droplets is included. The cloud cover fraction is calculated and in unsaturated regions the overlapping assumption is used (Skamarock *et al.*, 2007). Having been applied in many climate scenarios, the scheme has been extensively evaluated and has been confirmed to perform well when combined with Noah LSM (Mooney *et al.*, 2012; Warrach-Sagi *et al.*, 2013).

- The Eta surface layer scheme follows Janjic (2002) and is based on the similarity theory of Monin and Obukhov (1954). This scheme provides meteorological variables in the first vertical layer including the surface layer and the typical observational heights of 2 m for temperature and 10 m for wind and the transfer coefficient is calculated by the similarity theory. It calculates friction velocities that provide the surface heat and moisture fluxes for the planetary boundary layer

schemes. There are three particular boundary layer options, from which the Bougeault and Lacarrere scheme was selected for this study.

- Planetary boundary layer BouLac scheme of (Bougeault and Lacarrere, 1989) is classified as one-and-a-half order Turbulent Kinetic Energy (TKE) closure scheme. The comparison studies of different planetary boundary layer schemes under stable condition by Shin and Hong (2011) has shown better performance for simulation in which the BouLac scheme was applied. Simulation of thinner surface layers and local vertical mixing are only possible when TKE schemes are chosen. Providing a consistent prediction of TKE, the BouLac scheme performs better in experimental verifications.

The terrestrial input data for simulation CTL has been adapted from NESL's Mesoscale and Microscale Meteorology Database which provides land use and topography data with a resolution of 10 minutes, 2 minutes and 30 seconds and 24 categories of USGS land use parameters.

As mentioned earlier, to study the effect of an increase in the area of the urban and suburban built up areas on wind characteristic, in a separate simulation (NTV) the land cover of the metropolitan area of Adelaide was converted back to its native vegetation. Therefore the pre-European vegetation were adopted from a National Vegetation Information System (NVIS) provided by the Department of Sustainability, Environment, Water, Population and Communities of Australian Government (2007). As the data set suggests (Figure 5.3), the majority of native vegetation of Eucalypt Woodlands, Mallee woodland, scrubland which covered the Adelaide plain and surrounding areas including Yorke Peninsula and Kangaroo Island, were converted to cropland, building and roads and non-native vegetation.

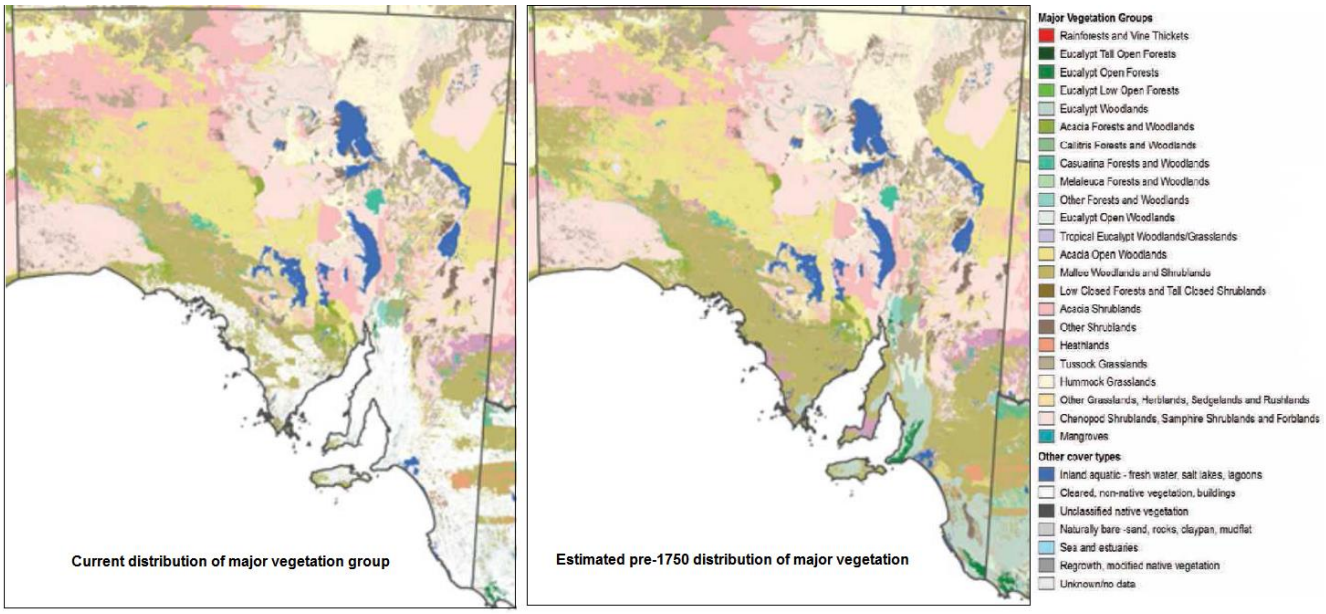

Figure 5.3. The change of vegetation in South Australia since 1750 (Department of the Environment and Water Resources, 2007).

The WRF model gets the land use, vegetation and soil parameters from the tables provided in the program. It also has the ability to use the USGS 24 land use categories which classifies the urban category as urban and built up, from which the chosen characteristic was second category (high density) in an urban parameter table (URBPARM.TBL).

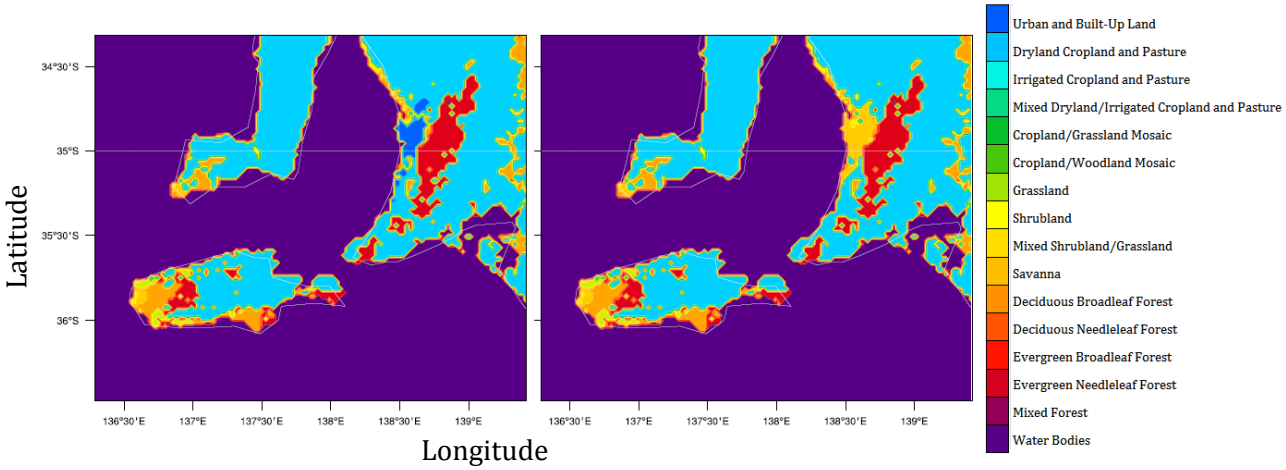

Figure 5.4. Land cover index from the model for CTL simulation (left) and NTV (right).

The values in the table were modified to address the current spatial distribution of population density. Figure 5.4 shows the land cover index of both simulations and Table 5.1 lists the values of physical parameters for the land cover of metropolitan for different simulations.

Table 5.1 Physical parameters of different land covers of metropolitan area.

Land Category	Urban and Built up (average building height= 5 m)		Mixed scrubland and grassland
Albedo	roof building wall ground	0.2 0.2 0.2	0.22~0.3
Emissivity	roof building wall ground	0.9 0.9 0.95	0.93~0.95
Fraction of urban land without vegetation	0.80		--------
Anthropogenic heat (W m^{-2})	35		--------

The categorization of the 3 classes of urban density, included as a property of each class in the urban parameter table, is based on the height of buildings and the width of the road and roofs. As the grid size of the finest domain is 3 km by 3 km, the exact simulation of the metropolitan area is not possible and so the values of the urban table were modified to address the characteristics of most of the Adelaide suburbs. Therefore the urban area has been modelled as a relatively high density residential area with an average height of 5 m for buildings with standard deviation of 3m, roof and road width of 9.4m and 20 percent of the land covered with natural vegetation.

5.4. Validation of model

The simulations were originally conducted for a period of a year starting from 1st January to 30th December of 2005. This period has been selected so that the model could

be evaluated for different locations around the Gulf and over the Adelaide Hills as hourly observation for different meteorological stations around Adelaide Airport and other side of the Gulf were available for this time period. There are 7 stations in the study area with valid observations for the period of 2005, as shown in Figure 5.5, and for which the results of simulation with current land cover could be evaluated for surface temperature, wind direction and wind speed.

Figure 5.5. Location (displayed by red flags)of available meteorological stations for the period of simulation(Google Earth, 2013), Adelaide metropolitan area is shown by yellow line.

As illustrated in the Figure 5.5, Adelaide Airport, Kent Town, Parafield and Edinburgh RAAF stations are located inside the metropolitan boundary and the Mount Lofty station is sited east of the range. The Edithburgh and Kingscote meteorological stations record the data of two small towns in Yorke Peninsula in the west and Kangaroo Island in the south of Gulf St Vincent.

5.4.1. Statistical Metrics

The model's performance was evaluated using the following statistical measures:

- r (the Pearson correlation coefficient)

The coefficient r determines the strength of linear relationship between model and observations and is represented by:

$$r = \left[\frac{\sum_{i=1}^{N}(O_i - \bar{O})(M_i - \bar{M})}{\sqrt{\sum_{i=1}^{N}(O_i - \bar{O})^2 (M_i - \bar{M})^2}} \right] \quad 5.1$$

- RMSE (Root mean square error)

The RMSE considers error compensation due to opposite sign differences and is calculated as

$$RMSE = \sqrt{\frac{\sum_{i=1}^{N}(O_i - M_i)^2}{N}} \quad 5.2$$

- Index of agreement (IA)

This dimensionless index determines the model skill in predicting the variations about the observed mean, and is calculated as

$$IA = 1 - \frac{N.RMSE^2}{\sum_{i=1}^{N}(|O_i - \bar{O}| + |M_i - \bar{O}|)^2} \quad 5.3$$

- Bias error

The mean bias provides the information on the overestimation/underestimation of any variable by the model and is defined as:

$$MB = \frac{1}{N}\sum_{i=0}^{N}(O_i - M_i) \qquad 5.4$$

In the equations, the summations are performed over the total number of model-observation pair values (N) and O_i and $M_i$represent the i^{th} observed and modelled values and $\bar{O}$ and $\bar{M}$ are the averaged values for the observations and model, respectively.

The results of statistical comparisons in 7 mentioned locations and for 3 variables are summarized in Table 5.2.

Table 5.2 Statistical evaluation of simulation of temperature, wind speed and direction at different locations.

	Temperature				Wind speed (m/s)				wind direction			
	IOA	r	RMSE (°C)	MB (°C)	IOA	r	RMSE (m/s)	MB (m/s)	IOA	r	RMSE (degree)	MB (degree)
Adelaide Airport	0.96	0.92	2.23	-0.11	0.83	0.70	2.19	0.36	0.94	0.89	53.32	-1.88
Edithburgh	0.94	0.89	2.15	0.30	0.82	0.69	2.02	0.20	0.96	0.92	43.03	-1.01
Edinburgh RAAF	0.96	0.93	2.44	0.18	0.80	0.53	2.19	-0.09	0.93	0.88	57.06	-2.14
Parafield	0.96	0.93	2.57	-0.32	0.77	0.62	2.26	0.74	0.93	0.88	57.12	6.58
Mount Lofty	0.87	0.84	4.25	2.65	0.72	0.57	2.82	-0.01	0.92	0.86	63.81	13.18
Kent Town	0.96	0.93	2.39	-0.03	0.62	0.52	2.91	1.91	0.93	0.87	59.58	6.67
Kingscote	0.91	0.84	3.05	0.47	0.73	0.58	2.70	1.19	0.94	0.89	55.92	-1.37

The proposed configuration of the model's physical scheme reproduces the surface temperature with RMSE below 3° C in most cases. The positive value of mean bias error in Edithburgh, Edinburgh RAAF, Mount Lofty and Kingscote stations demonstrates overestimation of the variable for these four locations while other sites show an underestimation of less than 0.5 degree in temperature predictions. The 0.96 of index of agreement for Kent Town supported by a correlation of 0.93 and mean bias error of close to zero, demonstrates the model's capability to predict the heat island that is developing in the urban areas.

The wind speed has a satisfactory performance, with the highest correlation of 0.70 for the Adelaide Airport station. The ability of the model to simulate the wind intensity inside the urban canopy (Kent Town) is poor with the mean bias value of 1.91 ms^{-1}, that is attributed to underestimation of aerodynamic roughness length over the urban area. With an average of 0.36 ms^{-1} mean error bias in wind speed, the Adelaide airport values are slightly overestimated.

With the index agreements of between 0.92 and 0.96 and correlations of between 0.88 and 0.92, the predicted wind directions are comparatively closest to the observation values, particularly for Adelaide Airport, Edithburgh and Kingscote.

Comparing the results with other studies (Jiménez *et al.*, 2010; Papanastasiou *et al.*, 2010; Mohan and Bhati, 2011; Carvalho *et al.*, 2012a; Carvalho *et al.*, 2012b; Meir *et al.*, 2013) the model performs well and captures the interaction between the urbanized region and the atmosphere in terms of temperature, wind speed and wind direction with similar accuracy. These studies used different datasets for initial and boundary condition, from NCEP (Papanastasiou *et al.*, 2010; Mohan and Bhati, 2011; Carvalho *et al.*, 2012a; Carvalho *et al.*, 2012b) to data from European Centre for Medium-Range Weather Forecast (Jiménez *et al.*, 2010; Meir *et al.*, 2013), and applied various combinations of physical schemes. Regarding the simulation of near surface temperature, Meir *et al.* (2013) have noted a good performance of the model in reproducing extreme heat events over New York city with an average RMSE of 2.5° over 27 sites. A high value of index of agreement (0.8) in temperature prediction has been documented in the study by Papanastasiou *et al.* (2010), however Mohan and Bhati (2011) pointed out that applying different physical schemes slightly affects the performance of the model in simulating meteorological variables.

Similarly the capability of the model in wind reproduction is associated with the selection of the model's parameterization (Mohan and Bhati, 2011), where the results of the statistical analysis of the wind data in research by Papanastasiou *et al.* (2010) have

shown that with a maximum correlation coefficient of 0.97 the model captures the direction of wind with relatively high accuracy. Furthermore, concerning the wind speed, the results of the studies by Jiménez *et al.* (2010) and Carvalho *et al.* (2012a) have shown the weak performance of the model in simulating the areas with regional features such as hills, valleys and mountains. Likewise Papanastasiou *et al.* (2010) has pointed out the underestimation of the model in the surface roughness length while simulating the urban areas.

In order to demonstrate a statistical summary of model performance for different variables and different locations, the Taylor value is also provided. In this application the model is compared to an "observed" reference with the standard deviation of each station being normalized with the respective observed data and its associated root mean square difference (RMSD) plotted in relation to the pattern correlation through Equation 5.5.

$$E^2 = \sigma_O^2 + \sigma_M^2 + 2\sigma_O\sigma_M R \qquad 5.5$$

in which, E is the debiased root mean square difference ($E^2 = RMSE^2 - MB^2$), R is correlation coefficient and σ_O and σ_M are the standard deviations of observation and models values, respectively. The values are normalized by being divided by the standard deviation of the observations. $\hat{E} = \frac{E}{\sigma_O}$, $\hat{\sigma}_M = \frac{\sigma_M}{\sigma_O}$, $\hat{\sigma}_O = 1$.

The comparison of performance of model for different coastal and inland locations is demonstrated in Figure 5.6. The more accurate the results, the closer the values get to the unit radius circle and the unit correlation line.

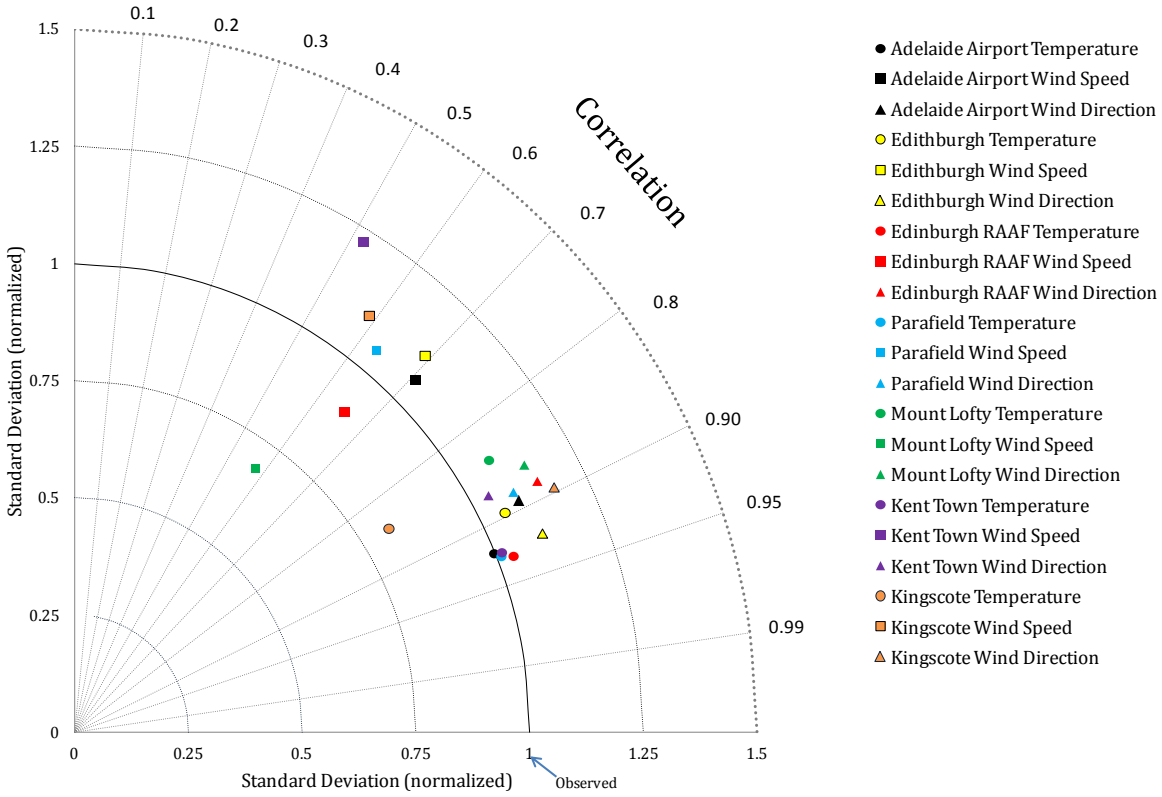

Figure 5.6. Taylor diagram of statistical values for all stations for three variables: temperature (circles), wind speed (squares) and wind direction (triangles).

Better predictions would produce higher correlation with standard deviation closer to the observations. For such simulations the values locate closer the normalized standard deviation of 1 and closer to x-axis (where the correlation is 1).

As shown in Figure 5.6, the modelled temperatures at different stations correspond well with the observations with a correlation of more than 0.8 and identical standard deviations between observed and predicted values for most of the locations. Similarly, the simulated wind directions show high correlation with observed value (0.86 to 0.92) and approximate average of 10 percent higher standard deviation for predicted values. The wind speed behaviour varies for different stations with acceptable performance for Edinburgh RAAF and Adelaide Airport and poor results in Mount Lofty and Kent Town. The lower correlation of the wind results in Kent Town and Mount Lofty is basically due to the location of the meteorological stations, as unlike the airport statins

these two stations are closely surrounded by buildings and woodlands respectively. Overall, as the characteristic of wind at the coastal site of Adelaide Airport is the main interest of the current study, the performance of the model is acceptable.

Examples of the comparison between observed and modelled values of temperature at 2m height, wind speed and wind direction at 10m height for Adelaide Airport for the period of February 2005 are plotted in Figure 5.7.

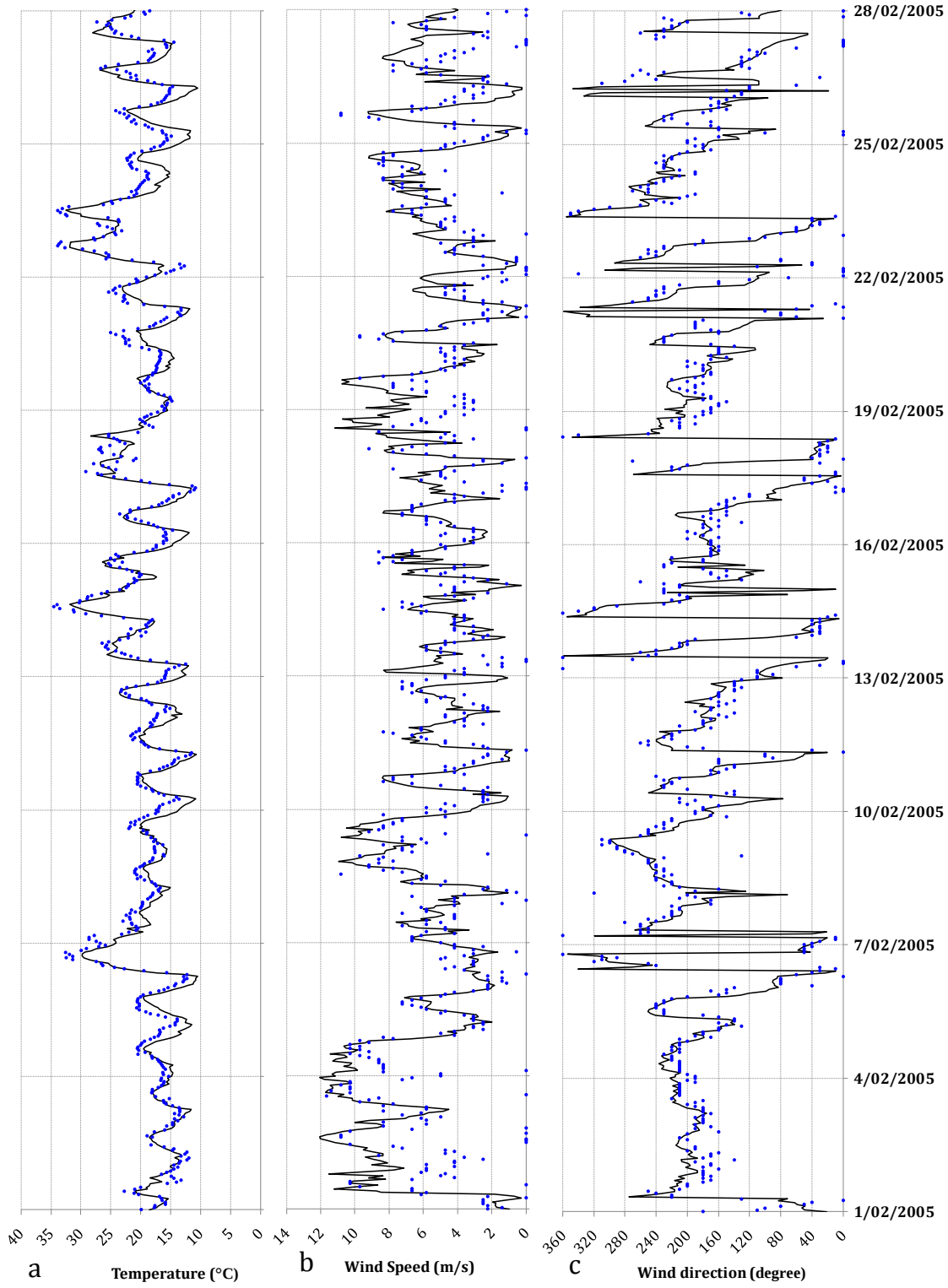

Figure 5.7. The performance of model to simulate 2m temperature (a), 10m wind speed (b) and 10m wind direction (c) in Adelaide airport in February 2005. Blue dots represent the observation and black lines are the model's outputs.

5.5. Modelling Metropolitan with pre-European Land cover

The possibility of a contribution from a change in the land surface cover on the near surface climate was tested by replacing the urban surface with pre-settlement native vegetation. Details of the land cover of the area were provided by the Department of Environment of the Australian Federal Government and suggest the native vegetation to have been eucalyptus woodlands with a tussock grass understorey for the metropolitan area. In order to implement the changes to the model, the urban and built up category of land in the finest scale domain was converted to mixed shrub land and grassland.

The surface friction force is strongly associated with the land surface vegetation and therefore changes to the surface from woodland to built up increases the surface drag force and reduces the near surface wind velocity. Moreover the littoral drift and Aeolian transport at coastline of Adelaide has been discussed to be sensitive to the wind climate over the gulf of St Vincent, therefore and in order to be able to analyse the possible changes to the climate of near surface wind without any friction related disruption, the wind data at a grid point over water were selected for study. As the finest grid lines are sized in 3 kilometres, the adjacent point over the water would be 1.5 kilometres further than shoreline.

5.5.1. Temperature

The change to the temperature at 2 m height at a coastal location (Adelaide Airport) and an inner suburb (Kent Town) are plotted in Figure 5.8. The average daily cycle of temperature at these two points was computed over the period of simulation.

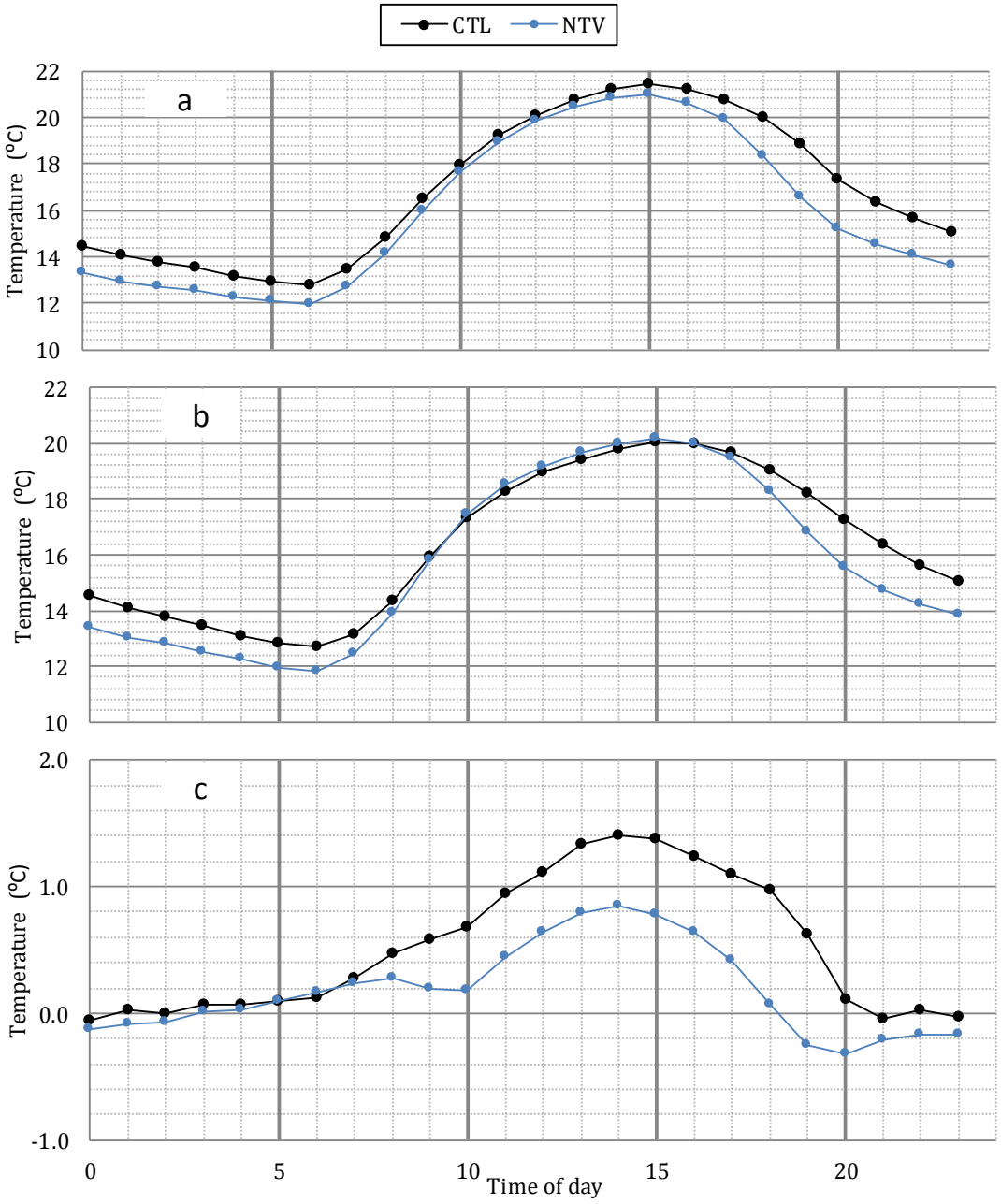

Figure 5.8. The Averaged daily cycle of temperature simulated with current land cover (black) and Native vegetation (blue) at an inner suburb (a), a coastal point (b) and the difference (c)=(a)-(b).

As expected the transformation of land surface from natural shrubby plants to buildings and roads increases the temperature, more noticeably during the night time when there is an absence of solar radiation. It is, as explained in the literature review, the result of re-

emission of stored heat in the urban canopy and therefore the temperature difference is greater in suburban areas. Evidently, the conversion of land surface cover from natural to urban had greater impact on the temperature of the inner suburb than the coastal location. It is clear that the average temperature difference of the mentioned locations is almost doubled during the morning and early afternoon. It confirms the significant impact of urbanization to the local climate change and once more underlines the fact that the observed temperature of the coastal site of Adelaide airport does not reflect the near surface temperature of metropolitan area (Section 4.8.1).

The difference between hourly averaged temperature of the simulation with current land cover (CTL) and simulation with native land cover (NTV) for an inner city location is plotted in Figure 5.9. While for all selected months, the early morning and night time temperatures are distinctly higher in CTL simulation, the time of maximum temperature difference between two simulations occurs around sunset time, which, as shown in the figure, is about two hours earlier in the cold months of May and July.

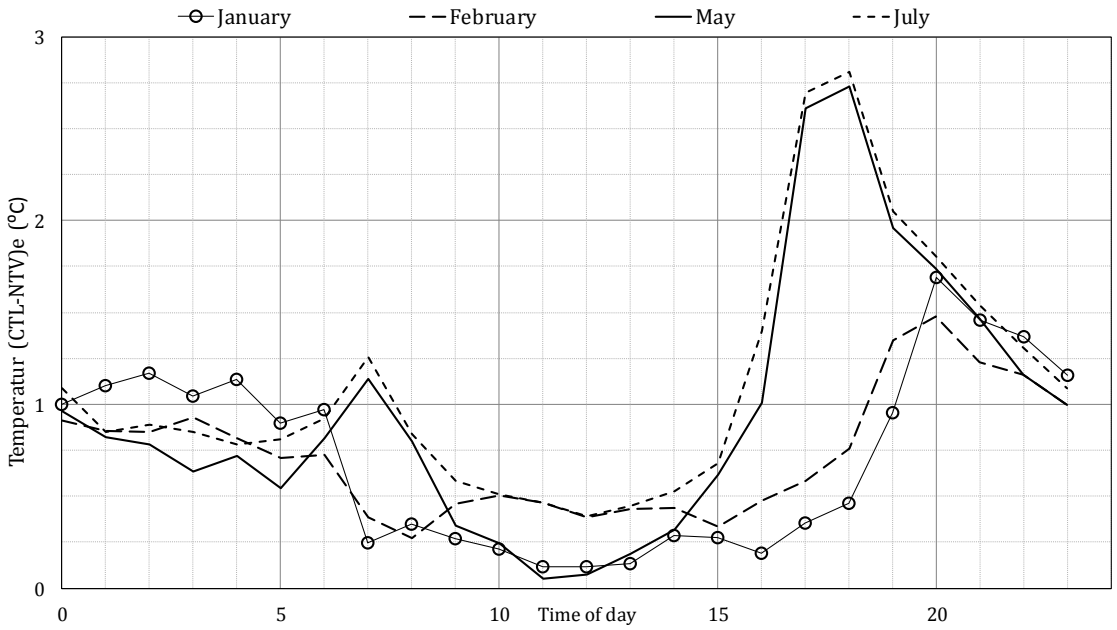

Figure 5.9. The difference between an hourly averaged temperature of an inner city location of two simulation ($T_{CTL} - T_{NTV}$) for two cold months of May and July and two warm months of January and March.

The individual comparison of each time step reveals a variation of between -3.5 and 6.5 degrees between two simulations temperature (considering a subtraction of simulations with native land cover from current surface coverage) for a location inside the city boundary corresponding to Kent Town.

An example of the difference in temperature distribution over the area is plotted for two times of 7 pm in 2005-11-01 and 11 am of 2005-11-12 (Figure 5.10). The dashed line is the latitude location of -35 degree where the southern boundary of city is located.

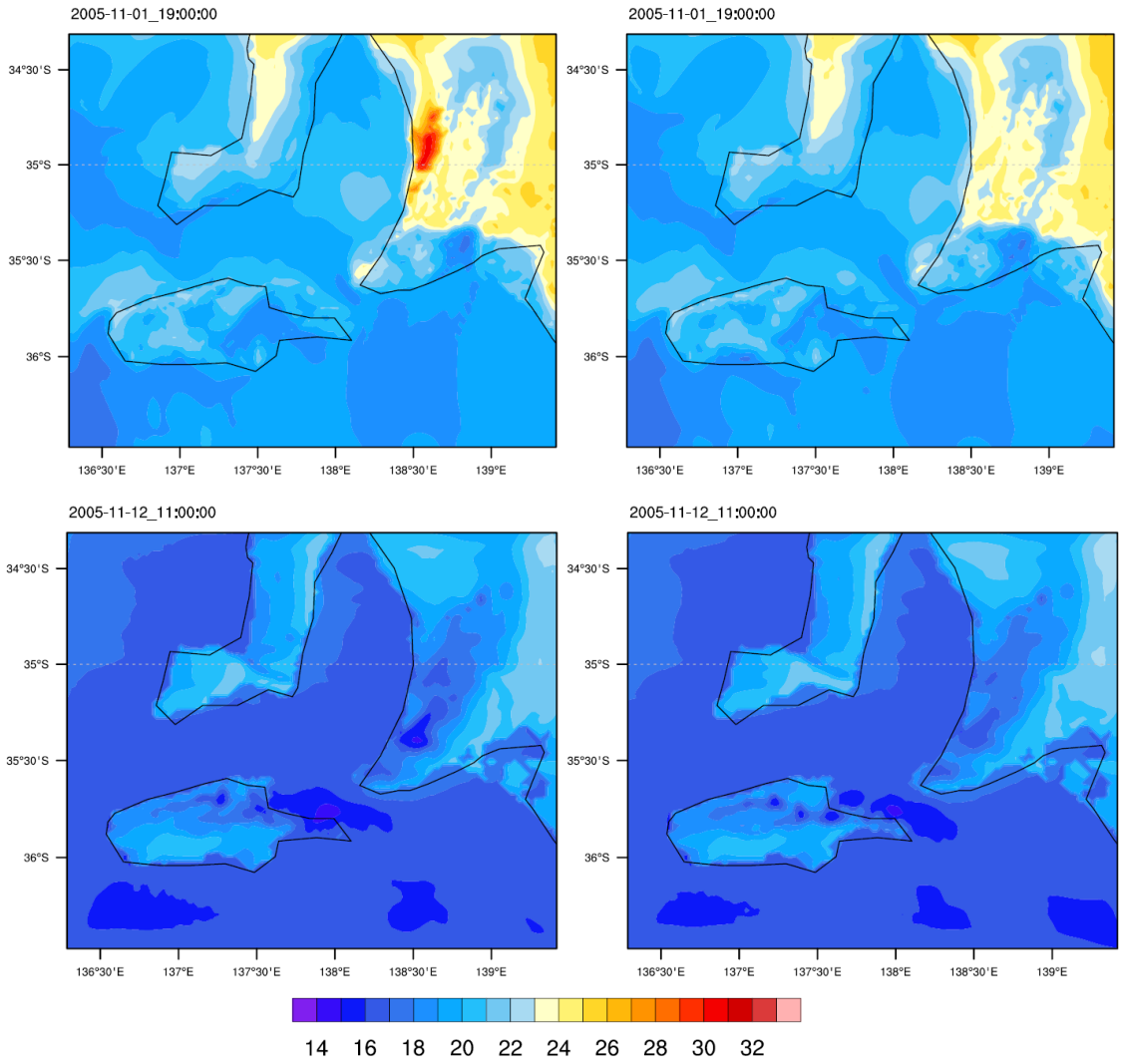

Figure 5.10. Two examples of 2m height temperature (°C) distribution over the area for two times steps; CTL (left) and NTV (right).

As the models have been run in a two-way nesting mode, the feedback from the interior domain at each time step, overwrites the overlapped region of the parent domain. This would lead to the appearance of difference in scales of much bigger than modified land cover scale and therefore the different surface temperature in two simulations may appear at any location (as some can be seen in Figure 5.10). The heated surface of the urban area at 7 pm of November 11 can clearly identify the location of metropolitan area of Adelaide.

5.5.2. Wind Speed

The WRF model generates the south–north (V) and west–east (U) component of the wind as separate variables; therefore the wind speed and direction of each time step were calculated using Equations 5.6 and 5.7.

$$WS = (U^2 + V^2)^{1/2} \tag{5.6}$$

$$WD = ArcTan\left(\frac{V}{U}\right) + 180^{\circ} \tag{5.7}$$

Winds from the west and south are considered as positive.

The analysis of wind speed over the Adelaide metropolitan area has shown an average difference of 0.5 m s^{-1} in the speed at 10 m height between the two simulations. The 13 to 25 of January wind speed for urban areas with different land cover simulation is plotted in Figure 5.11 (this date is just selected as an example). Since the differences are systematic but more noticeable in the high speed winds, the dissimilarity of land surface friction force (roughness length), only explains part of the wind speed dissimilarity. It appears that the characteristic of wind is also relatively related to the land surface properties.

To better evaluate the impact of land cover change on the strength of onshore winds and to avoid the effect of the surface drag force, the simulated data over water were analysed.

The comparison of simulations (Figure 5.12) suggests the presence of stronger wind over water when the metropolitan area is converted to natural vegetation at night (an example of which is shown with green ovals) and slightly weaker wind speed during the afternoon (blue ovals in the figure).

To minimize the drag force of surface and for the following 4 the averaging has been done for a location 3 km west of Adelaide Airport and over water hereafter refer as the water point.

The plot of monthly averaged vertical profiles of west-east and south-north winds in the lowest 2 km, resulting from the simulation with current land cover of the urban area, is provided in Figure 5.13. For an easier comparison the cold months were separated from warmer months.

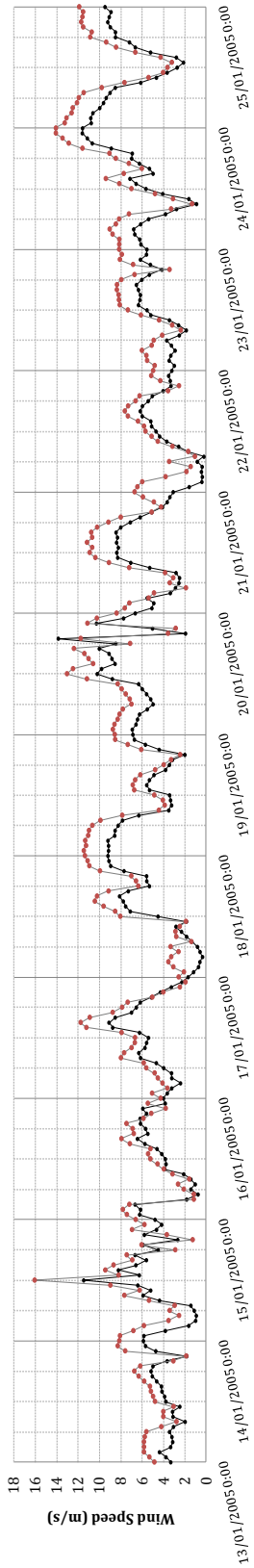

Figure 5.11. Area average wind speed at 10m height over the metropolitan area . CTL (black dots and thin black line) and NTV (red dots and thin grey line) for the period of 13 to 25 of January 2005

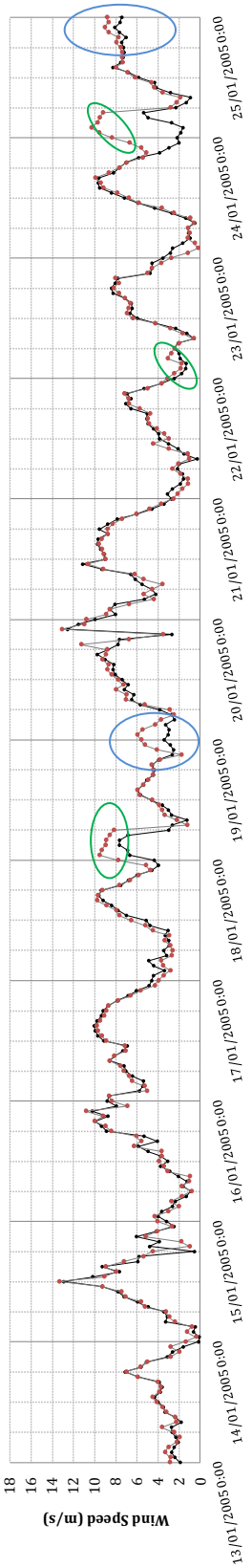

Figure 5.12. Same as Figure 5.11 for an adjacent point over water (green and blue ovals demonstrate the difference between two simulations in night times and afternoon respectively)

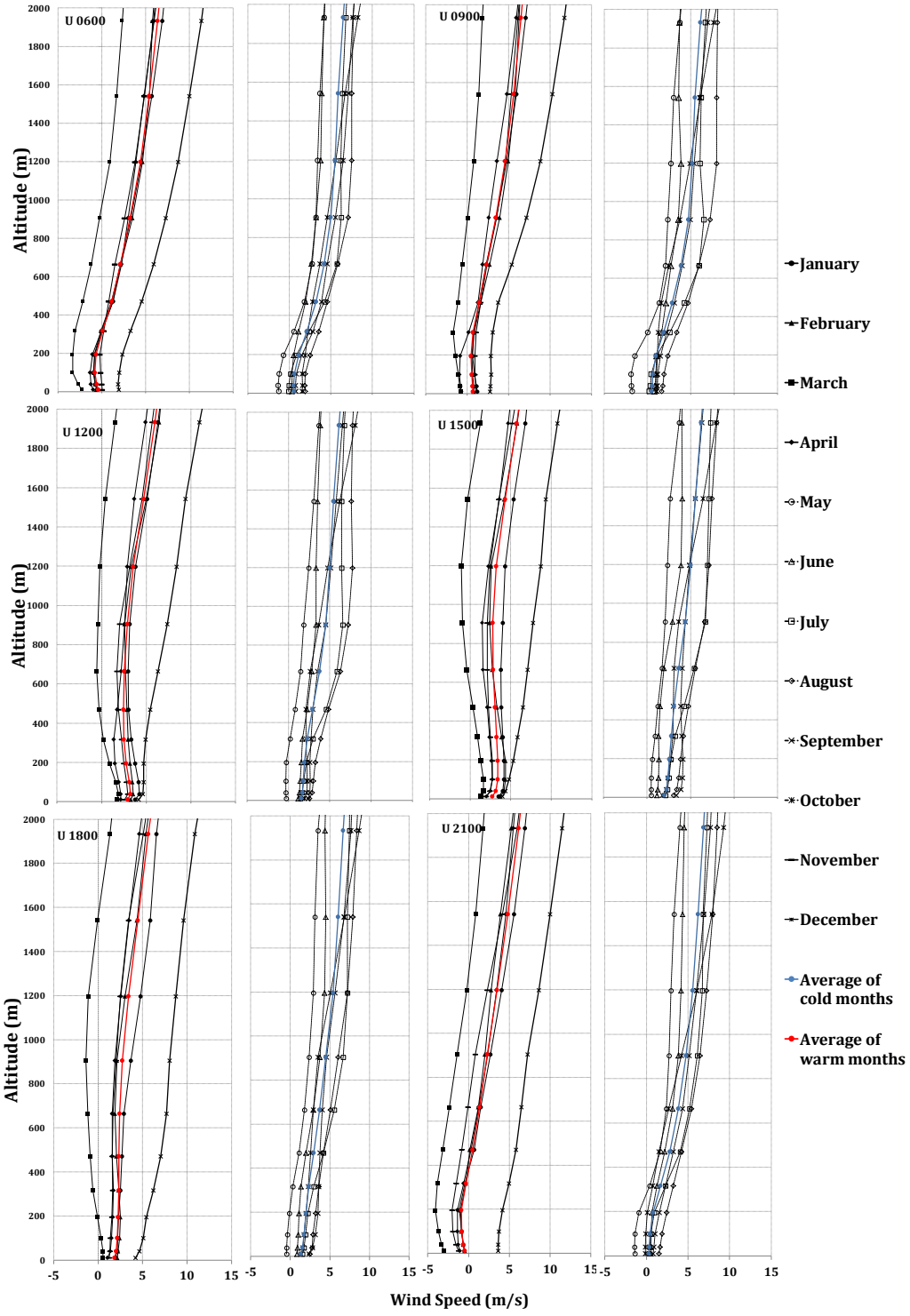

Figure 5.13. The monthly averaged u-wind component of the water point at lowest 2 km level of warm months (lines) and cold months (dashed line) at times of 0600, 0900, 1200, 1500, 1800 and 2100. The red and blue lines demonstrate the average of warm and cold months, respectively.

It appears that the U (west-east) components of wind of warmer months of January to April, November and December (with average of daily maximum temperature of considerably greater than 20°C) at lower elevation change direction from easterly to westerly (onshore) at sometime between 9 to 12 and grow in intensity until 3pm in the afternoon and by 6 pm they start moving back to the easterly direction and by 9 pm change to land breezes, whereas in most of the cold months of May to October winds are from the west during the period from 6 am to 9 pm.

The graph of V (south-north) component of wind, associated with the continental breeze, indicates the rotation of northerly to southerly wind, most likely due to Coriolis effect, to happen at some time between 12 and 3 pm and persist in growing in strength until 6 pm so that by 9 pm there is still a relatively strong southerly component to the wind. However the colder months are expecting a northerly wind component all through the day.

It should be noted again that the graphs has been provided for the water point, located over water and 3 km west of Adelaide Airport.

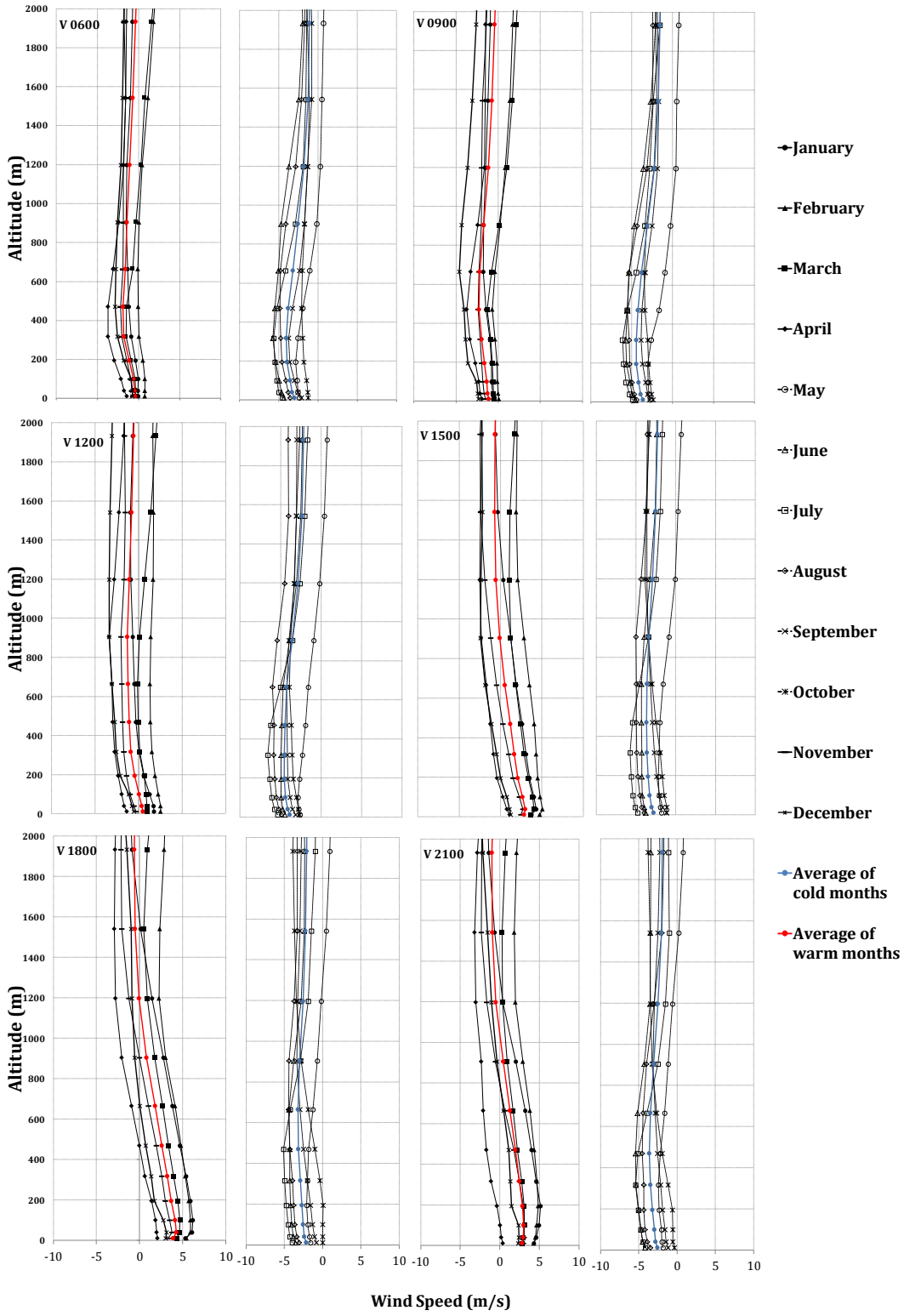

Figure 5.14. Same as Figure 5.13 for V-wind component.

For a better comparison of the response of onshore wind component to the change of the surface land cover in metropolitan areas, the wind profile of both simulations averaged for warmer months of January to April, November and December (hereafter referred to as WMP) are illustrated in Figure 5.15.

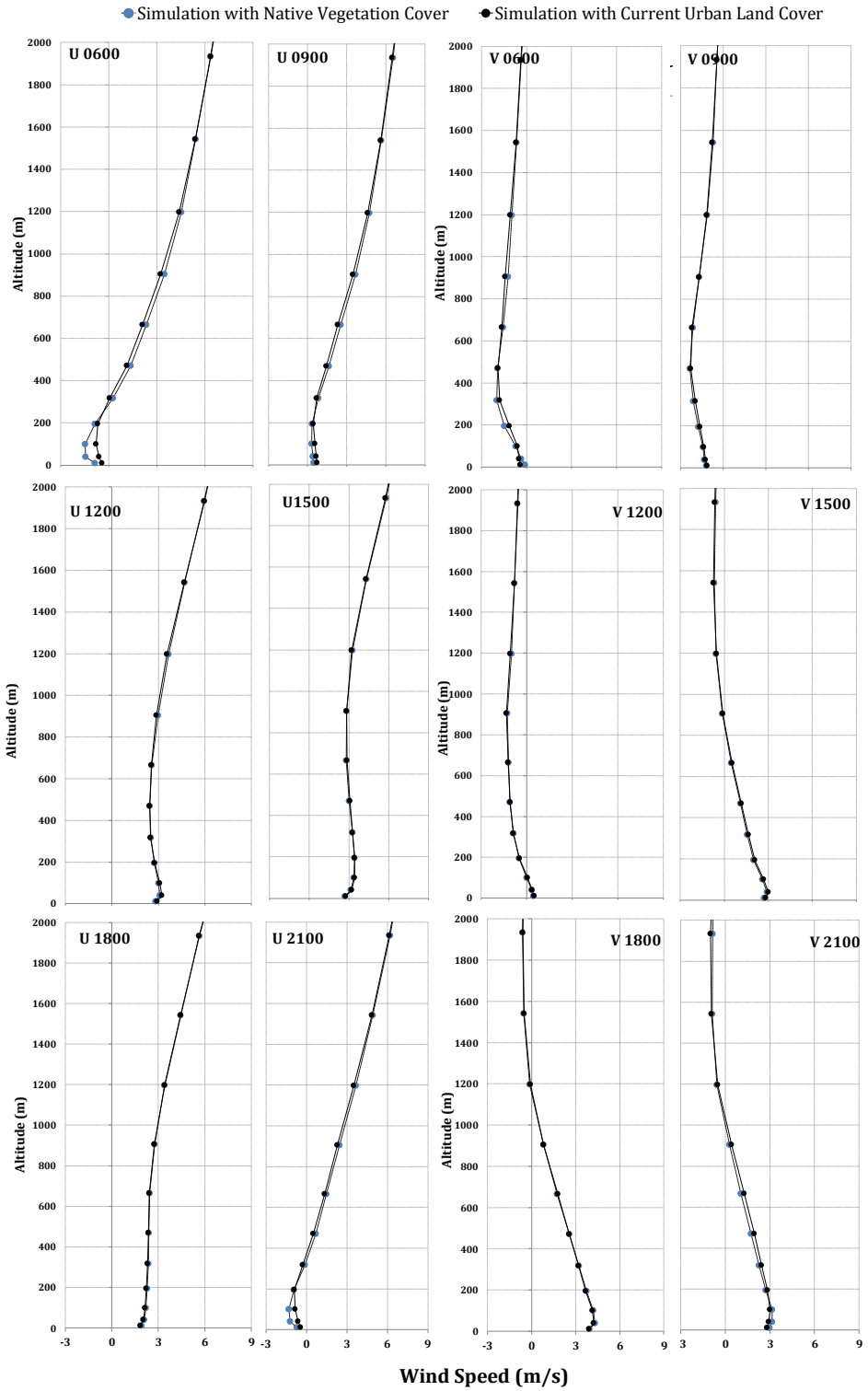

Figure 5.15. The warm period time-averaged U (two left columns) and V (two right columns) component of the water point simulated with CTL (black dots and thin line) and NTV (blue dots and thin dashed line) at times of 0600 and 0900 (top row), 1200and 1500 (middle row), 1800 and 2100 (bottom row).

Early in the morning, the easterly component of wind (offshore) is stronger when the urban land cover has been replaced by native vegetation and the rotation of wind to onshore westerly direction occurs later. Before 3 pm, the time that the westerly wind has had its full strength, the westerly wind component of simulation with urban land cover is slightly stronger at lower levels (below 400 m). Sometime between 6 pm and 9 pm the westerly (onshore) wind rotates to an offshore direction and grows in strength more noticeably with the absence of an urban area. The south-north component of wind does not show any significant difference in strength. Over the period of warmer months (November to April) and for each hour of the day, 10 m wind vectors has been averaged and the results, in form of a hodograph, is illustrated in Figure 5.16. The hodograph helps to demonstrate the changes to an hourly wind over the course of a day. The labels show the time and the circles represent the wind intensity interval of 1 m s^{-1}.

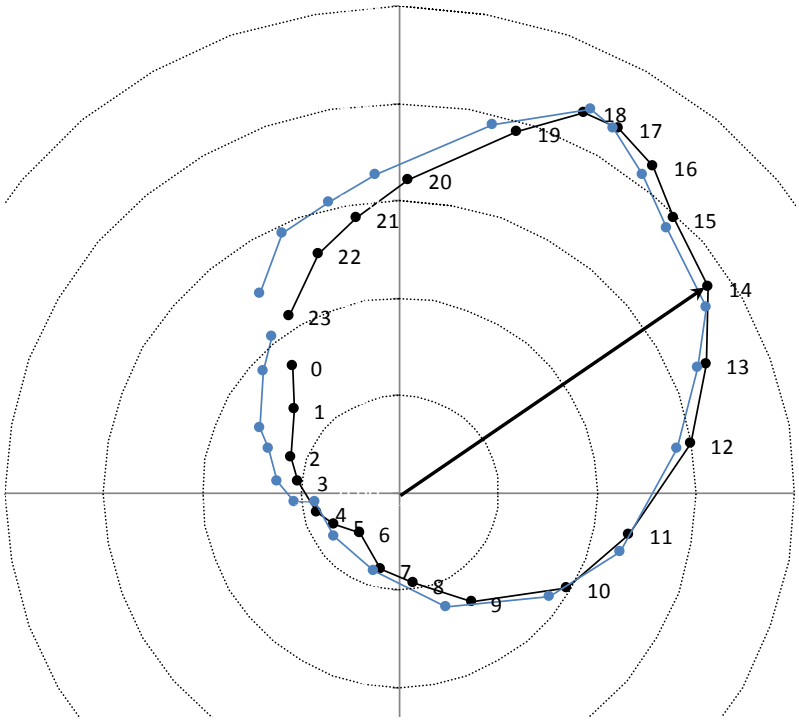

Figure 5.16. The hodograph of time-averaged wind of WMP at 10m height of the water point for CTL (black dots and line) and NTV (blue dots and line) simulations. The circles show the wind speed intervals of 1 m s^{-1} and the numbers denote the Australian Central Standard Time. An example of averaged wind vector for the hour of 1400 in CTL run is demonstrated by an arrow.

The time-averaged hodograph of the water point suggests that with the presence of an urban land cover, the morning wind shifts to an onshore direction, slightly earlier and grows relatively stronger and quicker than when it is replaced with vegetation. By 5 pm both simulations result in relatively similar wind components but the nocturnal offshore winds are significantly stronger over water when the adjacent land is covered with woodlands. The difference of the wind strength over water declines as it goes further over water. Figure 5.17 illustrates the horizontal extent of the difference of the 9 am wind (upper row) and 9 pm (lower row). The X-axis shows the intensity of east-west component of wind in m s^{-1}. The differences between two simulation's 9 pm offshore winds are observed to 21 km further over water while the 9 am difference disappear after 12 km distance from the shore.

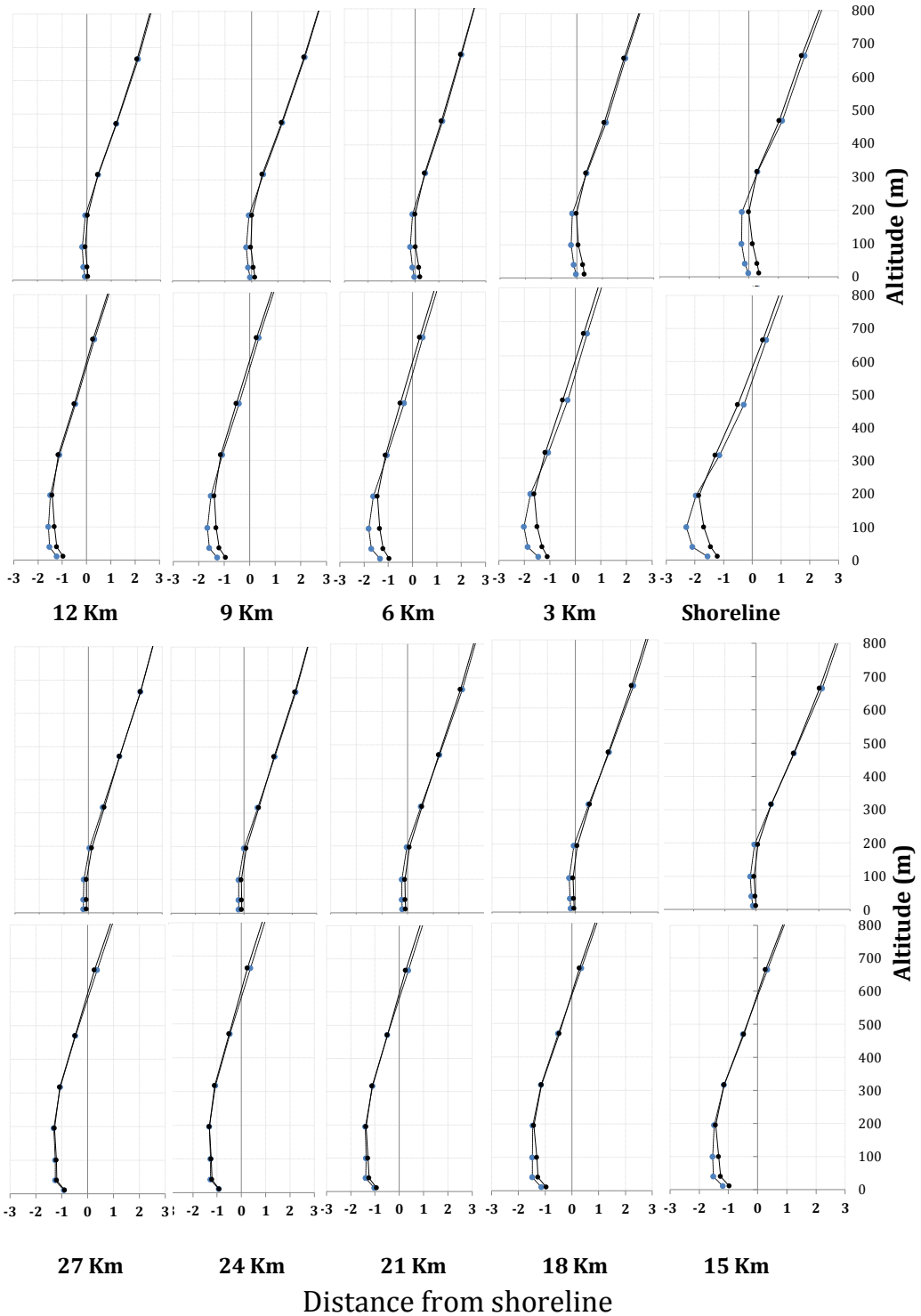

Figure 5.17. The averaged U-wind component profile of WMP in 9 am (above) and 9 pm (below) from shoreline to further 27 km over water.

In previous studies, as mentioned in literature review, the presence of urban areas has been shown to influence both horizontal and vertical wind profile (Oke, 1987; Eliasson and Holmer, 1990), and result in formation of what is known as heat island circulation (Figure 2.4). In order to study this effect, the change to the vertical wind profile of warmer months during the day in an urban location is plotted in Figure 5.18 (the positive values are the upward flow). As it appears in the figure, the afternoon upward wind in the first 1.5 kilometre is considerably stronger when the surface of land is covered with buildings and roads.

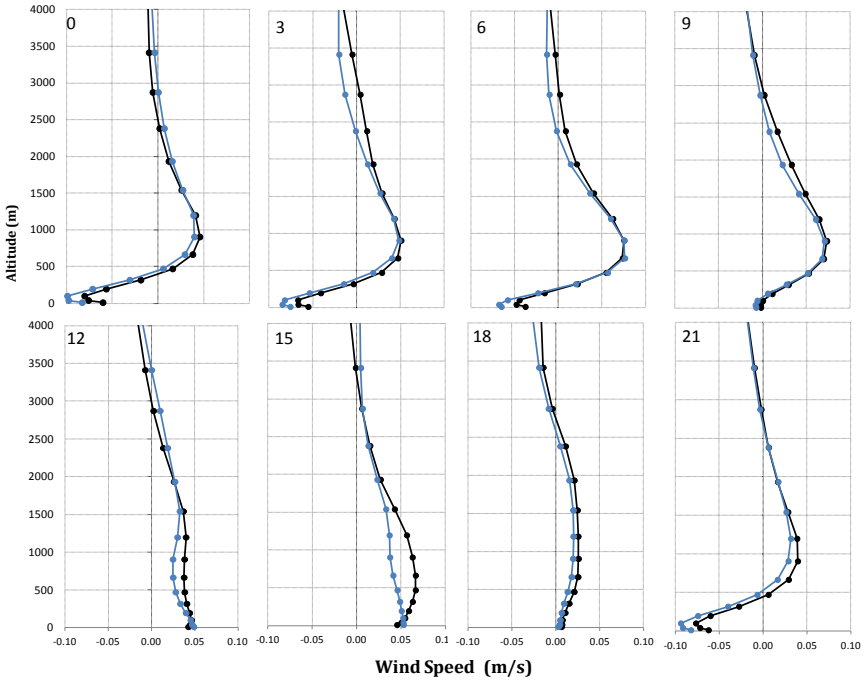

Figure 5.18. The vertical component of winds simulated with CTL (black) and NTV (blue) at times of 0000, 0300, 0600, 0900, 1200, 1500, 1800 and 2100.

Within the period of the 6 warm months of January to April, November and December of 2005, 65 days were considered as sea breeze days, using the sea breeze selection algorithm from Chapter 4. The behaviour of wind within the selected sea breeze days was compared with the days which were rejected as sea breeze days, called “non-sea breeze days”. The hodograph of averaged wind at 10 m heights of sea breeze and non-sea breeze days (Figure 5.19) shows the presence of a clear rotation of wind vectors in

the days which were selected as sea breeze days. It also suggests the presence of significantly stronger winds throughout the selected days, more noticeably at night.

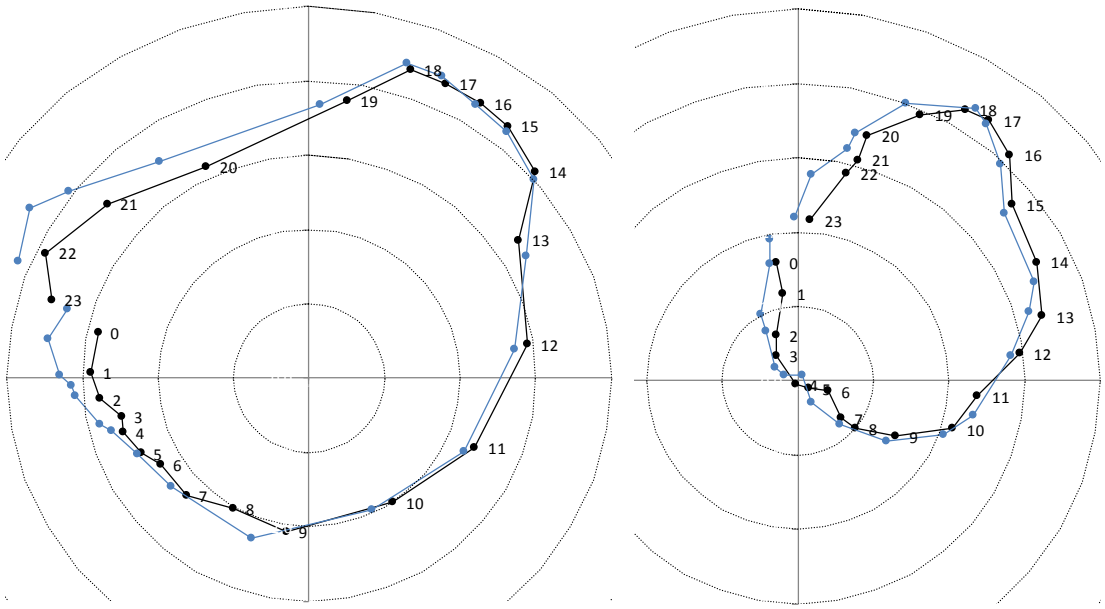

Figure 5.19. Hodograph of averaged sea breeze (left) and non-sea breeze day (right) of WMP, simulated with CTL (black) and NTV (blue). The circles show the wind speed intervals of 1 m s^{-1} and the numbers denote the Australian Central Standard Time.

Regardless of the day's category (as sea breeze or non-sea breeze days), the night time offshore winds are significantly stronger when the land surface is covered with vegetation. The afternoon onshore wind suggests the presence of stronger westerly wind components in the simulation with urban land cover, more noticeably in averaged non-sea breeze cases.

5.6. Discussion

In the previous chapter the weather for Adelaide for 12 months from January to December, 2005, was modelled using the WRF modelling system for two different land cover systems(Figure 5.4): one with buildings and roads (as its current state), and the other with the replacement of urban areas with the pre-settlement vegetation. The simulations were conducted with a selected combination of a physical scheme that is more suited for a coastal location with a mild atmospheric condition. The comparison of the modelling with current land cover and the observational record has shown a good agreement between the predicted values and observation, particularly for temperature and wind direction.

The result of the temperature modelling confirms the presence of an urban heat island over the metropolitan areas; however as the feedback from the inner domain reflected back to the parent domain, the impact of land cover conversion from native vegetation to urban and built-up areas, is on a larger scale than the metropolitan area of Adelaide. It is clearly demonstrated in Section 5.5.1 that the temperature difference between the two land surface coverings is more noticeable over the metropolitan area, however the magnitude of difference is significantly greater at night time, with an average of 2 degrees at sometime around 8 pm (Figure 5.8), which is the time when in the absence of solar radiation, the land starts cooling down. As the rate of heat convection from the surface substances are different for the two land surfaces and the heat storage capacity of urban surfaces is higher than natural shrub lands, the metropolitan areas do not cool down at the same rate as the native vegetation. Figure 5.9 reveals that the temperature difference is more noticeable for the months with colder air temperature (The averaged observed temperature of January, February, May and July are 22.3 °, 20.5°, 14.8 ° and 11.2 ° C respectively).

The result of simulations of the 10 m height wind over the urban areas has shown an average reduction of 0.5 m s^{-1} in the speed of predicted wind with urban land cover, which is a result of the change to the surface roughness length, whereas the comparison

of the simulated wind speed at a location over water, and close to the Adelaide coastline, has shown a significantly closer result (Figure 5.12). On the other hand, as the change to the coastal wind character is the main interest of this study, the wind behaviour over the Gulf, close to the shoreline, was of more interest.

It has been shown in Figure 5.12 that the conversion of land cover of the urban surface to its native vegetation has significantly increased the wind speed at night time, which as shown in Figure 5.16, these winds blow predominantly from north to east sector (offshore winds). This change can be attributed to the drag force on east winds, as they have to flow over the buildings, and the friction on urban surfaces results in a reduction in wind speed at lower levels. The monthly average of the wind component profile at different heights, shown in Figures 5.13 and 5.14, signifies the different behaviour of wind in different months. It clearly illustrates that for the warmer months, which includes the 6 months of January, February, March, April, November and December, on which the average of daily maximum observed temperature is higher than 23 ^{o}C, the westerly wind component of warmer months at below 800 metres height behave differently from the cold months average, as they are comparably getting stronger in the first 300 metres sometime around 9 am and continue growing until 3pm. By 9 pm the wind has rotated to an easterly direction for the warmer months, whereas the colder month average wind does not change in direction. The V-wind component shows persistence of a northerly direction for the whole day in colder months of May to October at almost all vertical levels, while in the warmer months northerly wind direction of the wind rotates to southerly direction at 12 pm and progresses until 6 pm, when it reaches its maximum intensity.

The change in the direction of easterly winds, as described in the literature review, is mainly attributed to the start of a locally generated gulf breeze, which, as concluded from an observational study by Physick and Byron-Scott (1977), starts prior to what is known as the northwest to southwest (offshore sector) southerly ocean breeze. The fact

that these phenomena are noticeable in warmer months is related to the higher probability of sea breezes occurring during this period.

The comparison of the wind profile of average wind in warmer months, for two different simulations of the metropolitan surface, one with urban as its current situation and the other with the metropolitan areas replaced with the native vegetation, shown in Figure 5.15, illustrates the reduction in intensity of the easterly component of night time wind with the conversion of land from native vegetation to urban and built up areas. An increase in the friction force, as a result of an increase of the roughness length reduces the intensity of the winds, as they flow over the urban areas. On the other hand, the intensification of the afternoon westerly winds occurs earlier for the urban land cover simulations, as by 12 pm the averaged wind profile of urban simulation is ahead of the simulation with native vegetation land cover. By 3 pm there is a slight difference between two simulation results, with the clearest picture as shown in Figure 5.16.

It is clear from the Figure 5.16 that by 9 am the winds of CTL simulation have changed in direction from westerly to easterly and continue to grow more rapidly than NTV simulations. By 2 pm the easterly wind reaches its maximum intensity for both simulations, which is slightly higher in CTL. From there until 5 pm, when the wind velocity is a maximum, the wind speeds of CTL simulation are higher than NTV. The wind rotates to a westerly direction between 7 and 8 pm in both cases. The differences in surface wind based on the changes to land cover extend less than 21 km over the water.

Throughout the mentioned figures, the change to the horizontal wind profile has been demonstrated and it appears that the conversion of land from natural vegetation to roads and buildings not only increases the near surface temperature, but also modifies the strength of the horizontal wind and the time of its rotation from onshore to offshore direction. Furthermore, Figure 5.18 illustrates the fact that the speed of the vertical wind profile changes as the land surface material changes. The figure captures the vertical profile of wind at a location over the urban area. It clearly shows the replacement of

early morning downward wind below 500 m to an upward direction at sometime between 9 am to 12 pm and its development to a maximum velocity around 3 pm and back to downward direction by 9 pm. 500 m is the altitude, which the horizontal wind system has shown a sensitivity to alteration of surface land cover. However, conversion of the urban surface to the native woodland, affects the intensity of maximum upward wind below 1500 m by reducing the upward wind at 650m by 40 percent, the fact that is attributed to the presence of vertical upward advection caused by urban heat island circulation formed over the metropolitan areas.

Following the effect of land surface alteration in lower level temperature and wind, the change to the wind behaviour of sea breeze and non-sea breeze days was analysed. In this part, the sea breeze selection was performed, using the mentioned algorithm in Chapter 3. For the period of the simulation (356 day), 95 days were selected as sea breeze days (26 %), which 68% of them (65 days) occur in six months of January, February, March, April, November and December. For the mentioned months, the daily hodograph of averaged sea breeze and non-sea breeze days were provided in Figure 5.19. In both cases the night time offshore wind are considerably stronger for the simulation with native vegetation as land cover, whereas the velocity of afternoon onshore wind of simulation with current urban surface is comparatively higher, more noticeably for the non-sea breeze cases.

It is clear from Figures 5.16 and 5.19 that replacing the native vegetation to urban and built up affects the land breeze in different ways. As the land breeze develops overland, the increase to the surface roughness length, as a result of land cover change, reduces the strength of the wind. Furthermore, changing the surface substances decelerates the land surface cooling rate, reducing the temperature difference of the land and sea surface during the night which consequently weakens the speed of the offshore winds. Similarly, the presence of heat island over the metropolitan area during the day affects the sea breeze by producing a greater thermal gradient over the land and water. This fact leads to an increase in the strength of the onshore winds, more noticeably on non-sea breeze

days (Figure 5.19) in which unlike sea breeze days, the absence of strong cool winds from the sea enables the land surface temperature to rise.

6. Summary and conclusion

An investigation of the long-term characteristics of the Adelaide sea breeze system was the main objective of current study. To carry this out the observational record of surface and upper air level meteorological data were used to categorize days as either sea breeze or non-sea breeze days. Due to the constraints imposed by the data availability, a set of criteria was applied to 3-hourly surface and 12-hourly upper air meteorological observations taken at the Bureau of Meteorology, Adelaide airport station to select sea breeze days. Later the behaviour of afternoon winds on selected sea breeze and non-sea breeze days was studied.

In order to corroborate the selection criteria for sea breeze days in Adelaide the wind characteristics on the other side of the gulf were utilised. The data from Edithburgh on Yorke Peninsula were only available from 1993 so the period 1993-2007 was analysed and represented in the form of wind hodographs. This allowed the sea breeze characteristics to be displayed clearly and for the selection criteria to be verified.

It is clear from the hodograph (Figure 4.5) that, despite the similarity of local circulation of wind on non-sea breeze days for Adelaide Airport and Edithburgh stations, the afternoon east-west component of the sea breeze days winds are from opposite directions. Being located on the opposite side of the gulf, the locally generated gulf breeze has been observed by Physick and Byron-Scott (1977) to have an easterly component on the western side of the gulf.

For the whole period of study, August 1955 to June 2008, 26.6% of the days were identified as sea breeze days, which of those 42% occur in summer and 10% in winter. Importantly, there has not been any noticeable change in the frequency of sea breeze days over the 53 years of the study; however there has been a significant increase in the intensity of afternoon winds, most noticeably on sea breeze days.

The results of regression analysis of intensity of the east-west and south-north components of winds on sea breeze and non-sea breeze days are provided in Tables 4.2 to Table 4.7. They show, as summarized in Table 4.8, that the intensity of the 15:00 (ACST) onshore and 21:00 offshore U component of the winds of spring, summer and autumn sea breeze days are progressively increasing over time, whereas except for autumn's 21:00 offshore wind there is not any significant change to the intensity of non-sea breeze day winds. Similarly, the 18:00 and 21:00 hour southerly component of sea breeze days wind has shown a growth over the period of study, where for non-sea breeze days, it is more evident in autumn and late night of summer. Tables 4.2 to 4.7 present the regression coefficient of the increasing rates of the afternoon wind intensity. The correlation between the average intensity of the wind component for each subsequent reading, Table 4.9, demonstrates that except for the east-west wind component of sea breeze days, which is considered to be locally generated, the afternoon east-west and north-south components of non-sea breeze days and the north-south component of sea breeze days, are highly correlated with the preceding and following time-step wind components. This supports the fact that these winds are potentially caused by synoptic scale flows rather than locally developed winds.

Later, the monthly averages of maximum air temperature at 1.2 m heights of Adelaide airport station, which have shown a noticeable increase over time, were compared against the afternoon wind components of both sea breeze and non-sea breeze days. The results, as shown in Table 4.10, indicate higher correlation between the north-south component and the maximum temperature, suggesting the role of land surface temperature on the intensity of southerly wind, known as the ocean breeze. On the other hand, the slight negative correlation between 21:00 hours north-south component of sea breeze days and air temperature indicates the greater likelihood of a land breeze (offshore wind) to occur on days with higher land temperatures.

The effect of South Australian climate drivers on the coastal wind regime was tested using the climate indices of SOI (the Southern Oscillation Index), IOD (the Indian

Ocean Dipole) and AOI (the Southern Annular mode or Antarctica Index). The oscillations of each component of afternoon wind around the trend line, the de-trended values, were compared against these indices. The results have shown no significant correlation between the values, rejecting any potential interaction between climate drivers and coastal wind circulations.

Although the presence of an increasing rate in the southerly component of sea breeze and non-sea breeze days afternoon wind were explained, using the near surface air temperature, the reason behind the significant growth of 15:00 hours westerly and 21:00 easterly wind component of sea breeze days (related to sea breeze and land breeze respectively) has not been identified. As the westerly component of the wind forms over the Gulf of St Vincent, there is a great possibility of the wind being affected by local climatic change. One of the more noticeable changes to the Adelaide plain is the development of the metropolitan area and growth of the population. Modification of urban geometry and rise in the population density modifies the land surface heat flux by increasing the anthropogenic heat emission and altering the thermal properties of land surface materials. These changes have been shown to intensify the sea breeze circulation by increasing the land surface temperature (Yoshikado, 1994; Ohashi and Kida, 2002; Cenedese and Monti, 2003; Freitas *et al.*, 2007). Moreover, the change to the roughness of the surface by replacing the natural vegetation of the land with roads and buildings alters the speed of near surface wind (Section 2.3) as it modifies the surface friction force.

To test the impact of the alteration to surface land covers on the sea breeze intensity, a numerical model, Weather Research and Forecasting (WRF), was employed to simulate the weather of the Adelaide coastline for a scenario on which the land surface was converted back to its native vegetation cover (NTV), taken from Bradshaw (2012). A control run (CTL) with the current urban condition was modelled alongside for the comparison purposes.

Model simulation extended over a 12 month period beginning on the 1st of January and ending on 31th of December 2005. Using the capability of the WRF for multi-nesting the model runs for three domains, the largest covers the central and eastern Australia whereas the smallest, with elements of 3 km by 3 km, which is centred at latitude 35.39 South and longitude of 137.85 and spans the Adelaide plain, Gulf St Vincent, Yorke Peninsula and Kangaroo Island.

The Noah land surface model coupled with a single layer urban canopy model was adopted. The Monin-Obukhov (Eta) scheme (Janjic, 2002), the BouLac scheme (Bougeault and Lacarrere, 1989) and WRF Single Moment 3 classes (WSM3) scheme were used by WRF in order to simulate surface layer physic, boundary layer processes and atmospheric microphysics process respectively.

The model results, extracted from the finer domain, were compared with observations collected by 7 near surface meteorological stations that provide hourly averaged data. The quality and reliability of the model were examined via several statistical indices. Regarding the model's capability to reproduce the near surface temperature, there is a good agreement between the simulated values and observed data of the Adelaide metropolitan area (includes Adelaide Airport, Edinburgh RAAF, Kent Town and Parafield). The high correlation and low mean bias score of the mentioned locations indicate the good performance of the model in simulation of urban surface temperature.

The assessment of the model's ability to predict the wind direction shows a high correlation between the observation data and simulated values, particularly in Edithburgh (a station located on the other side of the Gulf). Concerning the wind speed, with a slight over-prediction of 0.36 and 0.20 m s^{-1} and respective correlation of 0.7 and 0.69 at two coastal stations of Adelaide airport and Edithburgh, WRF is able to reproduce the observed wind speed of coastal areas, however the mean bias of 1.91 ms^{-1} in Kent Town station demonstrate the underestimation of aerodynamic roughness length over the urban areas.

Comparing the two land cover scenarios reveals that by replacing the native land cover with urban building and roads, the mean near-surface air temperature increased by 0.2 to 2 °C for inner city locations. The maximum difference occurs at night, in the absence of solar radiation, which reveals the importance of thermal property of land surface materials.

To avoid the model's under-prediction of surface drag force, the comparison analysis of wind was performed for an offshore location, close to Adelaide airport. The analysis of monthly-averaged wind profile suggests the presence of relatively stronger sea breeze circulation on the six warmer months of January to April, November and December. As the sea breeze activity was the objective of this study, the wind analyses were taken for the warmer months. By replacing the current metropolitan area with vegetation, the wind velocity at lower atmospheric level (below 1200 m) changes noticeably. The comparison of different components of the wind reveals that the east-west component of the wind is more sensitive to the surface land-use. It is concluded that land cover conversion from native vegetation to urban areas intensifies the onshore afternoon winds, noting that the progression of sea breeze toward the land is not affected by the change of surface roughness length. However at night, replacement of native low scrubland and grassland with metropolitan build-up areas weakens the offshore wind velocity as it flows over the city. The analysis of vertical wind profiles over the urban area confirms the presence of stronger upward motion of the air for the simulation with urban land cover, resulting from urban heat island circulation.

Out of 181 days from January to April, November and December, 65 days (36%) were selected as sea breeze days, using the sea breeze selection algorithm. The comparison of the hodograph of simulated wind averaged over sea breeze and non-sea breeze days indicate that the growth of the afternoon wind speed, attributed to change of the land surface from native to urban area, had greater impact on the afternoon wind velocity of non-sea breeze days.

In conclusion, the study has shown a progressive growth in the intensity of onshore breezes on the Adelaide coastline. Throughout the statistical analysis of near surface winds in selected sea breeze days, it has been explained that the growth to the southerly (V) component of winds, the continental breeze, is highly correlated with long-term rise in near surface temperature of the land, most likely associated with global warming. Furthermore, the numerical modelling of the Adelaide metropolitan area, confirms the important contribution of urban development in the characteristic of the locally generated breeze (U components of wind in this study). However as the urbanization in South Australia was accompanied with cropland expansion along both side of Gulf St. Vincent, the assessment of the level of such contribution is relatively complicated as it may strengthen or weaken the effect of urbanization on the local climate.

Taking everything into account, the ongoing changes to the near surface wind characteristic, more noticeably on sea breeze days, have the potential to change the littoral drift transport on the Adelaide shoreline, directly, by modifying the windblown sand transport, and indirectly, by changing the climate of locally-generated waves. Consequently, the combined effect of the mentioned modification to the wind regime and the expected rise in the sea surface level may affect the dynamics of the Adelaide coastline, which may impact the shoreline as seriously as a mild storm.

However, the ultimate effect of change of the afternoon wind intensity on the morphology of Adelaide beaches is beyond the scope of the current research and requires extensive analytical and numerical studies.

7. References

Abbs, DJ 1986. Sea-Breeze Interactions along a Concave Coastline in Southern Australia: Observations and Numerical Modeling Study". *Monthly weather review* 114**,** 831-848

Abbs, DJ & Physick, WL 1992. Sea Breeze Observation and Modelling: a review. *Australian Meteorological Magazine,* 41**,** 7-19

ABS, ABoS 2013. 3218.0 - Regional Population Growth, Australia, 2011-12. *In:* POPULATION DENSITY BY SA2, G. A.-J. (ed.). Canberra: Australian Burea of statistics

Andrys, J, Lyons, T & Kala, J 2013. Validation of WRF Downscaling Capabilities Over Western Australia to Detect Rainfall and Temperature Extremes. *In:* UNION, A. G. (ed.) *Fall Meeting 2013, abstract #GC43C-1054, "Australian Bureau of Meteorology.2009 . Australian Mean Sea Level Survey 2009. In: Centre, NT (ed.).Australian Government".*

Arnfield, AJ 2003. Two decades of urban climate research: A review of turbulence, exchanges of energy and water, and the urban heat island. *International Journal of Climatology,* 23**,** 1-26,DOI: Doi 10.1002/Joc.859.

Australian Burea of Meteorology. 2014a. The Bureau of Meteorology [Online]. Australian Government. Available: http://www.bom.gov.au/climate/cdo/about/sites.shtml [Accessed 29 April 2014]

Australian Burea of Meteorology. 2014b. Return to The Current SeasonS.O.I. (Southern Oscillation Index) Archives [Online]. http://www.bom.gov.au/climate/cdo/about/sites.shtml: Australian Government , Australian Bureau of Meteorology.

Australian Bureau of Meteorology. 2010. Australian Climate Influences [Online]. http://www.bom.gov.au/watl/about-weather-and-climate/australian-climate-influences.shtml: Commonwealth of Australia. [Accessed 15 April 2014]

Australian Bureau of Statistics. 2011. Census of Population and Housing: Basic Community Profile (Catalogue number 2001.0) [Online]. http://www.abs.gov.au/asstats/abs@.nfs/mf/2001.0. Available: http://www.censusdata.abs.gov.au

Australian Bureau of Statistics. 2012. Year Book Australia [Online]. http://www.abs.gov.au/asstats/abs@.nfs/productsbyCatalogue/02B2D95C0F67E84CCA257A07001BFB46?OpenDocument: Canberra. 92]

Azorin-Molina, C & Chen, D 2009. A climatological study of the influence of synoptic-scale flows on sea breeze evolution in the Bay of Alicante (Spain). *Theoretical and Applied Climatology,* 96**,** 249-260,DOI: 10.1007/s00704-008-0028-2.

Azorin-Molina, C & Martin-Vide , J 2007. Methodological approach to the study of the daily persistence of the sea breeze in Alicante (Spain). *Atmósfera* 20**,** 57-81

Azorin-Molina, C, Tijm, S & Chen, D 2011. Development of selection algorithms and databases for sea breeze studies. *Theoretical and Applied Climatology,* 106**,** 531-546,DOI: 10.1007/s00704-011-0454-4.

Baker, RD, Barry, HL, Aaron, B, Wei-Kuo, T & Joanne, S 2001. Influence of Soil Moisture, Coastline Curvature, and Land-Breeze. *Journal of Hydrometeorology,* vol 2

Barthelmie, RJ 1999. The effects of atmospheric stability on coastal wind climates. *Meteorological Applications,* 6**,** 39-47,DOI: 10.1017/s1350482799000961.

Belperio, AP 1993. Land subsidence and sea level rise in the Port Adelaide estuary: Implications for monitoring the greenhouse effect. *Australian Journal of Earth Sciences,* 40**,** 359-368,DOI: 10.1080/08120099308728087.

Bigot, S & Planchon, O 2003. Identification and Characterization of Sea Breeze Days in Northern France using Singular Value Decomposition. *International Journal of Climatology,* 23**,** 1397-1405

Borne, K, Chen, D & Nunez, M 1998. A method for finding sea breeze days under stable synoptic conditions and its application to the Swedish west coast. *International Journal of Climatology,* 18**,** 901-914,DOI: 10.1002/(sici)1097-0088(19980630)18:8<901::aid-joc295>3.0.co;2-f.

Bougeault, P & Lacarrere, P 1989. Parameterization of Orography-Induced Turbulence in a Mesobeta--Scale Model. *Monthly Weather Review,* 117**,** 1872-1890,DOI: 10.1175/1520-0493(1989)117<1872:pooiti>2.0.co;2.

Bradshaw, CJA 2012. Little left to lose: deforestation and forest degradation in Australia since European colonization. *Journal of Plant Ecology,* 5**,** 109-120,DOI: 10.1093/jpe/rtr038.

Carvalho, D, Rocha, A & Gómez-Gesteira, M 2012a. Ocean surface wind simulation forced by different reanalyses: Comparison with observed data along the Iberian Peninsula coast. *Ocean Modelling,* 56**,** 31-42,DOI: http://dx.doi.org/10.1016/j.ocemod.2012.08.002.

Carvalho, D, Rocha, A, Gómez-Gesteira, M & Santos, C 2012b. A sensitivity study of the WRF model in wind simulation for an area of high wind energy. *Environmental Modelling & Software,* 33**,** 23-34,DOI: http://dx.doi.org/10.1016/j.envsoft.2012.01.019.

Castillo, M, Inagaki, A & Kanda, M 2011. The Effects of Inner- and Outer-Layer Turbulence in a Convective Boundary Layer on the Near-Neutral Inertial Sublayer Over an Urban-Like Surface. *Boundary-layer meteorology,* 140**,** 453-469,DOI: 10.1007/s10546-011-9614-4.

Cenedese, A & Monti, P 2003. Interaction between an Inland Urban Heat Island and a Sea-Breeze Flow: A Laboratory Study. *Journal of Applied Meteorology,* 42**,** 1569-1583

Challa, VS, Indracanti, J, Rabarison, MK, Patrick, C, Baham, JM, Young, J, Hughes, R, Hardy, MG, Swanier, SJ & Yerramilli, A 2009. A simulation study of mesoscale coastal circulations in Mississippi Gulf coast. *Atmospheric Research,* 91**,** 9-25,DOI: http://dx.doi.org/10.1016/j.atmosres.2008.05.004.

Chen, F & Dudhia, J 2001. Coupling an Advanced Land Surface–Hydrology Model with the Penn State–NCAR MM5 Modeling System. Part I: Model Implementation and Sensitivity.

Monthly Weather Review, 129**,** 569-585,DOI: 10.1175/1520-0493(2001)129<0569:caalsh>2.0.co;2.

Chen, F, Miao, S, Tewari, M, Bao, J-W & Kusaka, H 2011. A numerical study of interactions between surface forcing and sea breeze circulations and their effects on stagnation in the greater Houston area. *Journal of Geophysical Research: Atmospheres,* 116**,** D12105,DOI: 10.1029/2010jd015533.

Cheng, CKM & Chan, JCL 2012. Impacts of land use changes and synoptic forcing on the seasonal climate over the Pearl River Delta of China. *Atmospheric Environment,* 60**,** 25-36,DOI: http://dx.doi.org/10.1016/j.atmosenv.2012.06.019.

Cheng, F-Y, Chin, S-C & Liu, T-H 2012. The role of boundary layer schemes in meteorological and air quality simulations of the Taiwan area. *Atmospheric Environment,* 54**,** 714-727,DOI: http://dx.doi.org/10.1016/j.atmosenv.2012.01.029.

Childs, PP & Raman, S 2005. Observations and Numerical Simulations of Urban Heat Island and Sea Breeze Circulations over New York City. *Pure and Applied Geophysics,* 162**,** 1955-1980

Church, JA, Hunter, JR, Mclnnes, KL & White, NJ 2006. Sea-level rise around the Australian coastline and the changing frequency of extreme sea-level events. *Australian Meteorological Magazine,* 55/4**,** 253-260

Clarke, H, Evans, JP & Pitman, AJ 2013. Fire weather simulation skill by the Weather Research and Forecasting (WRF) model over south-east Australia from 1985 to 2009. *International Journal of Wildland Fire,* 22**,** 739-756,DOI: http://dx.doi.org/10.1071/WF12048.

Clarke, RH 1955. Some Observation and Comments on the Sea Breeze. *Australian Meteorological Magazine,* 11**,** 47-68

Climatic Prediction Center. 2005. Antarctic Oscillation Index [Online]. National weather services Available: http://www.cpc.ncep.noaa.gov/products/precip/CWlink/daily_ao_index/aao/aao.shtml 2013]

Cooper, JAG & Pilkey, OH 2012. Pitfalls of Shoreline Stabilization: Selected Case Studies, Springer

Coppin, PA. 1979. Turbulent Fluxes Over a Uniform Urban Surface PhD Thesis, Flinders University of South Australia.

Crooks, G & Brooks, B 1987. Seafront Wind near Adelaide. *Bureau of Meteorology, Meteorologica Note,* 176

Crosman, E & Horel, J 2010. Sea and Lake Breezes: A Review of Numerical Studies. *Boundary-layer meteorology,* 137**,** 1-29,DOI: 10.1007/s10546-010-9517-9.

Cynthia, R, Soleckib, WD, Parshalla, L, Chopping, M, Popec, G & Goldberg, R 2005. Characterizing the urban heat island in current and future climates in New Jersey. *Environmental Hazards,* 6**,** 51-63

Dampier, W 1927. *A new voyage round the world,* London, Argonaut Press

Dandou, A, Tombrou, M & Soulakellis, N 2009. The Influence of the City of Athens on the Evolution of the Sea-Breeze Front. *Boundary-Layer Meteorology,* 131**,** 35-51

Das, S, Ashrit, R, Iyengar, G, Mohandas, S, Gupta, M, George, J, Rajagopal, EN & Dutta, S 2008. Skills of different mesoscale models over Indian region during monsoon season: Forecast errors. *Journal of Earth System Science,* 117**,** 603-620,DOI: 10.1007/s12040-008-0056-4.

Department of the Environment and Water Resources 2007. Australia's Native Vegetation: A summary of Australia's Major Vegetation Groups. *In:* AUSTRALIAN GOVERNMENT (ed.). http://www.environment.gov.au/system/files/resources/a9897cf2-9d38-4201-bea2-13dadf3af9a8/files/major-veg-summary.pdf:

Dong, Y & Dong, W 2012. Constructing Urban Development Model Based on the Local Climate. *Asia Pacific Conference on Environmental Science and Technology Advances in Biomedical Engineering.* Kuala Lumpur, Malaysia:

Drosdowsky, W 2005. The latitude of the subtropical ridge over Eastern Australia: The L index revisited. *International Journal of Climatology,* 25**,** 1291-1299,DOI: 10.1002/joc.1196.

Dudhia, J. 2010. WRF Physics Options [Online]. WRF Basic Tutorial: National Center For Atmospheric Research.

Dunsmuir, WTM, Spark, E, Kim, S-K & Chen, S 2003. Statistical prediction of sea breezes in Sydney Harbour. *Australian Meteorological Magazine,* 52**,** 117-126

Eliasson, I & Holmer, B 1990. Urban Heat Island Circulation in Göteborg, Sweden. *Theoretical and Applied climatology,* 42**,** 187-196,DOI: 10.1007/bf00866874.

Elnahas, MM & Williamson, TJ 1997. An improvement of the CTTC model for predicting urban air temperatures. *Energy and Buildings,* 25**,** 41-49,DOI: http://dx.doi.org/10.1016/S0378-7788(96)00986-3.

Erell, E & Williamson, T 2006. Simulating air temperature in an urban street canyon in all weather conditions using measured data at a reference meteorological station. *International Journal of Climatology,* 26**,** 1671-1694

Erell, E & Williamson, T 2007. Intra-urban differences in canopy layer air temperature at a mid-latitude city. *International Journal of Climatology,* 27**,** 1243-1255,DOI: Doi 10.1002/Joc.1469.

Estoque, MA 1962. The Sea Breeze as a Function of the Prevailing Synoptic Situation. *Journal of Atmospheric Sciences,* 19**,** 244-250

Evans, J, Ekström, M & Ji, F 2012. Evaluating the performance of a WRF physics ensemble over South-East Australia. *Climate Dynamics,* 39**,** 1241-1258,DOI: 10.1007/s00382-011-1244-5.

Evans, J & McCabe, M 2013. Effect of model resolution on a regional climate model simulation over southeast Australia. *Climate Research,* 56**,** 131-145,DOI: 10.3354/cr01151.

Evans, J, P. & Matthew, FM 2010. Evaluating a regional climate model's ability to simulate the climate of the South-east coast of Australia. *IOP Conference Series: Earth and Environmental Science,* 11**,** 012004

Feser, F, Rockel, B, von Storch, H, Winterfeldt, J & Zahn, M 2011. Regional Climate Models Add Value to Global Model Data: A Review and Selected Examples. *Bulletin of the American Meteorological Society,* 92**,** 1181-1192,DOI: 10.1175/2011bams3061.1.

Finkele, K 1998. Inland and Offshore Propagation Speeds of a Sea Breeze from Simulations and Measurements. *Boundary-layer meteorology,* 87**,** 307-329,DOI: 10.1023/a:1001083913327.

Finkele, K, Hacker, J, Kraus, H & Byron-Scott, RD 1995. A complete sea-breeze circulation cell derived from aircraft observations. *Boundary-layer meteorology,* 73**,** 299-317,DOI: 10.1007/bf00711261.

Freitas, E, Rozoff, C, Cotton, W & Dias, PS 2007. Interactions of an urban heat island and sea-breeze circulations during winter over the metropolitan area of São Paulo, Brazil. *Boundary-layer meteorology,* 122**,** 43-65,DOI: 10.1007/s10546-006-9091-3.

Frizzola, JA & Fisher, EL 1963. A Series of Sea Breeze Observations in the New York City Area. *Journal of Applied Meteorology,* 2**,** 722-739,DOI: 10.1175/1520-0450(1963)002<0722:asosbo>2.0.co;2.

Furberg, M, Steyn, DG & Baldi, M 2002. The climatology of sea breezes on Sardinia. *International Journal of Climatology,* 22**,** 917-932,DOI: 10.1002/joc.780.

Gero, A 2006. The impact of land cover change on storms in the Sydney Basin, Australia. *Global and Planetary Change,* 54**,** 57-79

Gero, AF & Pitman, AJ 2006. The Impact of Land Cover Change on a Simulated Storm Event in the Sydney Basin. *Journal of Applied Meteorology and Climatology,* 45**,** 283-300

Giannaros, TM & Melas, D 2012. Study of the urban heat island in a coastal Mediterranean City: The case study of Thessaloniki, Greece. *Atmospheric Research,* 118**,** 103-120,DOI: http://dx.doi.org/10.1016/j.atmosres.2012.06.006.

Giannaros, TM, Melas, D, Daglis, IA, Keramitsoglou, I & Kourtidis, K 2013. Numerical study of the urban heat island over Athens (Greece) with the WRF model. *Atmospheric Environment,* 73**,** 103-111,DOI: http://dx.doi.org/10.1016/j.atmosenv.2013.02.055.

Giorgi, F & Mearns, LO 1991. Approaches to the simulation of regional climate change: A review. *Reviews of Geophysics,* 29**,** 191-216,DOI: 10.1029/90rg02636.

Goodman, SJ. 1999. Heat Island [Online]. Available: http://weather.msfc.nasa.gov/urban/urban_heat_island.html

Google earth 2013. Adelaide Area, 35° 55’ 34.26” S, 138° 35’ 48.74” E. http://www.earth.google.com:

Grossi, P, Thunis, P, Martilli, A & Clappier, A 2000. Effect of Sea Breeze on Air Pollution in the Greater Athens Area. Part II: Analysis of Different Emission Scenarios. *Journal of Applied Meteorology and Climatology*

39**,** 563-575

Guan, H, Bennett, J, Ewenz, CM, Benger, SN, Vinodkumar, Zhu, S, Clay, R & Soebarto, V 2013. Characterisation, interpretation and implications of the Adelaide Urban Heat Island.

Haeger-Eugensson, M & Holmer, B 1999. Advection caused by the urban heat island circulation as a regulating factor on the nocturnal urban heat island. *International Journal of Climatology,* 19**,** 975-988,DOI: 10.1002/(sici)1097-0088(199907)19:9<975::aid-joc399>3.0.co;2-j.

Han, J-Y & Jin Baik, J 2008. A Theoretical and Numerical Study of Urban Heat Island–Induced Circulation and Convection. *Journal of the Atmospheric Sciences,* 65**,** 1859-1877

Han, J-YJB, Jong 2008. A Theoretical and Numerical Study of Urban Heat Island–Induced Circulation and Convection. *Journal of The Atmospheric Science,* 65**,** 1859-1877

Hendrickson, J & MacMahan, J 2009. Diurnal sea breeze effects on inner-shelf cross-shore exchange. *Continental Shelf Research,* 29**,** 2195-2206

Hernández-Ceballos, MA, Adame, JA, Bolívar, JP & De la Morena, BA 2013. A mesoscale simulation of coastal circulation in the Guadalquivir valley (southwestern Iberian Peninsula) using the WRF-ARW model. *Atmospheric Research,* 124**,** 1-20,DOI: http://dx.doi.org/10.1016/j.atmosres.2012.12.002.

Holbrook, NJ, Davidson, J, Feng, M, Hobday, AJ, Lough, JM, McGregor, S & Risbey, JS 2009. El Niño – Southern Oscillation. *Marine Climate Change in Australia, Impacts and Adaptation Responses.* the Marine Biodiversity and Resources Adaptation Network, Fisheries Research and Development Corporation, and CSIRO's Climate Adaptation .

Hong, S-Y, Dudhia, J & Chen, S-H 2004. A Revised Approach to Ice Microphysical Processes for the Bulk Parameterization of Clouds and Precipitation. *Monthly Weather Review,* 132**,** 103-120,DOI: 10.1175/1520-0493(2004)132<0103:aratim>2.0.co;2.

JAMST 2014. Indian Ocean Dipole *In:* NATIONAL OCEANIC AND ATMOSPHERE ADMINSTRATION (ed.). http://www.jamstec.go.jp/frcgc/research/d1/iod/e/iod/about_iod.html: Japan Agency for Marine-Earth Science and Technology

Janjic, Z 2002. Nonsingular Implementation of the Mellor-Yamada Level 2.5 Scheme in the NCEP Meso model. *National Centers for Environmental Prediction.* NCEP Off. ,DOI: citeulike-article-id:6651560.

Janjic, Z, R. Gall & Pyle, ME 2010. Scientific Documentation for the NMM Solver. *NCAR Technical Note.* NCAR/TN-477+STR: National Centre of Atmospheric Research (NCAR),DOI: 10.5065/D6MW2F3Z. .

Jauregui, E 1997. Heat island development in Mexico City. *Atmospheric Environment,* 31**,** 3821-3831

Jiménez, PA, González-Rouco, JF, García-Bustamante, E, Navarro, J, Montávez, JP, de Arellano, JV-G, Dudhia, J & Muñoz-Roldan, A 2010. Surface Wind Regionalization over Complex Terrain: Evaluation and Analysis of a High-Resolution WRF Simulation. *Journal of Applied Meteorology and Climatology,* 49**,** 268-287,DOI: 10.1175/2009jamc2175.1.

Johnson, GT, Oke, TR, Lyons, TJ, Steyn, DG, Watson, ID & Voogt, JA 1991. Simulation of surface urban heat islands under 'IDEAL' conditions at night part 1: Theory and tests against field data. *Boundary-Layer Meteorology,* 56**,** 275-294,DOI: 10.1007/bf00120424.

Kala, J, Lyons, T & Nair, U 2010. Numerical Simulations of the Impacts of Land-Cover Change on Cold Fronts in South-West Western Australia. *Boundary-Layer Meteorology,* 138**,** 121-138

Kambezidis, HD, Peppes, AA & Melas, D 1995. An Environmental Experiment over Athens Urban Area under Sea Breeze Conditions. *Atmospheric Research,* 36**,** 139-156

Kiehl, JT & Ramanathan, V 2006. *Frontiers of Climate Modeling,* Cambridge, Cambridge University Press,DOI: http://dx.doi.org/10.1017/CBO9780511535857.

Kim, Y-H & Baik, J-J 2002. Maximum Urban Heat Island Intensity in Seoul. *Journal of Applied Meteorology,* 41**,** 651-659

Kusaka, H & Kimura, F 2000. The effects of land-use Alternation on sea breeze and daytime Heat Island in Tokyo Metropolitan Area. *Journal of the Meteorological Society of Japan,* 78**,** 405-421

Kusaka, H, Kondo, H, Kikegawa, Y & Kimura, F 2001. A Simple Single-Layer Urban Canopy Model For Atmospheric Models: Comparison With Multi-Layer And Slab Models. *Boundary-Layer Meteorology,* 101**,** 329-358

Lin, C-Y, Chen, F, Huang, JC, Chen, WC, Liou, YA, Chen, WN & Liu, S-C 2008. Urban heat island effect and its impact on boundary layer development and land-sea circulation over northern Taiwan. *Atmospheric Environment,* 42**,** 5635-5649

Lo, JCF, Lau, AKH, Chen, F, Fung, JCH & Leung, KKM 2007. Urban Modification in a Mesoscale Model and the Effects on the Local Circulation in the Pearl River Delta Region. *Journal of Applied Meteorology and Climatology,* 46**,** 457-476,DOI: 10.1175/jam2477.1.

Logue, J 1986. Comparison of Wind Speeds Recorded Simultaneously by a Pressure-Tube Anemograph and a Cup-Generator Anemograph. *Meteorological Magazine,* 115**,** 178-185

Lynch, P 2008. The origins of computer weather prediction and climate modeling. *Journal of Computational Physics,* 227**,** 3431-3444,DOI: http://dx.doi.org/10.1016/j.jcp.2007.02.034.

Lyons, TJ 1975. Mesoscale wind spectra. *Quarterly Journal of the Royal Meteorological Society,* 101**,** 901-910,DOI: 10.1002/qj.49710143013.

Mahrer, Y & Pielke, RA 1977. The Effects of Topography on Sea and Land Breezes in a Two-Dimensional Numerical Model. *Monthly Weather Review,* 105**,** 1151-1162,DOI: 10.1175/1520-0493(1977)105<1151:teotos>2.0.co;2.

Makar, PA, Gravel, S, Chirkov, V, Strawbridge, KB, Froude, F, Arnold, J & Brook, J 2006. Heat flux, urban properties, and regional weather. *Atmospheric Environment,* 40**,** 2750-2766

Marshall, CH, Pielke, RA, Steyaert, LT & Willard, DA 2004. The Impact of Anthropogenic Land-Cover Change on the Florida Peninsula Sea Breezes and Warm Season Sensible Weather. *Monthly Weather Review,* 132**,** 28-52

Masselink, G & Pattiaratchi, C 1998. Morphodynamic Impact of Sea Breeze Activity on a Beach with Beach Cusp Morphology. *Journal of Coastal Research,* 14**,** 393-406

Masselink, G & Pattiaratchi, CB 2001. Characteristics of the Sea Breeze System in Perth, Western Australia, and Its Effect on the Nearshore Wave Climate. *journal of Coastal Research,* 17**,** 173-187,DOI: 10.2307/4300161.

MATLAB 2010. *Version 7.10.0,* Natick, Massachusetts:, The MathWorks Inc.

McAlpine, CA, Syktus, J, Deo, RC, Lawrence, PJ, McGowan, HA, Watterson, IG & Phinn, SR 2007. Modeling the impact of historical land cover change on Australia's regional climate. *Geophysical Research Letters,* 34**,** L22711,DOI: 10.1029/2007gl031524.

McInnes, KL, Suppiah, R, P.H.Whetton, K.J.Hennessy & R.N.Jones 2002. *Climate Change in South Australia: Report on assessment of climate change impacts and possible adaptation strategies relevant to South Australia*

Aspendale, Vic. : CSIRO Atmospheric Research

McPherson, RD 1970. A Numerical Study of the Effect of a Coastal Irregularity on the Sea Breeze. *Journal of Applied Meteorology,* 9**,** 767-777,DOI: 10.1175/1520-0450(1970)009<0767:ansote>2.0.co;2.

Meir, T, Orton, PM, Pullen, J, Holt, T, Thompson, WT & Arend, MF 2013. Forecasting the New York City Urban Heat Island and Sea Breeze during Extreme Heat Events. *Weather and Forecasting,* 28**,** 1460-1477,DOI: 10.1175/waf-d-13-00012.1.

Meng, X, Evans, J & McCABE, M 2011. Numerical modelling and land–atmosphere feedback of drought in southeast Australia. *IAHS Publ,* 344**,** 144-149

Mestayer, P, Almbauer, R & Tchepel, O 2003. Urban Field Campaigns. *In:* MOUSSIOPOULOS, N. (ed.) *Air Quality in Cities.* Springer Berlin Heidelberg,51-89DOI: 10.1007/978-3-662-05217-4_5.

Miao, S, Chen, F, LeMone, MA, Tewari, M, Li, Q & Wang, Y 2009. An Observational and Modeling Study of Characteristics of Urban Heat Island and Boundary Layer Structures in Beijing. *Journal of Applied Meteorology and Climatology,* 48**,** 484-501,DOI: 10.1175/2008jamc1909.1.

Mihalakakou, G, Santamouris, M, Papanikolaou, N, Cartalis, C & Tsangrassoulis, A 2004. Simulation of the Urban Heat Island Phenomenon in Mediterranean Climates. *Pure and Applied Geophysics,* 161**,** 429-451

Miller, C, Holmes, J, Henderson, D, Ginger, J & Morrison, M 2013. The Response of the Dines Anemometer to Gusts and Comparisons with Cup Anemometers. *Journal of Atmospheric and Oceanic Technology,* 30**,** 1320-1336,DOI: 10.1175/jtech-d-12-00109.1.

Miller, STK & Keim, BD 2003. Synoptic-Scale Controls on the Sea Breeze of the Central New England Coast. *Weather and Forecasting,* 18**,** 236-248,DOI: 10.1175/1520-0434(2003)018<0236:scotsb>2.0.co;2.

Mohan, M & Bhati, S 2011. Analysis of WRF Model Performance over Subtropical Region of Delhi, India. *Advances in Meteorology,* 2011,DOI: 10.1155/2011/621235.

Monin, AS & Obukhov, AM 1954. Basic laws of turbulent mixing in the surface layer of the atmosphere. *Tr. Akad. Nauk SSSR Geofiz. Inst* 24**,** 163-187

Mooney, PA, Mulligan, FJ & Fealy, R 2012. Evaluation of the Sensitivity of the Weather Research and Forecasting Model to Parameterization Schemes for Regional Climates of Europe over the Period 1990–95. *Journal of Climate,* 26**,** 1002-1017,DOI: 10.1175/jcli-d-11-00676.1.

Moroz, WJ 1967. A Lake Breeze on the Eastern Shore of Lake Michigan: Observations and Model. *Journal of the Atmospheric Sciences,* 24**,** 337-355,DOI: 10.1175/1520-0469(1967)024<0337:albote>2.0.co;2.

Morris, CJG & Simmonds, I 2000. Associations between Varying Magnitudes of the Urban Heat Island and the Synoptic Climatology in Melbourne, Australia. *International Journal of Climatology,* 20**,** 24

Narisma, GT & Pitman, AJ 2003. The Impact of 200 Years of Land Cover Change on the Australian Near-Surface Climate. *Journal of Hydrometeorology,* 4**,** 424-436,DOI: 10.1175/1525-7541(2003)4<424:tioyol>2.0.co;2.

National Centers for Environmental Prediction, NWSNUSDoC 2000. NCEP FNL Operational Model Global Tropospheric Analyses, continuing from July 1999. Boulder, CO: Research Data Archive at the National Center for Atmospheric Research, Computational and Information Systems Laboratory

Nelson, MA, Pardyjak, ER, Brown, MJ & Klewicki, JC 2007. Properties of the Wind Field within the Oklahoma City Park Avenue Street Canyon. Part II: Spectra, Cospectra, and Quadrant Analyses. *Journal of Applied Meteorology and Climatology,* 46**,** 2055-2073,DOI: 10.1175/2006jamc1290.1.

Ohashi, Y & Kida, H 2002. Local Circulations Developed in the Vicinity of Both Coastal and Inland Urban Areas: A Numerical Study with a Mesoscale Atmospheric Model. *Journal of Applied Meteorology,* 41**,** 30-45,DOI: 10.1175/1520-0450(2002)041<0030:lcditv>2.0.co;2.

Oke, TR 1981. Canyon geometry and the nocturnal urban heat island: Comparison of scale model and field observations. *Journal of Climatology,* 1**,** 237-254,DOI: 10.1002/joc.3370010304.

Oke, TR 1982. The energetic basis of the urban heat island. *Quarterly Journal of the Royal Meteorological Society,* 108**,** 1-24,DOI: 10.1002/qj.49710845502.

Oke, TR 1987. *Boundary Layer Climates*, Routledge

Oke, TR 1988. The urban energy balance. *Progress in Physical Geography,* 12**,** 471-508,DOI: 10.1177/030913338801200401.

Oke, TR, Johnson, GT, Steyn, DG & Watson, ID 1991. Simulation of surface urban heat islands under 'ideal' conditions at night part 2: Diagnosis of causation. *Boundary-Layer Meteorology,* 56**,** 339-358,DOI: 10.1007/bf00119211.

Papanastasiou, DK, Melas, D & Lissaridis, I 2010. Study of wind field under sea breeze conditions; an application of WRF model. *Atmospheric Research,* 98**,** 102-117,DOI: http://dx.doi.org/10.1016/j.atmosres.2010.06.005.

Pattiaratchi, C, Hegge, B, Gould, J & Eliot, I 1997. Impact of sea-breeze activity on nearshore and foreshore processes in southwestern Australia. *Continental Shelf Research,* 17**,** 1539-1560

Patz, JA, Campbell-Lendrum, D, Holloway, T & Foley, JA 2005. Impact of regional climate change on human health. *Nature,* 438**,** 310-317

Physick, W 1976. A Numerical Model of the Sea-Breeze Phenomenon over a Lake or Gulf. *Journal of the Atmospheric Sciences,* 33**,** 2107-2135,DOI: 10.1175/1520-0469(1976)033<2107:anmots>2.0.co;2.

Physick, WL & Byron-Scott, RAD 1977. Observations of the Sea Breeze in the Vicinity of a Gulf. *Weather,* 32**,** 373-381,DOI: 10.1002/j.1477-8696.1977.tb04481.x.

Pielke, S & Roger, A 2013. *Mesoscale Meteorological Modeling*, Academic Press,570,DOI: http://dx.doi.org/10.1016/B978-0-12-385237-3.00013-X.

Plummer, N, Lin, Z & Torok, S 1995. Trends in the diurnal temperature range over Australia since 1951. *Atmospheric Research,* 37**,** 79-86,DOI: http://dx.doi.org/10.1016/0169-8095(94)00070-T.

Prtenjak, MT & Grisogono, B 2007. Sea/land breeze climatological characteristics along the northern Croatian Adriatic coast. *Theoretical and Applied Climatology,* 90**,** 201-215,DOI: 10.1007/s00704-006-0286-9.

Psuty, NP 2005. Coastal Foredune Development under a Diurnal Wind Regime, Paracas, Peru. *Journal of Coastal Research***,** 68-73

Rasch, P 2012. Climate Change Modeling Methodology, Introduction. *In:* RASCH, P. J. (ed.) *Climate Change Modeling Methodology.* Springer New York,1-4DOI: 10.1007/978-1-4614-5767-1_1.

Rosenzweig, C, Solecki, WD, Parshall, L, Chopping, M, Pope, G & Goldberg, R 2005. Characterizing the urban heat island in current and future climates in New Jersey. *Global Environmental Change Part B: Environmental Hazards,* 6**,** 51-62

Rotach, MW 1993. Turbulence close to a rough urban surface part I: Reynolds stress. *Boundary-layer meteorology,* 65**,** 1-28,DOI: 10.1007/bf00708816.

Rotach, MW, Vogt, R, Bernhofer, C, Batchvarova, E, Christen, A, Clappier, A, Feddersen, B, Gryning, SE, Martucci, G, Mayer, H, Mitev, V, Oke, TR, Parlow, E, Richner, H, Roth, M, Roulet, YA, Ruffieux, D, Salmond, JA, Schatzmann, M & Voogt, JA 2005. BUBBLE – an Urban Boundary Layer Meteorology Project. *Theoretical and Applied climatology,* 81**,** 231-261,DOI: 10.1007/s00704-004-0117-9.

Sailor, DJ 1995. Simulated Urban Climate Response to Modifications in Surface Albedo and Vegetative Cover. *Journal of Applied Meteorology,* 34**,** 1694-1704,DOI: 10.1175/1520-0450-34.7.1694.

Salamanca, F, Martilli, A, Tewari, M & Chen, F 2010. A Study of the Urban Boundary Layer Using Different Urban Parameterizations and High-Resolution Urban Canopy Parameters with WRF. *Journal of Applied Meteorology and Climatology,* 50**,** 1107-1128,DOI: 10.1175/2010jamc2538.1.

Sarkar, A, Saraswat, R & Chandrasekar, A 1998. Numerical study of the effects of urban heat island on the characteristic features of the sea breeze circulation. *Journal of Earth System Science,* 107**,** 127-137

Schneider, SH & Dickinson, RE 1974. Climate modeling. *Reviews of Geophysics,* 12**,** 447-493,DOI: 10.1029/RG012i003p00447.

Sha, W, Grace, W & Physick, WL 1996. A Numerical Experiment on the Adelaide Gully Wind of South Australia. *Australian Meteorological Magazine,* 45**,** 19-40

Shigeta, Y, Ohashi, Y & Tsukamoto, O 2009. Urban Cool Island in Daytime Analysis by Using Thermal Image and Air Temperature Measurements. *The seventh International Conference on Urban Climate.* Yokohama, Japan:

Shin, H & Hong, S-Y 2011. Intercomparison of Planetary Boundary-Layer Parametrizations in the WRF Model for a Single Day from CASES-99. *Boundary-layer meteorology,* 139**,** 261-281,DOI: 10.1007/s10546-010-9583-z.

Simpson, JE 1994. *Sea Breeze and Local Wind,* New York Cambridge Univ. Press,234

Simpson, M, Raman, S, Suresh, R & Mohanty, U 2008. Urban effects of Chennai on sea breeze induced convection and precipitation. *Journal of Earth System Science,* 117**,** 897-909

Skamarock, WC, Klemp, JB, Dudhia, J, Gill, DO, Barker, DM, Wang, W & Powers, JG 2007. A Description of the Advanced Research WRF Version 2. *NCAR Technical Note.* Boulder, Colorado, USA: National Center for Atmospheric Research

Smith, S 1981. Comparison of Wind Speeds Recorded Simultaneously by Pressure-Tube and Meteorological Office Electrical Cup-Generator Anemographs. *Meteorological Magazine,* 110**,** 288-300

South Australian Coast Protection Board 1993. Maintaining the Adelaide Coastline. *Coastline.* 28 ed. Adelaide: Department for Environment and Heritage

State of Environment, SA 2011. Residential development of Adelaide and environs, pre-1910–2011, and planned development areas to 2038. *In:* VALUATION DATA SUPPLIED BY THE DEPARTMENT OF PLANNING, T. A. I. (ed.).

Steyn, DG 2003. Scaling the Vertical Structure of Sea Breezes Revisited. *Boundary-layer meteorology,* 107**,** 177-188

Steyn, DG & Faulkner, DA 1986. The climatology of sea breezes in the lower Fraser Valley.B. C. *Climatol. Bull,* 20**,** 21-39

Stone, DJ. 1969. Sea Breezes across Adelaide. B.A(Hons), University of Adelaide.

Sumner, GN 1977. Sea Breeze Occurrence in Hilly Terrain. *Weather,* 32**,** 200-208

Suppiah, R, Preston, B, P.H.Whetton, McInnes, KL, R.N.Jones, Macadam, I, Bathols, J & Kirono, D 2006. Climate change under enhanced greenhouse conditions in South Australia: An

updated report on: Assessment of climate change, impacts and risk management strategies relevant to South Australia. *In:* CLIMATE IMPACTS AND RISK GROUP, C. M. A. A. R. (ed.).

Tijm, ABC, Holtslag, AAM & van Delden, AJ 1999. Observations and Modeling of the Sea Breeze with the Return Current. *Monthly Weather Review,* 127**,** 625-640,DOI: 10.1175/1520-0493(1999)127<0625:oamots>2.0.co;2.

Tomlinson, CJ, Prieto-Lopez, T, Bassett, R, Chapman, L, Cai, XM, Thornes, JE & Baker, CJ 2013. Showcasing urban heat island work in Birmingham – measuring, monitoring, modelling and more. *Weather,* 68**,** 44-49,DOI: 10.1002/wea.1998.

Torok, SJ, Morris, CJG, Skinner, C & Plummer, N 2001. Urban heat island features of southeast Australian towns. *Australian Meteorological Magazine,* 50**,** 1-13

Townshend, JRG 1994. Global data sets for land applications from the Advanced Very High Resolution Radiometer: an introduction. *International Journal of Remote Sensing,* 15**,** 3319-3332,DOI: 10.1080/01431169408954333.

Trenberth, KE 1992. *Climate System Modeling*, Cambridge University Press

Tucker, R, Parker, J, Barnett, L, Cole, R, Cox, S, Davis, J, Deans, J, Detmar, S, Eaton, A, Fotheringham, D, Hutchens, C, Johnson, P, Murray–Jones, S, Orchard, F, Penney, S, Sandercock, R, Scriven, L, Townsend, M & Williams, G 2005. Adelaide's Living Beaches, A Strategy for 2005–2025. the Government of South Australia

Uno, W & Ueda, N 1988. An Observational Study of the Structure of the Nocturnal Urban Boundary Layer *Boundary-Layer Meteorol* 45**,** 59-83

Voice, M, Harvey, N & Walsh, K 2006. Vulnerability to climate change of Australia's coastal zone: Analysis of gaps in methods, data and system thresholds. *In:* VOICE, M., HARVEY, N. & WALSH, K. (eds.). CAnberra: Australian Greenhouse Office

von Storch, H, Langenberg, H & Feser, F 2000. A Spectral Nudging Technique for Dynamical Downscaling Purposes. *Monthly Weather Review,* 128**,** 3664-3673,DOI: 10.1175/1520-0493(2000)128<3664:asntfd>2.0.co;2.

Voogt, JA & Oke, TR 2003. Thermal remote sensing of urban climates. *Remote Sensing of Environment,* 86**,** 370-384,DOI: 10.1016/s0034-4257(03)00079-8.

Warrach-Sagi, K, Schwitalla, T, Wulfmeyer, V & Bauer, H-S 2013. Evaluation of a climate simulation in Europe based on the WRF–NOAH model system: precipitation in Germany. *Climate Dynamics,* 41**,** 755-774,DOI: 10.1007/s00382-013-1727-7.

Watson, P 2005. *Ideas. A History from Fire to Freud*, Phoenix,1118

Watts, A 1955. Sea breeze at Thorney Island. *Meteorol. Mag,* 84**,** 42-48

Williams, AAJ & Stone, RC 2009. An assessment of relationships between the Australian subtropical ridge, rainfall variability, and high-latitude circulation patterns *International Journal of Climatology,* 29**,** 691-709

Wright, WJ 1997. Tropical–extratropical cloudbands and Australian rainfall: I. climatology. *International Journal of Climatology,* 17**,** 807-829,DOI: 10.1002/(sici)1097-0088(19970630)17:8<807::aid-joc162>3.0.co;2-j.

Xian, Z & Pielke, RA 1991. The Effects of Width of Landmasses on the Development of Sea Breezes. *Journal of Applied Meteorology,* 30**,** 1280-1304,DOI: 10.1175/1520-0450(1991)030<1280:teowol>2.0.co;2.

Yerramilli, A, Challa, VS, Dodla, VBR, Dasari, HP, Young, JH, Patrick, C, Baham, JM, Hughes, RL, Hardy, MG & Swanier1, SJ 2010. Simulation of Surface Ozone Pollution in the Central Gulf Coast Region Using WRF/Chem Model: Sensitivity to PBL and Land Surface Physics. *Advances in Meteorology,* 2010**,** 24

Yoshikado, H 1992. Numerical Study of the Daytime Urban Effect and Its Interaction with the Sea Breeze. *Journal of Applied Meteorology,* 31**,** 1146-1164,DOI: 10.1175/1520-0450(1992)031<1146:nsotdu>2.0.co;2.

Yoshikado, H 1994. Interaction of the Sea Breeze with Urban Heat Islands of Different Sizes and Locations. *Journal of the Meteorological Society of Japan. Ser. II,* 72**,** 139-143

Yoshinori, S, Yukitaka, O & Osamu, T 2009. Urban Cool Island in Daytime Analysis by Using Thermal Image and Air Temperature Measurements. *The seventh International Conference on Urban Climate.* Yokohama, Japan:

Zhang, H, Sato, N, Izumi, T, Hanaki, K & Aramaki, T 2008. Modified RAMS-Urban Canopy Model for Heat Island Simulation in Chongqing, China. *Journal of Applied Meteorology and Climatology,* 47**,** 509-524

Appendix A: Adelaide Airport Station Metadata

The location of the Adelaide Airport station, duration and frequency of the meteorological observations are explained here. There has been some replacement of observation equipment for the station, the details of which are attached here.

Australian Government
Bureau of Meteorology

Basic Climatological Station Metadata

Current status

Metadata compiled: 28 JUL 2013

Station: ADELAIDE AIRPORT

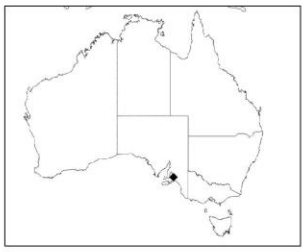

Bureau of Meteorology station number: 023034
Bureau of Meteorology district name: Adelaide Plains
State: SA

World Meteorological Organization number: 94672
Identification: YPAD

Network Classification: CLIMAT Stations, CLIMAT TEMP Stations, Regional Basic Synoptic Network
Station purpose: Synoptic, Upper Air, Aeronautical
Automatic Weather Station: Almos

Current Station Location				
Latitude	**Decimal**	-34.9524	**Hour Min Sec**	34°57'9"S
Longitude	**Decimal**	138.5204	**Hour Min Sec**	138°31'13"E
Station Height	2 m	**Barometer Height**	8.2 m	
Method of station geographic positioning			GPS	

Year opened: 1955
Status: Open

Station summary

No summary for this site has been written as yet.

Historical metadata for this site has not been quality controlled for accuracy and completeness. Data other than current station information, particularly earlier than 1998, should be considered accordingly. Information may not be complete, as backfilling of historical data is incomplete.

Prepared by National Climate Centre of the Bureau of Meteorology.
Contact us by phone on (03) 9669 4082, by fax on (03) 9669 4515, or by email on climatedata@bom.gov.au

Australian Government
Bureau of Meteorology

Basic Climatological Station Metadata
Current status

Station:	ADELAIDE AIRPORT			**Location:**	ADELAIDE AIRPORT			**State:**	SA
Bureau No.:	023034	**WMO No.:**	94672	**Aviation ID:**	YPAD	**Opened:**	16 Feb 1955	**Current Status:**	Still open
Latitude:	-34.9524	**Longitude:**	138.5204	**Elevation:**	2 m	**Barometer Elev:**	8.2 m	**Metadata compiled:**	28 JUL 2013

Observation summary

The table below indicates the approximate completeness of the record for individual element types within the Australian Data Archive for Meteorology. For elements not listed see the note below.

Completeness 0% → 100%

DAILY DATA HOLDINGS

OBSERVATION TYPE	FIRST MONTH	LAST MONTH	COMPLETENESS (% estimate)	SINGLE DAYS MISSED	FULL MONTHS MISSED
EVAPORATION	JAN 1982	JUN 2013	99.8	16	0
EVAPORIMETER - MAXIMUM WATER TEMPERATURE	JAN 1982	JUN 2011	97.0	285	1
GROUND MINIMUM TEMPERATURE	AUG 1959	JUN 2013	98.0	167	7
MAXIMUM AIR TEMPERATURE	FEB 1955	JUN 2013	99.9	16	0
MAXIMUM WIND GUST SPEED	FEB 1955	JUN 2013	99.2	163	0
SUNSHINE HOURS	AUG 1983	JUN 2013	99.6	40	0
WIND RUN ABOVE 10 FEET	JAN 1988	JUN 2013	70.1	219	84
WIND RUN BELOW 10 FEET	JAN 1982	JUN 2013	99.3	76	0
RAINFALL	JAN 1955	JUL 2013	100	N/A	N/A

Australian Government
Bureau of Meteorology

Basic Climatological Station Metadata
Current status

Station:	ADELAIDE AIRPORT			**Location:**	ADELAIDE AIRPORT			**State:**	SA
Bureau No.:	023034	**WMO No.:**	94672	**Aviation ID:**	YPAD	**Opened:**	16 Feb 1955	**Current Status:**	Still open
Latitude:	-34.9524	**Longitude:**	138.5204	**Elevation:**	2 m	**Barometer Elev:**	8.2 m	**Metadata compiled:**	28 JUL 2013

HOURLY DATA HOLDINGS - from 1 to 24 observations per day

OBSERVATION TYPE	FIRST MONTH	LAST MONTH	COMPLETENESS (% estimate)	FREQUENCY average daily	SINGLE DAYS MISSED	FULL MONTHS MISSED
AIR TEMPERATURE	FEB 1955	JUN 2013	99.8	8.1	15	0
DEW POINT	FEB 1955	JUN 2013	99.7	8.1	15	0
MEAN SEA LEVEL PRESSURE	FEB 1955	JUN 2013	99.8	8.1	15	0
SOIL TEMPERATURE - 10cm	FEB 1999	JUN 2013	98.4	2.0	26	0
TOTAL CLOUD AMOUNT	FEB 1955	JUN 2013	99.8	8.0	15	0
WIND SPEED	FEB 1955	JUN 2013	99.8	8.1	15	0
UPPER AIR TEMPERATURE	JUN 1954	JUN 2013	93.2	2.0	256	0
UPPER AIR WIND SPEED	JAN 1955	JUN 2013	94.6	4.0	55	15

Historical metadata for this site has not been quality controlled for accuracy and completeness. Data other than current station information, particularly earlier than 1998, should be considered accordingly. Information may not be complete, as backfilling of historical data is incomplete.

Prepared by National Climate Centre of the Bureau of Meteorology.
Contact us by phone on (03) 9669 4082, by fax on (03) 9669 4515, or by email on climatedata@bom.gov.au
 Page 3.

Australian Government
Bureau of Meteorology

Basic Climatological Station Metadata
Current status

Station:	ADELAIDE AIRPORT			**Location:**	ADELAIDE AIRPORT			**State:**	SA
Bureau No.:	023034	**WMO No.:**	94672	**Aviation ID:**	YPAD	**Opened:**	16 Feb 1955	**Current Status:**	Still open
Latitude:	-34.9524	**Longitude:**	138.5204	**Elevation:**	2 m	**Barometer Elev:**	8.2 m	**Metadata compiled:**	28 JUL 2013

RAINFALL INTENSITY DATA HOLDINGS

OBSERVATION TYPE	FIRST MONTH	LAST MONTH	COMPLETENESS (% estimate)	SINGLE DAYS MISSED	FULL MONTHS MISSED
RAINFALL INTENSITY	JAN 1967	JUN 2011	94.0	599	12

ONE-MINUTE DATA HOLDINGS

OBSERVATION TYPE	FIRST MONTH	LAST MONTH	COMPLETENESS (% estimate)	FREQUENCY average daily	SINGLE DAYS MISSED	FULL MONTHS MISSED
ALL ELEMENTS	DEC 2001	JUL 2013	99.6	1433.8	N/A	0

HALF-HOURLY DATA HOLDINGS

OBSERVATION TYPE	FIRST MONTH	LAST MONTH	COMPLETENESS (% estimate)	FREQUENCY average daily	SINGLE DAYS MISSED	FULL MONTHS MISSED
ALL ELEMENTS	JAN 1985	JUL 2013	103.3	49.6	N/A	0

UPPER-AIR EDT DATA HOLDINGS

OBSERVATION TYPE	FIRST MONTH	LAST MONTH	COMPLETENESS (% estimate)	FREQUENCY average daily	SINGLE DAYS MISSED	FULL MONTHS MISSED
Wind only flights	Jun 2000	Jul 2013	N/A	2.1	190	1
Wind, temperature and pressure flights	Apr 1991	Jul 2013	N/A	2.0	65	1

Holdings calculated up to 01 Jul 2013

The % complete figure is the completeness of observations averaged over all months of record, for the given station and observation type, taking gaps into account. For hourly holdings, the completeness is relative to the maximum number of daily observations for the site each month, and is therefore an estimate. For daily holdings, the completeness figure shown is exact.

The single days missed figure is the total number of days for which no observation was received, not including full missed months. The full months missed figure is the total of full month gaps over the period of record. Where an element is not included assumptions can generally be made about availability, and the list to use has been suggested below.

Unlisted element	Listed element to use
Minimum air temperature	Maximum air temperature
Wet bulb temperature	Dew point
Soil temperature at 20, 50 & 100cm	10cm soil temperature
Relative humidity	Dew point
Minimum temp. of water in evaporimeter	Evaporimeter - max water temp
Visual observations eg. weather, visibility	Total cloud amount
Sea related observations	Sea state

Australian Government
Bureau of Meteorology

Extended Climatological Station Metadata
All History

Station:	ADELAIDE AIRPORT			**Location:**	ADELAIDE AIRPORT			**State:**	SA
Bureau No.:	023034	**WMO No.:**	94672	**Aviation ID:**	YPAD	**Opened:**	16 Feb 1955	**Current Status:**	Still open
Latitude:	-34.9524	**Longitude:**	138.5204	**Elevation:**	2 m	**Barometer Elev:**	8.2 m	**Metadata compiled:**	28 JUL 2013

Instrument Location and Surrounding Features
20/12/2011(most recent)

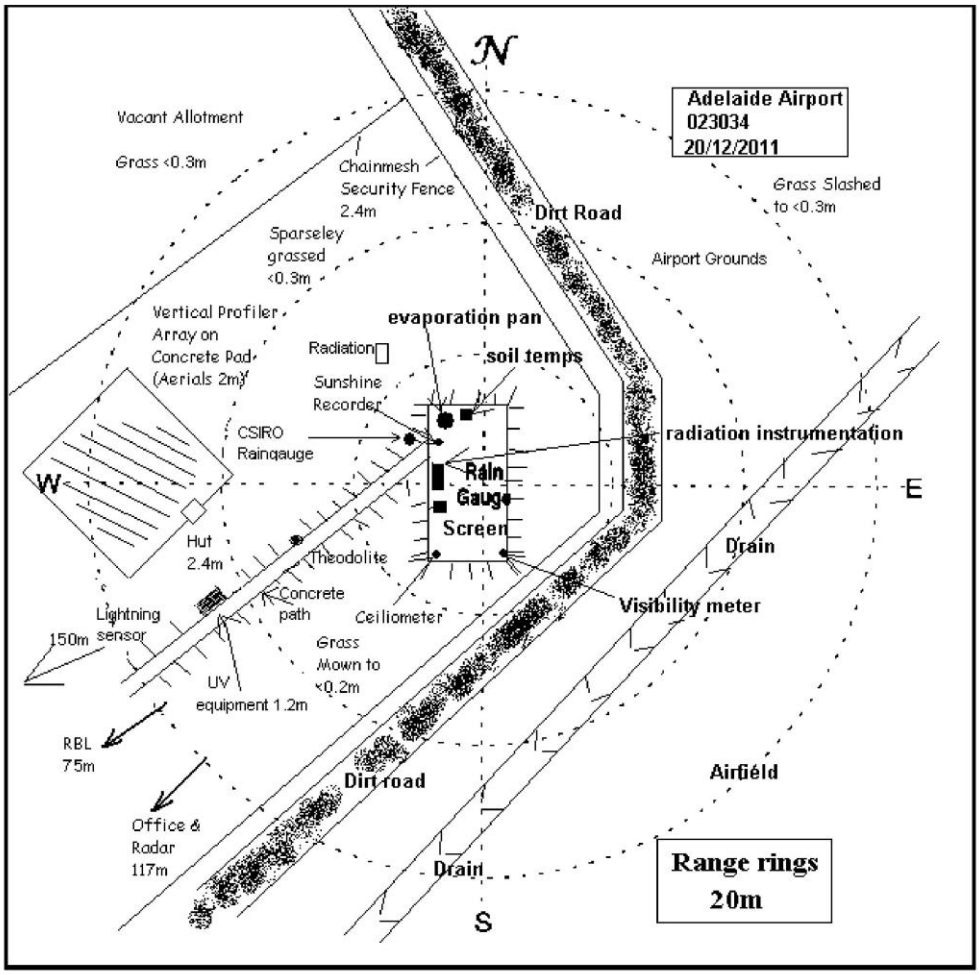

Historical metadata for this site has not been quality controlled for accuracy and completeness. Data other than current station information, particularly earlier than 1998, should be considered accordingly. Information may not be complete, as backfilling of historical data is incomplete.

Australian Government
Bureau of Meteorology

Extended Climatological Station Metadata
All History

Station:	ADELAIDE AIRPORT			**Location:**	ADELAIDE AIRPORT			**State:**	SA
Bureau No.:	023034	**WMO No.:**	94672	**Aviation ID:**	YPAD	**Opened:**	16 Feb 1955	**Current Status:**	Still open
Latitude:	-34.9524	**Longitude:**	138.5204	**Elevation:**	2 m	**Barometer Elev:**	8.2 m	**Metadata compiled:**	28 JUL 2013

Instrument Location and Surrounding Features
17/01/2011

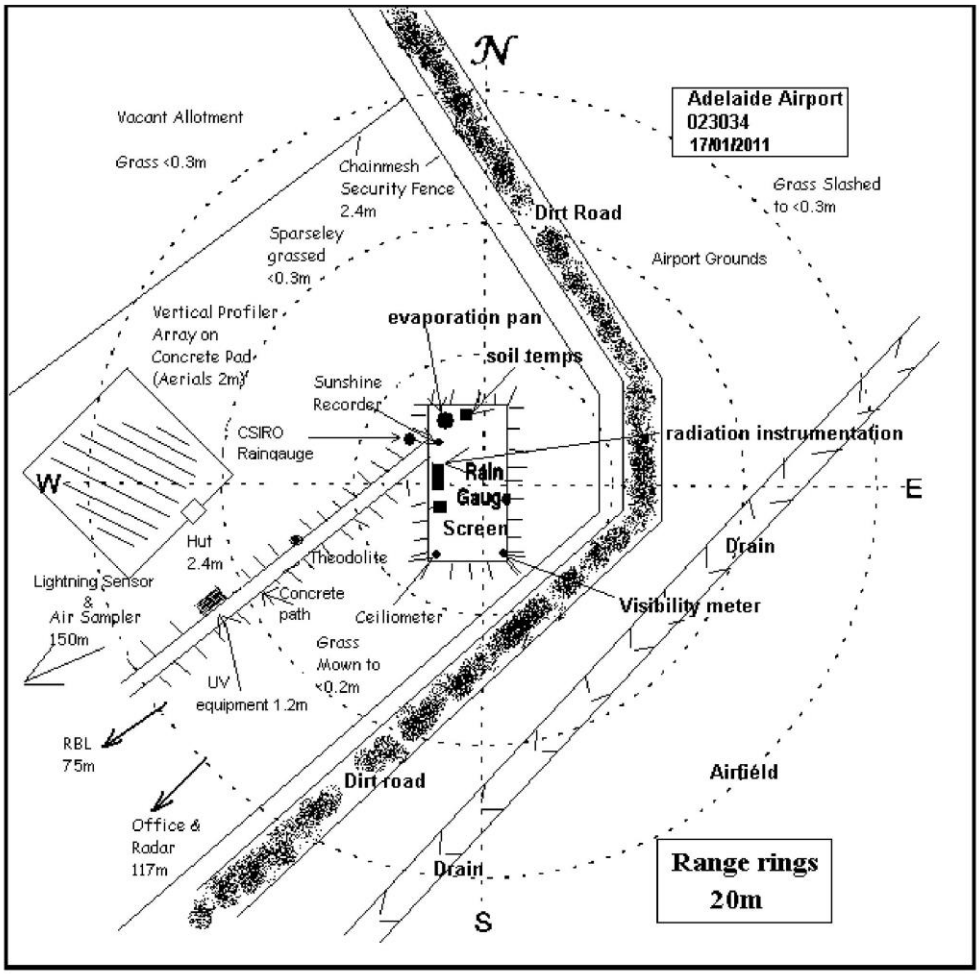

Historical metadata for this site has not been quality controlled for accuracy and completeness. Data other than current station information, particularly earlier than 1998, should be considered accordingly. Information may not be complete, as backfilling of historical data is incomplete.

Australian Government
Bureau of Meteorology

Extended Climatological Station Metadata
All History

Station:	ADELAIDE AIRPORT			**Location:**	ADELAIDE AIRPORT			**State:**	SA
Bureau No.:	023034	**WMO No.:**	94672	**Aviation ID:**	YPAD	**Opened:**	16 Feb 1955	**Current Status:**	Still open
Latitude:	-34.9524	**Longitude:**	138.5204	**Elevation:**	2 m	**Barometer Elev:**	8.2 m	**Metadata compiled:**	28 JUL 2013

Instrument Location and Surrounding Features
21/01/2010

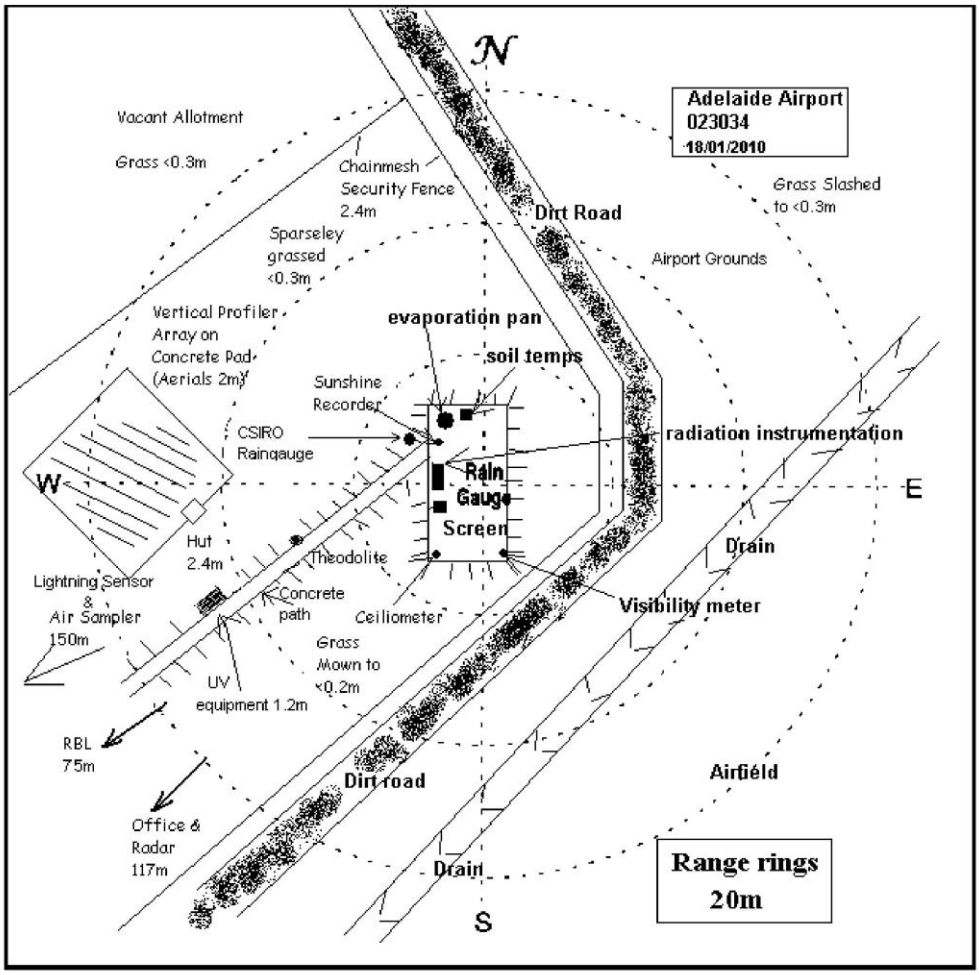

Historical metadata for this site has not been quality controlled for accuracy and completeness. Data other than current station information, particularly earlier than 1998, should be considered accordingly. Information may not be complete, as backfilling of historical data is incomplete.

Australian Government
Bureau of Meteorology

Extended Climatological Station Metadata
All History

Station:	ADELAIDE AIRPORT			**Location:**	ADELAIDE AIRPORT			**State:**	SA
Bureau No.:	023034	**WMO No.:**	94672	**Aviation ID:**	YPAD	**Opened:**	16 Feb 1955	**Current Status:**	Still open
Latitude:	-34.9524	**Longitude:**	138.5204	**Elevation:**	2 m	**Barometer Elev:**	8.2 m	**Metadata compiled:**	28 JUL 2013

Instrument Location and Surrounding Features
18/01/2010

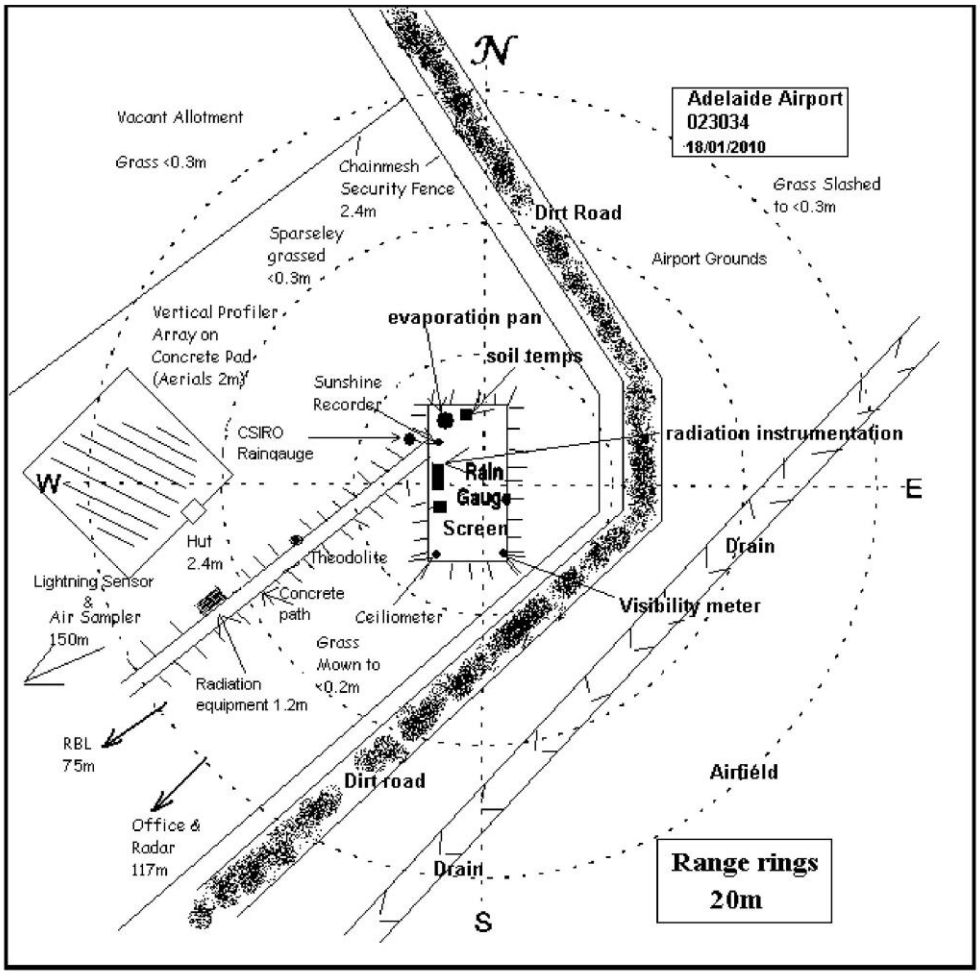

Historical metadata for this site has not been quality controlled for accuracy and completeness. Data other than current station information, particularly earlier than 1998, should be considered accordingly. Information may not be complete, as backfilling of historical data is incomplete.

Australian Government
Bureau of Meteorology

Extended Climatological Station Metadata
All History

Station:	ADELAIDE AIRPORT			**Location:**	ADELAIDE AIRPORT			**State:**	SA
Bureau No.:	023034	**WMO No.:**	94672	**Aviation ID:**	YPAD	**Opened:**	16 Feb 1955	**Current Status:**	Still open
Latitude:	-34.9524	**Longitude:**	138.5204	**Elevation:**	2 m	**Barometer Elev:**	8.2 m	**Metadata compiled:**	28 JUL 2013

Instrument Location and Surrounding Features
24/12/2008

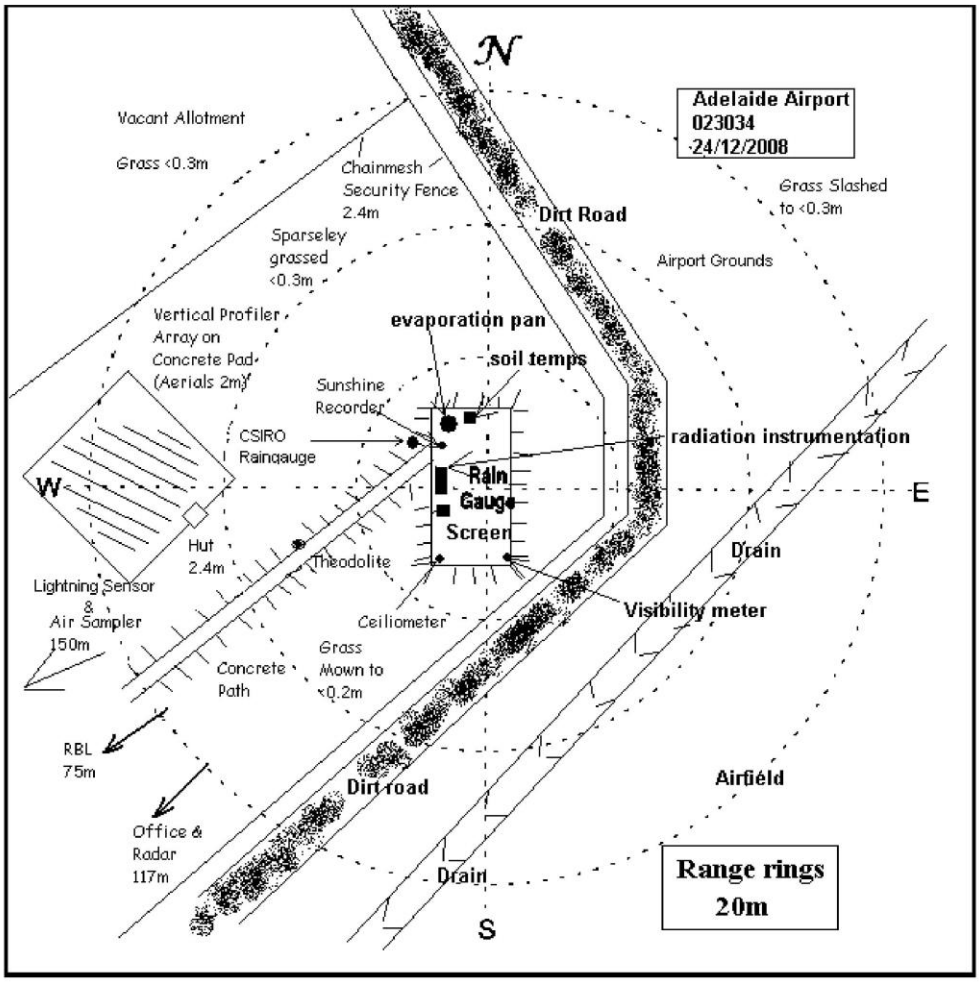

Historical metadata for this site has not been quality controlled for accuracy and completeness. Data other than current station information, particularly earlier than 1998, should be considered accordingly. Information may not be complete, as backfilling of historical data is incomplete.

Australian Government
Bureau of Meteorology

Extended Climatological Station Metadata
All History

Station:	ADELAIDE AIRPORT			**Location:**	ADELAIDE AIRPORT			**State:**	SA
Bureau No.:	023034	**WMO No.:**	94672	**Aviation ID:**	YPAD	**Opened:**	16 Feb 1955	**Current Status:**	Still open
Latitude:	-34.9524	**Longitude:**	138.5204	**Elevation:**	2 m	**Barometer Elev:**	8.2 m	**Metadata compiled:**	28 JUL 2013

Instrument Location and Surrounding Features
07/01/2008

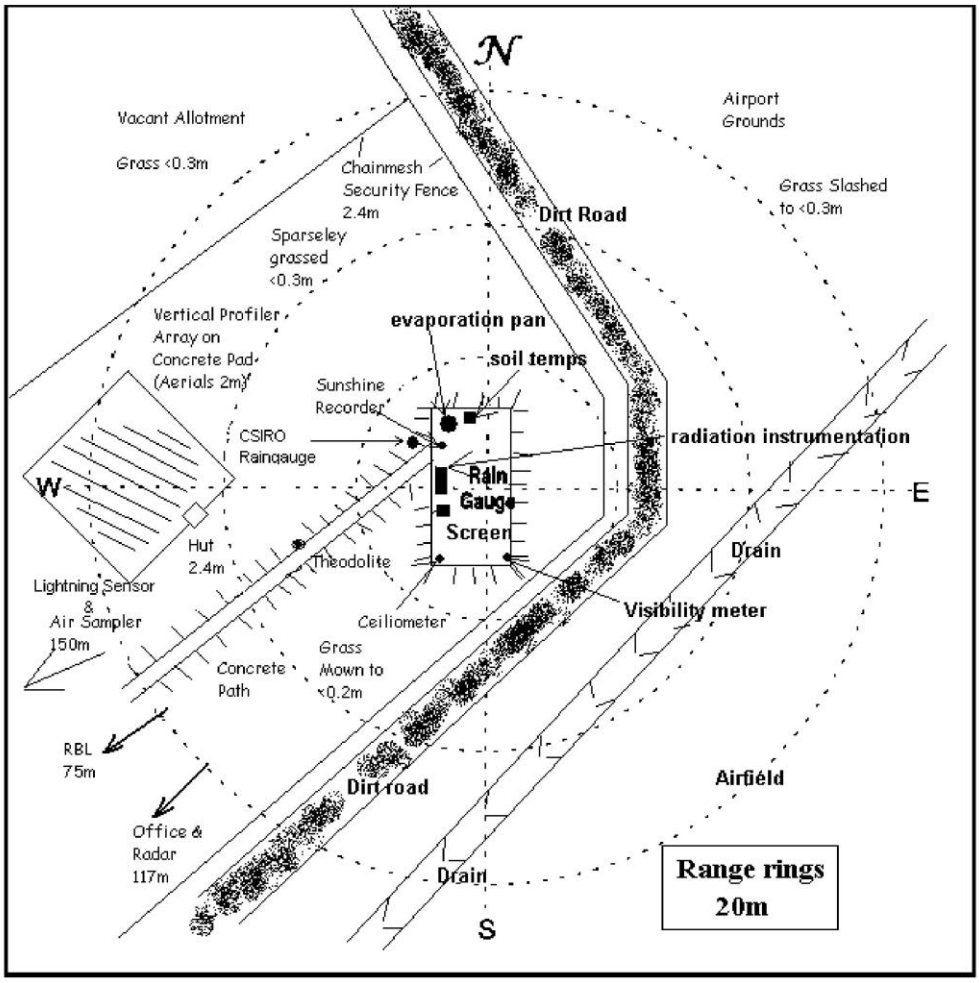

Australian Government
Bureau of Meteorology

Extended Climatological Station Metadata
All History

Station:	ADELAIDE AIRPORT			**Location:**	ADELAIDE AIRPORT			**State:**	SA
Bureau No.:	023034	**WMO No.:**	94672	**Aviation ID:**	YPAD	**Opened:**	16 Feb 1955	**Current Status:**	Still open
Latitude:	-34.9524	**Longitude:**	138.5204	**Elevation:**	2 m	**Barometer Elev:**	8.2 m	**Metadata compiled:**	28 JUL 2013

Instrument Location and Surrounding Features
21/03/2007

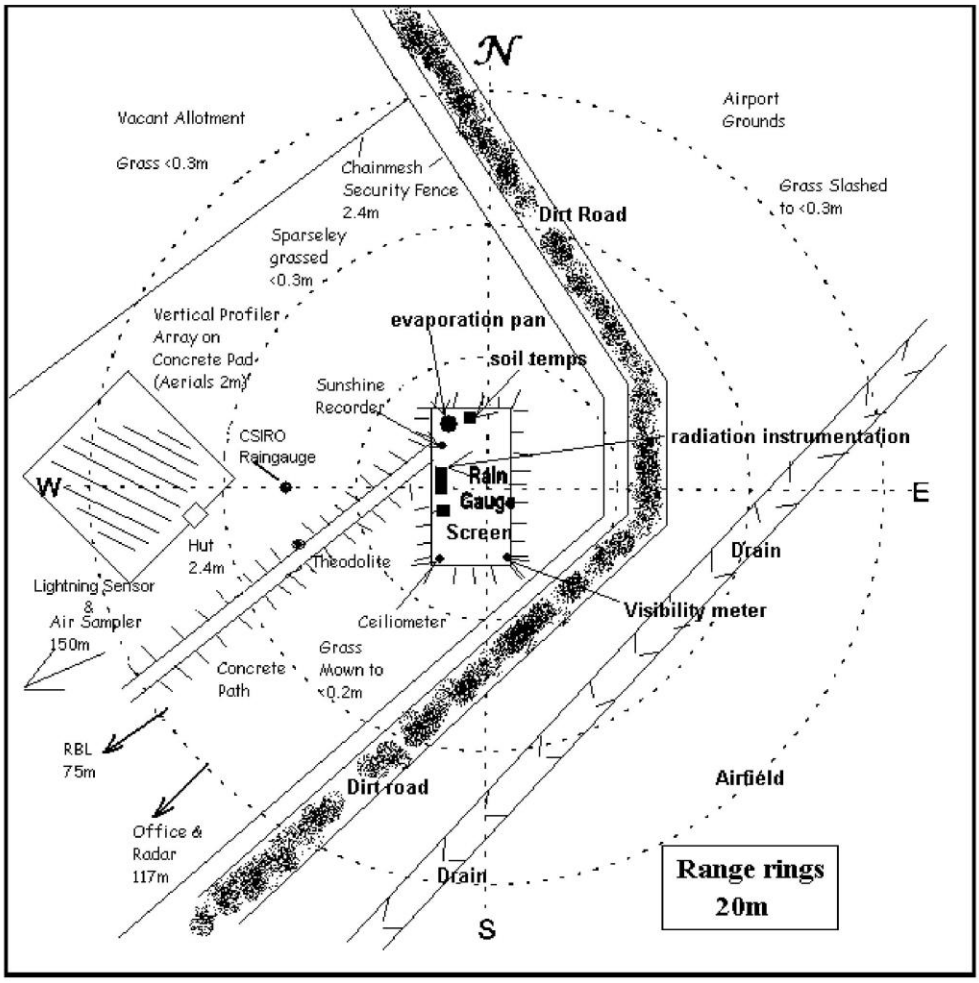

Australian Government
Bureau of Meteorology

Extended Climatological Station Metadata
All History

Station:	ADELAIDE AIRPORT			**Location:**	ADELAIDE AIRPORT			**State:**	SA
Bureau No.:	023034	**WMO No.:**	94672	**Aviation ID:**	YPAD	**Opened:**	16 Feb 1955	**Current Status:**	Still open
Latitude:	-34.9524	**Longitude:**	138.5204	**Elevation:**	2 m	**Barometer Elev:**	8.2 m	**Metadata compiled:**	28 JUL 2013

Instrument Location and Surrounding Features
12/01/2007

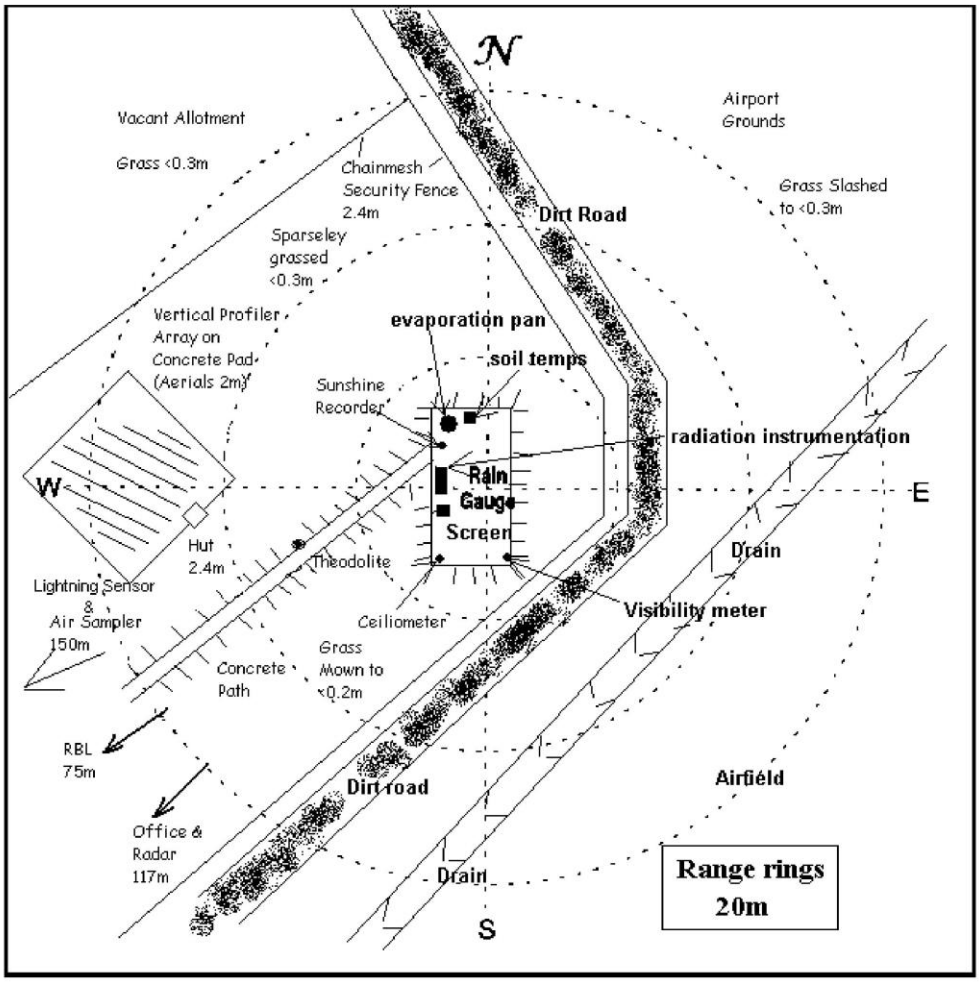

Australian Government
Bureau of Meteorology

Extended Climatological Station Metadata
All History

Station:	ADELAIDE AIRPORT			**Location:**	ADELAIDE AIRPORT			**State:**	SA
Bureau No.:	023034	**WMO No.:**	94672	**Aviation ID:**	YPAD	**Opened:**	16 Feb 1955	**Current Status:**	Still open
Latitude:	-34.9524	**Longitude:**	138.5204	**Elevation:**	2 m	**Barometer Elev:**	8.2 m	**Metadata compiled:**	28 JUL 2013

Instrument Location and Surrounding Features
13/01/2006

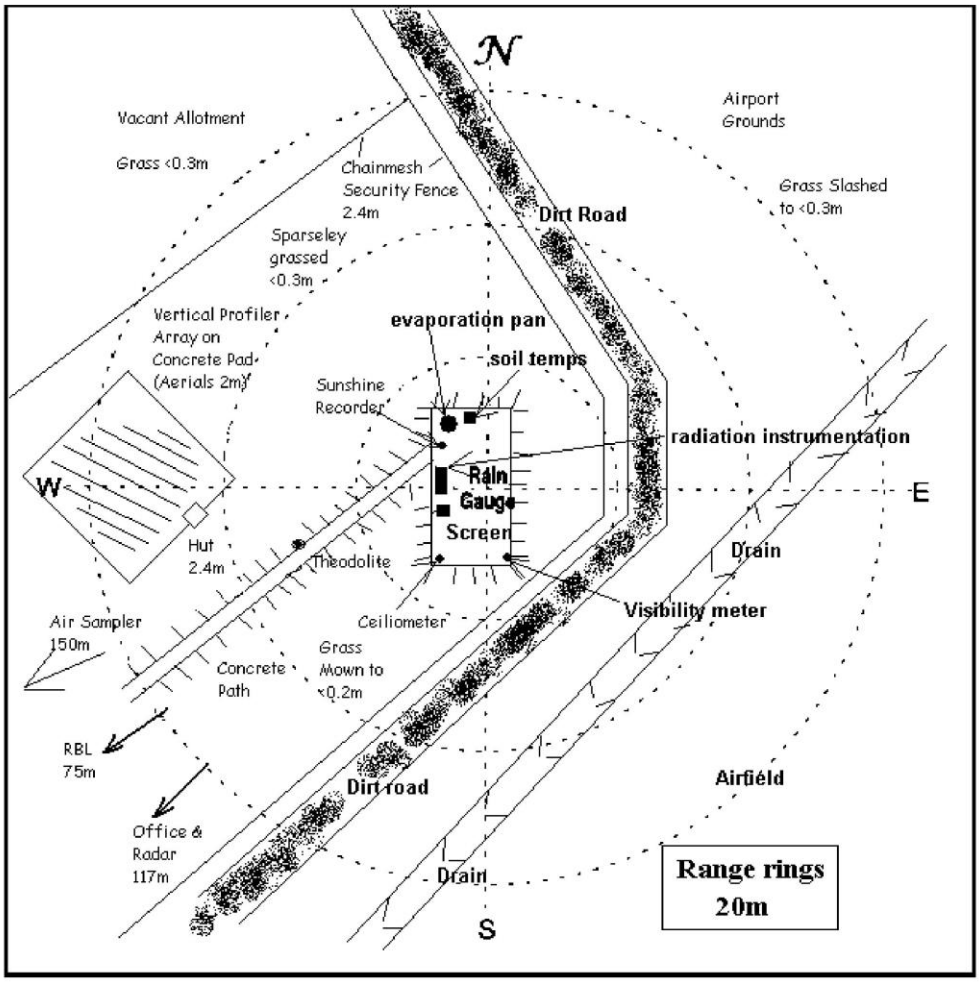

Historical metadata for this site has not been quality controlled for accuracy and completeness. Data other than current station information, particularly earlier than 1998, should be considered accordingly. Information may not be complete, as backfilling of historical data is incomplete.

Australian Government
Bureau of Meteorology

Extended Climatological Station Metadata
All History

Station:	ADELAIDE AIRPORT			**Location:**	ADELAIDE AIRPORT			**State:**	SA
Bureau No.:	023034	**WMO No.:**	94672	**Aviation ID:**	YPAD	**Opened:**	16 Feb 1955	**Current Status:**	Still open
Latitude:	-34.9524	**Longitude:**	138.5204	**Elevation:**	2 m	**Barometer Elev:**	8.2 m	**Metadata compiled:**	28 JUL 2013

Instrument Location and Surrounding Features
09/03/2005

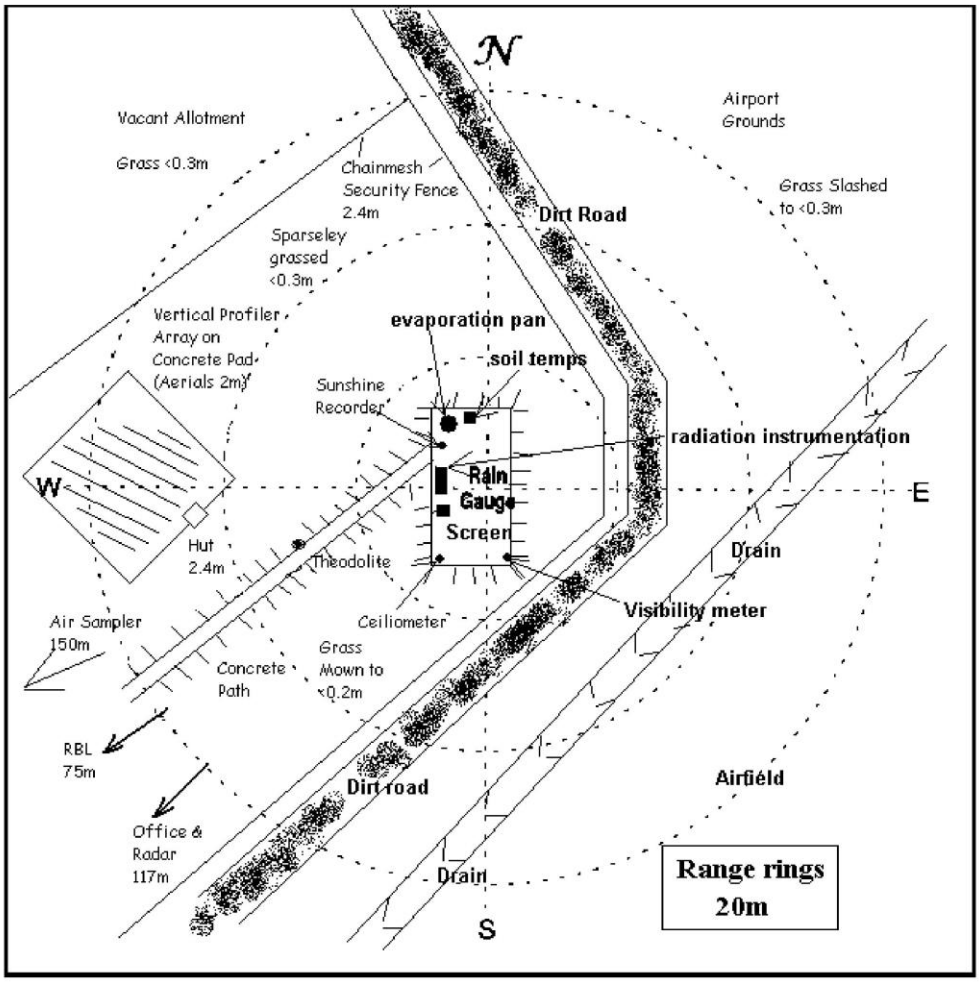

Historical metadata for this site has not been quality controlled for accuracy and completeness. Data other than current station information, particularly earlier than 1998, should be considered accordingly. Information may not be complete, as backfilling of historical data is incomplete.

Australian Government
Bureau of Meteorology

Extended Climatological Station Metadata
All History

Station:	ADELAIDE AIRPORT			**Location:**	ADELAIDE AIRPORT			**State:**	SA
Bureau No.:	023034	**WMO No.:**	94672	**Aviation ID:**	YPAD	**Opened:**	16 Feb 1955	**Current Status:**	Still open
Latitude:	-34.9524	**Longitude:**	138.5204	**Elevation:**	2 m	**Barometer Elev:**	8.2 m	**Metadata compiled:**	28 JUL 2013

Instrument Location and Surrounding Features
09/11/2004

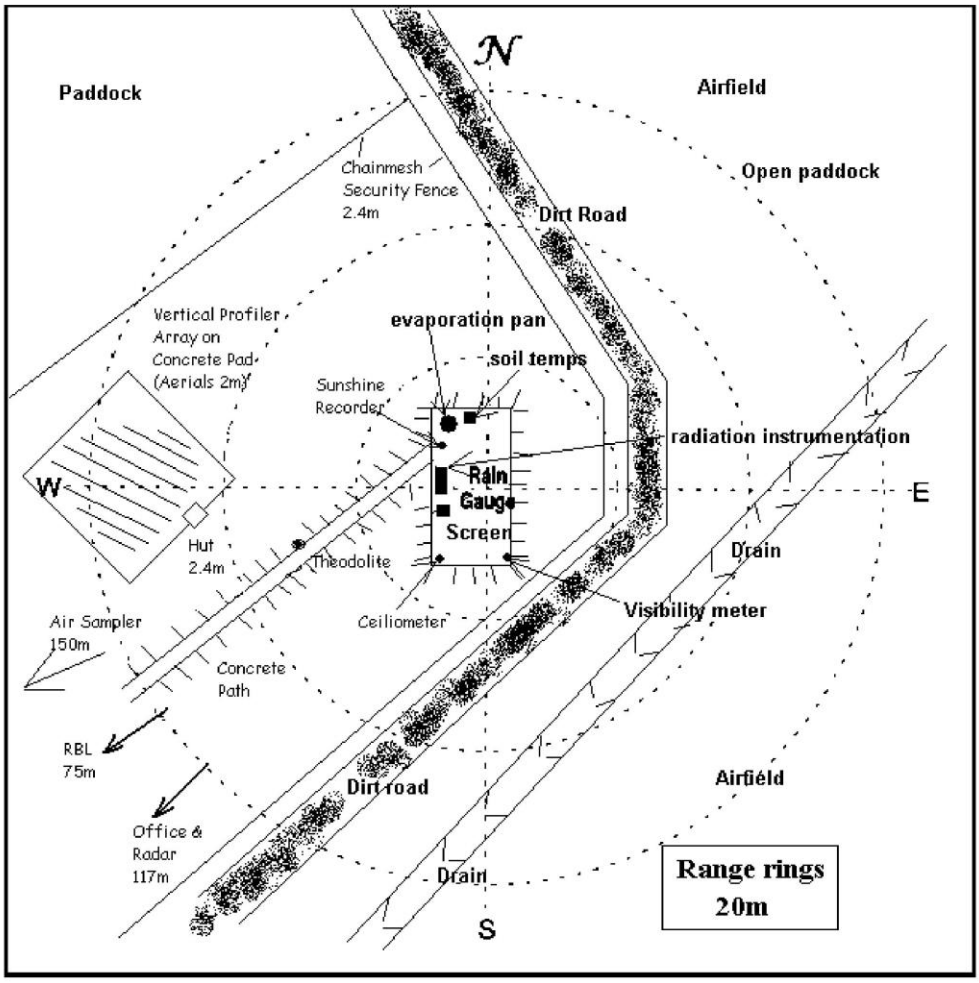

Historical metadata for this site has not been quality controlled for accuracy and completeness. Data other than current station information, particularly earlier than 1998, should be considered accordingly. Information may not be complete, as backfilling of historical data is incomplete.

Australian Government
Bureau of Meteorology

Extended Climatological Station Metadata
All History

Station:	ADELAIDE AIRPORT			**Location:**	ADELAIDE AIRPORT			**State:**	SA
Bureau No.:	023034	**WMO No.:**	94672	**Aviation ID:**	YPAD	**Opened:**	16 Feb 1955	**Current Status:**	Still open
Latitude:	-34.9524	**Longitude:**	138.5204	**Elevation:**	2 m	**Barometer Elev:**	8.2 m	**Metadata compiled:**	28 JUL 2013

Instrument Location and Surrounding Features
17/02/2004

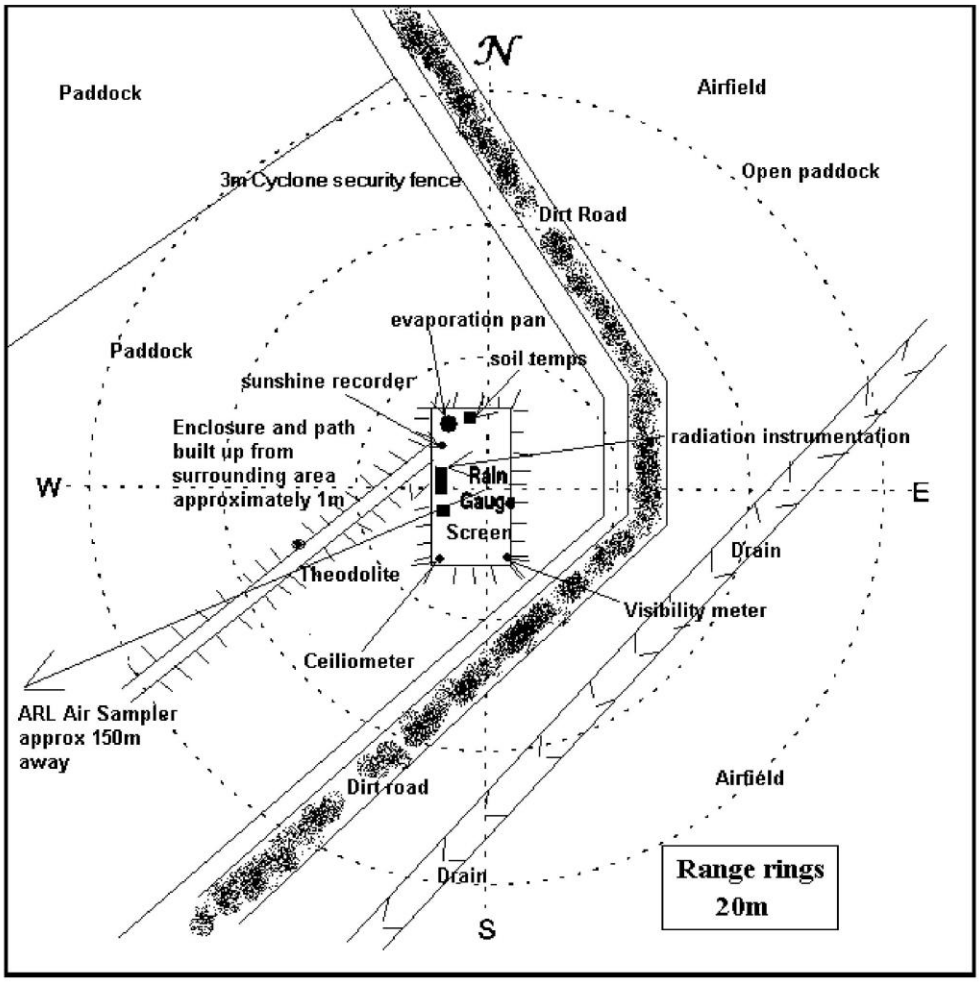

Historical metadata for this site has not been quality controlled for accuracy and completeness. Data other than current station information, particularly earlier than 1998, should be considered accordingly. Information may not be complete, as backfilling of historical data is incomplete.

Australian Government
Bureau of Meteorology

Extended Climatological Station Metadata
All History

Station:	ADELAIDE AIRPORT			**Location:**	ADELAIDE AIRPORT			**State:**	SA
Bureau No.:	023034	**WMO No.:**	94672	**Aviation ID:**	YPAD	**Opened:**	16 Feb 1955	**Current Status:**	Still open
Latitude:	-34.9524	**Longitude:**	138.5204	**Elevation:**	2 m	**Barometer Elev:**	8.2 m	**Metadata compiled:**	28 JUL 2013

Instrument Location and Surrounding Features
06/02/2004

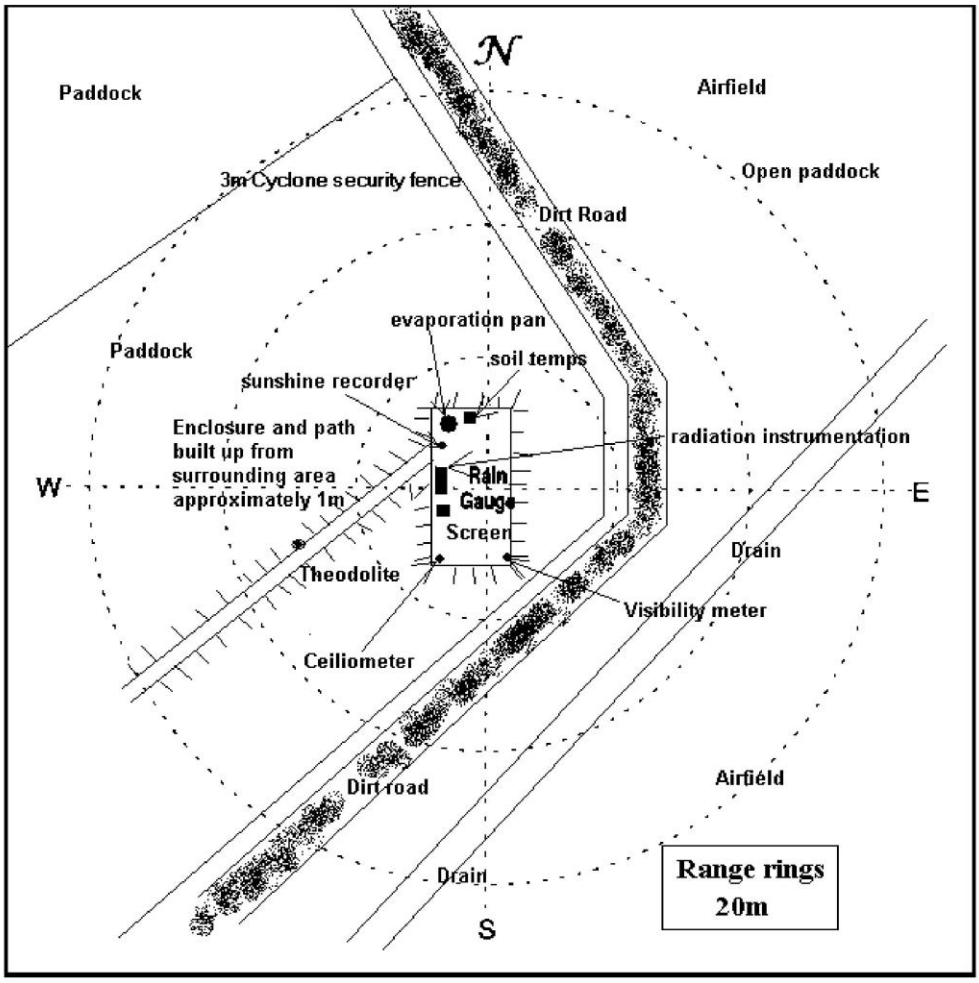

Historical metadata for this site has not been quality controlled for accuracy and completeness. Data other than current station information, particularly earlier than 1998, should be considered accordingly. Information may not be complete, as backfilling of historical data is incomplete.

Australian Government
Bureau of Meteorology

Extended Climatological Station Metadata
All History

Station:	ADELAIDE AIRPORT			**Location:**	ADELAIDE AIRPORT			**State:**	SA
Bureau No.:	023034	**WMO No.:**	94672	**Aviation ID:**	YPAD	**Opened:**	16 Feb 1955	**Current Status:**	Still open
Latitude:	-34.9524	**Longitude:**	138.5204	**Elevation:**	2 m	**Barometer Elev:**	8.2 m	**Metadata compiled:**	28 JUL 2013

Instrument Location and Surrounding Features
18/07/2003

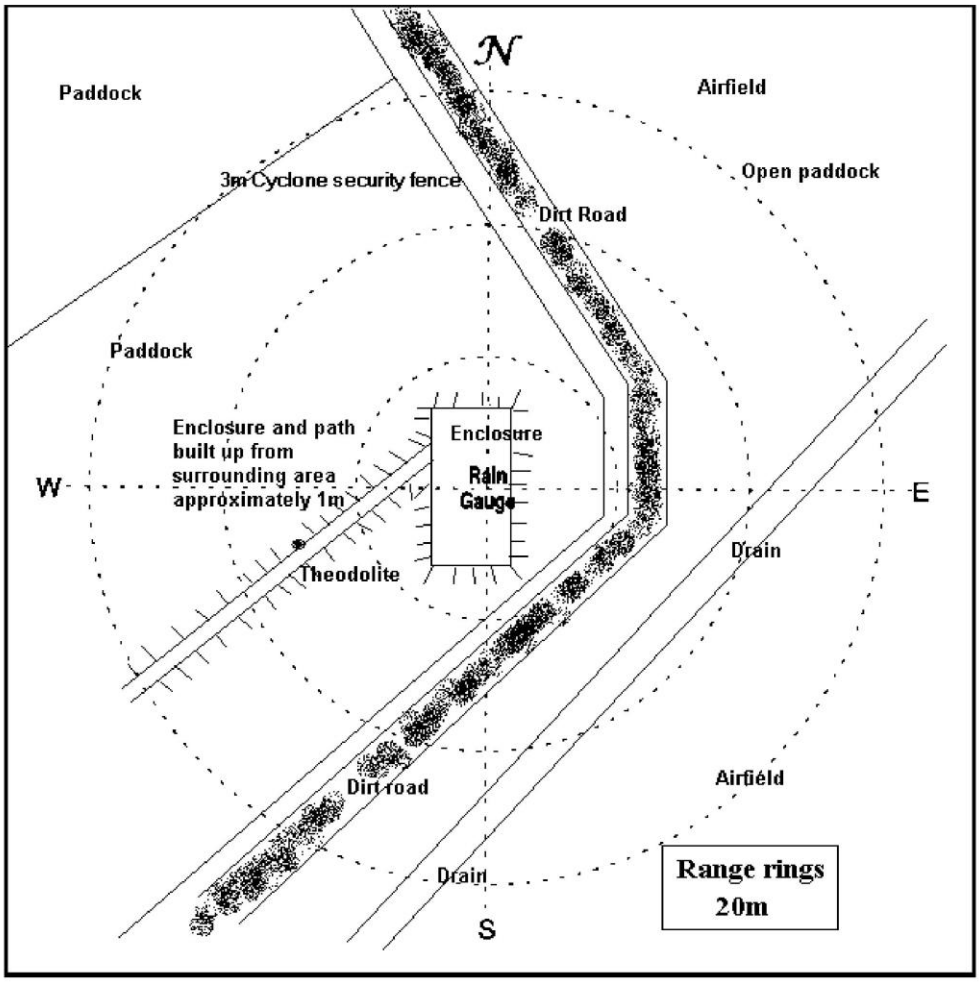

Historical metadata for this site has not been quality controlled for accuracy and completeness. Data other than current station information, particularly earlier than 1998, should be considered accordingly. Information may not be complete, as backfilling of historical data is incomplete.

Australian Government
Bureau of Meteorology

Extended Climatological Station Metadata
All History

Station:	ADELAIDE AIRPORT			**Location:**	ADELAIDE AIRPORT			**State:**	SA
Bureau No.:	023034	**WMO No.:**	94672	**Aviation ID:**	YPAD	**Opened:**	16 Feb 1955	**Current Status:**	Still open
Latitude:	-34.9524	**Longitude:**	138.5204	**Elevation:**	2 m	**Barometer Elev:**	8.2 m	**Metadata compiled:**	28 JUL 2013

Instrument Location and Surrounding Features
14/11/2000

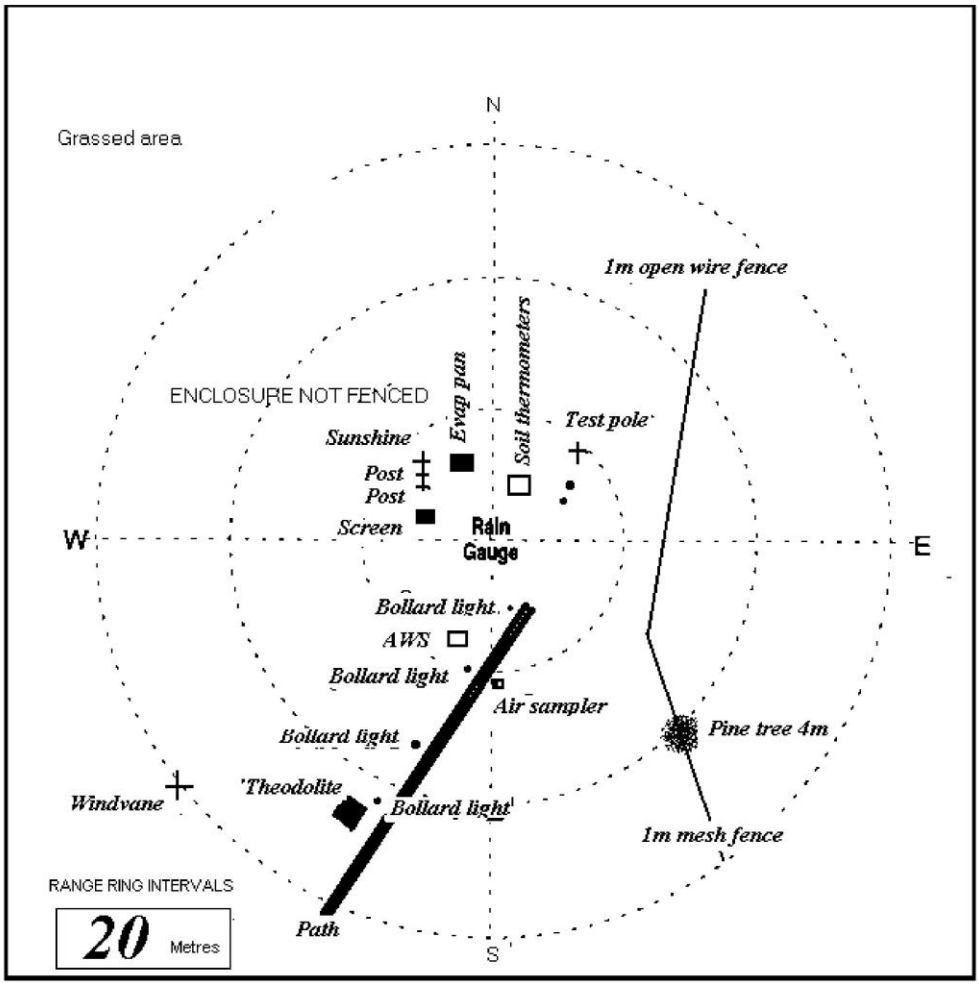

Historical metadata for this site has not been quality controlled for accuracy and completeness. Data other than current station information, particularly earlier than 1998, should be considered accordingly. Information may not be complete, as backfilling of historical data is incomplete.

Australian Government
Bureau of Meteorology

Extended Climatological Station Metadata
All History

Station:	ADELAIDE AIRPORT			**Location:**	ADELAIDE AIRPORT			**State:**	SA
Bureau No.:	023034	**WMO No.:**	94672	**Aviation ID:**	YPAD	**Opened:**	16 Feb 1955	**Current Status:**	Still open
Latitude:	-34.9524	**Longitude:**	138.5204	**Elevation:**	2 m	**Barometer Elev:**	8.2 m	**Metadata compiled:**	28 JUL 2013

Instrument Location and Surrounding Features
04/11/1999

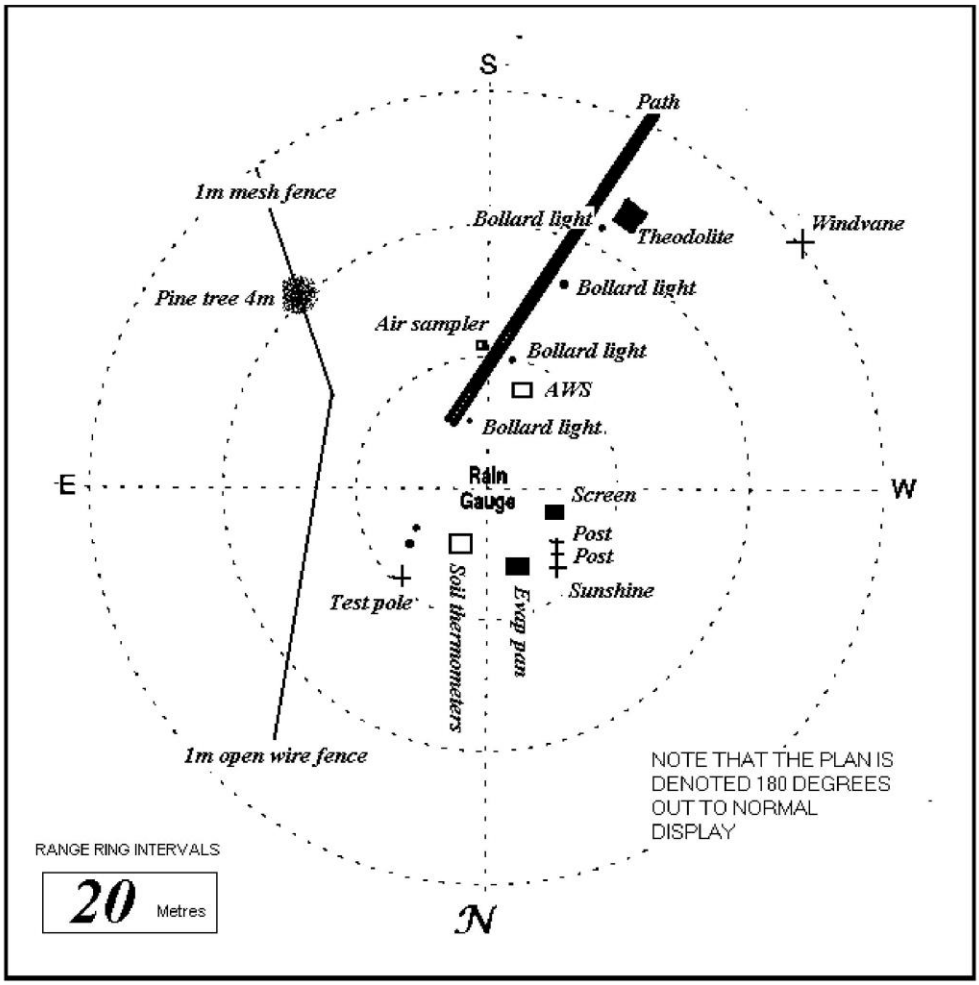

Historical metadata for this site has not been quality controlled for accuracy and completeness. Data other than current station information, particularly earlier than 1998, should be considered accordingly. Information may not be complete, as backfilling of historical data is incomplete.

Australian Government
Bureau of Meteorology

Extended Climatological Station Metadata
All History

Station:	ADELAIDE AIRPORT			**Location:**	ADELAIDE AIRPORT			**State:**	SA
Bureau No.:	023034	**WMO No.:**	94672	**Aviation ID:**	YPAD	**Opened:**	16 Feb 1955	**Current Status:**	Still open
Latitude:	-34.9524	**Longitude:**	138.5204	**Elevation:**	2 m	**Barometer Elev:**	8.2 m	**Metadata compiled:**	28 JUL 2013

Skyline Diagram
11/01/2013(most recent)

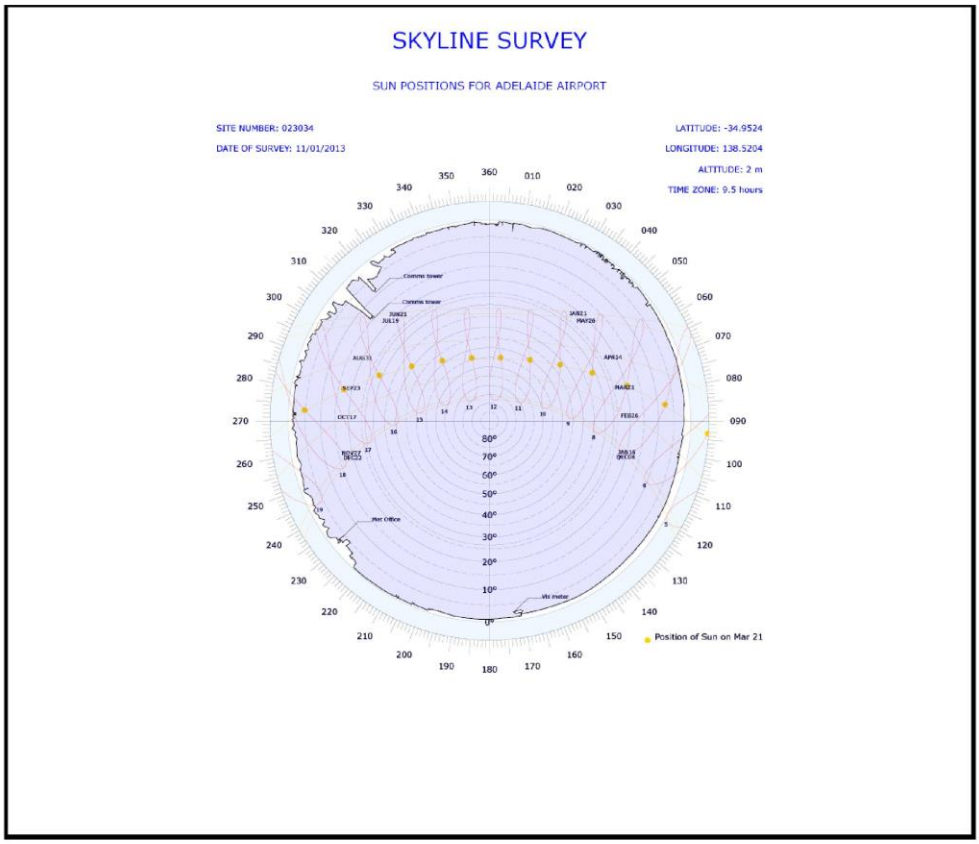

Historical metadata for this site has not been quality controlled for accuracy and completeness. Data other than current station information, particularly earlier than 1998, should be considered accordingly. Information may not be complete, as backfilling of historical data is incomplete.

Australian Government
Bureau of Meteorology

Extended Climatological Station Metadata
All History

Station:	ADELAIDE AIRPORT			**Location:**	ADELAIDE AIRPORT			**State:**	SA
Bureau No.:	023034	**WMO No.:**	94672	**Aviation ID:**	YPAD	**Opened:**	16 Feb 1955	**Current Status:**	Still open
Latitude:	-34.9524	**Longitude:**	138.5204	**Elevation:**	2 m	**Barometer Elev:**	8.2 m	**Metadata compiled:**	28 JUL 2013

Skyline Diagram
12/01/2007

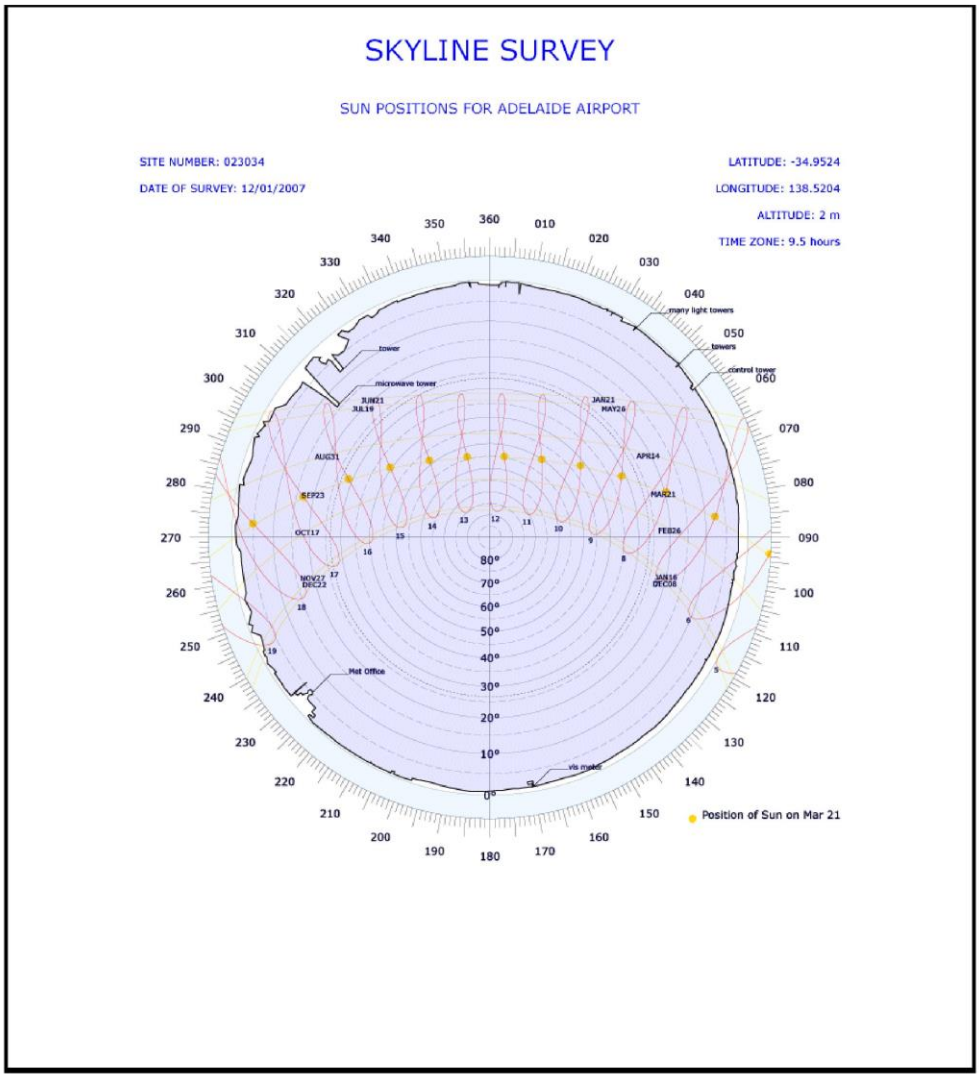

Historical metadata for this site has not been quality controlled for accuracy and completeness. Data other than current station information, particularly earlier than 1998, should be considered accordingly. Information may not be complete, as backfilling of historical data is incomplete.

Australian Government
Bureau of Meteorology

Extended Climatological Station Metadata
All History

Station:	ADELAIDE AIRPORT			**Location:**	ADELAIDE AIRPORT			**State:**	SA
Bureau No.:	023034	**WMO No.:**	94672	**Aviation ID:**	YPAD	**Opened:**	16 Feb 1955	**Current Status:**	Still open
Latitude:	-34.9524	**Longitude:**	138.5204	**Elevation:**	2 m	**Barometer Elev:**	8.2 m	**Metadata compiled:**	28 JUL 2013

Skyline Diagram
19/12/2002

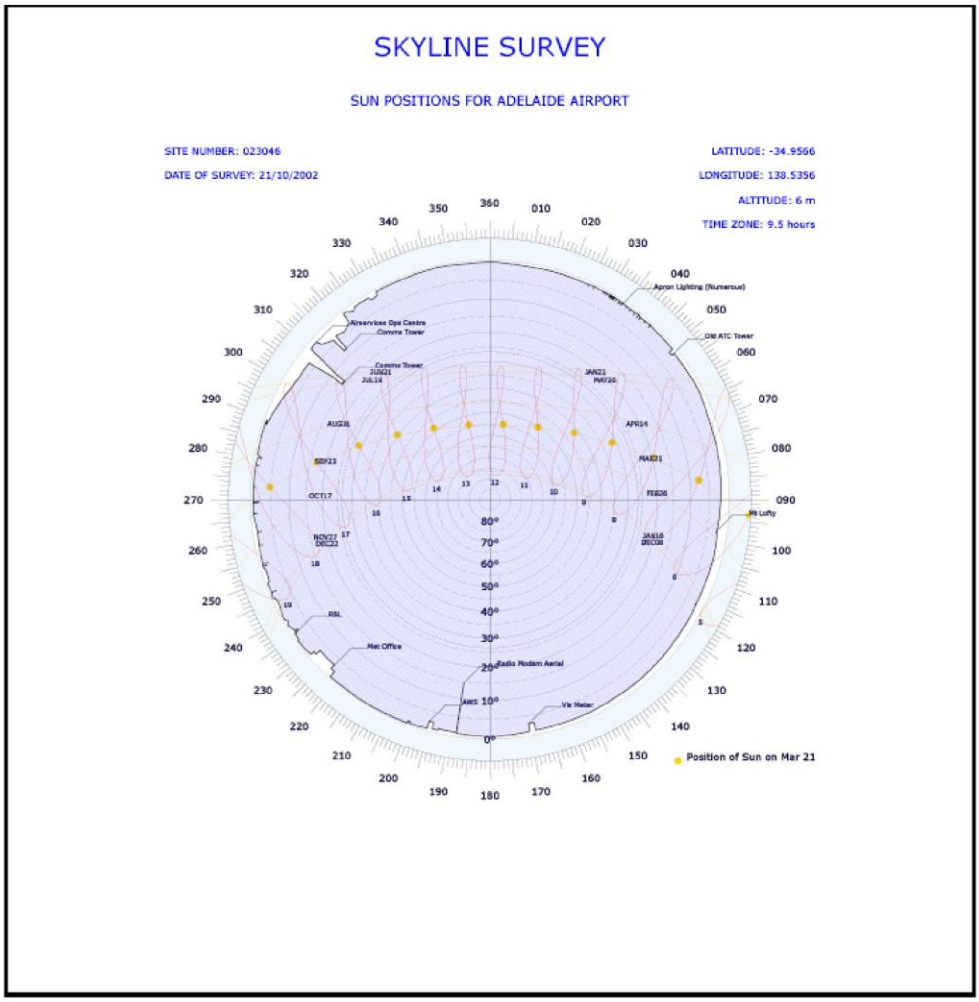

Historical metadata for this site has not been quality controlled for accuracy and completeness. Data other than current station information, particularly earlier than 1998, should be considered accordingly. Information may not be complete, as backfilling of historical data is incomplete.

Australian Government
Bureau of Meteorology

Extended Climatological Station Metadata
All History

Station:	ADELAIDE AIRPORT			**Location:**	ADELAIDE AIRPORT			**State:**	SA
Bureau No.:	023034	**WMO No.:**	94672	**Aviation ID:**	YPAD	**Opened:**	16 Feb 1955	**Current Status:**	Still open
Latitude:	-34.9524	**Longitude:**	138.5204	**Elevation:**	2 m	**Barometer Elev:**	8.2 m	**Metadata compiled:**	28 JUL 2013

Skyline Diagram
21/10/2002

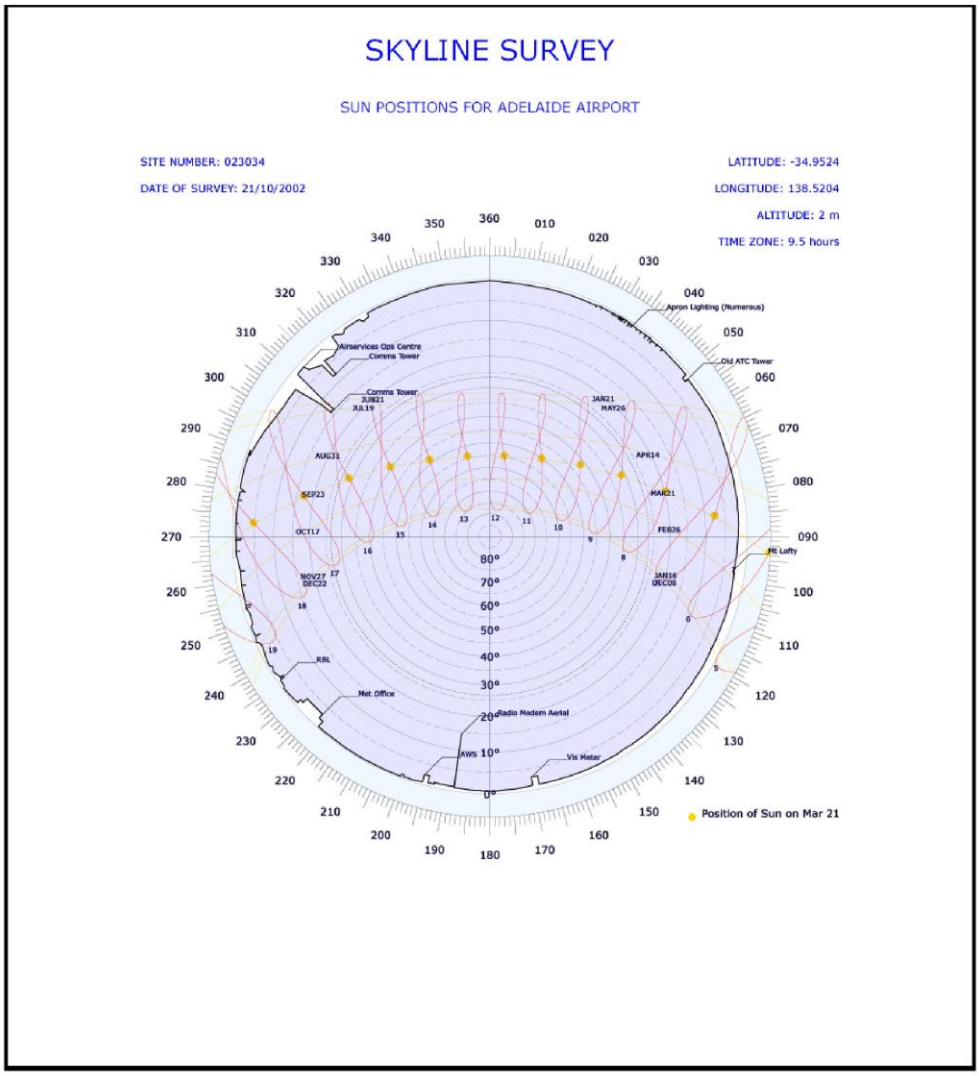

Historical metadata for this site has not been quality controlled for accuracy and completeness. Data other than current station information, particularly earlier than 1998, should be considered accordingly. Information may not be complete, as backfilling of historical data is incomplete.

 Page 24.

Australian Government
Bureau of Meteorology

Extended Climatological Station Metadata
All History

Station:	ADELAIDE AIRPORT			**Location:**	ADELAIDE AIRPORT			**State:**	SA
Bureau No.:	023034	**WMO No.:**	94672	**Aviation ID:**	YPAD	**Opened:**	16 Feb 1955	**Current Status:**	Still open
Latitude:	-34.9524	**Longitude:**	138.5204	**Elevation:**	2 m	**Barometer Elev:**	8.2 m	**Metadata compiled:**	28 JUL 2013

Skyline Diagram
04/11/1999

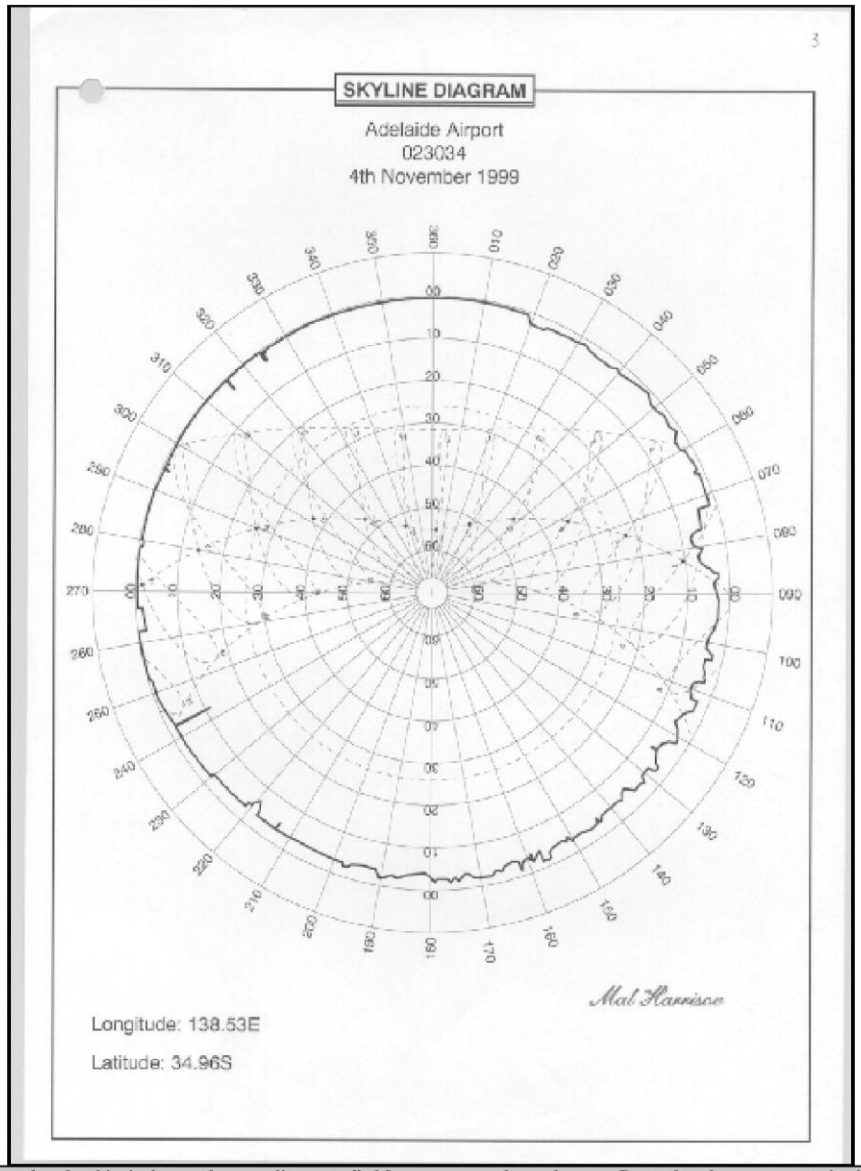

Historical metadata for this site has not been quality controlled for accuracy and completeness. Data other than current station information, particularly earlier than 1998, should be considered accordingly. Information may not be complete, as backfilling of historical data is incomplete.

 Page 25.

Australian Government
Bureau of Meteorology

Extended Climatological Station Metadata
All History

Station:	ADELAIDE AIRPORT			**Location:**	ADELAIDE AIRPORT			**State:**	SA
Bureau No.:	023034	**WMO No.:**	94672	**Aviation ID:**	YPAD	**Opened:**	16 Feb 1955	**Current Status:**	Still open
Latitude:	-34.9524	**Longitude:**	138.5204	**Elevation:**	2 m	**Barometer Elev:**	8.2 m	**Metadata compiled:**	28 JUL 2013

Station Observation Program Summary (Surface Observations) from 16/02/1955 to 15/04/1999

Current Observation	Continuous	Half Hourly	Hourly
Surface Observations	-	Y	Y

Current Observation	Program Type	12 AM	3 AM	6 AM	9 AM	12 PM	3 PM	6 AM	9 AM
Surface Observation	PERFORMED	Y	Y	Y	Y	Y	Y	Y	Y
Surface Observation	REPORTED	Y	Y	Y	Y	Y	Y	Y	Y
Surface Observation	SEASONAL	-	-	-	-	-	-	-	-

Station Observation Program Summary (Surface Observations) 28 JUL 2013 (most recent)

Current Observation	Continuous	Half Hourly	Hourly
Surface Observations	Y	Y	Y

Current Observation	Program Type	12 AM	3 AM	6 AM	9 AM	12 PM	3 PM	6 AM	9 AM
Surface Observation	PERFORMED	Y	Y	Y	Y	Y	Y	Y	Y
Surface Observation	REPORTED	Y	Y	Y	Y	Y	Y	Y	Y
Surface Observation	SEASONAL	-	-	-	-	-	-	-	-

Upper Air Routine 01/06/1954 to 01/08/2012

Flight type	Time UTC	Mon	Tue	Wed	Thur	Fri	Sat	Sun
Wind & Temp.	00:00	Y	Y	Y	Y	Y	Y	Y
Wind & Temp.	06:00	-	-	-	-	-	-	-
Wind & Temp.	12:00	Y	Y	Y	Y	Y	Y	Y
Wind & Temp.	18:00	-	-	-	-	-	-	-
Wind	00:00	Y	Y	Y	Y	Y	Y	Y
Wind	06:00	Y	Y	Y	Y	Y	Y	Y
Wind	12:00	Y	Y	Y	Y	Y	Y	Y
Wind	18:00	Y	Y	Y	Y	Y	Y	Y

Upper Air Routine 01/08/2012 (most recent)

Flight type	Time UTC	Mon	Tue	Wed	Thur	Fri	Sat	Sun
Wind & Temp.	00:00	Y	Y	Y	Y	Y	Y	Y
Wind & Temp.	06:00	-	-	-	-	-	-	-
Wind & Temp.	12:00	-	-	-	-	-	-	-
Wind & Temp.	18:00	-	-	-	-	-	-	-
Wind	00:00	Y	Y	Y	Y	Y	Y	Y
Wind	06:00	Y	Y	Y	Y	Y	Y	Y
Wind	12:00	Y	Y	Y	Y	Y	Y	Y
Wind	18:00	Y	Y	Y	Y	Y	Y	Y

Historical metadata for this site has not been quality controlled for accuracy and completeness. Data other than current station information, particularly earlier than 1998, should be considered accordingly. Information may not be complete, as backfilling of historical data is incomplete.

Australian Government
Bureau of Meteorology

Extended Climatological Station Metadata
All History

Station:	ADELAIDE AIRPORT			**Location:**	ADELAIDE AIRPORT			**State:**	SA
Bureau No.:	023034	**WMO No.:**	94672	**Aviation ID:**	YPAD	**Opened:**	16 Feb 1955	**Current Status:**	Still open
Latitude:	-34.9524	**Longitude:**	138.5204	**Elevation:**	2 m	**Barometer Elev:**	8.2 m	**Metadata compiled:**	28 JUL 2013

Station Equipment History

Equipment Install/Remove

Cloud Height
17/DEC/2002 INSTALL Ceilometer (Type Vaisala CT25K S/N - W09412) Surface Observations
02/MAR/2010 REPLACE Ceilometer (Now Vaisala CT25K S/N - A50403) Surface Observations
19/OCT/2006 REPLACE Ceilometer (Now Vaisala CT25K S/N - U14501) Surface Observations
14/FEB/2006 REPLACE Ceilometer (Now Vaisala CT25K S/N - W09406) Surface Observations
16/FEB/1955 INSTALL Cloud Base Searchlight (Type 63 Degree S/N - Unknown) Surface Observations
16/DEC/2002 REMOVE Cloud Base Searchlight (Type 63 Degree S/N - CBM5145) Surface Observations
02/SEP/1997 REPLACE Cloud Base Searchlight (Now 63 Degree S/N - CBM5145) Surface Observations

River Height
23/JAN/1997 INSTALL River Height Gauge (Type Druck Pressure Transducer S/N - 896399) Flood Warning
10/AUG/2001 REMOVE River Height Gauge (Type Druck Pressure Transducer S/N - 1063834) Flood Warning
13/MAR/2001 REPLACE River Height Gauge (Now Druck Pressure Transducer S/N - 1063834) Flood Warning

Wind Run
17/DEC/2002 INSTALL Wind Run Anemometer (Type Munro S/N - 8689) Surface Observations
16/FEB/1955 INSTALL Wind Run Anemometer (Type Synchrotac S/N - CBM056) Surface Observations
16/DEC/2002 REMOVE Wind Run Anemometer (Type Synchrotac S/N - CBM056) Surface Observations
04/JUN/2004 REPLACE Wind Run Anemometer (Now Munro S/N - 8684) Surface Observations
22/JUN/2004 REPLACE Wind Run Anemometer (Now Munro S/N - 8689) Surface Observations
07/OCT/2004 REPLACE Wind Run Anemometer (Now Munro S/N - CBM360) Surface Observations
24/MAY/2006 REPLACE Wind Run Anemometer (Now Munro S/N - CBM519) Surface Observations
01/MAR/2007 REPLACE Wind Run Anemometer (Now Synchrotac S/N - CBM668) Surface Observations

Spectral Radiation
01/MAR/2003 INSTALL Photometer Head (Type SPO2 Mk1 S/N - 1001) Radiation
07/MAR/2003 REPLACE Photometer Head (Now SPO2 Mk1 S/N - 1013) Radiation

Sea Surface Temperature (No Electronic History)

Sea Water Temperature (No Electronic History)

Evaporation
01/DEC/1977 INSTALL Evaporation Pan (Type Class A S/N - NONE) Surface Observations
17/DEC/2002 INSTALL Evaporation Pan (Type Class A S/N - NONE) Surface Observations
16/DEC/2002 REMOVE Evaporation Pan (Type Class A S/N - NONE) Surface Observations
12/JAN/2008 REPLACE Evaporation Pan (Now Class A S/N - NONE) Surface Observations

Minimum Temperature
04/NOV/1999 INSTALL Thermometer, Alcohol, Min (Type Dobbie S/N - 18970) Surface Observations
17/DEC/2002 INSTALL Thermometer, Alcohol, Min (Type WIKA S/N - 31914) Surface Observations
16/DEC/2002 REMOVE Thermometer, Alcohol, Min (Type Dobbie S/N - M3600) Surface Observations
02/JAN/2002 REPLACE Thermometer, Alcohol, Min (Now Dobbie S/N - M3600) Surface Observations

Soil Temperature 50cm
17/DEC/2002 INSTALL Thermometer, Soil, 50cm (Type Amarol S/N - 0269691) Surface Observations
01/JAN/1994 INSTALL Thermometer, Soil, 50cm (Type Dobros S/N - CBM132) Surface Observations
16/DEC/2002 REMOVE Thermometer, Soil, 50cm (Type Dobros S/N - CBM132) Surface Observations

Sub Surface Temperature (No Electronic History)

Electrical Conductivity (No Electronic History)

Maximum Temperature

Australian Government
Bureau of Meteorology

Extended Climatological Station Metadata
All History

Station:	ADELAIDE AIRPORT			**Location:**	ADELAIDE AIRPORT			**State:**	SA
Bureau No.:	023034	**WMO No.:**	94672	**Aviation ID:**	YPAD	**Opened:**	16 Feb 1955	**Current Status:**	Still open
Latitude:	-34.9524	**Longitude:**	138.5204	**Elevation:**	2 m	**Barometer Elev:**	8.2 m	**Metadata compiled:**	28 JUL 2013

Station Equipment History (continued)

Equipment Install/Remove(Continued)

17/DEC/2002 INSTALL Thermometer, Mercury, Max (Type Dobbie S/N - 23403) Surface Observations
16/FEB/1955 INSTALL Thermometer, Mercury, Max (Type Dobbie S/N - M1437) Surface Observations
16/DEC/2002 REMOVE Thermometer, Mercury, Max (Type Dobbie S/N - M1437) Surface Observations
14/MAR/2004 REPLACE Thermometer, Mercury, Max (Now Dobbie S/N - M2467) Surface Observations
23/JUL/2010 REPLACE Thermometer, Mercury, Max (Now WIKA S/N - 28860) Surface Observations

Soil Temperature 20cm

17/DEC/2002 INSTALL Thermometer, Soil, 20cm (Type Dobros S/N - 0011822) Surface Observations
01/JAN/1994 INSTALL Thermometer, Soil, 20cm (Type Unknown S/N - Unknown) Surface Observations
16/DEC/2002 REMOVE Thermometer, Soil, 20cm (Type Dobros S/N - 9604821) Surface Observations
02/JUL/2004 REPLACE Thermometer, Soil, 20cm (Now Amarol S/N - 0270779) Surface Observations
20/JUL/2007 REPLACE Thermometer, Soil, 20cm (Now Amarol S/N - 0270787) Surface Observations
31/AUG/1998 REPLACE Thermometer, Soil, 20cm (Now Dobros S/N - 9604821) Surface Observations
22/MAY/2003 REPLACE Thermometer, Soil, 20cm (Now Dobros S/N - M4052) Surface Observations
24/AUG/2009 REPLACE Thermometer, Soil, 20cm (Now Unknown S/N - 9566407) Surface Observations

Solar Radiation

07/NOV/1994 INSTALL Global Pyranometer Mount (Type Unknown S/N - Unknown) Radiation
01/MAR/2003 INSTALL Global Pyranometer Mount (Type Unknown S/N - Unknown) Radiation
01/MAR/2003 INSTALL Pyranometer (Type Kipp&Zonen CM11 S/N - 924032) Radiation
01/MAR/2003 INSTALL Pyranometer (Type Kipp&Zonen CM11 S/N - 924697) Radiation
07/NOV/1994 INSTALL Pyranometer (Type Unknown S/N - Unknown) Radiation
17/APR/1999 REMOVE Global Pyranometer Mount (Type Unknown S/N - Unknown) Radiation
17/APR/1999 REMOVE Pyranometer (Type Unknown S/N - Unknown) Radiation
07/MAR/2003 REPLACE Pyranometer (Now Kipp&Zonen CM11 S/N - 924032) Radiation
26/JAN/2004 REPLACE Pyranometer (Now Kipp&Zonen CM11 S/N - 924032) Radiation
16/DEC/2006 REPLACE Pyranometer (Now Kipp&Zonen CM11 S/N - 924032) Radiation
11/NOV/2008 REPLACE Pyranometer (Now Kipp&Zonen CM11 S/N - 924032) Radiation
01/OCT/2004 REPLACE Pyranometer (Now Kipp&Zonen CM11 S/N - 924032) Radiation
07/MAR/2003 REPLACE Pyranometer (Now Kipp&Zonen CM11 S/N - 924697) Radiation
26/JAN/2004 REPLACE Pyranometer (Now Kipp&Zonen CM11 S/N - 924697) Radiation
16/DEC/2006 REPLACE Pyranometer (Now Kipp&Zonen CM11 S/N - 924698) Radiation
11/NOV/2008 REPLACE Pyranometer (Now Kipp&Zonen CM11 S/N - 924698) Radiation
01/OCT/2004 REPLACE Pyranometer (Now Kipp&Zonen CM11 S/N - 924698) Radiation

Soil Temperature 5cm

17/DEC/2002 INSTALL Thermometer, Soil, 5cm (Type Dobros S/N - 9566475) Surface Observations

Oxygen Content (No Electronic History)

Sea Water Level (No Electronic History)

Surface Inclination (No Electronic History)

Terrestial Minimum Temperature

01/SEP/1959 INSTALL Thermometer, Terrestrial, Min (Type Dobbie S/N - Unknown) Surface Observations
17/DEC/2002 REPLACE Thermometer, Terrestrial, Min (Now Dobbie S/N - 13200) Surface Observations
06/FEB/2005 REPLACE Thermometer, Terrestrial, Min (Now Dobbie S/N - 23336) Surface Observations
26/MAY/2009 REPLACE Thermometer, Terrestrial, Min (Now Dobbie S/N - 29111) Surface Observations
13/JAN/2006 REPLACE Thermometer, Terrestrial, Min (Now Dobbie S/N - 43081) Surface Observations

Australian Government
Bureau of Meteorology

Extended Climatological Station Metadata
All History

Station:	ADELAIDE AIRPORT			**Location:**	ADELAIDE AIRPORT			**State:**	SA
Bureau No.:	023034	**WMO No.:**	94672	**Aviation ID:**	YPAD	**Opened:**	16 Feb 1955	**Current Status:**	Still open
Latitude:	-34.9524	**Longitude:**	138.5204	**Elevation:**	2 m	**Barometer Elev:**	8.2 m	**Metadata compiled:**	28 JUL 2013

Station Equipment History (continued)

Equipment Install/Remove(Continued)

29/MAY/2007 REPLACE Thermometer, Terrestrial, Min (Now Dobbie S/N - 43081) Surface Observations
28/APR/2006 REPLACE Thermometer, Terrestrial, Min (Now Dobbie S/N - M3517) Surface Observations
16/DEC/2002 REPLACE Thermometer, Terrestrial, Min (Now Dobbie S/N - M3517) Surface Observations
06/NOV/1999 REPLACE Thermometer, Terrestrial, Min (Now Dobbie S/N - M3592) Surface Observations
22/APR/2010 REPLACE Thermometer, Terrestrial, Min (Now Unknown S/N - 43073) Surface Observations
09/DEC/2010 REPLACE Thermometer, Terrestrial, Min (Now WIKA S/N - 31176) Surface Observations
02/MAY/2011 REPLACE Thermometer, Terrestrial, Min (Now WIKA S/N - 31877) Surface Observations

Visibility

17/DEC/2002 INSTALL Visibility Meter (Type Vaisala FD12 S/N - W10308) Surface Observations

Solar Radiation (Direct)

01/MAR/2003 INSTALL Pyrheliometer (Type Carter Scott DN5 S/N - 5014) Radiation

Magnetic Bearing (No Electronic History)

Wind Direction

16/FEB/1955 INSTALL Anemometer (Type Dines S/N - Unknown) Surface Observations
02/AUG/2005 INSTALL Anemometer (Type Synchrotac Cups - Type 732 S/N - 64453) Surface Observations
21/OCT/1988 INSTALL Anemometer (Type Synchrotac Type 706 S/N - Unknown) Surface Observations
01/FEB/1995 INSTALL Anemometer (Type Synchrotac Type 706 S/N - WS-90WD-90) Surface Observations
04/MAY/1987 INSTALL Mast Anemometer (Type Pipe, Guyed S/N - Unknown) Infrastructure
01/FEB/1995 INSTALL Mast Anemometer (Type Pivot, Standard 8m S/N - NONE) Infrastructure
01/FEB/1995 INSTALL Mast Anemometer (Type Pivot, Standard 8m S/N - NONE) Infrastructure
17/DEC/2002 INSTALL Mast Anemometer (Type Pivot, Standard 8m S/N - NONE) Infrastructure
17/DEC/2002 INSTALL Wind Run Anemometer (Type Munro S/N - 8689) Surface Observations
16/FEB/1955 INSTALL Wind Run Anemometer (Type Synchrotac S/N - CBM056) Surface Observations
22/OCT/1988 REMOVE Anemometer (Type Dines S/N - Unknown) Surface Observations
01/FEB/1995 REMOVE Anemometer (Type Synchrotac Type 706 S/N - Unknown) Surface Observations
16/DEC/2002 REMOVE Mast Anemometer (Type Pipe, Guyed S/N - Unknown) Infrastructure
28/SEP/2004 REMOVE Mast Anemometer (Type Pivot, Standard 8m S/N - NONE) Infrastructure
02/FEB/1995 REMOVE Mast Anemometer (Type Pivot, Standard 8m S/N - NONE) Infrastructure
16/DEC/2002 REMOVE Wind Run Anemometer (Type Synchrotac S/N - CBM056) Surface Observations
02/AUG/2005 REPLACE Anemometer (Now Synchrotac Type 706 S/N - 419) Surface Observations
04/JUN/2004 REPLACE Wind Run Anemometer (Now Munro S/N - 8684) Surface Observations
22/JUN/2004 REPLACE Wind Run Anemometer (Now Munro S/N - 8689) Surface Observations
07/OCT/2004 REPLACE Wind Run Anemometer (Now Munro S/N - CBM360) Surface Observations
24/MAY/2006 REPLACE Wind Run Anemometer (Now Munro S/N - CBM519) Surface Observations
01/MAR/2007 REPLACE Wind Run Anemometer (Now Synchrotac S/N - CBM668) Surface Observations

Air Temperature

01/FEB/1995 INSTALL Temperature Probe - Dry Bulb (Type Rosemount S/N - NONE) Surface Observations
17/DEC/2002 INSTALL Temperature Probe - Dry Bulb (Type Rosemount ST2401 S/N - 0528) Surface Observations
16/DEC/2002 REMOVE Temperature Probe - Dry Bulb (Type Rosemount S/N - NONE) Surface Observations
01/FEB/1967 INSTALL Thermograph (Type Fielden S/N - Unknown) Surface Observations
01/OCT/1988 REMOVE Thermograph (Type Fielden S/N - Unknown) Surface Observations
04/JUN/1981 REPLACE Thermograph (Now Fielden S/N - Unknown) Surface Observations
17/DEC/2002 INSTALL Thermometer, Mercury, Dry Bulb (Type Dobbie S/N - 18716) Surface Observations

Australian Government
Bureau of Meteorology

Extended Climatological Station Metadata
All History

Station:	ADELAIDE AIRPORT			**Location:**	ADELAIDE AIRPORT			**State:**	SA
Bureau No.:	023034	**WMO No.:**	94672	**Aviation ID:**	YPAD	**Opened:**	16 Feb 1955	**Current Status:**	Still open
Latitude:	-34.9524	**Longitude:**	138.5204	**Elevation:**	2 m	**Barometer Elev:**	8.2 m	**Metadata compiled:**	28 JUL 2013

Station Equipment History (continued)

Equipment Install/Remove(Continued)

06/OCT/1998 INSTALL Thermometer, Mercury, Dry Bulb (Type Dobbie S/N - 4967) Surface Observations
16/DEC/2002 REMOVE Thermometer, Mercury, Dry Bulb (Type Dobbie S/N - 4967) Surface Observations

Wet Bulb Temperature

01/FEB/1995 INSTALL Temperature Probe - Wet Bulb (Type Rosemount S/N - NONE) Surface Observations
17/DEC/2002 INSTALL Temperature Probe - Wet Bulb (Type Rosemount ST2401 S/N - 0666) Surface Observations
16/DEC/2002 REMOVE Temperature Probe - Wet Bulb (Type Rosemount S/N - NONE) Surface Observations
17/DEC/2002 INSTALL Thermometer, Mercury, Wet Bulb (Type Dobbie S/N - 20404) Surface Observations
16/FEB/1955 INSTALL Thermometer, Mercury, Wet Bulb (Type Dobbie S/N - 4622) Surface Observations
16/DEC/2002 REMOVE Thermometer, Mercury, Wet Bulb (Type Dobbie S/N - 4622) Surface Observations
12/JAN/2007 REPLACE Thermometer, Mercury, Wet Bulb (Now Dobbie S/N - 20219) Surface Observations

Lightning

22/FEB/2006 INSTALL Lightning Sensor (Type Vaisala TSS928 (Thunderstorm Sensor) S/N - Z5030001) Surface Observations

Turbidity (No Electronic History)

Total Column Ozone Amount (No Electronic History)

Pressure

16/FEB/1955 INSTALL Barometer (Type Kew pattern mercury S/N - 1769) Surface Observations
16/FEB/1955 INSTALL Barometer (Type Kew pattern mercury S/N - 1846) Surface Observations
07/MAY/1992 INSTALL Barometer (Type Vaisala PA11A S/N - 458180) Surface Observations
17/DEC/2002 INSTALL Barometer (Type Vaisala PTB220B S/N - W4920008) Surface Observations
01/DEC/1996 REMOVE Barometer (Type Kew pattern mercury S/N - 1769) Surface Observations
01/JUL/1992 REMOVE Barometer (Type Kew pattern mercury S/N - 1846) Surface Observations
16/DEC/2002 REMOVE Barometer (Type Vaisala PA11A S/N - 458180) Surface Observations

Humidity

01/FEB/1967 INSTALL Hygrograph (Type Fielden S/N - Unknown) Surface Observations
01/MAY/1995 INSTALL Hygrograph (Type Fielden S/N - Unknown) Surface Observations
01/OCT/1988 REMOVE Hygrograph (Type Fielden S/N - Unknown) Surface Observations
31/AUG/1999 REMOVE Hygrograph (Type Fielden S/N - Unknown) Surface Observations

Sunshine Hours

17/DEC/2002 INSTALL Sunshine Recorder (Type Campbell-Stokes S/N - 6243) Surface Observations
17/AUG/1983 INSTALL Sunshine Recorder (Type Campbell-Stokes S/N - CBM008) Surface Observations
16/DEC/2002 REMOVE Sunshine Recorder (Type Campbell-Stokes S/N - CBM008) Surface Observations

Pressure Trend

04/MAY/1987 INSTALL Barograph (Type Weekly S/N - 5582) Surface Observations
17/DEC/2002 INSTALL Barograph (Type Weekly S/N - CBM0003) Surface Observations
01/JUL/1992 REMOVE Barograph (Type Weekly S/N - 5582) Surface Observations

Snow Height (No Electronic History)

Wind Speed

16/FEB/1955 INSTALL Anemometer (Type Dines S/N - Unknown) Surface Observations
02/AUG/2005 INSTALL Anemometer (Type Synchrotac Cups - Type 732 S/N - 64453) Surface Observations
21/OCT/1988 INSTALL Anemometer (Type Synchrotac Type 706 S/N - Unknown) Surface Observations
01/FEB/1995 INSTALL Anemometer (Type Synchrotac Type 706 S/N - WS-90WD-90) Surface Observations
04/MAY/1987 INSTALL Mast Anemometer (Type Pipe, Guyed S/N - Unknown) Infrastructure

Australian Government
Bureau of Meteorology

Extended Climatological Station Metadata
All History

Station:	ADELAIDE AIRPORT			**Location:**	ADELAIDE AIRPORT			**State:**	SA
Bureau No.:	023034	**WMO No.:**	94672	**Aviation ID:**	YPAD	**Opened:**	16 Feb 1955	**Current Status:**	Still open
Latitude:	-34.9524	**Longitude:**	138.5204	**Elevation:**	2 m	**Barometer Elev:**	8.2 m	**Metadata compiled:**	28 JUL 2013

Station Equipment History (continued)

Equipment Install/Remove(Continued)

01/FEB/1995	INSTALL Mast Anemometer (Type Pivot, Standard 8m S/N - NONE) Infrastructure
01/FEB/1995	INSTALL Mast Anemometer (Type Pivot, Standard 8m S/N - NONE) Infrastructure
17/DEC/2002	INSTALL Mast Anemometer (Type Pivot, Standard 8m S/N - NONE) Infrastructure
17/DEC/2002	INSTALL Wind Run Anemometer (Type Munro S/N - 8689) Surface Observations
16/FEB/1955	INSTALL Wind Run Anemometer (Type Synchrotac S/N - CBM056) Surface Observations
22/OCT/1988	REMOVE Anemometer (Type Dines S/N - Unknown) Surface Observations
01/FEB/1995	REMOVE Anemometer (Type Synchrotac Type 706 S/N - Unknown) Surface Observations
16/DEC/2002	REMOVE Mast Anemometer (Type Pipe, Guyed S/N - Unknown) Infrastructure
28/SEP/2004	REMOVE Mast Anemometer (Type Pivot, Standard 8m S/N - NONE) Infrastructure
02/FEB/1995	REMOVE Mast Anemometer (Type Pivot, Standard 8m S/N - NONE) Infrastructure
16/DEC/2002	REMOVE Wind Run Anemometer (Type Synchrotac S/N - CBM056) Surface Observations
02/AUG/2005	REPLACE Anemometer (Now Synchrotac Type 706 S/N - 419) Surface Observations
04/JUN/2004	REPLACE Wind Run Anemometer (Now Munro S/N - 8684) Surface Observations
22/JUN/2004	REPLACE Wind Run Anemometer (Now Munro S/N - 8689) Surface Observations
07/OCT/2004	REPLACE Wind Run Anemometer (Now Munro S/N - CBM360) Surface Observations
24/MAY/2006	REPLACE Wind Run Anemometer (Now Munro S/N - CBM519) Surface Observations
01/MAR/2007	REPLACE Wind Run Anemometer (Now Synchrotac S/N - CBM668) Surface Observations
Rainfall	
01/JAN/1967	INSTALL Pluviograph (Type Dines syphoning S/N - Unknown) Rainfall Intensity
30/APR/1998	REMOVE Pluviograph (Type Dines syphoning S/N - Unknown) Rainfall Intensity
16/FEB/1955	INSTALL Raingauge (Type 203 mm (8in) - 200mm capacity S/N - NONE) Surface Observations
17/DEC/2002	INSTALL Raingauge (Type 203 mm (8in) - 200mm capacity S/N - NONE) Surface Observations
01/FEB/1995	INSTALL Raingauge (Type HS TB3A-0.2 S/N - 94-285) Surface Observations
19/MAR/2007	INSTALL Raingauge (Type Not Listed S/N - Unknown) External Clients
18/JUN/2007	INSTALL Raingauge (Type Not Listed S/N - Unknown) External Clients
22/MAR/1993	INSTALL Raingauge (Type Rimco 7499 TBRG S/N - 096) Flood Warning
17/DEC/2002	INSTALL Raingauge (Type Rimco 7499 TBRG S/N - 82488) Rainfall Intensity
17/DEC/2002	INSTALL Raingauge (Type Rimco 7499 TBRG S/N - 82488) Surface Observations
16/DEC/2002	REMOVE Raingauge (Type 203 mm (8in) - 200mm capacity S/N - NONE) Surface Observations
10/AUG/2001	REMOVE Raingauge (Type Rimco 7499 TBRG S/N - 096) Flood Warning
16/DEC/2002	REMOVE Raingauge (Type Rimco 8020 TBRG S/N - 78111) Rainfall Intensity
06/MAR/2000	REMOVE Raingauge (Type Rimco 8020 TBRG S/N - 78111) Surface Observations
16/DEC/2002	REMOVE Raingauge (Type Rimco 8020 TBRG S/N - 78111) Surface Observations
09/DEC/1998	REPLACE Raingauge (Now HS TB3A-0.2 S/N - 96 -181) Rainfall Intensity
09/DEC/1998	REPLACE Raingauge (Now HS TB3A-0.2 S/N - 96 -181) Surface Observations
13/JAN/2006	REPLACE Raingauge (Now Rimco 7499 TBRG S/N - 87561) Rainfall Intensity
13/JAN/2006	REPLACE Raingauge (Now Rimco 7499 TBRG S/N - 87561) Surface Observations
06/OCT/1998	REPLACE Raingauge (Now Rimco 8020 TBRG S/N - 75521) Rainfall Intensity
06/OCT/1998	REPLACE Raingauge (Now Rimco 8020 TBRG S/N - 75521) Surface Observations
14/NOV/2000	REPLACE Raingauge (Now Rimco 8020 TBRG S/N - 78111) Rainfall Intensity
14/NOV/2000	REPLACE Raingauge (Now Rimco 8020 TBRG S/N - 78111) Surface Observations
17/APR/1997	SHARE Raingauge (Type HS TB3A-0.2 S/N - 94-285) Rainfall Intensity
15/MAR/2000	SHARE Raingauge (Type HS TB3A-0.2 S/N - 94-285) Surface Observations

Australian Government
Bureau of Meteorology

Extended Climatological Station Metadata
All History

Station:	ADELAIDE AIRPORT			**Location:**	ADELAIDE AIRPORT			**State:**	SA
Bureau No.:	023034	**WMO No.:**	94672	**Aviation ID:**	YPAD	**Opened:**	16 Feb 1955	**Current Status:**	Still open
Latitude:	-34.9524	**Longitude:**	138.5204	**Elevation:**	2 m	**Barometer Elev:**	8.2 m	**Metadata compiled:**	28 JUL 2013

Station Equipment History (continued)

Equipment Install/Remove(Continued)

17/APR/1997 SHARE Raingauge (Type HS TB3A-0.2 S/N - 96 -181) Rainfall Intensity
15/MAR/2000 SHARE Raingauge (Type HS TB3A-0.2 S/N - 96 -181) Surface Observations
17/APR/1997 SHARE Raingauge (Type Rimco 8020 TBRG S/N - 75521) Rainfall Intensity
15/MAR/2000 SHARE Raingauge (Type Rimco 8020 TBRG S/N - 75521) Surface Observations
17/APR/1997 SHARE Raingauge (Type Rimco 8020 TBRG S/N - 78111) Rainfall Intensity
15/MAR/2000 SHARE Raingauge (Type Rimco 8020 TBRG S/N - 78111) Surface Observations

Soil Temperature 100cm

17/DEC/2002 INSTALL Thermometer, Soil, 100cm (Type Amarol S/N - 0269679) Surface Observations
01/JAN/1994 INSTALL Thermometer, Soil, 100cm (Type Dobros S/N - M2243) Surface Observations
16/DEC/2002 REMOVE Thermometer, Soil, 100cm (Type Dobros S/N - M2243) Surface Observations
13/DEC/2004 REPLACE Thermometer, Soil, 100cm (Now Amarol S/N - A9564488) Surface Observations

Soil Temperature 10cm

01/JAN/1994 INSTALL Thermometer, Soil, 10cm (Type Dobros S/N - 9572455) Surface Observations
17/DEC/2002 INSTALL Thermometer, Soil, 10cm (Type Dobros S/N - 9725451) Surface Observations
16/DEC/2002 REMOVE Thermometer, Soil, 10cm (Type Dobros S/N - 9572455) Surface Observations

Solar Radiation (Long Wave)

01/MAR/2003 INSTALL Pyrgeometer (Type Epply PIR S/N - 27703F3) Radiation

RF Reflectivity

01/JUN/1954 INSTALL Radar (Type 277F S/N - Unknown) Upper Air
01/JUN/1954 INSTALL Radar (Type 277F S/N - Unknown) WeatherWatch
18/FEB/2009 INSTALL Radar (Type WF100-5C S/N - Unknown) Upper Air
01/JUN/1972 INSTALL Radar (Type WF44 S/N - NONE) Upper Air
01/JUN/1972 INSTALL Radar (Type WF44 S/N - NONE) WeatherWatch
18/FEB/2009 INSTALL Radar Interface (Type BOM S/N - Unknown) Upper Air
01/JUN/1972 INSTALL Radar Tower (Type Lattice WF44 - 18 ft S/N - NONE) Infrastructure
01/MAY/1972 REMOVE Radar (Type 277F S/N - Unknown) Upper Air
01/MAY/1972 REMOVE Radar (Type 277F S/N - Unknown) WeatherWatch
17/NOV/2008 REMOVE Radar (Type WF44 S/N - NONE) Upper Air
17/NOV/2008 REMOVE Radar (Type WF44 S/N - NONE) WeatherWatch
16/DEC/2002 REMOVE Radar Tower (Type Lattice WF44 - 18 ft S/N - NONE) Infrastructure

The following table summarises information on field performance checks available electronically over the period indicated. The number of instances an instrument was found to fail field performance checks should only be used as a guide. A system of data quality flags is implemented by the National Climate Centre to indicate the data quality of an observation as determined by a mutli-stage quality control process.

Available Date Range	Element	Fail Field Performance Check
01/JUL/2003 - 11/JUL/2013	Cloud Height	0
04/MAY/1987 - 11/JAN/2013	Wind Run	1
14/NOV/2000 - 11/JAN/2013	Evaporation	0
14/NOV/2000 - 11/JAN/2013	Minimum Temperature	0
28/FEB/1996 - 11/JAN/2013	Soil Temperature 50cm	0
04/MAY/1987 - 11/JAN/2013	Maximum Temperature	0

Australian Government
Bureau of Meteorology

Extended Climatological Station Metadata
All History

Station:	ADELAIDE AIRPORT			**Location:**	ADELAIDE AIRPORT			**State:**	SA
Bureau No.:	023034	**WMO No.:**	94672	**Aviation ID:**	YPAD	**Opened:**	16 Feb 1955	**Current Status:**	Still open
Latitude:	-34.9524	**Longitude:**	138.5204	**Elevation:**	2 m	**Barometer Elev:**	8.2 m	**Metadata compiled:**	28 JUL 2013

Station Equipment History (continued)

Available Date Range	Element	Fail Field Performance Check
28/FEB/1996 - 11/JAN/2013	Soil Temperature 20cm	0
19/DEC/2002 - 11/JAN/2013	Soil Temperature 5cm	0
04/MAY/1987 - 11/JAN/2013	Terrestial Minimum Temperature	2
01/JUL/2003 - 11/JUL/2013	Visibility	1
04/MAY/1987 - 03/JUL/2013	Wind Direction	2
28/FEB/1996 - 11/JUL/2013	Air Temperature	0
04/MAY/1987 - 11/JUL/2013	Wet Bulb Temperature	1
21/JUL/2009 - 27/JUL/2012	Lightning	2
04/MAY/1987 - 11/JUL/2013	Pressure	2
26/JAN/1989 - 11/JAN/2013	Pressure Trend	0
04/MAY/1987 - 03/JUL/2013	Wind Speed	2
04/MAY/1987 - 11/JUL/2013	Rainfall	3
28/FEB/1996 - 11/JAN/2013	Soil Temperature 100cm	0
28/FEB/1996 - 11/JAN/2013	Soil Temperature 10cm	0
01/MAR/2000 - 30/NOV/2012	RF Reflectivity	1

Station Detail Changes

16/DEC/2002 CLASSIFICATION Building (FBL)
26/JUN/2002 CLASSIFICATION CLIMAT Stations (CLC)
26/JUN/2002 CLASSIFICATION CLIMAT TEMP Stations (CLT)
09/MAY/2006 CLASSIFICATION Category A (TAF A)
10/JAN/2011 CLASSIFICATION Critical (ASOSCRIT)
01/FEB/1995 CLASSIFICATION Fielden (FFD) ENDED 16-12-2002
01/JUL/1998 CLASSIFICATION Information and Observations (MIO) ENDED 18-11-2002
18/NOV/2002 CLASSIFICATION Observations Only (MO)
01/JUL/1998 CLASSIFICATION Rawinsonde Stations (RS)
14/FEB/1997 CLASSIFICATION Regional Basic Synoptic Network (RBSN)
15/SEP/2006 OBJECT Document/023034060915email
18/JUN/2007 OBJECT Document/023034070514piezo-email
18/DEC/2002 OBJECT Document/BAROMETER COEFFICIENTS
28/JUN/2012 OBJECT Document/CEILOMETER STATUS
11/JUL/2013 OBJECT Document/CEILOMETER STATUS
07/JUN/2011 OBJECT Document/CEILOMETER STATUS
03/MAR/2009 OBJECT Document/RAPIC TX CAL DATA
20/MAR/2013 OBJECT Document/RBL RM Schedule 20-3-13
09/NOV/2004 OBJECT Document/SKYLINE DATA
12/JAN/2007 OBJECT Document/SKYLINE DATA
19/DEC/2002 OBJECT Document/SKYLINE DATA
21/OCT/2002 OBJECT Document/SKYLINE DATA
04/NOV/1999 OBJECT Document/SKYLINE DATA
27/JAN/2011 OBJECT Document/SKYLINE DATA - ANEMOMETER
04/JUL/2002 OBJECT Document/SKYLINE DATA - RADAR
30/AUG/2010 OBJECT Document/Urban Heat Island Study

Australian Government
Bureau of Meteorology

Extended Climatological Station Metadata
All History

Station:	ADELAIDE AIRPORT			**Location:**	ADELAIDE AIRPORT			**State:**	SA
Bureau No.:	023034	**WMO No.:**	94672	**Aviation ID:**	YPAD	**Opened:**	16 Feb 1955	**Current Status:**	Still open
Latitude:	-34.9524	**Longitude:**	138.5204	**Elevation:**	2 m	**Barometer Elev:**	8.2 m	**Metadata compiled:**	28 JUL 2013

Station Equipment History (continued)

Station Detail Changes(Continued)

28/JUN/2012	OBJECT Document/VISIBILITY METER STATUS
11/JUL/2013	OBJECT Document/VISIBILITY METER STATUS
07/JUN/2011	OBJECT Document/VISIBILITY METER STATUS
06/MAR/2012	OBJECT Document/VISIBILITY METER STATUS
06/MAR/2012	OBJECT Document/YPAD visibility - DRI21 calibration scales
21/FEB/2011	OBJECT Document/metconsole_stationconfig_023034110221
13/NOV/2008	OBJECT Document/sondestrategy
19/FEB/2009	OBJECT Document/tag and testing 2009-02-20
16/FEB/1955	STATION - (nondb seeding) Opened
16/FEB/1955	STATION - (nondb seeding) aero_ht Changed to 6.1
16/FEB/1955	STATION - (nondb seeding) bar_ht Changed to 4
16/FEB/1955	STATION - (nondb seeding) bar_ht_deriv Changed to SURVEY
16/FEB/1955	STATION - (nondb seeding) name Changed to ADELAIDE AIRPORT
16/FEB/1955	STATION - (nondb seeding) stn_ht Changed to 6
16/FEB/1955	STATION - (nondb seeding) stn_ht_deriv Changed to SURVEY
16/FEB/1955	STATION - (nondb seeding) wmo_num Changed to 94672
16/FEB/1955	STATION aero_ht_deriv Changed to SURVEY
16/FEB/1955	STATION aviation_id Changed to YPAD
16/DEC/2002	STATION bar_ht Changed to 8.2
16/DEC/2002	STATION bar_ht_deriv Changed to SURVEY
16/DEC/2002	STATION latitude Changed to -34.9524
16/FEB/1955	STATION latitude Changed to -34.95660WSG84
16/DEC/2002	STATION latlon_deriv Changed to GPS
16/FEB/1955	STATION latlon_deriv Changed to GPS
16/DEC/2002	STATION latlon_error Changed to
16/DEC/2002	STATION longitude Changed to 138.5204
16/FEB/1955	STATION longitude Changed to 138.53562WSG84
16/FEB/1955	STATION lu_0_100m Changed to Airport
04/NOV/1999	STATION lu_0_100m Changed to Airport
16/FEB/1955	STATION lu_100m_1km Changed to Airport
04/NOV/1999	STATION lu_100m_1km Changed to Airport
16/FEB/1955	STATION lu_1km_10km Changed to City area, buildings < 10 metres (3 storey)
04/NOV/1999	STATION lu_1km_10km Changed to City area, buildings > 10 metres (3 storey)
04/NOV/1999	STATION soil_type Changed to black soil
16/DEC/2002	STATION soil_type Changed to sand
16/DEC/2002	STATION stn_ht Changed to 2
16/DEC/2002	STATION stn_ht_deriv Changed to SURVEY
16/DEC/2002	STATION surface_type Changed to bare ground
17/JAN/2011	STATION surface_type Changed to fully covered by grass
04/NOV/1999	STATION surface_type Changed to fully covered by grass
13/JAN/2006	STATION surface_type Changed to mostly covered by grass
17/FEB/2004	STATION surface_type Changed to partly covered by grass

System Changes

14/OCT/2009	SYSTEM External Clients Ceased

Historical metadata for this site has not been quality controlled for accuracy and completeness. Data other than current station information, particularly earlier than 1998, should be considered accordingly. Information may not be complete, as backfilling of historical data is incomplete.

Australian Government
Bureau of Meteorology

Extended Climatological Station Metadata
All History

Station:	ADELAIDE AIRPORT			**Location:**	ADELAIDE AIRPORT			**State:**	SA
Bureau No.:	023034	**WMO No.:**	94672	**Aviation ID:**	YPAD	**Opened:**	16 Feb 1955	**Current Status:**	Still open
Latitude:	-34.9524	**Longitude:**	138.5204	**Elevation:**	2 m	**Barometer Elev:**	8.2 m	**Metadata compiled:**	28 JUL 2013

Station Equipment History (continued)

System Changes(Continued)

01/MAR/1977	SYSTEM External Clients Commenced
13/OCT/2009	SYSTEM External Clients Commenced
10/AUG/2001	SYSTEM Flood Warning Ceased
22/MAR/1993	SYSTEM Flood Warning Commenced
01/JUN/1954	SYSTEM Infrastructure Commenced
17/APR/1999	SYSTEM Radiation Ceased
07/NOV/1994	SYSTEM Radiation Commenced
01/MAR/2003	SYSTEM Radiation Commenced
01/JAN/1967	SYSTEM Rainfall Intensity Commenced
23/DEC/2009	SYSTEM Reference Standards Commenced
16/FEB/1955	SYSTEM Surface Observations Commenced
01/JUN/1954	SYSTEM Upper Air Commenced
17/NOV/2008	SYSTEM WeatherWatch Ceased
01/JUN/1954	SYSTEM WeatherWatch Commenced

Australian Government
Bureau of Meteorology

Notes on these metadata

The following notes have been compiled to assist with interpreting the metadata provided in this document. These notes are subject to change as the network evolves. Changes in station-specific metadata occur more frequently, both as recent changes are recorded and historical information is transferred from paper file to electronic database.

Reliability of the metadata

The Commonwealth Bureau of Meteorology maintains information on more than 20,000 stations which have operated since observations began in the mid 1800s. The amount of information available for each of these sites and its associated uncertainty are influenced by a number of factors including the type and purpose of the station and the time over which it operated.

Early information about stations was held only on paper file. In 1998 a corporate electronic database was established to help maintain information about the network and its components. The number of parameters recorded about a station is now much greater than before this database was established. The national database has also helped improve consistency in the metadata through the implementation of predefined fields. As a result, and through the refinement of operating procedures, station metadata recorded since 1998 are of a higher overall standard than previously, although occasional omissions and errors are still possible.

The Bureau is part way through a task of entering historical information held on paper file into the corporate database. **Until this process is completed there will remain large gaps in the information contained in these metadata documents and considerable caution should be used when deriving conclusions from the metadata.** As an example, two consecutive entries about a rain gauge dated 50 years apart may appear in the equipment metadata. This may either mean that nothing happened to that instrument over the 50 years, or that information for the intervening period has yet to be entered into the database. Similarly, if no information was available about instruments at a site when it was first established, fields which were required to have a value present may have used the earliest information available as a best-guess estimate. Sometimes this was the metadata current when the database was established in 1998. In some instances there may be gaps in metadata relevant to the post 1998 period.

For the above reasons it is recommended that all metadata prior to 1998 be considered as indicative only, and used with caution, unless it has been quality controlled. The Bureau of Meteorology should be contacted if further information or confirmation of the data is required. Depending on the nature of the inquiry there may be a fee associated with this request. Contact details are provided in the telephone book for each capital city or the Bureau's web site at:
http://www.bom.gov.au

The following pages contain explanatory notes for selected terms found in this document.

Station Number

The Bureau of Meteorology station number uniquely specifies a station and is not intended to change over time time, although on very rare occasions a station number may change or be deleted from the record (usually to correct an error). Generally a new station number is established if an existing station changes in a way that would affect the climate data record for that site (measured in terms of air temperature and precipitation). Significant station moves are an example of this.

Some stations also possess a World Meteorological Organization (WMO) station number. The WMO number is different to the Bureau of Meteorology number. It also uniquely specifies a station at any given time but can be reassigned to another station if the new station takes priority in the global reporting network. Only selected stations will have a WMO number. Significant stations may maintain their WMO number for many decades.

Australian Government
Bureau of Meteorology

Notes on these metadata

Network Classification

SUPPORTING the BASIC CLIMATE SERVICE
Global Climate Observing System (GCOS)
GCOS Upper Air Network (GUAN)
GCOS Surface Network (GSN)
National Climate Network {not yet assigned}
Reference Climate Stations (RCS)
Regional Basic Climatological Network (RBCN)
CLIMAT Stations (CLC)
CLIMAT TEMP Stations (CLT)
SUPPORTING the NATIONAL WEATHER WATCH SYSTEM
WMO Global Observing System (GOS)
GOS Upper Air Network
GOS Satellite Network
Global Atmospheric Watch
Background Atmospheric Pollution Monitoring Network (BAPMON)
Basic Ozone Network
Basic Solar and Terrestrial Radiation Network
Regional Basic Synoptic Network (RBSN)
WMO Global Oceanic Observing System (GOOS)
SUPPORTING the BASIC WEATHER SERVICE (BWS)
BWS Land Network
Significant Land Locations
Capital City Mesonets
National Benchmark Network for Agrometeorology (NBNA)
BWS Marine Network
Significant Coastal Loactions
Open Ocean Network
BWS Upper Air Network
Major Significant Locations
BWS Remote Sensing Network
Weather Watch Radar Network
Fire Weather Wind Mesonets
High Resolution Satellite
SUPPORTING the BASIC HYDROLOGICAL SERVICE
Regional Flood Warning Network
Water Resources Assessment Network
Global Hydrological Network
Global Terrestrial Observing System (GTOS)
World Hydrological Cycle Observing System (WHYCOS)
National Hydrological Network

Networks of stations are defined for a variety of purposes (as defined in above table).

Australian Government
Bureau of Meteorology

Notes on these metadata

Network Classification Continued....

Stations may be included in several different networks, which may change over time. The table on the previous page lists current network classifications related to the scientific purpose of the network. Some of these networks - the GCOS network for instance - are components of a global network. Entries in the database for some networks may not be complete, thus not properly representing the status of the network. The composition of the network will usually change over time. While several of the networks have international significance, other network classifications have been developed to aid operational management.

Station Purpose

The station purpose can be classified according to the observation program listed below. Parameters in brackets list some of the various different configurations which occur.

- Synoptic [Seasonal, River Height, Climatological, Telegraphic Rain, Aeronautical, Upper Air]
- Climatological [Seasonal, Telegraphic Rain]
- Aeronautical
- Rainfall [River Height]
- River Height
- Telegraphic Rain [Non-Telegraphic River Height, Telegraphic River Height]
- Non-Telegraphic Rain [Telegraphic River Height]
- Evaporation [Rainfall, River Height, Telegraphic River Height, Non-Telegraphic River Height, Telegraphic Rain, Non-Telegraphic Rain]
- Pluviograph [Rainfall, Telegraphic Rain, Non-Telegraphic Rain, River Height, Telegraphic River Height, Non-Telegraphic River Height]
- Radiation
- Lightning Flash Counter
- Public Information
- Local Conditions
- Radar Site
- Unclassified
- No Routine Observations

Note: Telegraphic observations are those which are sent by some electronic means be it a phone or telegram to the responsible Bureau office. It is a term which is historically linked to analogue non automatic data transmission.

Station Observation Program Summary

Surface Observations

The following terms are used to describe the frequency of surface observations at a site. Historical observation programs will typically be missing for many sites until the database is backfilled with information.

Set a)

- Continuous Program
  - More than half hourly observations sent (eg an automatic weather station {AWS} which continuously transmits 10 minute observations). This will automatically include half hourly and hourly observations programs.
- Half hourly observations
  - Half hourly observations sent. This will automatically include hourly observations.
- Hourly observations
  - Hourly observations sent only. Stations report on non-synoptic hours (ie. 0100, 0200, 0400, 0500, etc)

Australian Government
Bureau of Meteorology

Notes on these metadata

Surface observations continued....

Set b)

- Performed
  - Observations performed, instruments read and observations recorded
- Reported
  - Observations performed, instruments read and reported real time
- Seasonal
  - The program may only be performed during a defined season (such as Fire Weather observations) or the routine program may increase in reporting frequency and/or parameters. The program dates are currently modified at the start and end of each season for stations performing seasonal observations. Historically this was not always the case.

Current Station Equipment Summary

Equipment listed in this metadata product is catalogued under one of systems listed below, appropriate to its application. The "Infrastructure" category has been included since it contains information about the mast height of an anemometer (if present).

- Flood Warning
- Infrastructure
- Radiation
- Rainfall Intensity
- Surface Observations
- Upper Air
- Weather Watch {RADAR}

Station Equipment History

Equipment Install/Remove

One of four types of actions can be performed on an instrument in this listing:

Install - A new instrument is installed at the site. This can be either a completely new addition (eg the first barometer at the site), or the replacement of an existing instrument with a different type (eg replacing mercury barometer with electronic barometer)

Remove - An instrument can be removed either when it is no longer necessary to measure a particular element, or when the element is to be measured by an instrument of a different type (see under "Install" above)

Replace - This occurs when one instrument is replaced with another of the same type (eg Kew pattern mercury barometer replacing another Kew pattern mercury barometer)

Share - The same instrument is used for observations under two (or more) systems (eg a rain gauge may be used within both Surface Observations and Rainfall Intensity systems)

Unshare - The instrument is no longer shared between systems

Australian Government
Bureau of Meteorology

Notes on these metadata

Calibration

During a site inspection an instrument will be calibrated as either being within or not within the specified tolerance in accuracy.

Where a quantative calibration result can be achieved by comparison to a transfer standard (eg barometer comparisons and tipping bucket rain gauge calibrations), the instrument will be recorded as being within or outside the required tolerance. Instruments (such as 203mm rain gauges, screens and evaporation pans) where quantitative calibrations cannot be derived should be regarded as meeting specifications when the instrument is in 'good working order'.

This product provides a summary table of the number of times an instrument was found to be out of calibration

Station Detail Changes

This set of metadata indicates when some aspect of the general information about a station has changed.

- STATION

Metadata which are categorised as pertaining to STATION are items of (textual) information describing a specific attribute of the station. A reference to (nondB seeding) indicates initial information of this field has been sourced from a previous database.

Station position

- Latitude and longitude

Derivation of station latitude and longitude, defined by the location of the rain gauge when it is present, has changed over time. Current practice is to locate or verify open and operational station latitude and longitude based on Global Positioning System equipment. Methods used to locate a station as described in this product (latlon_deriv) are as follows: GPS, MAP 1:10000, MAP 1:12500, MAP 1:25000, MAP 1:50000, MAP 1:100000, MAP 1:250000, SURVEY, and Unknown (which is more commonly represented by a null value). The field latlon_error should be used with caution as the method of determining this value has been interpreted in different ways over time.

- Height

Determination of heights for observing sites is by survey where possible. Otherwise height may be determined using a Digital Aneroid Barometer and a known surveyed point, or derived from map contours. The source of height is provided in the corresponding parameter with a suffix of "_deriv".

Heights which may appear in these metadata are:

- aero_ht
  - The official elevation of the aerodrome which normally corresponds to the altitude of the highest threshold of the runways at that airport;
- bar_ht
  - this represents the height of the mercury barometer cistern or the digital aneroid barometer above mean sea level (MSL);
- stn_ht
  - this normally represents the height of the rain gauge above MSL

Australian Government
Bureau of Meteorology

Notes on these metadata

- Land Use

To assist the long term understanding of climate change it is important to be able to determine the differences over time which are attributed to variations in the climate. Since land use has an effect on the micro climate around the site, and changes in land use will therefore affect the climate record, it is important that the characteristics of the site are monitored. Soil types are recorded as they affect the land use and also add to the knowledge of the site details.

Defined Land use Types.

- Non-vegetated (barren, desert)
- Coastal or Island
- Forest
- Open farmland, grassland or tundra
- Small town, less than 1000 population
- Town 1000 to 10,000 population
- City area with buildings less than 10 metres (3 stories)
- City area with buildings greater than 10 metres (3 stories)
- Airport

The land use code is entered on the station inspection form in the ranges 0 to 100 m, 100 to 1 km and 1km to 10 km; ie:

- lu_0_100m: Land Use 0 to 100 metres from the enclosure
- lu_100m_1km: Land Use 100 metres to 1 kilometre
- lu_1km_10km: Land Use 1 kilometre to 10 kilometres

Defined Soil Type (At Enclosure).

- unable to determine
- sand
- black soil
- clay
- rock
- red soil
- other

Surface Type (At Enclosure).

- unable to determine
- fully covered by grass
- mostly covered by grass
- partly covered by grass
- bare ground
- sand
- concrete
- asphalt
- rock
- other

Appendix B: Climatic Indices and their Correlation with monthly averaged components of wind

The monthly record of climatic indices of Southern Oscillation, Antarctic Oscillation and Indian Ocean Dipole are presented along with the correlation analysis of each index with the detrended monthly averaged intensity of each component of wind. The 3 years and 5 years filtering results is also attached.

Monthly Southern Oscillation Index (SOI) Since January 1956

Year	Jan	Feb	Mar	Apr	May	Jun	Jul	Aug	Sep	Oct	Nov	Dec
1956	11.3	12.4	9.4	11.1	17.9	12.3	12.6	11	0.2	18.3	1.9	10.3
1957	5.6	-2.2	-0.9	1.2	-12.2	-2.3	0.9	-9.5	-10.6	-1.3	-11.9	-3.5
1958	-16.8	-6.9	-1.4	1.2	-8.2	0.2	2.2	7.8	-3.4	-1.9	-4.7	-6.5
1959	-8.7	-14	8.4	3.6	2.8	-6.3	-5	-5	0.2	4.2	11.1	8.2
1960	0.3	-2.2	5.6	7.8	5.2	-2.3	4.8	6.6	6.9	-0.7	7.2	6.7
1961	-2.5	6.3	-20.9	9.4	1.3	-3.1	2.2	0.1	0.8	-5	7.2	13.8
1962	17	5.3	-1.4	1.2	12.3	5	-0.4	4.6	5.1	10.3	5.2	0.6
1963	9.4	3	7.3	6.1	2.8	-9.6	-1	-2.4	-5.2	-12.9	-9.3	-11.6
1964	-4	-0.3	8.4	13.5	2.8	7.4	6.8	14.3	14.1	12.8	2.6	-3
1965	-4	1.6	2.9	-12.9	-0.3	-12.8	-22.6	-11.4	-14.2	-11.1	-17.9	1.6
1966	-12	-4.1	-13.9	-7.1	-9	1	-1	4	-2.2	-2.5	-0.1	-4
1967	14.6	12.9	7.8	-3	-3.5	6.6	1.6	5.9	5.1	-0.1	-4	-5.5
1968	4.1	9.6	-3	-3	14.7	12.3	7.4	0.1	-2.8	-1.9	-3.4	2.1
1969	-13.5	-6.9	1.8	-8.8	-6.6	-0.6	-6.9	-4.4	-10.6	-11.7	-0.1	3.7
1970	-10.1	-10.7	1.8	-4.6	2.1	9.9	-5.6	4	12.9	10.3	19.7	17.4
1971	2.7	15.7	19.2	22.6	9.2	2.6	1.6	14.9	15.9	17.7	7.2	2.1
1972	3.7	8.2	2.4	-5.5	-16.1	-12	-18.6	-8.9	-14.8	-11.1	-3.4	-12.1
1973	-3	-13.5	0.8	-2.1	2.8	12.3	6.1	12.3	13.5	9.7	31.6	16.9
1974	20.8	16.2	20.3	11.1	10.7	2.6	12	6.6	12.3	8.5	-1.4	-0.9
1975	-4.9	5.3	11.6	14.4	6	15.5	21.1	20.7	22.5	17.7	13.8	19.5
1976	11.8	12.9	13.2	1.2	2.1	0.2	-12.8	-12.1	-13	3	9.8	-3
1977	-4	7.7	-9.5	-9.6	-11.4	-17.7	-14.7	-12.1	-9.4	-12.9	-14.6	-10.6
1978	-3	-24.4	-5.8	-7.9	16.3	5.8	6.1	1.4	0.8	-6.2	-2	-0.9
1979	-4	6.7	-3	-5.5	3.6	5.8	-8.2	-5	1.4	-2.5	-4.7	-7.5
1980	3.2	1.1	-8.5	-12.9	-3.5	-4.7	-1.7	1.4	-5.2	-1.9	-3.4	-0.9
1981	2.7	-3.2	-16.6	-5.5	7.6	11.5	9.4	5.9	7.5	-5	2.6	4.7
1982	9.4	0.6	2.4	-3.8	-8.2	-20.1	-19.3	-23.6	-21.4	-20.2	-31.1	-21.3
1983	-30.6	-33.3	-28	-17	6	-3.1	-7.6	0.1	9.9	4.2	-0.7	0.1
1984	1.3	5.8	-5.8	2	-0.3	-8.7	2.2	2.7	2	-5	3.9	-1.4
1985	-3.5	6.7	-2	14.4	2.8	-9.6	-2.3	8.5	0.2	-5.6	-1.4	2.1
1986	8	-10.7	0.8	1.2	-6.6	10.7	2.2	-7.6	-5.2	6.1	-13.9	-13.6
1987	-6.3	-12.6	-16.6	-24.4	-21.6	-20.1	-18.6	-14	-11.2	-5.6	-1.4	-4.5
1988	-1.1	-5	2.4	-1.3	10	-3.9	11.3	14.9	20.1	14.6	21	10.8
1989	13.2	9.1	6.7	21	14.7	7.4	9.4	-6.3	5.7	7.3	-2	-5
1990	-1.1	-17.3	-8.5	-0.5	13.1	1	5.5	-5	-7.6	1.8	-5.3	-2.4
1991	5.1	0.6	-10.6	-12.9	-19.3	-5.5	-1.7	-7.6	-16.6	-12.9	-7.3	-16.7
1992	-25.4	-9.3	-24.2	-18.7	0.5	-12.8	-6.9	1.4	0.8	-17.2	-7.3	-5.5
1993	-8.2	-7.9	-8.5	-21.1	-8.2	-16	-10.8	-14	-7.6	-13.5	0.6	1.6

Monthly Southern Oscillation Index (SOI) Since January 1956 (continued)												
1994	-1.6	0.6	-10.6	-22.8	-13	-10.4	-18	-17.2	-17.2	-14.1	-7.3	-11.6
1995	-4	-2.7	3.5	-16.2	-9	-1.5	4.2	0.8	3.2	-1.3	1.3	-5.5
1996	8.4	1.1	6.2	7.8	1.3	13.9	6.8	4.6	6.9	4.2	-0.1	7.2
1997	4.1	13.3	-8.5	-16.2	-22.4	-24.1	-9.5	-19.8	-14.8	-17.8	-15.2	-9.1
1998	-23.5	-19.2	-28.5	-24.4	0.5	9.9	14.6	9.8	11.1	10.9	12.5	13.3
1999	15.6	8.6	8.9	18.5	1.3	1	4.8	2.1	-0.4	9.1	13.1	12.8
2000	5.1	12.9	9.4	16.8	3.6	-5.5	-3.7	5.3	9.9	9.7	22.4	7.7
2001	8.9	11.9	6.7	0.3	-9	1.8	-3	-8.9	1.4	-1.9	7.2	-9.1
2002	2.7	7.7	-5.2	-3.8	-14.5	-6.3	-7.6	-14.6	-7.6	-7.4	-6	-10.6
2003	-2	-7.4	-6.8	-5.5	-7.4	-12	2.9	-1.8	-2.2	-1.9	-3.4	9.8
2004	-11.6	8.6	0.2	-15.4	13.1	-14.4	-6.9	-7.6	-2.8	-3.7	-9.3	-8
2005	1.8	-29.1	0.2	-11.2	-14.5	2.6	0.9	-6.9	3.9	10.9	-2.7	0.6
2006	12.7	0.1	13.8	15.2	-9.8	-5.5	-8.9	-15.9	-5.1	-15.3	-1.4	-3
2007	-7.3	-2.7	-1.4	-3	-2.7	5	-4.3	2.7	1.5	5.4	9.8	14.4
2008	14.1	21.3	12.2	4.5	-4.3	5	2.2	9.1	14.1	13.4	17.1	13.3
2009	9.4	14.8	0.2	8.6	-5.1	-2.3	1.6	-5	3.9	-14.7	-6.7	-7
2010	-10.1	-14.5	-10.6	15.2	10	1.8	20.5	18.8	25	18.3	16.4	27.1
2011	19.9	22.3	21.4	25.1	2.1	0.2	10.7	2.1	11.7	7.3	13.8	23
2012	9.4	2.5	2.9	-7.1	-2.7	-10.4	-1.7	-5	2.7	2.4	3.9	-6
2013	-1.1	-3.6	11.1	0.3	8.4	13.9	8.1	-0.5	3.9	-1.9	9.2	0.6

Source: http://www.bom.gov.au/climate/current/soihtm1.shtml

Monthly Antarctic Oscillation Index (AAO) index since January 1979

Year	Jan	Feb	Mar	Apr	May	Jun	Jul	Aug	Sep	Oct	Nov	Dec
1979	0.209	0.356	0.899	0.678	0.724	1.7	2.412	0.546	0.629	0.16	-0.423	-0.951
1980	-0.447	-0.98	-1.424	-2.068	-0.479	0.286	-1.944	-0.997	-1.701	0.577	-2.013	-0.356
1981	0.231	0.039	-0.966	-1.462	-0.344	0.352	-0.986	-2.118	-1.509	-0.26	0.626	1.116
1982	-0.554	0.277	1.603	1.531	0.118	0.92	-0.415	0.779	1.58	-0.702	-0.849	-1.934
1983	-1.34	-1.081	0.166	0.149	-0.437	-0.263	1.114	0.792	-0.696	1.193	0.727	0.475
1984	-1.098	-0.544	0.251	-0.204	-1.237	0.426	0.89	-0.548	0.327	-0.009	-0.024	-1.476
1985	-0.795	0.215	-0.134	0.031	-0.066	-0.331	1.914	0.595	1.507	0.471	1.085	1.24
1986	0.158	-1.588	-0.77	-0.087	-1.847	-0.619	0.089	-0.157	0.849	0.306	-0.222	0.886
1987	-0.95	-0.708	-0.133	-0.286	0.039	-0.702	-1.531	1.485	-0.799	0.455	1.06	0.272
1988	-0.612	0.551	-0.219	-0.077	-0.749	-1.055	0.576	-0.745	-0.689	-2.314	0.401	1.074
1989	0.618	0.849	0.632	-0.573	2.691	1.995	1.458	-0.132	-0.121	0.136	0.572	-0.445
1990	-0.352	1.151	0.414	-1.879	-1.803	0.093	-1.215	0.466	1.482	0.139	-0.359	-0.312
1991	0.869	-0.852	0.522	-0.639	-0.539	-1.155	-1.22	0.036	-0.513	-0.623	-0.804	-2.067
1992	0.073	-1.627	-1.01	-0.439	-2.032	-2.193	-0.566	-0.35	0.435	-0.319	0.122	0.244
1993	-2.021	0.437	-0.378	0.087	1.26	1.218	1.957	1.083	1.061	0.748	0.324	1.028
1994	0.723	1.157	0.693	-0.052	-0.153	-1.682	-0.492	1.91	-0.947	-0.578	-0.793	0.933
1995	1.448	0.533	-0.154	0.649	1.397	-0.802	-3.01	-0.696	1.173	-0.057	0.143	1.47
1996	0.332	-0.525	0.543	0.115	0.983	-0.252	0.021	-1.502	-1.314	0.966	-1.667	-0.023
1997	0.369	-0.244	0.701	-0.458	1.028	-0.458	0.78	0.768	0.122	-0.595	-1.905	-0.835
1998	0.413	0.39	0.736	1.927	-0.038	1.031	1.45	0.904	-0.122	0.4	0.817	1.435
1999	0.999	0.456	0.18	0.949	1.639	-1.325	0.316	0.042	-0.012	1.653	0.901	1.784
2000	1.273	0.62	0.133	0.233	1.127	0.117	0.059	-0.674	-1.853	0.347	-1.537	-1.29
2001	-0.471	-0.265	-0.555	0.515	-0.262	0.386	-0.928	0.91	1.161	1.277	0.996	1.474
2002	0.747	1.334	-1.823	0.165	-2.798	-1.112	-0.591	-0.099	-0.864	-2.564	-0.924	1.308
2003	-0.988	-0.357	-0.188	0.224	0.385	-0.775	0.727	0.678	-0.323	-0.025	-0.712	-1.323
2004	0.807	-1.182	0.432	0.151	0.46	1.195	1.474	-0.071	0.254	-0.042	-0.242	-0.973
2005	-0.129	1.243	0.158	0.355	-0.297	-1.428	-0.252	0.228	0.241	0.031	-0.551	-1.968
2006	0.339	-0.211	0.501	-0.169	1.695	0.438	0.926	-1.727	-0.324	0.879	0.101	0.638
2007	-0.083	0.075	-0.57	-1.035	-0.612	-1.198	-2.631	-0.108	0.031	-0.434	-0.984	1.929
2008	1.208	1.147	0.587	-0.873	-0.49	1.348	0.32	0.087	1.386	1.215	0.92	1.194
2009	0.963	0.456	0.605	0.029	-0.733	-0.47	-1.234	-0.686	-0.017	0.085	-1.915	0.607
2010	-0.757	-0.775	0.108	0.377	1.021	2.071	2.424	1.51	0.402	1.335	1.516	0.205
2011	0.052	1.074	-0.296	-0.87	1.266	-0.099	-1.384	-1.202	-1.25	0.388	-0.908	2.573
2012	1.583	-0.283	0.275	0.666	0.153	-0.197	1.259	0.489	0.562	-0.444	-1.701	-0.764
2013	0.071	0.716	1.375	0.611	0.36	-0.271	0.945	-1.561	-1.658	-0.458	0.189	0.061

Source: http://www.cpc.ncep.noaa.gov/products/precip/CWlink/daily_ao_index/aao/monthly.aao.index.b79.current.ascii.table

Monthly Indian Ocean Dipole Index (IOD) since January 1958

Year	Jan	Feb	Mar	Apr	May	Jun	Jul	Aug	Sep	Oct	Nov	Dec
1958	0.19	0.22	0.17	-0.08	-0.65	-1.25	-1.88	-2.17	-2.02	-1.74	-0.88	-0.40
1959	-0.18	0.01	-0.02	-0.51	-0.57	-0.81	-1.10	-0.94	-0.82	-0.66	-0.26	0.22
1960	0.20	0.00	-0.27	-0.58	-1.10	-1.18	-0.99	-1.10	-1.23	-1.24	-1.04	-0.80
1961	-0.36	-0.28	-0.12	0.01	0.58	1.30	2.25	2.96	3.17	2.83	2.49	2.33
1962	2.11	1.78	1.27	0.56	-0.19	-0.65	-0.71	-0.62	-0.44	-0.21	0.16	0.48
1963	0.76	0.82	0.65	0.26	0.17	0.44	0.65	1.29	1.74	1.48	0.66	-0.05
1964	-0.73	-1.18	-1.48	-1.30	-1.33	-1.53	-1.99	-2.29	-2.22	-1.74	-1.56	-1.24
1965	-0.69	-0.72	-0.93	-0.95	-0.88	-0.84	-0.65	-0.14	0.08	0.19	0.12	0.05
1966	-0.33	-0.51	-0.54	-0.36	-0.17	0.28	0.81	0.98	0.81	0.58	0.21	-0.03
1967	0.29	0.31	0.41	0.69	0.90	0.86	1.26	1.57	1.55	1.43	1.39	1.41
1968	1.28	1.26	1.16	1.11	0.49	0.06	-0.48	-0.74	-1.17	-1.01	-0.90	-0.60
1969	-0.29	-0.04	0.02	-0.28	-0.44	-0.71	-0.80	-0.79	-0.34	-0.18	0.20	0.51
1970	0.58	0.69	0.92	0.44	-0.22	-0.49	-1.04	-1.63	-1.57	-1.37	-1.06	-0.71
1971	-0.18	0.19	0.36	0.10	-0.13	-0.64	-1.30	-1.67	-1.47	-1.08	-0.64	-0.35
1972	0.05	0.10	0.10	0.65	1.43	1.89	2.19	2.40	2.36	2.14	1.68	1.25
1973	0.89	0.27	0.04	-0.07	-0.32	-0.69	-1.07	-1.39	-1.30	-0.90	-0.30	0.33
1974	0.76	0.80	0.64	0.49	0.25	-0.24	-0.60	-0.98	-1.35	-1.47	-1.45	-1.24
1975	-1.05	-0.59	-0.21	0.20	0.43	0.59	-0.03	-0.82	-1.10	-1.24	-1.06	-0.44
1976	0.27	0.58	0.76	1.11	1.56	1.70	1.53	1.42	1.00	0.52	0.35	0.20
1977	0.40	0.48	0.24	0.24	0.36	0.08	0.00	0.51	0.48	0.54	0.16	-0.16
1978	-0.91	-1.02	-1.36	-0.94	-0.55	-0.19	-0.12	-0.01	-0.21	-0.37	-0.06	-0.10
1979	0.15	0.29	0.19	0.11	0.04	-0.03	0.02	0.19	-0.07	0.05	0.02	-0.03
1980	-0.23	-0.15	-0.07	-0.16	-0.45	-0.68	-1.07	-1.46	-1.49	-1.42	-1.04	-0.61
1981	-0.20	0.15	0.56	0.61	0.26	-0.16	-0.71	-1.09	-1.16	-0.79	-0.30	0.29
1982	0.68	0.98	1.21	1.36	1.49	1.71	2.06	2.43	2.44	2.05	1.37	0.46
1983	-0.73	-1.42	-1.30	-0.57	0.35	1.26	1.73	1.61	1.06	0.52	-0.03	-0.22
1984	-0.21	0.04	-0.07	-0.10	-0.21	-0.43	-0.85	-1.06	-1.10	-1.09	-1.17	-1.31
1985	-1.35	-1.23	-1.14	-1.19	-0.95	-0.81	-0.74	-0.88	-0.33	-0.40	-0.22	-0.26
1986	-0.14	-0.45	-0.19	-0.24	-0.50	-0.58	-0.37	-0.22	-0.18	-0.01	0.15	0.20
1987	0.02	0.06	0.47	0.70	0.89	1.31	1.84	1.98	1.87	1.79	1.74	1.22
1988	0.67	0.58	0.13	-0.27	-0.20	-0.10	-0.21	-0.14	-0.07	0.13	0.04	0.21
1989	0.24	-0.03	-0.57	-0.88	-1.13	-1.06	-0.77	-0.56	-0.22	-0.07	-0.02	-0.19
1990	-0.12	-0.20	-0.30	-0.59	-0.51	-0.64	-0.39	-0.33	0.03	0.16	0.40	0.33
1991	0.44	0.67	1.00	1.21	1.54	1.67	1.61	1.34	1.16	0.95	0.54	0.03
1992	-0.59	-1.10	-1.54	-1.89	-1.90	-1.91	-2.04	-2.05	-1.70	-1.63	-1.31	-0.76
1993	-0.64	-0.52	-0.26	-0.12	-0.21	-0.16	-0.06	-0.10	-0.14	-0.24	-0.09	-0.19
1994	-0.04	0.29	0.91	1.30	1.88	2.42	2.66	2.84	2.73	2.45	1.83	1.42
1995	0.72	0.28	-0.08	-0.18	-0.38	-0.38	-0.26	-0.29	-0.46	-0.31	-0.33	-0.34

Monthly Indian Ocean Dipole Index (IOD) since January 1958 (continued)												
1996	-0.25	-0.35	-0.59	-0.81	-1.24	-1.64	-1.82	-2.42	-2.74	-2.62	-2.29	-1.80
1997	-1.04	-0.44	-0.06	0.15	0.49	1.02	1.66	2.37	3.29	3.55	3.35	2.96
1998	2.12	1.13	0.62	0.41	-0.15	-0.48	-0.80	-1.41	-2.03	-2.04	-1.80	-1.56
1999	-1.02	-0.56	-0.39	-0.32	-0.14	-0.14	-0.06	0.01	0.04	-0.19	-0.39	-0.45
2000	-0.30	-0.12	0.15	0.32	0.47	0.56	0.49	0.38	0.18	-0.11	-0.62	-0.66
2001	-0.66	-0.33	0.03	0.56	0.55	0.43	0.27	-0.10	-0.37	-0.33	-0.29	-0.29
2002	-0.03	-0.14	-0.29	-0.24	-0.29	-0.38	0.23	0.87	1.10	1.13	1.01	0.69
2003	0.24	0.04	0.09	0.46	0.61	0.79	0.91	0.91	0.67	0.65	0.49	0.49
2004	0.61	0.62	0.07	-0.21	-0.49	-0.61	-0.56	-0.09	0.07	0.12	-0.01	-0.50
2005	-0.98	-0.86	-0.76	-0.75	-0.58	-0.47	-0.88	-1.15	-1.25	-1.27	-1.23	-1.19
2006	-1.17	-1.04	-0.95	-0.85	-0.55	-0.15	0.27	0.92	1.34	1.37	1.25	0.92
2007	0.43	0.07	0.20	0.12	0.10	0.27	0.48	0.39	0.36	0.10	-0.08	-0.42
2008	-0.50	-0.63	-0.25	-0.08	0.24	0.35	0.66	0.63	0.40	0.15	0.01	-0.02
2009	-0.05	0.13	0.45	0.60	0.42	0.37	0.32	0.21	0.11	0.36	0.60	0.63

Source: http://www.jamstec.go.jp/frcgc/research/d1/iod/DATA/dmi_HadISST.txt

Correlation coefficient between monthly averaged U and V components of wind and climatic indices

		Non Sea breeze days								**Sea breeze days**							
Wind Components		U				V				U				V			
Month	Time of the day	12:00	15:00	18:00	21:00	12:00	15:00	18:00	21:00	12:00	15:00	18:00	21:00	12:00	15:00	18:00	21:00
	Indices																
January	SOI	-0.5	-0.4	-0.5	-0.4	0.0	-0.1	-0.2	-0.2	-0.1	-0.2	-0.1	-0.3	0.0	0.2	0.2	0.0
	AAO	-0.1	-0.2	-0.2	-0.1	0.0	0.1	0.1	-0.3	0.2	0.0	-0.3	-0.1	0.2	0.1	0.2	-0.1
	IOD	-0.1	-0.1	-0.1	-0.1	-0.2	-0.2	-0.3	-0.1	0.1	0.0	-0.1	-0.3	0.1	0.2	0.3	0.0
February	SOI	-0.3	-0.5	-0.4	-0.3	0.0	0.0	-0.3	-0.1	0.0	0.0	-0.2	-0.2	-0.1	0.1	0.0	0.0
	AAO	0.1	0.1	0.1	0.2	0.3	0.4	0.0	0.1	0.3	-0.1	-0.1	-0.3	-0.2	0.0	-0.2	-0.1
	IOD	0.0	0.0	0.0	-0.1	0.0	-0.1	-0.3	0.0	0.2	0.2	0.2	0.0	-0.1	0.0	0.0	0.1
March	SOI	-0.3	-0.3	-0.3	-0.1	-0.2	0.1	0.0	-0.1	-0.1	0.0	-0.1	-0.1	0.1	0.0	0.0	0.0
	AAO	-0.2	-0.1	-0.2	-0.1	0.0	0.2	0.1	-0.1	-0.1	0.0	0.1	-0.4	-0.1	0.2	0.4	0.2
	IOD	0.1	0.2	0.2	0.1	-0.1	-0.2	0.0	0.0	0.0	0.4	0.0	-0.1	0.1	0.2	0.1	0.1
April	SOI	-0.3	-0.3	0.0	0.2	0.1	-0.1	0.0	0.1	-0.3	0.0	0.0	-0.2	0.1	0.2	0.1	0.0
	AAO	0.1	-0.1	0.0	0.1	0.2	0.0	-0.1	0.0	0.0	-0.3	-0.1	-0.3	0.0	-0.1	-0.2	0.0
	IOD	0.1	0.1	0.1	-0.1	-0.1	-0.2	-0.1	-0.3	0.3	-0.1	0.1	0.2	0.2	0.0	0.0	0.3
May	SOI	-0.1	-0.1	-0.1	0.0	-0.1	-0.2	-0.1	-0.2	0.2	0.0	0.3	0.3	0.0	-0.2	0.0	-0.1
	AAO	0.1	-0.1	0.1	0.2	0.3	0.2	0.0	0.0	-0.2	-0.2	0.0	0.4	0.1	-0.1	-0.2	0.0
	IOD	-0.1	0.0	0.0	0.0	0.1	0.1	0.1	0.1	-0.1	0.0	-0.2	0.1	0.0	0.1	-0.1	0.1
June	SOI	-0.1	-0.2	-0.1	0.0	-0.1	-0.1	-0.2	-0.1	-0.2	-0.2	0.1	0.1	0.2	0.2	0.2	0.1
	AAO	0.2	0.1	0.0	-0.1	-0.1	0.0	0.0	0.0	-0.1	-0.2	0.0	-0.1	-0.1	0.0	0.0	-0.1
	IOD	-0.2	0.0	0.0	0.0	0.1	0.1	0.2	0.2	0.1	0.2	0.1	0.2	0.0	-0.1	-0.2	-0.1
July	SOI	0.1	0.1	0.0	0.0	-0.2	-0.3	-0.2	-0.3	-0.2	-0.2	-0.1	0.3	0.3	0.3	0.0	0.2
	AAO	-0.3	-0.3	-0.4	-0.4	0.1	0.4	0.1	0.0	-0.3	-0.2	-0.2	-0.2	-0.3	0.0	0.1	0.2
	IOD	-0.1	-0.1	0.0	-0.1	0.0	0.1	0.2	0.2	0.2	0.1	0.0	-0.2	-0.1	-0.2	0.0	-0.2
August	SOI	0.1	0.0	0.0	0.1	-0.1	-0.2	-0.1	-0.1	-0.2	0.0	0.0	0.2	0.0	0.0	-0.1	-0.1
	AAO	-0.2	-0.2	-0.3	-0.2	0.3	0.3	0.1	0.2	0.2	-0.2	-0.3	-0.3	0.1	0.0	-0.1	0.1
	IOD	-0.3	-0.2	-0.2	-0.3	0.2	0.1	0.1	0.1	0.0	-0.2	-0.2	-0.2	0.2	0.1	0.0	0.1
September	SOI	-0.2	-0.1	-0.1	-0.1	-0.2	-0.3	-0.3	-0.2	-0.2	-0.1	0.1	0.2	-0.2	-0.3	-0.3	-0.2
	AAO	**-0.5**	**-0.5**	-0.5	-0.3	0.1	0.2	0.4	0.3	-0.2	-0.2	-0.3	-0.2	0.0	0.1	0.0	-0.1
	IOD	0.0	0.0	0.0	0.0	0.1	0.0	0.0	0.2	0.2	0.1	0.0	-0.2	0.2	0.3	0.2	0.2
October	SOI	0.2	0.1	0.2	0.2	-0.3	-0.5	-0.4	-0.4	0.1	0.0	0.1	-0.1	-0.3	-0.3	-0.2	-0.3
	AAO	-0.4	-0.4	-0.5	-0.4	-0.1	-0.2	-0.2	-0.4	-0.1	-0.2	0.1	0.2	0.2	0.2	0.1	0.3
	IOD	-0.2	-0.1	0.0	0.0	0.4	0.5	**0.5**	**0.5**	0.1	-0.1	0.0	0.0	0.1	0.2	0.2	0.2
November	SOI	-0.4	-0.4	-0.3	-0.3	0.1	0.2	0.0	0.0	0.0	-0.1	0.1	-0.1	0.2	0.3	0.3	0.2
	AAO	-0.2	-0.2	-0.1	-0.2	0.1	0.0	-0.1	-0.1	-0.2	0.0	0.0	-0.4	0.3	0.3	0.3	0.3
	IOD	0.2	0.2	0.2	0.2	0.1	0.2	0.2	0.2	-0.1	0.1	-0.1	0.0	-0.1	-0.1	-0.2	-0.3
December	SOI	0.0	-0.2	-0.1	0.0	-0.2	-0.3	-0.3	-0.4	0.0	0.1	0.0	0.0	0.1	0.2	0.2	0.2
	AAO	-0.2	-0.3	-0.3	-0.3	0.2	0.3	0.2	0.0	-0.1	-0.1	0.0	0.0	-0.3	0.0	-0.3	-0.1
	IOD	-0.2	-0.2	-0.2	-0.2	0.2	0.2	0.2	0.3	0.2	0.1	-0.1	-0.2	0.0	0.0	0.1	0.0

Correlation coefficient between monthly averaged U and V components of wind and climatic indices after applying 3 years filtering

		Non Sea breeze days								**Sea breeze days**							
Wind Components		U				V				U				V			
Month	Time of the day	12:00	15:00	18:00	21:00	12:00	15:00	18:00	21:00	12:00	15:00	18:00	21:00	12:00	15:00	18:00	21:00
	Indices																
January	SOI	**-0.6**	-0.5	**-0.5**	**-0.5**	-0.1	-0.1	-0.4	-0.3	-0.2	**-0.5**	-0.3	-0.3	0.0	0.1	0.0	-0.1
	AAO	-0.3	**-0.5**	**-0.6**	-0.3	-0.4	-0.2	-0.3	**-0.7**	0.4	-0.1	**-0.5**	0.1	0.5	0.2	0.2	-0.2
	IOD	-0.2	-0.2	-0.3	-0.3	-0.4	-0.2	-0.4	-0.3	0.2	-0.2	-0.2	-0.2	0.1	0.1	0.1	-0.2
February	SOI	-0.1	-0.3	-0.2	-0.3	-0.1	-0.2	-0.4	-0.3	-0.2	-0.2	-0.2	-0.2	-0.3	-0.1	-0.1	0.2
	AAO	-0.1	-0.1	-0.2	-0.1	0.2	0.2	-0.3	-0.2	0.3	-0.2	-0.4	**-0.5**	-0.2	0.3	0.0	0.0
	IOD	0.2	0.2	0.3	0.0	0.1	0.1	-0.3	-0.1	0.1	0.1	-0.1	0.0	-0.2	-0.1	0.2	0.2
March	SOI	-0.2	-0.2	-0.1	0.0	-0.2	0.2	0.1	-0.1	0.0	0.4	0.0	-0.2	0.0	-0.1	-0.2	0.1
	AAO	-0.2	0.0	-0.1	-0.1	-0.2	0.0	-0.4	-0.3	-0.2	0.0	0.4	-0.2	-0.1	0.1	0.4	0.5
	IOD	-0.3	-0.1	0.0	0.0	-0.3	-0.2	-0.1	0.0	0.1	0.4	-0.1	-0.1	0.2	0.1	0.3	0.4
April	SOI	-0.5	**-0.5**	-0.3	0.1	0.0	-0.1	0.0	0.1	0.0	-0.2	-0.3	-0.2	0.5	0.5	0.2	0.2
	AAO	-0.2	-0.2	-0.1	0.2	0.1	-0.3	-0.4	-0.4	-0.2	**-0.6**	-0.1	-0.1	0.1	-0.2	-0.3	0.1
	IOD	0.0	0.1	0.2	0.1	-0.4	-0.5	-0.4	**-0.6**	0.1	-0.1	0.3	0.2	0.3	0.0	0.0	0.3
May	SOI	-0.2	-0.2	-0.3	-0.2	-0.1	-0.3	-0.3	-0.5	0.3	0.0	0.0	0.2	0.0	-0.2	-0.2	0.0
	AAO	-0.1	-0.3	0.0	0.2	0.4	0.1	0.0	0.0	-0.3	**-0.6**	-0.1	**0.6**	0.4	-0.2	-0.2	-0.1
	IOD	0.0	0.3	0.3	0.4	-0.1	-0.2	-0.2	-0.1	-0.1	0.0	-0.1	0.4	0.1	0.1	-0.1	-0.2
June	SOI	-0.4	**-0.6**	-0.4	-0.3	0.0	-0.1	0.0	0.0	-0.3	-0.1	-0.1	0.2	0.1	0.2	0.3	0.2
	AAO	-0.1	-0.2	0.0	0.2	-0.5	-0.5	-0.5	-0.3	0.0	0.2	-0.1	-0.4	-0.1	0.0	**0.5**	-0.1
	IOD	-0.1	0.0	0.5	**0.6**	0.4	0.4	0.3	0.4	-0.1	0.1	0.0	0.3	-0.1	-0.1	-0.3	0.0
July	SOI	0.1	-0.2	0.0	0.0	-0.1	-0.2	-0.3	-0.3	0.0	-0.1	-0.3	0.1	0.3	0.2	-0.1	0.1
	AAO	**-0.7**	**-0.7**	**-0.6**	**-0.5**	**0.6**	**0.8**	**0.5**	**0.6**	-0.3	-0.5	**-0.7**	-0.4	-0.5	0.0	-0.3	0.3
	IOD	-0.1	0.0	0.1	0.1	0.4	0.4	0.4	0.3	-0.1	-0.1	0.1	0.0	0.1	0.1	0.1	0.1
August	SOI	0.0	0.0	-0.1	0.1	0.0	0.0	-0.1	0.0	-0.2	0.0	0.0	0.2	0.1	0.0	0.1	-0.1
	AAO	-0.3	-0.4	-0.3	-0.2	0.1	0.1	0.0	0.1	0.3	0.0	-0.1	-0.2	0.1	0.0	-0.1	0.1
	IOD	-0.4	-0.4	-0.3	-0.4	0.0	0.0	0.2	0.0	0.0	-0.1	-0.3	-0.1	0.3	0.3	0.2	0.1
September	SOI	0.1	0.1	0.0	0.1	-0.2	-0.4	-0.3	-0.1	-0.3	-0.1	0.2	0.1	0.0	-0.1	-0.1	-0.1
	AAO	-0.4	**-0.6**	-0.5	-0.4	0.5	**0.6**	**0.6**	0.2	0.1	0.5	0.0	0.2	-0.1	0.0	-0.3	-0.4
	IOD	-0.1	-0.2	-0.2	-0.2	0.2	0.2	0.2	0.3	0.3	0.1	-0.2	0.0	-0.1	0.0	-0.1	-0.1
October	SOI	0.2	0.1	0.2	0.4	-0.1	-0.3	-0.2	-0.2	-0.2	-0.1	0.0	0.1	0.1	-0.1	-0.2	-0.3
	AAO	-0.4	-0.4	**-0.5**	-0.4	-0.3	-0.3	-0.4	-0.4	-0.5	-0.2	0.2	**0.6**	0.0	0.1	0.0	0.2
	IOD	0.1	0.0	0.1	0.0	0.2	0.3	0.4	0.3	0.4	0.0	0.0	-0.2	-0.3	0.1	0.1	0.0
November	SOI	-0.3	-0.3	-0.4	-0.4	0.4	0.4	0.2	0.2	-0.2	-0.2	-0.2	0.0	0.2	0.3	0.1	0.2
	AAO	-0.5	**-0.5**	-0.3	-0.4	0.5	0.4	0.3	0.3	**-0.6**	**-0.5**	-0.1	**-0.5**	0.4	0.4	0.1	0.1
	IOD	0.3	0.2	0.2	0.2	0.1	0.2	0.2	0.0	0.1	0.1	-0.2	0.0	0.0	-0.1	-0.2	-0.3
December	SOI	0.2	-0.2	-0.1	0.1	0.0	-0.1	-0.1	-0.4	0.1	0.0	-0.1	0.2	0.1	0.1	0.1	0.1
	AAO	-0.1	**-0.6**	-0.4	**-0.6**	0.5	**0.6**	0.5	-0.1	0.1	-0.3	-0.5	-0.1	0.1	0.2	-0.4	-0.1
	IOD	-0.1	-0.3	-0.4	-0.3	0.4	0.3	0.3	0.2	0.2	-0.1	-0.2	-0.2	0.2	0.2	0.1	0.1

Correlation coefficient between monthly averaged U and V components of wind and climatic indices after applying 5 years filtering

		Non Sea breeze days								**Sea breeze days**							
Wind Components		U				V				U				V			
Month	Time of the day	12:00	15:00	18:00	21:00	12:00	15:00	18:00	21:00	12:00	15:00	18:00	21:00	12:00	15:00	18:00	21:00
	Indices																
January	SOI	**-0.6**	-0.5	**-0.5**	**-0.6**	-0.1	-0.2	-0.4	-0.3	-0.1	-0.4	-0.2	0.0	0.0	-0.1	-0.1	0.0
	AAO	-0.2	**-0.5**	**-0.7**	-0.3	**-0.6**	-0.4	-0.5	**-0.8**	**0.5**	-0.1	**-0.6**	0.4	**0.5**	0.1	0.0	-0.3
	IOD	-0.2	-0.1	-0.3	-0.2	-0.5	-0.2	-0.4	-0.4	0.4	0.1	-0.3	0.0	0.4	0.1	0.1	-0.1
February	SOI	0.1	-0.2	-0.2	-0.3	0.0	0.0	-0.3	-0.4	0.0	0.0	-0.2	-0.3	-0.2	0.1	0.1	0.2
	AAO	0.2	-0.3	-0.4	**-0.5**	0.2	0.3	-0.5	-0.5	**0.6**	0.1	**-0.5**	**-0.6**	0.1	0.5	0.2	0.3
	IOD	0.2	0.1	0.2	0.0	0.3	0.3	0.0	-0.1	0.1	0.2	-0.1	-0.2	-0.1	0.1	0.4	0.2
March	SOI	-0.2	-0.2	-0.1	0.1	-0.2	0.3	0.1	-0.2	0.0	**0.6**	0.2	0.0	0.1	-0.2	-0.2	0.2
	AAO	0.2	0.4	0.3	0.0	-0.2	-0.1	-0.4	-0.1	-0.1	0.2	0.5	0.1	0.1	0.2	0.4	**0.6**
	IOD	-0.3	0.0	0.1	0.0	**-0.5**	-0.1	0.1	0.0	0.0	**0.6**	0.1	-0.1	0.3	0.0	0.2	0.5
April	SOI	**-0.6**	**-0.6**	-0.3	0.1	-0.1	-0.2	-0.1	0.0	0.0	-0.2	-0.4	-0.1	**0.5**	0.4	0.2	0.2
	AAO	-0.3	-0.2	-0.1	0.2	0.2	-0.4	-0.4	**-0.5**	-0.4	**-0.8**	0.1	-0.3	0.2	-0.4	**-0.6**	-0.1
	IOD	0.1	0.3	0.5	0.5	**-0.5**	**-0.6**	**-0.6**	**-0.6**	-0.1	-0.1	0.3	0.0	0.5	0.0	-0.1	0.3
May	SOI	0.0	-0.1	-0.2	0.0	-0.4	-0.5	**-0.6**	**-0.6**	0.3	0.2	-0.1	0.1	-0.2	-0.1	-0.4	-0.1
	AAO	-0.1	-0.3	0.1	0.3	**0.7**	0.4	0.4	0.4	**-0.5**	**-0.7**	-0.1	**0.8**	**0.5**	**-0.5**	0.1	-0.3
	IOD	-0.1	0.2	0.2	**0.5**	-0.1	-0.3	-0.4	-0.2	0.0	-0.2	-0.2	**0.6**	0.3	0.2	0.0	-0.3
June	SOI	-0.4	**-0.6**	-0.4	0.0	0.1	0.2	0.2	0.1	-0.3	0.2	-0.1	0.1	-0.1	0.1	0.2	0.3
	AAO	0.3	0.3	0.5	**0.6**	-0.5	-0.4	**-0.5**	-0.1	0.0	0.1	-0.3	**-0.5**	0.1	0.3	0.5	0.1
	IOD	-0.2	-0.2	0.2	0.5	0.3	0.3	0.2	0.4	-0.2	0.3	0.0	0.4	-0.1	0.0	-0.3	0.1
July	SOI	0.0	-0.1	-0.1	-0.2	-0.2	-0.2	-0.3	-0.3	0.3	0.0	-0.1	-0.1	-0.1	0.0	-0.1	0.1
	AAO	**-0.8**	**-0.8**	**-0.7**	**-0.6**	**0.6**	**0.9**	**0.6**	**0.7**	-0.2	**-0.5**	**-0.7**	-0.4	-0.4	0.1	-0.1	0.2
	IOD	-0.1	-0.2	0.1	0.1	0.5	0.4	0.4	0.4	-0.2	-0.1	0.0	0.0	-0.1	0.1	0.0	0.0
August	SOI	-0.1	0.0	-0.1	0.1	-0.1	-0.1	-0.2	-0.1	-0.2	-0.1	0.1	0.1	0.2	0.2	0.3	0.2
	AAO	0.0	-0.1	0.0	0.1	0.2	0.2	0.1	0.1	0.2	0.1	0.0	-0.2	0.2	-0.1	0.0	0.2
	IOD	-0.2	-0.2	-0.2	-0.2	0.1	0.1	0.2	0.1	0.0	-0.1	-0.3	0.0	0.1	0.0	0.0	-0.1
September	SOI	0.2	0.1	-0.1	0.1	-0.3	-0.4	-0.4	-0.2	-0.3	0.0	0.4	0.1	0.1	0.0	0.2	0.3
	AAO	-0.2	**-0.6**	-0.5	**-0.5**	**0.6**	**0.7**	**0.7**	**0.6**	0.4	0.4	0.0	0.0	0.2	0.4	-0.1	-0.4
	IOD	-0.1	-0.2	-0.1	-0.1	0.4	0.3	0.1	0.3	0.2	0.1	-0.1	0.1	-0.1	-0.1	-0.2	-0.3
October	SOI	0.2	0.1	0.3	**0.5**	-0.2	-0.4	-0.3	-0.2	-0.3	0.0	-0.3	0.2	0.2	-0.1	-0.2	-0.2
	AAO	-0.3	-0.3	-0.4	-0.2	-0.2	-0.2	-0.4	-0.3	**-0.6**	-0.4	0.1	**0.7**	0.0	-0.1	-0.1	0.0
	IOD	0.0	-0.1	0.0	-0.2	0.4	0.4	**0.5**	0.3	0.4	0.0	0.2	-0.1	-0.4	0.1	0.0	-0.1
November	SOI	-0.2	-0.2	-0.4	-0.4	0.4	0.4	0.2	0.2	0.1	-0.1	-0.3	0.0	0.4	0.4	0.2	0.2
	AAO	**-0.5**	**-0.6**	-0.3	-0.4	**0.6**	0.5	0.3	0.3	**-0.6**	**-0.5**	0.1	**-0.6**	**0.5**	**0.5**	0.0	0.1
	IOD	0.1	-0.2	-0.2	0.1	0.2	0.3	0.2	-0.1	0.3	-0.1	-0.3	-0.1	-0.1	-0.3	**-0.5**	**-0.6**
December	SOI	0.3	-0.1	0.0	0.3	0.0	-0.1	-0.1	-0.4	0.4	0.0	-0.2	0.5	0.1	-0.1	-0.1	0.1
	AAO	0.3	**-0.7**	-0.5	**-0.5**	**0.5**	**0.7**	**0.6**	-0.2	0.2	-0.4	**-0.6**	0.0	0.3	0.2	-0.5	-0.1
	IOD	-0.1	-0.4	-0.5	-0.5	**0.6**	0.5	0.4	-0.1	0.4	-0.1	-0.3	-0.3	0.4	0.3	0.2	0.0